The Adsorption of Organic Molecules on Metal and Semiconductor Surfaces

by

Gilles Rousseau

A thesis presented in partial fulfilment for
the degree of Doctor of Philosophy in the
Faculty of Science of the University of Glasgow

Chemistry Department

September 2003

Acknowledgements

I would like to thank my supervisor, Dr. Malcolm Kadodwala, for his help and patience, for giving me the opportunity to carry out this work and for his expert guidance throughout the course of this project. His dedication to his work and that of the Surface Science group has made working here a privilege.

I would also like to thank my friends and colleagues with whom I have had the privilege to know and work with in my time at Glasgow. Especially Shona, Andrew, Nicolas, Chris, Ewan, Ian, David, Paula, Tim, Dave and Peter and countless other people I have probably forgotten to mention.

I owe a great date of gratitude to Dr Vin Dhanak, George Miller, Dr Chris Muryn and Dr Alex Shard for their help during the eleven and a half weeks spent at the Daresbury Laboratory.

I would also like to thank the members of staff (Dr Lutz Hecht, Dr Kelvin Tyler, Dr. David Lennon and Stuart MacKay) with whom I consulted when a problem came up.

I am indebted to the mechanical workshop (John Gillan), the electronic workshop (Jarnail Bhumbra and Ray Pallister) and the glass-blowing workshop (William McCormack and Arlene Douglas) whose help was much appreciated, especially when the equipment started to go wrong or break down.

Many thanks to my long-suffering family, for their love and support, especially over the past few years. Finally, many thanks to my wife Fiona for her support during my PhD and especially during my writing-up period.

Acronyms and Abbreviations used in this Thesis

AES	Auger Electron Spectroscopy
AFM	Atomic Force Microscopy
ARPEFS	Angle Resolved Photoemission Extended Fine Structure
ARUPS	Angle Resolved Ultraviolet Photoemission Spectroscopy
CHA	Concentric Hemispherical Analyser
CIO	Coadsorption Induced Ordering
DFT	Density Functional Theory
EELS	Electron Energy Loss Spectroscopy
FCC	Face Centred Cubic
FMO	Frontier Molecular Orbital
FTMS	Fourier Transform Mass Spectrometry
HCP	Hexagonal Close Packed
HREELS	High Resolution Electron Energy Loss Spectroscopy
HV	High Vacuum
LEED	Low Energy Electron Spectroscopy
ML	Monolayer
NEXAFS	Near Edge X-ray Absorption Fine Structure
NIXSW	Normal Incidence X-ray Standing Wavefield
QMS	Quadrupole Mass Spectrometer
RAIRS	Reflectance Absorbance Infrared Spectroscopy
RFA	Retarding Field Analyser
SEXAFS	Surface Extended X-ray Fine Structure
STM	Scanning Tunnelling Microscopy
TDS	Temperature Desorption Spectroscopy
TPD	Temperature Programmed Desorption
TSP	Titanium Sublimation Pump
2PPE	Two Photon Photoemission
UPS	Ultraviolet Photoemission Spectroscopy
UHV	Ultra High Vacuum
XPS	X-ray Photoemission Spectroscopy
XSW	X-ray Standing Wavefield

Abstract

The first part of this project focused on the effects of coadsorbates on the adsorption of organic molecules bonded to Cu(111). First, the influence of coadsorbed CO on the structure and bonding of thiophene was investigated using a combination of LEED, AES, TPD and synchrotron-based NIXSW and NEXAFS techniques. It was found that the coadsorption of CO does not induce an ordering of the disordered chemisorbed thiophene layer, in contrast to the behaviour of related benzene coadsorption systems where CO induces ordering of benzene disordered layers. Detailed analysis of our NIXSW and NEXAFS data showed that CO and thiophene both adopt atop adsorption sites within the coadsorbed overlayer, the same site adopted by both molecules in pure layers, and the orientation of the thiophene molecules within the coadsorbed layer is also similar to that adopted in the pure layer. The results of our NIXSW measurements, however, showed that CO molecules within the coadsorbed layer are tilted, which contrasts with a linear geometry observed in pure CO layers of a similar coverage. We propose that the lack of any significant cooperative effects between the CO and thiophene within the coadsorbed overlayers is due to the relatively weak adsorbate – substrate interactions.

The second coadsorption study concerned the influence of sulfur precovered Cu(111) surfaces on the adsorption of thiophene, benzene, cyclohexene and cyclohexane molecules using TPD, AES, LEED, XPS and UPS. The characterisation experiments established that all four molecules are reversibly adsorbed on all the surfaces studied, and more importantly our TPD and UPS data clearly showed that the co-adsorption of sulfur influences the bonding of each of the probe molecules in particular ways. At a pre-coverage of 0.12 ML of sulfur, the desorption of thiophene and benzene in our TPD experiments is shifted to higher temperatures, clearly showing that co-adsorbed sulfur at this precise coverage stabilises the adsorption of the aromatic molecules. With increasing S pre-coverage, the stabilising effects of sulfur on these two molecules diminish and by *ca.* 0.33 ML of sulfur destabilisation takes place. The stabilisation of cyclohexene is also effective but occurred at higher sulfur coverages (up to θ_S = 0.33ML). We believe that steric blocking by sulfur adatoms is responsible for the destabilisation of thiophene, benzene and cyclohexene. For cyclohexane, however,

stabilisation does not occur and the appearance of a new desorption peak indicates the formation of a less stable adsorption state at all sulfur coverages studied. We believe that the stabilisation of thiophene, benzene and cyclohexene on Cu(111) in presence of sulfur can be explained in terms of a simple electrostatic model. The formation of induced anti-parallel dipoles, which are caused by the charge transfer from the unsaturated molecules to the substrate and from the substrate to sulfur adatoms, provoke an increase of charge donation from the π-levels of the unsaturated molecules into unoccupied levels of the substrate. This model illustrates the enhancement of the bond strength of the π-bonded species to Cu(111) experimentally observed. A similar electrostatic model can also be used to describe the destabilisation of the cyclohexane molecules. The electrostatic field set up by sulfur results in the formation of induced parallel dipoles which reduce the charge transfer from the substrate to the saturated molecule and destabilise the saturated molecule.

In the second part of this project, the surface reactivity of thiophene, benzene and benzonitrile with Si(100)-(2×1), Si(111)-(7×7) and Ge(100)-(2×1) was investigated using synchrotron-based valence band photoemission. To the best of our knowledge, the adsorption of thiophene and benzonitrile on the Ge(100)-(2×1) surface has not been reported in the literature. For the three molecules studied, our experimental results show that the relative reaction rates for the (2×1) semiconductor surfaces studied give Si(100) > Ge(100), with Si(100) being more reactive than the Ge(100) surface as a result of the higher degree of polarisation within the Si dimers than the Ge dimers. The detailed analysis of the collected valence band data reveals that the adsorption of thiophene, benzene and benzonitrile on all three semiconductor surfaces leads to the formation of 2,5-dihydrothiophene-, 1,4-cyclohexadiene- and benzoimine-like moieties, respectively. The adsorption of thiophene, benzene and benzonitrile occurs on the terraces of Si(100)-(2×1) and Si(111)-(7×7), whereas our UP spectra indicate that benzene and benzonitrile adsorb initially on the Ge dimers located next to the step edges of the Ge(100)-(2×1) surface. The formation of the 2,5-dihydrothiophene- and 1,4-cyclohexadiene-like surface species on Si(100) and Ge(100) is consistent with a [4+2] cycloaddition (Diels–Alder) mechanism. For benzonitrile, however, a 1,2-dipolar cycloaddition reaction between the unsaturated cyano group and the Si and Ge surface dimers results in the formation of the benzoimine-like species. In contrast to the two other surfaces, the formation of the 2,5-dihydrothiophene-, 1,4-cyclohexadiene- and benzoimine-like

moieties on Si(111)-(7×7) cannot occur *via* a cycloaddition reaction, due to the absence of the required "π-bonded" dimers. The results presented here would therefore imply that although the electronic/physical properties of the three substrates may influence the mechanism of a reaction, they do not appear to significantly affect which species is the most stable product.

ELSEVIER

Surface Science 511 (2002) 190–202

SURFACE SCIENCE

www.elsevier.com/locate/susc

The structure of a coadsorbed layer of thiophene and CO on Cu(1 1 1)

G.B.D. Rousseau [a], N. Bovet, S.M. Johnston [a], D. Lennon [a], V. Dhanak [b], M. Kadodwala [a,*]

[a] *Department of Chemistry, Joseph Black Building, University of Glasgow, Glasgow G12 8QQ, UK*
[b] *CLRC Daresbury Laboratory, Warrington WA4 4AD, UK*

Received 28 September 2001; accepted for publication 16 February 2002

Abstract

The influence of coadsorbed CO on the structure and bonding of thiophene (C_4H_4S), an aromatic heterocycle, on Cu(1 1 1) has been investigated using a combination of near edge X-ray absorption fine structure spectroscopy, normal incidence X-ray standing wavefield absorption (NIXSW) and temperature programmed desorption. The coadsorption of CO does not induce an ordering of the disordered chemisorbed thiophene layer. This lack of ordering contrasts with the behaviour of related benzene coadsorption systems where CO induces ordering of disordered layers. The results of NIXSW measurements show that CO and thiophene both adopt atop adsorption sites within the coadsorbed overlayer, the same site adopted by both in pure layers. The orientation of the thiophene within the coadsorbed layer is also similar to that adopted in a pure layer. However, the CO molecules within the coadsorbed layer are tilted, which contrasts with a linear geometry observed in pure CO layers of a similar coverage. It is suggested that the lack of any significant cooperative effects between the CO and thiophene within the coadsorbed overlayers is due to the relatively weak adsorbate–substrate interactions. © 2002 Published by Elsevier Science B.V.

Keywords: Copper; Carbon monoxide; X-ray standing waves; Adsorption kinetics

1. Introduction

In general heterogeneous catalytic reactions on metal surfaces involve more than one adsorbed species. This has motivated many studies of model coadsorption systems, which have attempted to determine how two adsorbed species interact with each other, and to what extent their structure and bonding is altered. The majority of this previous work has involved studying the effects of simple electron withdrawing (NO, CO, halogen, oxygen) or donating (alkali metal) adsorbates on the bonding of simple adsorbates such as CO and benzene [1,2]. From this body of work some general trends in the behaviour of coadsorption systems have been established. Namely when electron withdrawing and electron donating species are adsorbed together cooperative effects within the overlayer are observed. The most apparent manifestation of these cooperative effects is the

* Corresponding author. Tel.: +44-141-330-4380; fax: +44-141-330-4888.
E-mail address: malcolmk@chem.gla.ac.uk (M. Kadodwala).

0039-6028/02/$ - see front matter © 2002 Published by Elsevier Science B.V.
PII: S0039-6028(02)01487-5

ELSEVIER

Surface Science 494 (2001) 251–264

SURFACE SCIENCE

www.elsevier.com/locate/susc

Photoemission studies of the surface reactivity of thiophene on Si(100)-(2 × 1), Si(111)-(7 × 7) and Ge(100)-(2 × 1)

Gilles B.D. Rousseau [a], Vin Dhanak [b], Malcolm Kadodwala [a,*]

[a] *Department of Chemistry, University of Glasgow, Joseph Black Building, Glasgow, Scotland G12 8QQ, UK*
[b] *CCLRC Daresbury Laboratory, Warrington WA4 4AD, UK*

Received 10 March 2001; accepted for publication 30 July 2001

Abstract

The surface reactivity of thiophene with Si(100)-(2 × 1), Si(111)-(7 × 7) and Ge(100)-(2 × 1) has been investigated using valence band photoemission. The data clearly show that for all three surfaces thiophene adsorption leads to the formation of the same surface moiety. Based on comparisons of the photoemission data with gas phase spectra we believe that this moiety is a 2,5-dihydrothiophene-like species. The formation of a 2,5-dihydrothiophene-like species on Si(100)-(2 × 1) and Ge(100)-(2 × 1) is consistent with a 4 + 2 cycloaddition (Diels–Alder) mechanism being responsible for the reaction between thiophene and the two surfaces. The relative reactivities of Si(100)-(2 × 1) and Ge(100)-(2 × 1) towards thiophene are also consistent with a Diels–Alder mechanism. In contrast to the two other surfaces, the formation of a 2,5-dihydrothiophene-like moiety on Si(111)-(7 × 7) cannot occur via a Diels–Alder mechanism, because of the absence of the required "π-bonded" silicon dimers. The results presented would imply that although the electronic/physical properties of the three substrates may influence the mechanism of a reaction, they do not appear to significantly affect which species is the most stable product. © 2001 Published by Elsevier Science B.V.

Keywords: Germanium; Silicon; Photoelectron spectroscopy

1. Introduction

Fundamental studies of the adsorption and subsequent reactivity of simple organic molecules on group IV semiconductors have always been of interest to the surface science community. Apart from the intrinsic interest of the physical and chemical properties of these covalently bonded surfaces, work has been motivated by their technological importance. Recently, studies of interfaces between organic molecules and semiconductors have gained further importance because of technological opportunities offered by interfacing organic and biological materials to electronic devices.

The majority of studies of the adsorption of small organic molecules on group IV semiconductor surfaces have been performed on Si(100)-(2 × 1) [1] and Si(111)-(7 × 7) [2], with fewer studies involving Ge(100)-(2 × 1) [3–6]. The Si(100)-(2 × 1) and Si(111)-(7 × 7) surfaces have significantly different structures and electronic properties. The Si(100)-(2 × 1) surface has the least complicated surface structure, consisting of rows of buckled silicon dimers which have π-bonding character [7–9]. The

* Corresponding author. Tel.: +44-141-330-4380; fax: +44-141-330-4888.

E-mail address: malcolmk@chem.gla.ac.uk (M. Kadodwala).

0039-6028/01/$ - see front matter
PII: S0039-6028(01)01480-7

Contents

Chapter 1. Introduction and Literature Review

1.1 Introduction

In the first part of this project, we wish to rationalise the influence of coadsorbates on the structure and bonding of simple organic probe molecules adsorbed on Cu(111). With heterogeneous catalytic reactions on metal surfaces which normally involve more than one adsorbed species, this has motivated many studies of model coadsorption systems that have attempted to determine how two adsorbed species interact with each other and to what extent their structure and bonding is altered. Previous investigations have shown that the possible effects of coadsorbates is to induce 2-dimensional order within a chemisorbed overlayer, to affect the local geometry of coadsorbed molecules, and to stabilise (promote) or destabilise (poison) the adsorption and reactivity of the coadsorbates.

It has been previously established that when carbon monoxide (CO) and benzene (C_6H_6) are adsorbed together on transition metal surfaces, cooperative effects within the overlayer are observed.[1,2] The most apparent manifestation of these cooperative effects is the re-ordering of molecules with the coadsorbed overlayer. Indeed, benzene adsorption on many transition metal surfaces leads to the formation of disordered overlayers, however ordered structures are formed when CO is coadsorbed.[1] It has been postulated that the formation of induced anti-parallel dipoles formed by the transfer of charge from the benzene to the substrate and from the substrate to CO is the driving force for this ordering.[2]

In the first Result Section of the present study (Chapter 4), we wish to discover whether thiophene (C_4H_4S), an heterocyclic aromatic molecule, can be induced to form ordered structures by the coadsorption of CO, as it was previously established by our group that thiophene does not form any ordered structures on clean Cu(111) using the LEED technique.[3,4] It was also shown by our group that thiophene can undergo a coverage driven phase transition from a roughly flat (so-called "α-phase") to a more upright geometry (so-called "β-phase").[4] The use of the synchrotron-based NEXAFS and NIXSW techniques should also enable us to detect any possible change in the local registry and/or orientation of adsorbed thiophene brought about by the presence of coadsorbed CO.

The poisoning properties of sulfur over transition metal catalysts are well known and have been widely documented in the literature, however Hutchings *et al.* have recently demonstrated the promotional properties of sulfur for the selective hydrogenation reaction of crotonaldehyde to crotyl alcohol on supported gold and copper catalysts.[5-8] In view of Hutchings' recent work, the second coadsorption study performed during the course of this project focused on the effects of coadsorbed sulfur on the adsorption of thiophene, benzene, cyclohexene (C_6H_{10}) and cyclohexane (C_6H_{12}) molecules on Cu(111) single crystal surfaces. By performing these studies, we aimed to discover whether sulfur could act as a promoter for the adsorption of these four probe molecules.

The second part of this project concerns the interaction of simple organic molecules adsorbed on group IV semiconductors. Such systems have recently become of increasing importance due to the technological opportunities offered by interfacing organic and biological materials to electronic devices. The majority of recent studies have been based on the adsorption of small organic molecules on Si(100)-(2×1)[9] and Si(111)-(7×7),[10] with fewer studies involving Ge(100)-(2×1).[11-14] The Si(100)-(2×1) and Ge(100)-(2×1) surfaces have been shown to be structurally identical with similar electronic properties,[15-17] with both surfaces consisting of rows of buckled silicon dimers which possess π-bonding character.[18-20] On the other hand, Si(111)-(7×7) has a more complex reconstruction than the (2×1); this surface contains silicon atoms in a variety of chemically distinct environments and exhibits significantly different structures and electronic properties.[21,22]

It has recently been proposed by two groups, led by Hamers and Bent, that the π-bonded dimers of the (2×1) reconstructed Si(100) and Ge(100) surfaces can undergo cycloaddition reactions with dienes.[9,23] In light of this work, we intended to develop an improved understanding of the relationship between surface structural and electronic properties and chemical activity. Specifically we wished to determine whether the absence of π-bonded dimers, and hence the lack of a cycloaddition reaction pathway, on Si(111)-(7×7) has a significant effect on its reactivity towards a diene. Towards this end, the adsorption of thiophene, benzene and benzonitrile molecules on the Si(100), Si(111) and Ge(100) surfaces were systematically performed. This approach enabled us to readily compare data from each system and hence facilitate the establishment of structure–reactivity relationships.

1.2 Literature Review

In order to study the effects of coadsorbates on the adsorption of organic molecules bonded to Cu(111), it is important to first review previous investigations which have dealt with the adsorption of CO, sulfur, thiophene, benzene, cyclohexane and cyclohexene on pure coinage metal surfaces (mostly Cu(111)), then followed by a brief overview of previous coadsorption studies which are relevant to this project.

A brief description of the Si(100)-(2×1), Si(111)-(7×7) and Ge(100)-(2×1) surfaces used during this project will be given in the second part of this section, followed by a literature review of previous work involving the adsorption of thiophene, benzene and benzonitrile on these three semiconductor surfaces.

1.2.1 Pure and Coadsorption Studies

1.2.1.1 Carbon Monoxide Adsorbed on clean Cu(111)

The adsorption of CO on Cu(111) has been previously investigated using the LEED,[24,25] RAIRS,[26,29] EELS,[26] TDS,[27] and ARPEFS[28] techniques and surface potential measurements.[25] The early LEED studies[24] of the CO/Cu(111) system suggested the formation of three distinctive overlayer structures. The first ordered structure to appear upon CO adsorption on Cu(111) at 89 K corresponds to a $(\sqrt{3}\times\sqrt{3})R30°$ LEED pattern at coverage of 0.33 ML.[24] Further adsorption leads to the formation of a second coexisting LEED structure which was attributed to two domains of a hexagonal (1.5×1.5)R18° mesh on the surface.[24] The final structure formed at saturation coverage was assigned to a further compressed, out-of-registry overlayer of hexagonally close packed CO molecules, (1.4×1.4) structure.[24]

The results from thermal desorption spectroscopy reveal that the CO molecules are weakly bond to the Cu(111) surface, as the molecules desorb below 195 K.[27] The Gibbs free activation energy of desorption deduced from these TPD experiments was found to exhibit a dramatic rise in transition from the higher coverage (1.5×1.5)R18° phase to the lower coverage $(\sqrt{3}\times\sqrt{3})R30°$ phase.[27] Surface potential measurements also demonstrated an abrupt change in heat of adsorption, from ~ 38 kJ/mole to 50

kJ/mole, at the transition from the (1.5×1.5)R18° phase to the (√3×√3)R30° phase, respectively.[25]

The use of RAIRS,[26,29] EELS[26] and ARPEFS[28] led to a further understanding of the CO/Cu(111) systems. It was found that CO adsorbs on an atop site with the carbon end down for the first two coverage phases,[26,28,29] with a C-Cu bond length of 1.91 (1) Å in the (√3×√3)R30° phase and 1.91 (2) Å in the (1.5×1.5) R18° phase.[28] For coverages greater than 0.44 ML, it was established by EELS, RAIRS and LEED that both bridged and linear CO species exist in this coverage range, and the proportion of bridged species present in the overlayer is very sensitive to adsorption temperature.[26]

Theoretically, the bonding of CO to copper surfaces is generally well understood and can be described by the Blyholder model.[30] In this model, the 5σ MO of the CO molecule donates charge to the Cu(4s,4p), and back donation from the metal into the unoccupied 2π* orbital of CO occurs.[31] The 2π* MO resides primarily on the carbon atom,[31] in good agreement with the experimental results which suggested that the CO molecule adsorbs with the carbon end down. This transfer of electronic charge from the copper substrate to the molecule leads to a positive charge on the metal which stabilises the repulsive interaction between the occupied 5σ MO and the metal valence electrons.

1.2.1.2 Sulfur Adsorbed on Cu(111)

The phenomenon of sulfur-induced reconstruction on low-index-copper surfaces has been described for the first time by Domange and Oudar in 1968 using LEED and radioactive ^{35}S tracer[32]. With the improvement of surface science techniques, numerous quantitative methods have been applied to the S/Cu(111) complex and have provided new physical pictures of how sulfur induces the reconstruction of (111) face of copper (Table 1).

In the first investigation of the S/Cu(111) system[32], three ordered phases were detected as a function of increasing H_2S exposure at room temperature (it has been suggested that the adsorption of H_2S is associative below 200 K but dissociative above this temperature, with the subsequent desorption of gaseous H_2 taking place at room

temperature and leaving only atomic sulfur on the Cu(111) surface).[33] These three ordered structures were: a $(\sqrt{3}\times\sqrt{3})R30°$ phase, a transitory 'complex' phase, and finally a $(\sqrt{7}\times\sqrt{7})R19°$ phase.[32] The $(\sqrt{3}\times\sqrt{3})R30°$ structure has not been reproduced since then. It has been proposed that this phase might have been associated with a narrow range of coverage and/or temperature as it is the case for the formation of the $(\sqrt{3}\times\sqrt{3})R30°$-S on Ni(111).[34] Ruan *et al.* suspected that this structure in the original study may have been an artefact.[35] Furthermore, the 'complex' phase described in the earliest investigation has been identified by STM[35] and SXRD[36] and assigned as $\begin{vmatrix} 4 & 1 \\ -1 & 4 \end{vmatrix}$ in matrix notation. This structure occurs at $\theta_S = 0.35$ ML and consists of two Cu_4S units per surface unit mesh with the sulfur atom adsorbed in the fourfold hollow site on top of the Cu tetramers. This structure is commonly known has the 'zigzag' structure on account of the STM images obtained. Originally, it was suggested that the $(\sqrt{7}\times\sqrt{7})R19°$ phase was to be associated with the formation of a compound copper-sulfide overlayer.[32] Subsequent structural investigations of this phase have been carried out by a variety of methods including NIXSW,[37-39] SEXAFS,[37] STM,[35] and SXRD.[36] Numerous structural models of this structure have been proposed, however disagreements still exist. The two investigations based on the NIXSW[39] and STM[35] data favoured the model proposed on the basis of SXRD[36] which involves one Cu_4S tetramer per surface unit mesh (compared to two Cu_4S tetramers for the 'zigzag' structure)[35] and two additional S atoms per surface unit mesh occupying the Hexagonal Close Packed (HCP) and Face Centred Cubic (FCC) sites on the underlying unreconstructed Cu(111) layer (Fig. 1).

Five other ordered structures due to the presence of adsorbed S on Cu(111) have also recently been described. Wahlström *et al.* observed the formation of four other ordered structures on Cu(111) using STM, core level and valence band photoelectron techniques.[40,41] The particularity of the honeycomb-like $(\sqrt{43}\times\sqrt{43})R7.5°$ phase and the three other structures labelled I, II and III by the authors was due to their detection that only took place at low temperature. More recently, Driver and Woodruff reported a new S-induced adsorption phase on Cu(111) observed by STM.[42] This structure was formed by dissociation of adsorbed methanethiolate in an electron beam and coexisted with the 'zigzag' and $(\sqrt{7}\times\sqrt{7})R19°$ structures. This new phase had a near-

square geometry and the authors interpreted it as a significant pseudo-(100)c(2×2)-S model which appeared to a commensurate $\begin{vmatrix} 5 & 0 \\ 1 & 3 \end{vmatrix}$ structure.

Table 1. *Long-range-ordered structures formed by S adsorption on Cu(111).*

Surface	Phase	Coverage θ_S / ML	Temperature / K
Cu(111)	$(\sqrt{43}\times\sqrt{43})R7.5°$	0.05 to 0.25	<170
	Structure I, II & III	0.25 to 0.35	<230
	$(\sqrt{3}\times\sqrt{3})R30°$	0.33	300
	$\begin{vmatrix} 4 & -1 \\ 1 & 4 \end{vmatrix}$ ('zigzag')	0.33 to 0.43	300
	$(\sqrt{7}\times\sqrt{7})R19°$	0.43	300
	Pseudo-(100)c(2×2) or $\begin{vmatrix} 5 & 0 \\ 1 & 3 \end{vmatrix}$ By electron-induced decomposition	–	300

Fig.1 *Schematic top and side views of surface model of the $(\sqrt{7}\times\sqrt{7})R19°$-S structure proposed by Foss et al[36] and Jackson and co-workers[39] on the basis of their SXRD and NIXSW results. The Cu substrate atoms are drawn unshaded, and the outermost layer Cu atoms are lightly shaded. Darkly shaded spheres represent the S atoms.*

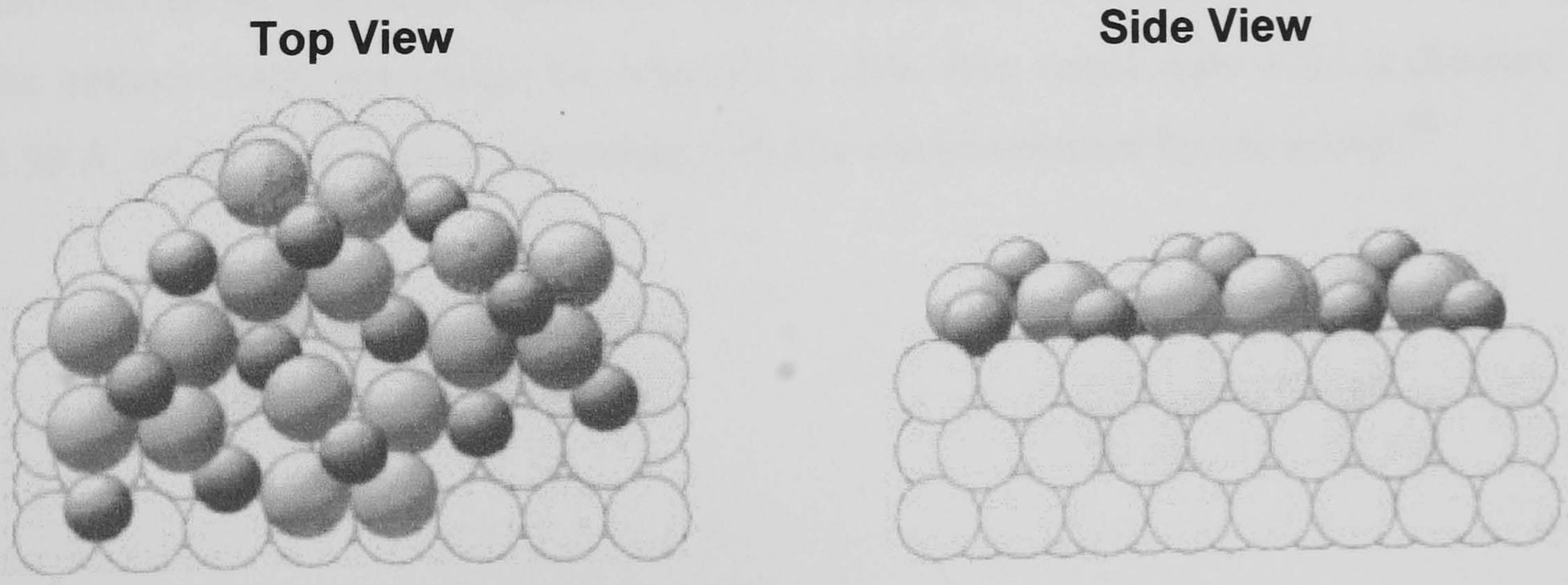

1.2.1.3 Thiophene Adsorbed on Cu(111)

In the first study of thiophene adsorbed on Cu(111) at room temperature, Richardson and Campuzano found that relatively large exposures of thiophene were required to saturate the surface.[43] From their angle-resolved photoemission data, the authors suggested that the thiophene molecules were in a flat orientation and weakly π - bonded to the Cu(111) surface.

For the adsorption of thiophene at cryogenic temperature, a LEED, TPD and AES study performed by our group[3,4] showed that thiophene is reversibly adsorbed on the Cu(111) surface and does not form any ordered structures. Synchrotron-based NIXSW and NEXAFS data of the C_4H_4S/Cu(111) system was also collected by our group in order to determine the adsorption site and orientation of the molecule.[3,4] It was found that the bonding of thiophene to Cu(111) is dominated by its sulfur atom and the molecule can undergo a coverage driven phase transition due to the energy advantage of increasing the thiophene packing density. In the low coverage phase the thiophene molecule forms a π-bonded species which adopts an atop adsorption site with a Cu-S separation of 2.62 Å and with the ring inclined by 26° (labelled as the "α - phase"). At higher coverages, the molecule undergoes a compressional phase transformation to a more weakly bound sulfur lone-pair bonded species with the thiophene molecule still occupying an atop site with a Cu-S distance of 2.83 Å and the ring now inclined at 44° to the surface (the so-called "β-state").

Information on the orientation and S-Cu surface distance was also obtained in a separate study by Ohta *et al.*[44] who studied the adsorption of thiophene on Cu(111) using S K-edge NEXAFS and SEXAFS at cryogenic temperature. In this study, thiophene surfaces were prepared at sub-monolayer coverages. The S K-edge NEXAFS showed that the thiophene molecules are oriented a flat, π-bonded orientation. Although the authors could not assign the adsorption sites, they could state a S-Cu distance of 2.50 Å, which was in good agreement with the results obtained by our group.[4]

1.2.1.4 Benzene Adsorbed on Cu(111)

The adsorption of benzene on Cu(111) was previously studied using the TPD, HREELS and NEXAFS techniques by Bent *et al.*[45] Their TPD spectra showed three peaks which corresponded to desorption of benzene multilayers at 152 K, second benzene layer at 157 K and a broader peak centred at 225 K attributed to first benzene layer desorption. Their HREELS and NEXAFS results indicated that the molecules in the first layer were chemisorbed and bonded with their π rings approximately parallel to the surface, whereas benzene molecules in the second layer were physisorbed and adopted a more upright or almost perpendicular orientation. They concluded that the peak at 157 K was due to bilayer formation and concluded that the broad monolayer feature at 225 K was due to repulsive interaction between flat lying benzene molecules within the monolayer.

Two Photon Photoemission (2PPE) spectroscopy was employed by Velic *et al* to characterise the electronic states of the C_6H_6/Cu(111) system at 85 K.[46] Their work function versus benzene coverage measurements showed three distinct linear trends that coincided with the formation of the first layer, second layer and multilayers. Their work agreed with the bilayer model proposed by Bent and co-workers.

The broadening feature of the monolayer peak with increasing benzene coverage on Cu(111) observed by Bent *et al.*[45] was also studied by Weiss and co-workers using the STM technique.[47] In their STM images, it was found that benzene aligns along the step edges. This was then extended to the idea that the adsorbed molecules on the step edges perturb the site adjacent to them on the terrace and supports the formation of island of benzene molecules. Islands of benzene molecules therefore have attractive lateral interactions, in contrast to the conclusion drawn by Bent and co-workers.[45] Weiss explains the broadening to lower desorption temperature as desorption of islands of benzene of different sizes.[47]

Interestingly, in a recent thermal desorption and ARUPS study of the adsorption of benzene on a pseudomorphic Cu monolayer on Ni(111) by Koschel and co-workers,[48] the authors suggested that the chemical properties of the Cu monolayer were quite similar to those of the Cu(111) surface, and their TPD and ARUPS data for benzene adsorbed on the pseudomorphic Cu monolayer on Ni(111) provided similar results to the Bent work.[45] For instance, it was found that the benzene is weakly

chemisorbed as desorption of the first layer occurred in the temperature range between 155 and 230 K with no sign of dissociation, and from their ARUPS spectra, the plan of the molecule is parallel to the Cu/Ni(111)surface at low benzene coverages.[48] The authors also observed a tilting of the adsorbed molecules for the saturated first benzene layer on Cu/Ni(111).[48]

1.2.1.5 Cyclohexane Adsorbed on Cu(111)

The first adsorption/desorption behaviour of cyclohexane on the Cu(111) surface was studied by Xi and Bent using the TPD technique.[49] At low exposures, a single peak was observed at 175 K and the authors attributed this peak to desorption of cyclohexane monolayer. For higher exposure, an additional peak centred at 135 K appeared which showed zero-order desorption and was assigned to the desorption of cyclohexane condensed layers. Further, the plot of the amount of molecularly desorbing cyclohexane as derived from the TPD peak area versus cyclohexane exposure showed a linear increase. This was consistent with the fact that no decomposition products were detected in their TPD and there was no carbon deposition on the surface as monitored by Auger electron spectroscopy. From these observations, Xi and Bent concluded that the desorption behaviour for cyclohexane on Cu(111) is reversible.

Cyclohexane was also used as a probing molecule for studying the "softened" C-H modes on transition metal surfaces.[50] Using a combination of EELS[50,51], RAIRS and LEED[51] techniques, Raval *et al.* proposed that two types of C-H bonds in the molecularly adsorbed species were involved; one relatively little perturbed, and the other one "softened", shifted down in frequency. The "softening" of the C-H stretching mode was thought to arise from the C-H···M interaction, resulting of an electron transfer from the bonding CH σ orbital into the metal orbitals and from the filled metal orbitals into the antibonding CH σ^* orbital. The authors also suggested that at low coverage, the cyclohexane molecules in the first layer were adsorbed in C_{3V} symmetry with the carbon skeleton approximately parallel to the surface. With increasing coverage, differences in the vibrational spectra acquainted a possible change in the adsorption symmetry from C_{3V} to C_S and also indicated a change in the orientation of the molecule, accompanied by a decrease in the intensity of the CH softening mode peak. The authors

also observed the clean desorption of cyclohexane molecules from the Cu(111) surface taking place at a temperature of 165 K.

In a recent theoretical investigation, Fosser *et al.*[52] performed ab initio calculations of the same system and the authors indicated that the soft modes previously seen for cyclohexane on the Cu(111) surface are in fact derived from the totally symmetric ν_2 mode (symmetric CH_2 stretch). The authors believed that a new mechanism came into play. Their calculated data revealed that there is a significant transfer of charge from the Cu substrate into the adsorbed cyclohexane molecules, however the authors suggested that this charge is back-donated into empty Rydberg orbitals of the C_6H_{12} molecule, and not into the orbital of C–H σ^* character.

1.2.1.6 Cyclohexene Adsorbed on Au(111)

To the best of our knowledge, there is currently only one publication available in the literature discussing the adsorption of cyclohexene on a coinage metal single crystal. Syomin and Koel have recently investigated the adsorption of cyclohexene (and cyclohexane) on Au(111) by means of TPD and Fourier-Transform RAIRS.[53] Their TPD spectra indicated that both molecules were reversibly adsorbed, with desorption from multilayer films at 143 K for the two molecules studied. Peaks at 213 and 198 K were observed and these desorption features were attributed by the authors to molecular desorption of cyclohexene and cyclohexane monolayers, respectively. RAIRS was utilised to characterise the cyclohexane and cyclohexene adsorbed layers. The "soft" C - H mode was also observed on the infrared spectra of C_6H_{12} at submonolayer coverages, indicating that the molecular plane of the molecule was parallel to the surface with three hydrogens pointed directly into the surface. As it was the case for the adsorption of cyclohexane on copper surfaces, the cyclohexane molecules started to tilt with increasing coverage. For the adsorption of cyclohexene at 1 ML and below, the bands of the olefinic C-H group stretching mode were absent in the spectra. The author attributed this observation to a possible flat orientation of the C_6H_{10} molecule on Au(111), with the C=C double bond in a parallel geometry.

1.2.1.7 Coadsorption Studies

1.2.1.7.1 Carbon Monoxide

The majority of previous investigations relevant to the first co-adsorption study of the current project has involved studying the effects of CO on the adsorption of benzene bonded to various transition metal surfaces (Ni,[54,55] Pt,[1,2,56] Pd,[57] and Rh[1,58] and Ru[59]). From this body of work some general trends in the behaviour of these coadsorption systems have been established. Namely when CO, an electron withdrawing species, and benzene, an electron donating species, are adsorbed together cooperative effects within the overlayer are observed.[2] The most apparent manifestation of these cooperative effects is the re-ordering of the benzene molecules in the presence of coadsorbed CO.[2] For instance, it was observed that benzene adsorption on pure Pt(111) does not lead to ordering in the adsorbed layer, however benzene ordered structures are formed when CO is coadsorbed.[1] The mechanisms postulated for the ability of CO to induce ordering within benzene overlayers involve the charge transfer from benzene to the substrate, and from the substrate to CO which causes the formation of anti-parallel dipoles which interact attractively and induce ordering.[2] Further evidence for the role of anti-parallel dipoles in the ordering of coadsorbed layers comes from studies of overlayer containing adsorbates of the same type (either both electron withdrawing or both donating). In these systems where the induced dipoles are parallel, no ordering within the layers occurs.

In parallel to the above model which proposed that the formation of induced anti-parallel dipoles is the driving force for ordering,[2] Neuber *et al.*[58] also suggested that although anti-parallel induced surface dipoles may determine the structure of an ordered coadsorbate system, they may not be exclusively necessary to produce ordered structures. Although the so-called coadsorption induced ordering (CIO) model may play a role in the formation of benzene ordered structures, Neuber and co-workers believed that based on simple packing considerations, tightly packed repulsive bodies will naturally order to minimise their total energy.[58]

1.2.1.7.2 Sulfur

1.2.1.7.2.1 Sulfur Poisoning

It is well known that the presence of sulfur-containing molecules, commonly found as impurities in fuels and oil-derived feedstock, can have negative effects on the performance of catalytic processes.[60] A typical example of how sulfur can deactivate transition metal catalysts was proposed by Campbell and Koel.[33] They demonstrated that the rate of the water gas-shift reaction ($H_2O + CO \rightarrow CO_2 + H_2$) over Cu(111) decreases linearly with sulfur coverage. The authors attributed this poisoning to a steric blocking by the sulfur adatoms of the sites required for dissociative water adsorption.[32]

Other examples concern the poisoning effects of sulfur on the reactivity of thiophene over transition metal single crystal surfaces. Thiophene is frequently used as a test molecule in hydrodesulfurisation process studies (HDS) and its decomposition on Mo(100),[61,62] Mo(110),[63-65] Ru(0001),[66-68] Ni(100),[69] Ni(111),[70,71] Pd(111),[72,73] Pt(111),[74,75] Rh(111),[76] W(211)[77] and Re(0001)[78] have shown to produce gaseous hydrogen, surface sulfur and surface carbon, and in certain cases C_xH_y fragments were also detected. More importantly, previous investigations found that sulfur pre-covered W(211),[79] Ni(111),[70] Ru(0001)[66] surfaces and various sulfide-modified molybdenum surfaces (Mo(110)–p(2×2)-S,[65] MoS_x,[63,80] MoS_2(0002)[84,85] and MoS_x/Al2O3 catalyst)[86] were less active for thiophene decomposition. This was also true for benzene adsorbed on sulfur pre-adsorbed Pt(111) surfaces.[93]

A possible explanation of how sulfur affects the reactivity of transition metal surfaces was recently proposed by Rodriguez and Hrbek.[94] They observed that sulfur perturbs the electronic properties of Pt, Pd, Ni, Rh, Mo and W transition metals[63,87-92] by withdrawing charge from the metal d-band and reducing the DOS near the Fermi level (electronic effect). From the methanation reaction study on Ni(100),[83] Goodman also suggested that sulfur can withdraw electron charge from the metal and therefore influence chemisorption and reactions over a relatively large spatial region. Goodman indicated that some ten nickel atoms were poisoned by each sulfur adatom at low coverage, compared to 2.6 copper atoms in the case of the water-gas shift reaction studied by Campbell and Koel.[33]

1.2.1.7.2.2 Promotional Effects of Sulfur on Coinage Metals

For the past 10 years, Hutchings and co-workers have shown that partial poisoning of supported copper or gold catalysts using sulfur-containing molecules can instead be a viable approach for the design of selective catalysts, whilst also maintaining catalytic activity.[5-8] They showed for the first time that the modification of Cu/Al_2O_3 catalysts by a wide range of sulfur components including thiophene, thiophane, DMSO, DMS, SO_2 and CS_2 significantly enhanced the selective formation of but-2-en-1-ol (crotyl alcohol) from the hydrogenation of but-2-enal (crotonaldehyde), with higher rates of synthesis obtained after thiophene treatment.[5] The effect of the modification with sulfur on the α,β-unsaturated aldehyde was therefore to enhance the selectivity for C=O bond hydrogenation rather than C=C bond hydrogenation.[6] In a recent paper by Bailie and Hutchings,[8] it was reported that similar effects were observed for thiophene doping of Cu supported on SiO_2 and MgO indicating that the effect was primarily due to interaction between copper and sulfur, and any interaction with the support was of secondary importance.[8] Thiophene doping of supported gold catalysts (Au/ZnO and Au/ZrO_2 *appropriately* prepared) was recently studied,[7] and an increase in the rate of formation of crotyl alcohol for the hydrogenation of the crotonaldehyde was also observed by the authors at very low levels of thiophene doping on the supported gold catalysts.

Pre-treatment of supported Ni, Pd, Pt, Ru, and Rh catalysts with thiophene doping showed that sulfur poisoned all the reactive sites and hence no selectivity could be induced for the hydrogenation of C=O bonds and instead enhanced the selectivity for C=C bond hydrogenation to butanal.[8] This argument suggested that the beneficial effects of sulfur modification of metal catalysts to promote the selective hydrogenation of the C=O bond of α,β-unsaturated aldehydes could only be restricted to supported Cu and Au catalysts for which sulfur appears to act as an electronic promoter.

The promotional effect of another electronegative element, chlorine, has also been reported by Lambert *et al.* for the stabilisation of benzene formed from the dissociative chemisorption of dichlorocyclobutadiene ($C_4H_4Cl_2$) on a Cu(110) surface at low Cl coverages.[95] To explain this result, Lomas and Pacchioni performed a theoretical *ab initio* cluster model wavefunctions calculation to study the effects of Cl on the bonding mechanism of benzene adsorbed on Cu surfaces.[96] They suggested that

the experimentally observed enhancement of the chemisorption bond strength of benzene on Cu(110) in the presence of coadsorbed Cl could be explained by a simple electrostatic model where the adsorption of Cl created a surface dipole layer which lowered the metal Fermi level. An increase in charge donation from benzene to the Cu substrate, which over-compensated the reduction in charge back-donation, was induced and furthermore resulted in a reinforcement of the chemisorption bond strength. On the other hand, Lomas and Pacchioni observed that on Pd(111) the stabilisation effect of Cl was not observed because the back donation contribution of Pd to the overall bonding is more important than on Cu, and any increase in charge donation from benzene to Pd is not sufficient to overcompensate any decrease in back donation.[96]

1.2.2 Semiconductor Studies

1.2.2.1 Si(100)-(2×1), Ge(100)-(2×1) and Si(111)-(7×7) Surfaces

The phenomenon of reconstruction is well known in surface science and this process, which is driven by the energetics of the systems, takes place on the clean group IV semiconductor surfaces. In the case of Si(100) and Ge(100), the formation of the two surfaces leaves two "dangling bonds" per surface atom and the presence of these bonds causes two adjacent surface atoms to be drawn together as pairs, thus forming rows of the so-called surface dimers (Fig. 2). Numerous experimental and theoretical studies have shown that the bonding within these dimers can be described in terms of σ and π bonds.[9,97,102] Analogies between the double bonds of the surface dimers and the C=C double bonds of alkenes can be made. However the π overlap is significantly less than would be found for the C=C bonds, suggesting that these dimers might be better thought of as di-radicals, with each Si and Ge atoms having a single unpaired electron.[103] Further, it is widely recognised that the dimers of the Si(100) and Ge(100) surfaces can tilt, and a charge transfer from the "down" atom to the "up" atom occurs, thereby adding zwitterionic character to the dimers (Fig. 3).[97] Ge(100) is structurally similar to the Si(100) surface, i.e. it can be viewed as having π-like character,[9] however the germanium surface possesses a 4% wider lattice constant and a 6% longer dimer distance.[104,105]

Since its discovery through LEED in 1959 by Schlier and Farnsworth,[106] the Si(111)-(7×7) surface has been extensively studied. The structure of this very complex reconstruction was given by Takayanagi *et al.* in the so-called dimer-adatom-stacking (DAS) model[107] and is depicted in Fig. 7. In this model, the energy associated with the dangling bonds is decreased by reducing their number from 49 to 19 in the (7×7) unit cell. The 19 dangling bonds are associated with 12 adatoms (AD), six rest-atoms (RA) and one corner hole in a unit cell, while the layer below consists of 42 atoms. Due to their position, all adatoms are not electronically equivalent. Because of a stacking fault in the unit cell, the two triangular halves are inequivalent and are generally referred to as the faulted and unfaulted halves. From a chemical point of view, the complexity of the (7×7) reconstruction offers a wide range bonding opportunities and the reactions are most likely to take place at these dangling bonds.[107,108]

Fig.2. *Schematic diagram representing the reconstruction of the Si(100)-(2×1) surface.* ***(a)*** *unreconstructed (1×1) surface; the Si atoms of the topmost layer are highlighted in orange; these atoms are bonded to only two other Si atoms, both of which are in the second layer (shaded grey).* ***(b)*** *reconstructed (2×1) surface; the Si atoms of the topmost layer form a covalent bond with an adjacent surface atom are thus drawn together as pairs; they are said to form "dimers".*

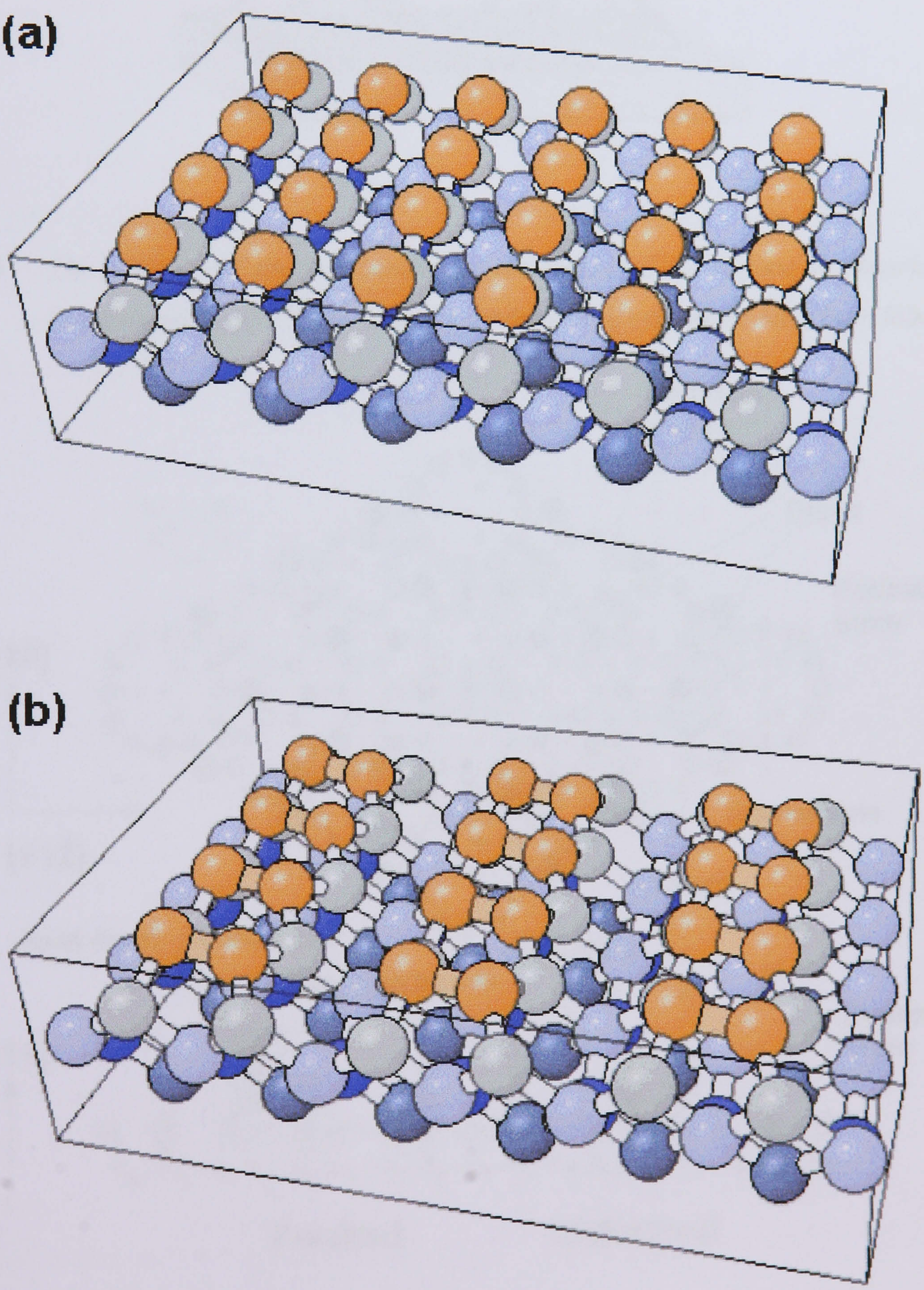

Fig.3 *Schematic illustrations of the tilted dimers of the Si(100)-(2x1) and Ge(100)-(2x1) surfaces according to Ref. [97]. The zwitterionic character of the dimers is also depicted.*[97]

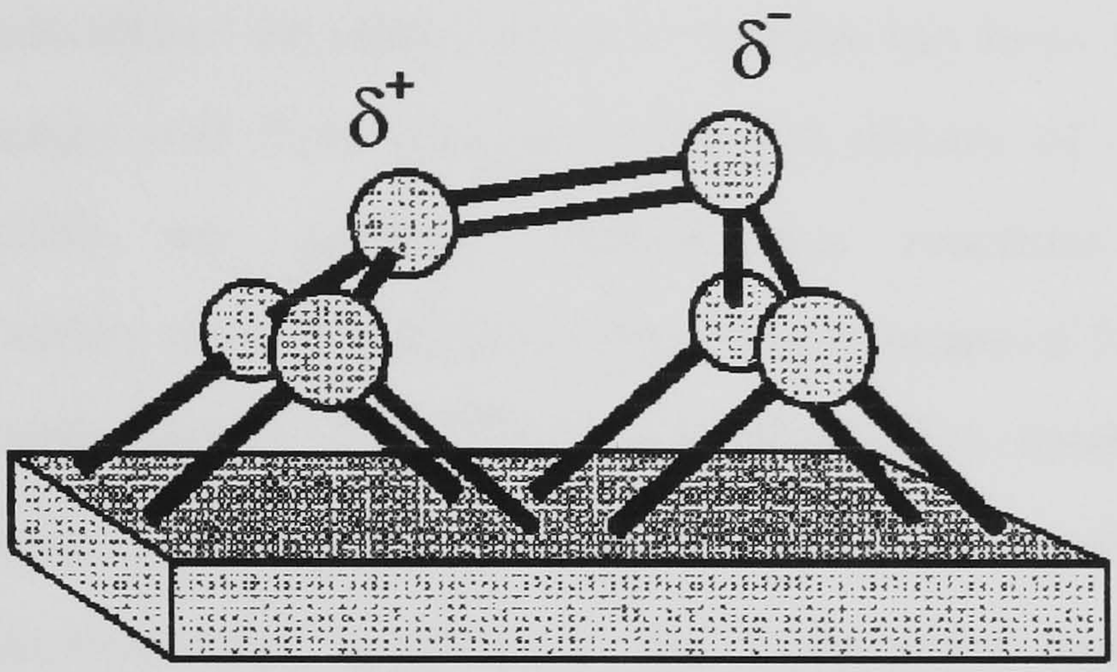

Fig.4 *The structure of the DAS model for the Si(111)-(7x7) surface as observed by Takayanagi et al.*[107] *The adatoms, pedestal and rest atoms have been labelled.*

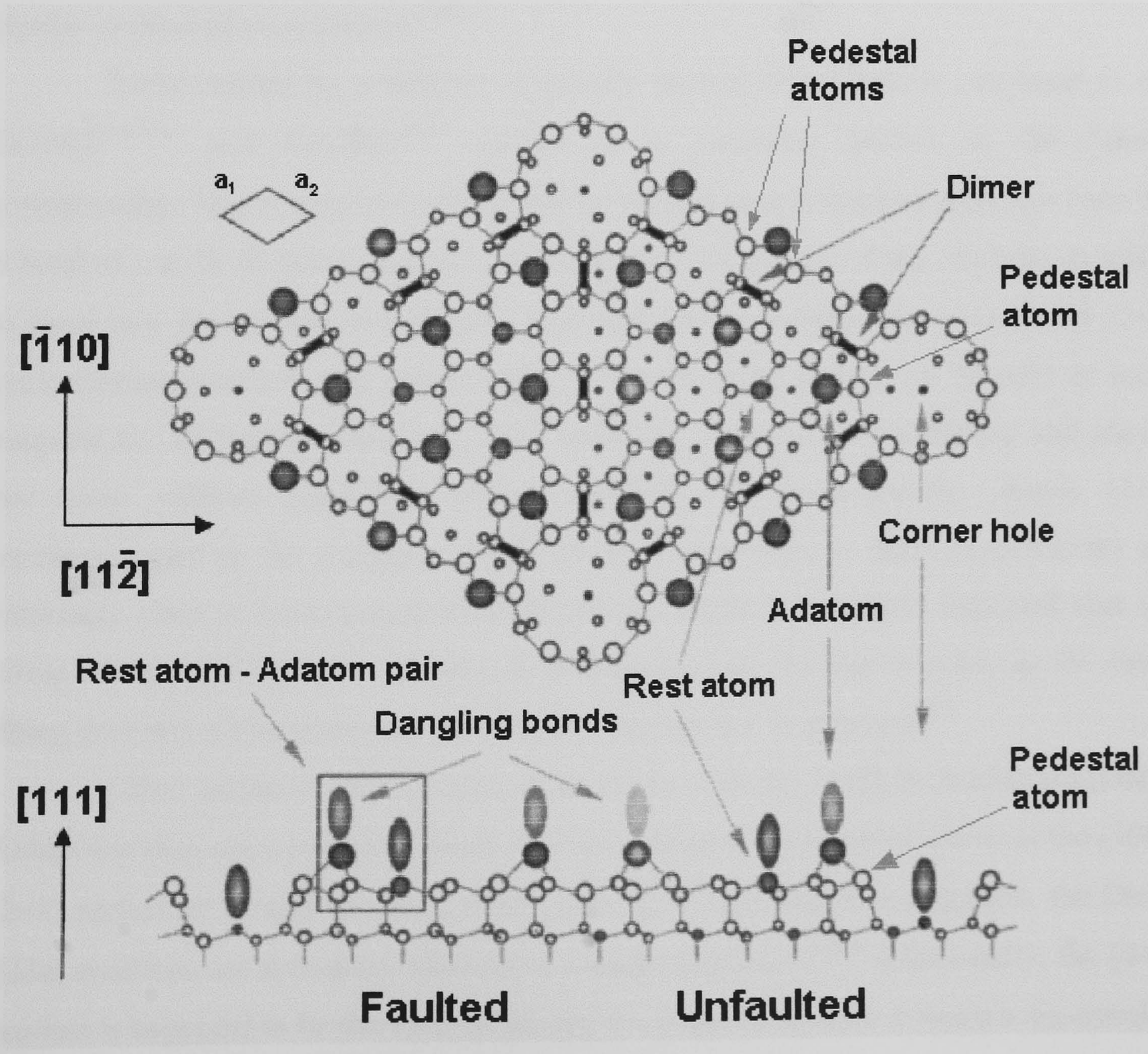

1.2.2.2 Cycloaddition Reactions

The most interesting recent development in the understanding of the chemical activity of organic adsorbates on semiconductor surfaces has been the proposal by two groups lead by Hamers and Bent that the π-bonded dimers of (2×1) reconstructed Si(100) and Ge(100) can undergo cycloaddition reactions with dienes.[9,23] Cycloadditions are widely used in organic synthesis as a means of forming new carbon-carbon bonds and new carbon rings.[109] In a cycloaddition reaction, two π-bonded molecules react to form a new cyclic molecule by the formation of two new σ bonds. The best-known cycloaddition reaction is the Diels-Alder reaction, in which a conjugated diene reacts with an alkene, called the dieneophile, to form a six-membered ring. The cycloaddition reactions are typically designated by the number of π electrons of each reactant molecule in the reaction, hence the Diels-Alder reaction is also known as the [4+2] reaction. Other cycloadditions include the [2+2] reaction, 1,2-, 1,3- and 1,4-dipolar cycloaddition reactions.[109]

Early studies by a number of groups showed that ethylene can bond to the Si(100)[110,111] and Ge(100)[112] surface in a geometry known as the "di-σ" configuration. This adsorption process can be viewed as utilising two electrons from the π bond of one Si=Si dimer and two electrons from the π bond of the ethylene molecule to form two new strong Si-C bonds. This reaction corresponds to a concerted [2+2] cycloaddition reaction and, surprisingly, it occurs quite readily on Si(100) at room temperature. In organic chemistry, such reactions are symmetry-forbidden and should not occur without significant energy activation.[109] Consequently, simple [2+2] reactions (such as the reaction of two ethylene molecules to form cyclobutane) are extremely slow at room temperature. However, recent calculations indicated that the tilting of the Si(100) surface dimers plays a crucial role for this reaction, as the dimer tilting provides a low-symmetry pathway for the reaction to proceed.[23]

Other surface science studies have shown that the [4+2] cycloaddition (Diels-Alder) reaction also occurs in a facile way for a range of conjugated dienes at the (100)-(2×1) surface of Si and Ge. In contrast to the [2+2] cycloaddition reactions, the Diels-Alder reactions are symmetry-allowed in organic chemistry.[109] Additionally, the [4+2] product is expected to be thermodynamically more stable because it forms a six-member

ring at the interface, while the [2+2] reaction is predicted to form a more highly strained four-member ring.[23]

1.2.2.3 Thiophene Adsorbed on Si(100)-(2×1) and Si(111)-(7×7)

In the first adsorption study of thiophene on Si(100)-(2×1) performed at 300 K by Jeong *et al.*[113] using LEED, AES, UPS, and semiempirical calculations, it was found that the thiophene molecules are molecularly adsorbed on the Si(100) surface and that the overall structure of the reconstructed (2×1) surface is sustained after chemisorption. From their AES data, the saturation coverage with respect to the atomic density of surface silicon was estimated to be ~ 0.6 ML. Their theoretical calculations using cluster models indicated that two adjacent C atoms of thiophene are di-σ bonded to one silicon dimer with the sulfur atom interacting with the neighbouring silicon dimer.

Recently, the surface reactions of thiophene on Si(100)-(2×1) was also investigated by Qiao and co-workers using a combination of XPS, UPS, and HREELS.[114] The authors identified two adsorption states at 120 K, which corresponded to physisorbed and chemisorbed thiophene, with the former desorbing below 200 K. The authors reported that the chemisorbed state was strongly bonded to the surface and their HREELS data revealed that chemisorbed thiophene is a 2,5-dihydrothiophene-like species. The author suggested that the formation of this surface moiety was the result of a Diels-Alder cycloaddition reaction with the dimers of the Si(100)-(2×1) surface. With increasing thiophene exposure, the authors observed a reorientation from nearly parallel to tilted relative to the surface plane. Using XPS, HREELS and UPS, the authors were able to follow the thermal evolution of the molecule and it was found that above 400 K, the chemisorbed species either desorbs as molecular thiophene or decomposes possibly via α-thiophenyl and Si-H, and metallocycle-like intermediate and atomic S. By 1000 K, only silicon carbide was left on the substrate.

On Si(111)-(7×7), a combined thermal desorption and photoemission study by MacPherson *et al.*[115] showed that adsorption of thiophene at room temperature leads to two molecular desorption states which were supposed to involve no C-H bond breakage

but rather a σ bond through the lone-pair electrons of sulfur and a π-bonded state (similar to thiophene on Cu(111) at low coverage). However, a recent HREELS and STM investigation by Cao *et al.*[116] demonstrated that thiophene undergoes a [4+2] cycloaddition (Diels-Alder) reaction toward the adjacent rest atom-adatom pairs on Si(111)-(7×7).

1.2.2.4 Benzene Adsorbed on Si(100)-(2×1), Si(111)-(7×7) and Ge(100)-(2×1) Surfaces

The adsorption of benzene on the Si(100) surface has been extensively studied.[117-128] and despite many experimental and theoretical investigations, the adsorption mechanism is not yet well understood and results in a number of different predictions. Amongst the structures proposed in the literature is the 1,4-cyclohexadiene-like "butterfly" configuration, in which the benzene molecule is di-σ-bonded to the two dangling bonds of the same Si surface dimer. This model is supported by TPD and ARUPS,[121] STM,[123] vibrational IR spectroscopy, and NEXAFS,[125] and first-principles cluster calculations.[121] Other STM experiments[122] suggest the 1,3-cyclohexadiene-like "tilted" structure. Finally, semi-empirical calculations,[119,124] STM, and IR spectroscopy experiments[124] favour a tetra-σ-bonded configuration where benzene is bonded to two adjacent surface dimers. Another open issue concerns the occurrence and nature of metastable adsorption states. Indeed, the results of STM and IR spectroscopy[122,124] support the hypothesis that benzene is initially chemisorbed in a metastable, "butterfly"-like state, and then slowly converts (within minutes) to a lower-energy final state, which is a "tilted" structure according to Ref. [122], or a tetra-σ-bonded one according to Ref. [124]. Further IR experiments[125] suggest that, at room temperature, benzene is predominantly adsorbed in the butterfly configuration, while the existence of a less stable structure, consistent with a tetra-σ-bonded configuration, is proposed.

The molecular adsorption of benzene on the Si(111)-(7×7) surface at room temperature was studied by TPD,[129] HREELS,[130,132] valence band photoemission[131] and semi-empirical (PM3) and density functional theory (DFT) method with cluster models.[133] The early understanding of the π-type of interaction, based on the TDS

results by MacPherson *et al.*[129] and HREELS studies of Taguchi and co-workers,[130] was challenged by the recent synchrotron photoemission study, where Carbone *et al.* suggested the formation of a 1,4-cyclohexadiene-like species upon molecular adsorption of benzene on Si(111)-(7×7).[131] This system was also re-investigated by Xu *et al.* using HREELS at a higher instrumental resolution,[132] and their results clearly unveiled the presence of rehybridisation of carbon atoms within chemisorbed benzene, which strongly suggests the σ-attachment of benzene to the Si(111)-(7×7) surface. A 1,4-cyclohexadiene-like adsorption configuration with benzene di-σ bonded to a pair of neighbouring adatom and rest atom was proposed.[132] This configuration was also confirmed by both semi-empirical and DFT theoretical calculations recently performed.[133]

The electronic structure of benzene adsorbed on a single-domain Ge(100)-(2×1) was investigated by Fink *et al.* at cryogenic temperature using ARUPS and TPD.[134] The detailed analysis of their ARUPS spectra indicated that benzene chemisorbs with C_{2v} symmetry and a 1,4-cyclohexadiene-like electronic structure. The molecule was flat-lying and di-σ-bonded to a Ge=Ge dimer via two carbon atoms in opposite ring (1,4) positions. From their TPD data, it was found that the adsorption of benzene on the germanium surface is reversible, and benzene desorption on Ge(100) led to two peaks centred at approximately 230 and 250 K. The authors assigned these two features to desorption of chemisorbed benzene from terrace and step sites.

1.2.2.5 Benzonitrile Adsorbed on Si(100)-(2×1) and Si(111)-(7×7)

The covalent attachment and binding configuration of benzonitrile on Si(100)-(2×1) were studied by Tao *et al.* using a combination of TPD, HREELS, XPS, UPS and DFT calculations.[135] The authors were able to identified both physisorbed and chemisorbed benzonitrile at an adsorption temperature of 110 K, with the physisorbed molecules desorbing at ~ 180 K and chemisorbed benzonitrile desorbing molecularly at ~ 490 K. Further, their HREELS data demonstrated that chemisorbed benzonitrile directly interacts with Si=Si dimers of the Si(100)-(2×1) surface, evidenced by the disappearance of the C≡N stretching mode coupled with the appearance of the C=N stretching mode and the retention of all vibrational signatures of a phenyl ring in their

vibration spectra. The detailed analysis of their XPS and UPS data confirmed the direct involvement of the C≡N group of chemisorbed benzonitrile in the surface binding, leaving a nearly unperturbed phenyl ring protruding into vacuum.

The cycloaddition of benzonitrile with Si(111)-(7×7) was also investigated by the same group using HREELS, XPS, UPS, STM and DFT calculation.[135] Their vibrational data revealed that the interaction between chemisorbed benzonitrile and the surface occurs through the interaction of the cyano group of the molecule with adjacent adatom-rest atom pair of Si(111)-(7×7), evidenced by the disappearance of C≡N stretching mode, appearance of C=N stretching mode, and retention of all vibrational signatures of phenyl ring. Confirmation of the covalent attachment of benzonitrile on Si(111) was provided by UPS, where the authors found that when compared with physisorbed molecules, the photoemission from π_{CN} orbitals of chemisorbed benzonitrile was significantly reduced, suggesting the direct involvement of π_{CN} in the surface binding. As for benzonitrile adsorbed on Si(100), Tao *et al.* were able to show that the covalent attachment of benzonitrile on Si(111)-(7×7) occurs in a highly selective manner.

1.3 References

1. C.M. Mates, G.A. Somorjai, Surf. Sci., 160 (1985) 542
2. C.M. Mates, C.T. Kao, G.A. Somorjai, Surf. Sci., 206 (1988) 145
3. P. Milligan, J. McNamarra, B. Murphy, B.C.C. Cowie, D. Lennon, M. Kadodwala, Surf. Sci., 412/413 (1998) 166
4. P.K. Milligan, B. Murphy, D. Lennon, B.C.C. Cowie, M. Kadodwala, J. Phys. Chem. B, 105 (2001) 140
5. G.J. Hutchings, F. King, I.P. Okoye, M.B. Padley, C.H. Rochester, J. Catal. 148 (1994) 464
6. J.E. Bailie, G.J. Hutchings, Chem. Commun., (1999) 2151
7. J.E. Bailie, H.A. Abdullah, J.A. Anderson, C.H. Rochester, N.V. Richardson, N. Hodge, J.-G. Zhang, A. Burrows, C.J. Kiely, G.J. Hutchings, Phys. Chem. Chem. Phys., 3 (2001) 4113
8. J.E. Bailie, G.J. Hutchings, J. Mol. Catal. A: Chem., 177 (2002) 209
9. R.J. Hamers, S.K. Coulter, M.D. Ellison, J.S. Hovis, D.F. Padowitz, M.P. Schwartz, C.M. Greenlief, J.N. Russell, Acc. Chem. Res., 33 (2000) 617
10. R.J. Hamers, Y. Wand, Chem. Rev., 96 (1996) 1261
11. A.V. Teplyakov, P. Lal, Y.A. Noah, S.F. Bent, J. Am. Chem. Soc., 120 (1998) 7377
12. S.W. Lee, L.N. Nelen, H. Ihm, T. Scoggins, C. Greenlief, Surf. Sci., 410 (1998) L773
13. S.W. Lee, J.S. Hovis, S.K. Coulter, R.J. Hamers, C.M. Greenlief, Surf. Sci., 462 (2000) 6
14. P. Lal, A.V. Teplyakov, Y.A. Noah, M.J. Kong, G.T. Wang, S.F. Bent, J. Chem. Phys., 110 (1999) 10545
15. S.D. Kevan, Phys. Rev. B, 32 (1985) 2344
16. J.A. Kubby, J.E. Griffith, R.S. Becker, J.S. Vickers, Phys. Rev. B, 36 (1987) 6079
17. E. Landemark, C.J. Karlsson, L.S.O. Johannsson, R.I.G. Uhrberg Phys. Rev. B, 49 (1994) 16523
18. D.J. Chadi, Phys. Rev. Lett., 43 (1979) 43
19. R.I.G. Uhrberg, G.V. Hannson, J.M. Nicholls, S.A. Flodstrom, Phys. Rev. B, 24 (1981) 4684.
20. R.J. Hamers, R.M. Tromp, J.E. Demuth, Surf. Sci., 181 (1987) 346

21. K. Tayayanagi, Y. Tanishiro, M. Takahashi, S. Takahashi, J. Vac. Sci. Technol. A, 3 (1985) 1502
22. K.B. Brommer, N. Needels, B.E. Larson, J.D. Joannopoulos, Phys. Rev. Lett., 68 (1992) 1355
23. S.F. Bent, J. Phys. Chem. B, 106 (2002) 2830
24. P. Hollins, J. Pritchard, Surf. Sci., 89 (1979) 486
25. P. Hollins, J. Pritchard, Surf. Sci., 99 (1980) L389
26. R. Raval, S.F. Parker, M.E Pemble, P. Hollins, J. Pritchard, M.A. Chesters, Surf. Sci., 203 (1988) 353
27. W. Kirstein, B. Krüger,F. Thieme, Surf. Sci., 176 (1986) 505
28. E.J. Moler, S.A. Kellar, W.R.A. Huff, Z. Hussain, Y. Chen, D.A. Shirley, Phys. Rev. B, 54 (1996) 10862
29. C.J. Hirschmugl, G.P. Williams, F.M. Hoffmann, Y.J. Chabal, J. Electron. Spectrosc. Rel. Phenom., 54/55 (1990) 109
30. G. Blyholder, J. Phys. Chem., 68 (1964) 2772
31. G. Attard, C. Barnes, *Surfaces*, Oxford Chemistry Premiers, Oxford University Press, Oxford, 1998
32. J.L. Domange, J. Oudar, Surf. Sci., 11 (1968) 124
33. C.T. Campbell, B.E. Koel, Surf. Sci., 183 (1987) 100
34. D. P. Woodruff, J. Phys. Condens. Matter, 6 (1994) 6067
35. L. Ruan, I. Stensgaard, F. Besenbacher, E. Laegsgaard, Ultramicroscopy, 42/44 (1992) 498
36. M. Foss, R. Feidenhans'l, M. Nielsen, E. Findeisen, T. Buslaps, R.L. Johnson, F. Besenbacher, Surf. Sci., 388 (1997) 5
37. N.P. Prince, D.L. Seymour, M.J. Ashwin, C.F. McConville, D.P. Woodruff, R.G. Jones, Surf. Sci., 230 (1990) 13
38. Y. Kitajima, Y. Takata, H. Sato, T. Yokoyama, T. Ohta, H. Kuroda, Jpn. J. Appl. Phys., 32 (1993) 377
39. G.J. Jackson, S.M. Driver, D.P. Woodruff, B.C.C. Cowie, R.G. Jones, Surf. Sci., 453 (2000) 183
40. E. Wahlström, I. Ekvall, T. Kihlgren, H. Olin, S.-A. Lindgren, L. Wallden, Phys. Rev. B, 64 (2001) 155406
41. E. Wahlström, I. Ekvall, H. Olin, S.-A. Lindgren, L. Wallden Phys. Rev. B, 60 (1999) 10699

42. S.M. Driver, D.P. Woodruff, Surf. Sci., 479 (2001) 1
43. N.V Richardson, J.C.Campuzano, Vacuum, 31 (1981) 449
44. A. Imanishi, T. Yokoyama, Y. Kitajima, T. Ohta, Bull. Chem. Soc. Jap., 71 (1998) 831
45. M. Xi, M. Yang, S.K. Jo, B.E. Bent, J. Chem. Phys., 101 (1994) 9122
46. D. Velic, A. Hotzel, M. Wolf, G. Ertl, J. Chem. Phys., 109 (1998) 9155
47. S.J. Stranick, M.M. Kamna, P.S. Weiss, Surf. Sci., 338 (1995) 41
48. H. Koschel, G. Held, P. Trischberger, W. Widdra, H.P. Steinruck, Surf. Sci., 437 (1999) 125
49. M. Xi, B.E. Bent, J. Phys. Chem., 97 (1993) 4167
50. R. Raval, M.A. Chesters, Surf. Sci., 219 (1989) L505
51. R. Raval, S.F. Parker, M.A. Chesters, Surf. Sci., 289 (1993) 227
52. K.A. Fosser, R.G. Nuzzo, P.S. Bagus, C. Wöll, Angew. Chem. Int. Ed., 41 (2002) 1735
53. D. Syomin, B.E. Koel, Surf. Sci., 498 (2002) 61
54. W. Huber, H.-P. Steinrück, T. Pache, D. Menzel, Surf. Sci., 217 (1989) 103
55. W. Huber, P. Zebisch, T. Bonemann, H.-P. Steinrück, Surf. Sci., 258 (1991) 16
56. A. Wander, G. Held, R.Q. Hwang, G.S. Blackman, M.L. Xu, P. de Andres, M.A. Van Hove, G.A. Somorjai, Surf. Sci., 249 (1991) 21
57. H. Ohtami, M.A. Van Hove, G.A. Somorjai, J. Phys. Chem., 92 (1988) 3974
58. M. Neuber, F. Schneider, C. Zubragel, M. Neumann, J. Phys. Chem., 99 (1995) 9160
59. P.A. Heimann, P. Jakob, T. Pache, H.-P. Steinrück, D. Menzel, Surf. Sci., 210 (1989) 282
60. G.J. Speight, *The Technology of Petroleum*, Second Edition (Dekker, New York, 1991)
61. F. Zaera, E.B. Kollin, J.L. Gland, Surf. Sci., 184 (1987) 75
62. J.A. Rodriguez, Surf. Sci, 278 (1992) 326
63. J.A. Rodriguez, J. Dvorak, T. Jirsak, Surf. Sci. Lett., 457 (2000) L413
64. J.A. Rodriguez, Surf. Sci, 278 (1992) 326
65. J.T. Roberts, C.M. Friend, Surf. Sci., 186 (1987) 201
66. R.A. Cocco, B.J. Tatarchuk, Surf. Sci., 218 (1989) 127
67. R.A. Cocco, B.J. Tatarchuk, Surf. Sci., 218 (1989) 147
68. W.H. Heise, B.J. Tatarchuk, Surf. Sci., 207 (1989) 297

69. F. Zaera, E.B. Kollin, J.L. Gland, Langmuir, 3 (1987) 555
70. G.R. Schoofs, R.E. Preston, J.B. Benziger, Langmuir, 1 (1985) 313
71. D.R. Huntley, D.R. Mullins, M.P. Wingeier, J. Phys. Chem., 100 (1996) 19620
72. T.E. Caldwell, I.M. Abdelrehim, D.P. Land, Surf. Sci. Lett., 367 (1996) L26
73. T.M. Gentle, Energy Res. Abstr., 9 (1984) 28229
74. J. Stohr, J.L. Gland, E.B. Collin, R.J. Koestner, A.L. Johnson, E.L. Muetterties, F. Sette, Phys. Rev. Lett., 53 (1984) 2161
75. J.F. Lang, R.I. Masel, Surf. Sci., 183 (1987) 44
76. F.P. Netzer, E. Bertel, A. Goldman, Surf. Sci., 201 (1988) 257
77. R.E. Preston, J.B. Benziger, J. Phys. Chem., 89 (1985) 5010
78. D.G. Kelly, J.A. Odriozola, G.A. Somorjai, J. Phys. Chem., 91 (1987) 5695
79. R.E. Preston, J.B. Benziger, J. Phys. Chem., 89 (1985) 5010
80. M. Salmeron, G.A. Somorjai, A. Wold, R. Chianelli, K.S. Liang, Chem. Phys. Lett., 90 (1982) 105
81. D.G. Kelly, M. Salmeron, G.A. Somorjai, Surf. Sci., 175 (1986) 465
82. A.J. Gellman, M.H. Farias, M. Salmeron, G.A. Somorjai, Surf. Sci., 136 (1984) 217
83. D.W. Goodman, Appl. Surf. Sci., 19 (1984) 1
84. S.L. Petterson, K. Shultz, Langmuir, 12 (1996) 941
85. M. Salmeron, G.A. Somorjai, A. Wold, R. Chianelli, K.S. Liang, Chem. Phys. Lett., 90 (1982) 105
86. T.L. Tarbuck, K.R. McCrea, J.W. Logan, J.L. Heisler, M.E. Bussell, J. Phys. Chem. B, 102 (1998) 7845
87. J.A. Rodriguez, M. Kuhn, J. Hrbek, Chem. Phys. Lett., 251 (1996) 13
88. J.A. Rodriguez, S. Chaturvedi, T. Jirsak, Phys. Lett., 296 (1998) 421
89. P.J. Feibelman, D.R. Hamann, Surf. Sci., 149 (1985) 48
90. S. Wilke, M. Scheffler, Phys. Rev. Lett., 76 (1996) 3380
91. D.R. Mullin, P.F. Lyman, S.H. Overbury, Surf. Sci., 277 (1992) 64
92. J.A. Rodriguez, M. Kuhn, J. Hrbek, J. Phys. Chem., 100 (1996) 3799
93. E.L. Garfunkel, M.H. Farias, G.A. Somorjai, J. Am. Chem. Soc., 107 (1985) 349
94. J.A. Rodriguez, J. Hrbek, Acc. Chem. Res., 32 (1999) 719
95. J.R. Lomas, C.J. Baddeley, M.S. Tikhov, R.M. Lambert, Langmuir, 11 (1995) 3048
96. J.R. Lomas, G. Pacchioni, Surf. Sci., 365 (1996) 297

97. D.J. Chadi, Phys. Rev. Lett., 43 (1979) 43
98. R.I.G. Uhrberg, G.V. Hannson, J.M. Nicholls, S.A. Flodstrom, Phys. Rev. B, 24 (1981) 4684
99. R.J. Hamers, R.M. Tromp, J.E. Demuth, Surf. Sci., 181 (1987) 346
100. S.D. Kevan, Phys. Rev. B, 32 (1985) 2344
101. J.A. Kubby, J.E. Griffith, R.S. Becker, J.S. Vickers, Phys. Rev. B, 36 (1987) 6079
102. E. Landemark, C.J. Karlsson, L.S.O. Johannsson, R.I.G. Uhrberg, Phys. Rev. B, 49 (1994) 16523
103. A. Redondo, W.A. Goddard, J. Vac. Sci. Technol., 21 (1982) 344
104. X. Torrelles, H.A. van der Vegt, V.H. Etgens, P. Fajardo, S. Alvarez, S. Ferrer, Surf. Sci., 364 (1996) 242
105. P. Krüger, J. Pollmann, Phys. Rev. Lett., 74 (1995) 1155
106. R.E. Schlier, H.E. Farnsworth, J. Chem. Phys., 30 (1959) 917
107. K. Takayanagi, Y. Tanishiro, M. Takahashi, S. Takahashi, J. Vac. Sci. Technol. A, 3 (1985) 1502
108. K.B. Brommer, N. Needels, B.E. Larson, J.D. Joannopoulos, Phys. Rev. Lett., 68 (1992) 1355
109. J. McMurry, *Organic chemistry*, Pacific Grove, California: Brooks-Cole, 3rd ed., (1992)
110. C. Huang, W. Widdra, W.H. Weinberg, Surf. Sci. 315 (1994) L953
111. W. Widdra, C. Huang, S.I. Yi, W.H. Weinberg, J. Chem. Phys., 105 (1996) 5605
112. A. Fink, R. Huber, W. Widdra, J. Chem Phys, 115 (2001) 2768
113. H.D. Jeong, Y.S. Lee, S. Kim, J. Chem. Phys., 105 (1996) 5200
114. M.H. Qiao, Y. Cao, F. Tao, Q. Liu, J.F. Deng, G.Q. Xu, J. Phys. Chem. B, 104 (2000) 11211
115. C.D. MacPherson, K.T. Leung, Phys. Rev.B, 51 (1995) 17995
116. Y. Cao, K.S. Yong, Z.Q. Wang, W.S. Chin, Y.H. Lai, J.F. Deng, G.Q. Xu, J. Am. Chem. Soc., 122 (2000) 1812
117. Y. Taguchi, M. Fujisawa, T. Takaoka, T. Okada, M. Nishijima, J. Chem. Phys. 95 (1991) 6870
118. B.I. Craig, Surf. Sci. Lett., 280 (1993) L279
119. H.D. Jeong, S. Ryu, Y.S. Lee, S. Kim, Surf. Sci. Lett. 344 (1995) L1226
120. R. Konecny, D.J. Doren, Surf. Sci., 417 (1998) 169

121. S. Gokhale, P. Trischberger, D. Menzel, W. Widdra, H. Droge, H.-P. Steinruck, U. Birkenheuer, U. Gutdeutsch, N. Rosch, J. Chem. Phys. 108 (1998) 5554; U. Birkenheuer, U. Gutdeutsch, N. Rosch, Surf. Sci., 409 (1998) 213
122. B. Borovsky, M. Krueger, E. Ganz, Phys. Rev. B, 57 (1998) R4269
123. K.W. Self, R.I. Pelzel, J.H.G. Owen, C. Yan, W. Widdra, W.H. Weinberg, J. Vac. Sci. Technol. A, 16 (1998) 1031
124. G.P. Lopinski, D. J. Moffatt, and R. A. Wolkow, Chem. Phys. Lett., 282 (1998) 305; G.P. Lopinski, T.M. Fortier, D.J. Moffatt, R.A. Wolkow, J. Vac. Sci. Technol. A, 16 (1998) 1037; R.A. Wolkow, G.P. Lopinski, D.J. Moffatt, Surf. Sci. Lett., 416 (1998) L1107
125. M.J. Kong, A.V. Teplyakov, J.G. Lyubovitsky, S. F. Bent, Surf. Sci., 411 (1998) 286
126. P.L. Silvestrelli, F. Ancilotto, F. Toigo, Phys. Rev. B, 62 (2000) 1596
127. M. Staufer, U. Birkenheuer, T. Belling, F. Nortemann, N. Rosch, W. Widdra, K.L. Kostov, T. Moritz, D. Menzel, J. Chem. Phys., 112 (2000) 2498
128. P. Kruse, R.A. Wolkow, Appl. Phys. Lett, 81 (2002) 4422
129. C.D. MacPherson, D.Q. Hu, K.T. Leung, Solid State Commun., 80 (1991) 217
130. Y. Taguchi, M. Fujisawa, M. Nishijima, Chem. Phys. Lett., 178 (1991) 363
131. M. Carbone, M.N. Piancastelli, R. Zanoni, G. Comtet, G. Dujardin, L. Hellner, Surf. Sci., 407 (1998) 275
132. Y. Cao, X.M. Wei, W.S. Chin, Y.H. Lai, J.F. Deng, S.L. Bernasek, G.Q. Xu, J. Phys. Chem. B, 103 (1999) 5698
133. Z.H. Wang, Y. Cao, G.Q. Xu, Chem. Phys. Lett, 338 (2001) 7
134. A. Fink, D. Menzel, W. Widdra, J. Phys. Chem. B, 105 (2001) 3828
135. F. Tao, Z.H. Wang, G.Q. Xu, J. Phys. Chem. B, 106 (2002) 3557
136. F. Tao, Z.H. Wang, X.F. Chen, G.Q. Xu, Phys. Rev. B, 65 (2002) 115311

Chapter 2. Theory

2.1 Introduction

A review of the variety of experimental techniques that enabled us to study the adsorption of atoms and molecules on single crystal surfaces during the course of the current work is given in this section. These techniques are Temperature Programmed Desorption (TPD), Low Energy Electron Diffraction (LEED), Auger Electron Spectroscopy (AES), Ultraviolet Photoemission Spectroscopy (UPS), X-ray Photoelectron Spectroscopy (XPS), Normal Incidence X-ray Standing Wavefield (NIXSW) absorption and finally Near Edge X-ray Absorption Fine Structure (NEXAFS). More extensive reviews of the theoretical backgrounds of the above surface sensitive techniques can be found in Ref. [1-8,11,15,16]. Here we will concentrate on the aspects that will be of importance in Chapters 4 to 8 (Results Sections).

2.2 Temperature Programmed Desorption (TPD)

TPD is a surface science technique that enables one to study the desorption of adsorbed atoms and/or molecules from a single crystal surface and thus can provide information on the strength of the interactions between the surface and the adsorbed species. In a TPD experiment, a heating ramp is applied to an adsorbate covered surface and the rate of desorption is monitored by a Quadrupole Mass Spectrometer (QMS) placed directly in front of the sample. The temperature ramp is applied to the sample in such a way that the heating rate (β) is linear in time (t) and obeys the relationship:

$$T(t) = T_0 + \beta t \qquad (1)$$

where T_0 is the initial sample temperature. If the pumping speed of the chamber is very large compared to the rate of desorption, the pressure rise in the chamber caused by the desorption process is proportional to the desorption rate and peaks present in the corresponding pressure-temperature curve represent different adsorption states.

As the temperature rises and the thermal energy available becomes sufficient to break surface bonds, desorption is observed. For the simplest case of an adsorbate in which the activation energy for desorption is constant as a function of coverage, a single desorption peak is obtained. The temperature at which maximum desorption occurs on the pressure vs. temperature curve (T_{max}) corresponds to the maximum desorption rate. In the current work, the TPD technique was mainly employed to identify the different adsorption states.

The main information of interest that can be gained from a TPD experiment are the activation energy of desorption (E_d), the order of desorption (n = 0, 1, 2, etc.), and the rate constant for desorption (k_d). Desorption from a single crystal surface under UHV conditions obeys an Arrhenius dependency and the rate constant for desorption k_d can be represented by:

$$k_d = A \exp\left(\frac{-E_d}{RT}\right) \qquad (2)$$

where A is a pre-exponential factor ($\approx 10^{13}\ s^{-1}$), R is the gas constant ($\approx 8.314\ J.mol^{-1}.K^{-1}$) and T is the temperature (in K). Equation (2) implies that the rate of desorption should increase exponentially. The reason a maximum is observed in the pressure-temperature curve is because as k_d increases, the surface coverage decreases. Hence desorption can be described by the following equation:

$$-\frac{d\theta}{dt} = k_d \theta^n \tag{3}$$

where θ is the number of adsorbed molecules (surface coverage) and n is the order of the reaction. Re-arranging Equation (3) gives:

$$\frac{d\theta}{dt} = \frac{d\theta}{dT} \times \frac{dT}{dt} = \frac{d\theta}{dT}\beta \tag{4}$$

where $\beta = \frac{dT}{dt}$ which corresponds to the heating rate. By exchanging $\frac{d\theta}{dt}$ for $\frac{d\theta}{dT}\beta$ and substituting into Equation (2) gives:

$$-\frac{d\theta}{dT} = \theta^n \frac{A}{\beta} \exp\left(\frac{-E_d}{RT}\right) \tag{5}$$

At T_{max}, $-\frac{d^2\theta}{dT^2} = 0$, as the rate of desorption is at a maximum, differentiating Equation (5) with respect to T gives the general expression:

$$\frac{E_d}{RT_{max}^{\ 2}} = \frac{A}{\beta} n\theta^{n-1} \exp\left(\frac{-E_d}{RT_{max}}\right) \tag{6}$$

So for a 1st order desorption:

$$\frac{E_d}{RT_{max}^{\ 2}} = \frac{A}{\beta} \exp\left(\frac{-E_d}{RT_{max}}\right) \tag{7}$$

and 2nd order desorption:

$$\frac{E_d}{RT_{max}^{\ 2}} = 2\frac{A}{\beta}\theta \exp\left(\frac{-E_d}{RT_{max}}\right) \tag{8}$$

As is obvious from Equation (7) and (8), the second order desorption processes are coverage dependent due to the term θ in Equation (8). A "rule of thumb" in assigning the reaction kinetics of a TPD experiment from the spectra is that the 1st order desorption spectra are asymmetric about T_{max}. On the other hand the 2nd order desorption spectra are symmetric about T_{max}. Also, as the 1st order desorption processes are independent of coverage, if the maximum desorption temperature T_{max} for chemisorbed adsorbates shift with changing coverage then the process being studied follows the 2nd order kinetics.

Great care must be taken however in using these rules. Adsorbate-adsorbate lateral interactions can invalidate the simple determination of 1st or 2nd order kinetics. For instance, in some adsorption systems which ostensibly exhibit first order kinetics,

increasing coverage may lead to the desorption peak maximum to shift to lower temperature due to repulsive interactions which destabilise neighbouring atoms. Further, first order kinetic desorption processes with variable activation energies may also give symmetric desorption peaks. If E_d varies with coverage then T_{max} becomes coverage dependent. However a plot of $\ln(\theta \cdot T_{max})$ versus $\frac{1}{T_{max}}$ gives a straight line for 2nd order desorption with a fixed E_d.

2.3 Low Energy Electron Diffraction (LEED)

In a LEED experiment, incident electrons with kinetic energies ranging from 20 to 1000 eV are elastically backscattered from a surface without energy loss. Electrons in this energy range possess inelastic free paths of between 5 and 20 Å and are therefore ideal for probing the surface structure as they only travel a few atomic layers into the surface. These electrons have de Broglie wavelengths of the same order of magnitude as the interatomic spacing between atoms/molecules at single crystal surfaces and may give characteristic diffraction patterns if the adsorbates are arranged periodically on the surface. An estimation of the wavelength λ of these electrons can be made by modifying the de Broglie equation:

$$\lambda(\mathring{A}) = \left(\frac{150.6}{E(eV)}\right)^{\frac{1}{2}} \qquad (9)$$

Fig.1. *Schematic diagram of the diffraction of a beam of electrons from a hypothetical one dimensional array of point scatterers of equal spacings a. From "Surface", by Attard and Barnes, Oxford University Press, 1998.*[1]

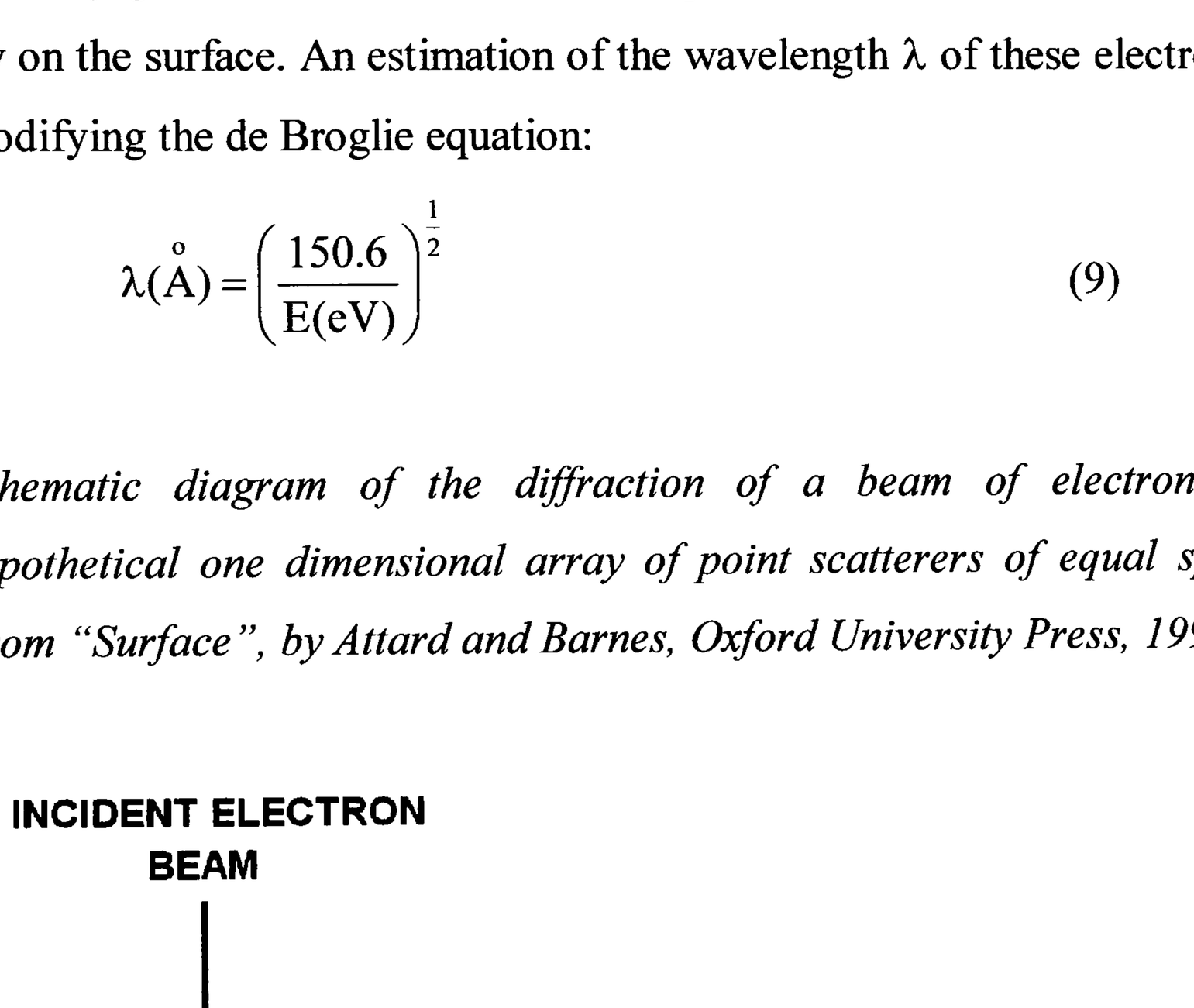

Fig. 1 illustrates electron scattering at an angle θ_a from atoms in a one-dimensional chain. Δ_a represents the path length difference. For constructive

interference between scattered electron waves, the path length difference must be equal to an integral number of wavelengths therefore we must have:

$$\Delta_a = n\lambda \tag{10}$$

where n can take values 0, 1, 2, 3, etc. The wavelength λ can also be expressed by recalling the de Broglie relationship:

$$\lambda = \frac{h}{mv} \tag{11}$$

where h is the Planck's constant, m is the mass of the electron and v its velocity. Simple geometry applied to Fig. 1 gives:

$$\Delta_a = a \sin\theta_a \tag{12}$$

and combining equations (10) and (12) yields:

$$n\lambda = a \sin\theta_a \tag{13}$$

or:

$$\sin\theta_a = \frac{n\lambda}{a} \tag{14}$$

Hence, for a fixed wavelength λ and lattice spacing a, only well-defined values of θ_a are allowed for which constructive interference will be observed. This means that discrete diffracted beams will be seen at particular angles.

An alternative way of representing the condition for diffraction is in terms of 'electron wavevectors' and the so-called 'reciprocal lattice vectors'. The magnitude of the incident wavevector of an electron k_0 is defined as:

$$|k_0| = \frac{2\pi}{\lambda} \tag{15}$$

where $|k_0|$ is a measure of the electron momentum. This can be demonstrated by combining equation (15) with the de Broglie relationship (equation (11)):

$$|k_0| = \frac{2\pi}{h} \cdot mv \tag{16}$$

where the term mv corresponds to the momentum of the electron. Substitution of equation (14) into equation (15) and eliminating "λ" then gives:

$$|k_0| \sin\theta_a = \left(\frac{2\pi}{a}\right) n \tag{17}$$

Fig. 2 shows that $|k_0| \sin\theta_a$ is in fact the component of momentum parallel to the surface of the incident electron ($k_{\|}$).

Fig.2. *Diagram showing the components of the wavevector k_0. From this diagram, we have* $|k_{\parallel}| = |k_0| \cdot \sin\theta_a$ *and* $|k_{\perp}| = |k_0| \cdot \cos\theta_a$

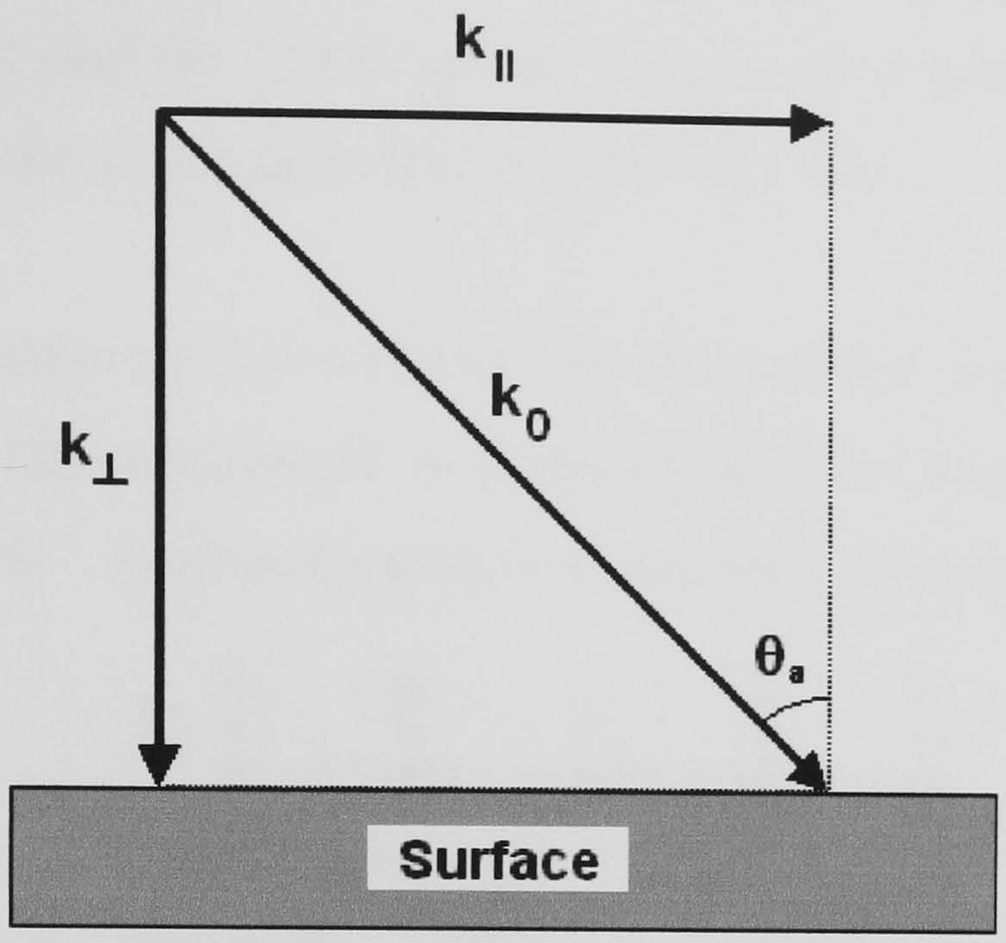

As n can only take values of 0, ± 1, ± 2, ± 3, etc., the component of the momentum parallel to the surface can only be exchanged with the surface in quantised units of $\frac{2\pi}{a}$ (equation (17)). Therefore $\left\{\frac{2\pi}{a}\right\}$ is the magnitude of a one-dimensional reciprocal lattice vector associated with the diffraction of the electron beam. Conservation of momentum in the scattering process means that in order for the electron to change direction, they must exchange momentum with the one-dimension lattice. Hence:

$$\Delta k_{\parallel} = |k_0| \sin\theta_a = \left(\frac{2\pi}{a}\right) n \qquad (18)$$

where $\Delta k_{\parallel}$ represents the change in parallel momentum in quantised units of $(2\pi/a)$.

If we now introduce periodicity in a second orthogonal array of scatterers in which the lattice spacing is b, the condition for constructive interference can be derived in an identical manner to equation (14):

$$\sin\theta_b = \frac{n\lambda}{b} \qquad (19)$$

and the conservation of momentum for this one-dimensional array is now:

$$\Delta k_{\parallel} = |k_0| \sin\theta_b = \left(\frac{2\pi}{b}\right) m \qquad (20)$$

where m is analogous to n and take values from 0, ± 1, ± 2, ± 3, etc.

For diffraction to occur from a two-dimensional array, both equations (18) and (20) must be satisfied simultaneously. In this case the two-dimensional diffraction is allowed only at the intersection of the one–dimensional reciprocal lattice generated in the a and b directions, and the LEED pattern consists of a series of diffraction spots corresponding to this points of intersection as depicted in Fig. 3.

Fig.3. *Diffraction pattern observed from two-dimensional array. Diffraction spots occur when* $\Delta k_{\|}$ *corresponds to a two-dimensional reciprocal lattice vector. From "Surface", by Attard and Barnes, Oxford University Press, 1998.*[1]

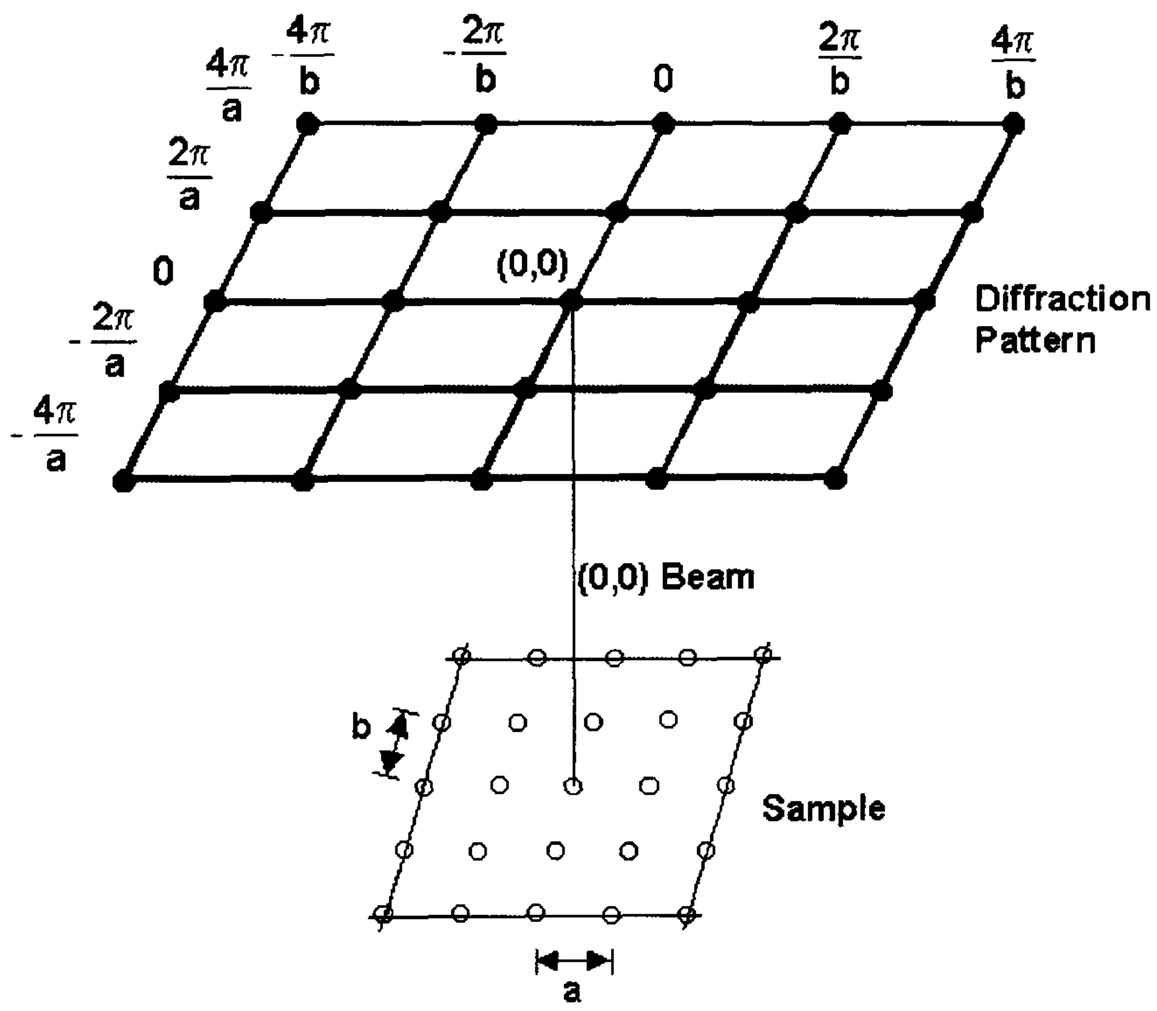

For diffraction to be observed from the two-dimensional array, the exchange of parallel momentum is restricted to a two-dimensional reciprocal lattice vector G such as:

$$G = \Delta k_{\|} = n\frac{2\pi}{a} + m\frac{2\pi}{b} \qquad (21)$$

The reciprocal lattice vector G can also be related to the corresponding real space lattice through the relationship:

$$G = na^* + mb^* \qquad (22)$$

with:
$$|a^*| = \frac{2\pi}{|a|} \qquad (23)$$

and
$$|b^*| = \frac{2\pi}{|b|} \qquad (24)$$

and
$$a \cdot b^* = a^* \cdot b = 0 \qquad (25)$$

where a and b are the elementary vectors of the real space lattice array and a* and b* are the elementary vectors of the reciprocal space lattice array. The condition for diffraction is then given by:

$$k_0^{\parallel} = k_S^{\parallel} + G \qquad (26)$$

where $k_S^{\parallel}$ is the parallel component of the scattered electron.

The number of diffracted beams emerging from the surface at a given primary beam energy E(eV) and the angle made by a diffracted beam with a particular real space direction can be provided by the Ewald sphere construction (Fig. 4). The Ewald sphere is a geometrical representation of equation (26) and consists of a circle (in two-dimensional space) of radius $|k_0|$. In Fig. 4(a) the number of reciprocal lattice points contained in the circle generated by $|k_0|$ gives the total number of diffracted beams emerging from the surface, and in Fig. 4(b) the angle θ made by a diffracted beam with a particular real space direction is given by the intersection between the circle and the reciprocal lattice rods.

Fig.4. *Ewald sphere construction. From "Surface", by Attard and Barnes, Oxford University Press, 1998.*[1]

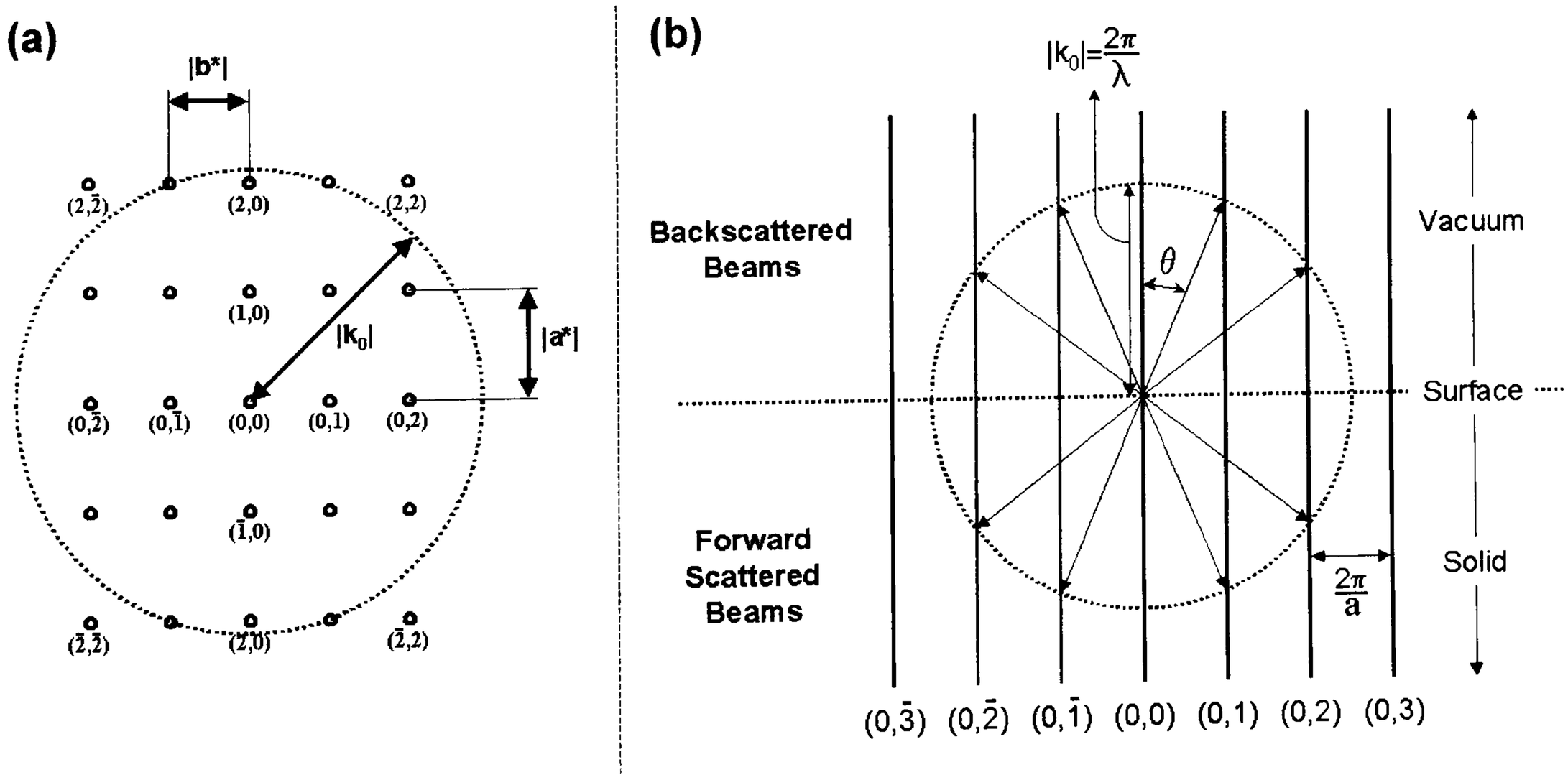

2.4 Auger Electron Spectroscopy (AES)

Auger electrons arise from an "auto-ionisation" process within an excited atom. A schematic representation of the Auger effect is depicted in Fig. 5. An incident photon (or electron) causes photoemission of a core electron (electron 1). The hole (or electron vacancy) created in the core level by photoemission can be neutralised by an electron transition from an electron level of lower binding energy ("down electron" – electron 2). The quantum of energy ΔE (equal to the difference in binding energy between the core hole and the down electron) now becomes available and may either be removed from the atom as a photon (X-ray fluorescence) or transferred to a third electron (Auger electron) which can escape into the vacuum with a kinetic energy E_{Kin}. The kinetic energy of the $KL_1L_{2,3}$ Auger electron as represented in Fig. 5 is:

$$E_{Kin} = E_K - E_{L_1} - E_{L_{2,3}} - \phi \qquad (27)$$

where ϕ is the work function of the surface under study. ϕ is defined as the minimum energy required to remove an electron from the highest occupied energy level in the solid to the vacuum level.

Fig.5. *Schematic representation of a $KL_1L_{2,3}$ Auger process. The energy levels in this diagram are not drawn to scale. From "Surface", by Attard and Barnes, Oxford University Press, 1998.*[1]

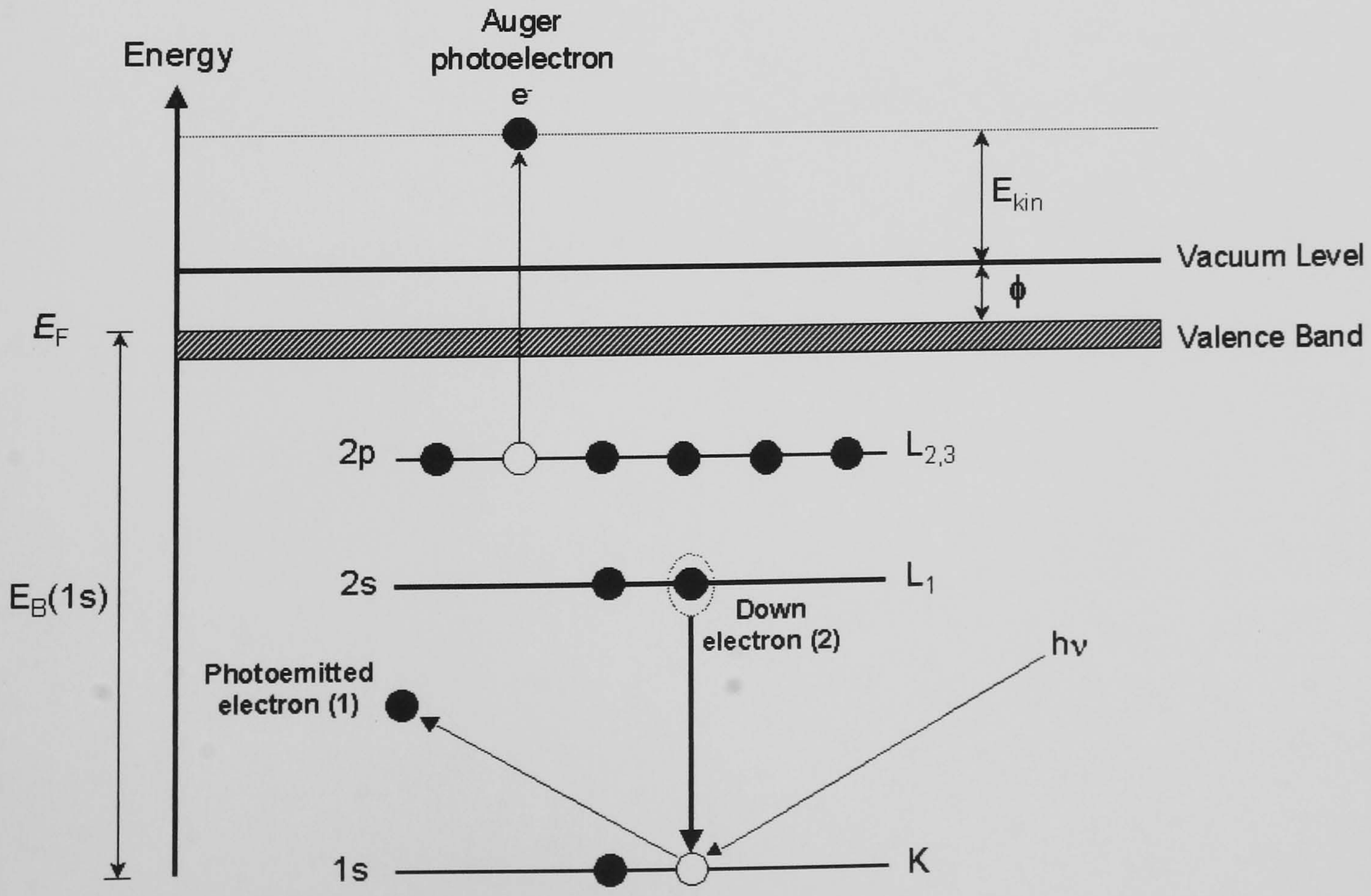

The kinetic energy of an Auger electron, in contrast to photoemission, is seen to be independent of the energy of incident photon or electron beam which gives rise to the initial core hole. The kinetic energy of the Auger electrons are characteristic solely of the binding energies of the electrons within the atom, therefore AES can be employed to identify all atomic species with three or more electrons (i.e. all elements other than H and He). For elements of high atomic numbers ($Z \geq 20$), the relative probabilities of Auger emission become small and the X-ray fluorescence processes dominate.

Finally, the AES technique can be used to quantify the amount of adsorbate on a surface, as the AES signal is proportional to the surface concentration. Provided that a point of reference is available, i.e. a peak associated with a known surface coverage, then AES may be used to yield absolute coverages of an element. However, this quantifying method is only valid for coverages of up to a saturated monolayer. For surface layers of thickness greater than one atomic layer, Auger electrons from the atoms in the first layer must pass through the second layer to reach the detector, and inelastic energy losses may occur en route to the detector, therefore leading to a smaller contribution from the first monolayer compared to the outermost layer and subsequently providing an inaccurate calculated coverages.

2.5 X-ray Photoemission Spectroscopy (XPS)

X-ray photoelectron spectroscopy is one of the most versatile techniques used for analysing surfaces chemically. Its basis lies in Einstein's explanation of the photoelectric effect. XPS is, in principle, a particularly simple process. Fig 6 illustrates schematically the energetics of a photoemission experiments. A photon of energy hν from an X-ray beam penetrates the surface, is then adsorbed by an electron with a binding energy E_B below the vacuum level (providing that hν is greater than the work function ϕ) which finally emerged from the solid with a kinetic energy E_{Kin}. The energy of the emitted photoelectron is therefore given by:

$$E_{Kin} = h\nu - E_B - \phi \qquad (28)$$

Fig.6. *Schematic diagram summarising the XPS process with X-ray excitation of a 1s core electron. The energy levels in this diagram are not drawn to scale. From "Surface", by Attard and Barnes, Oxford University Press, 1998.*[1]

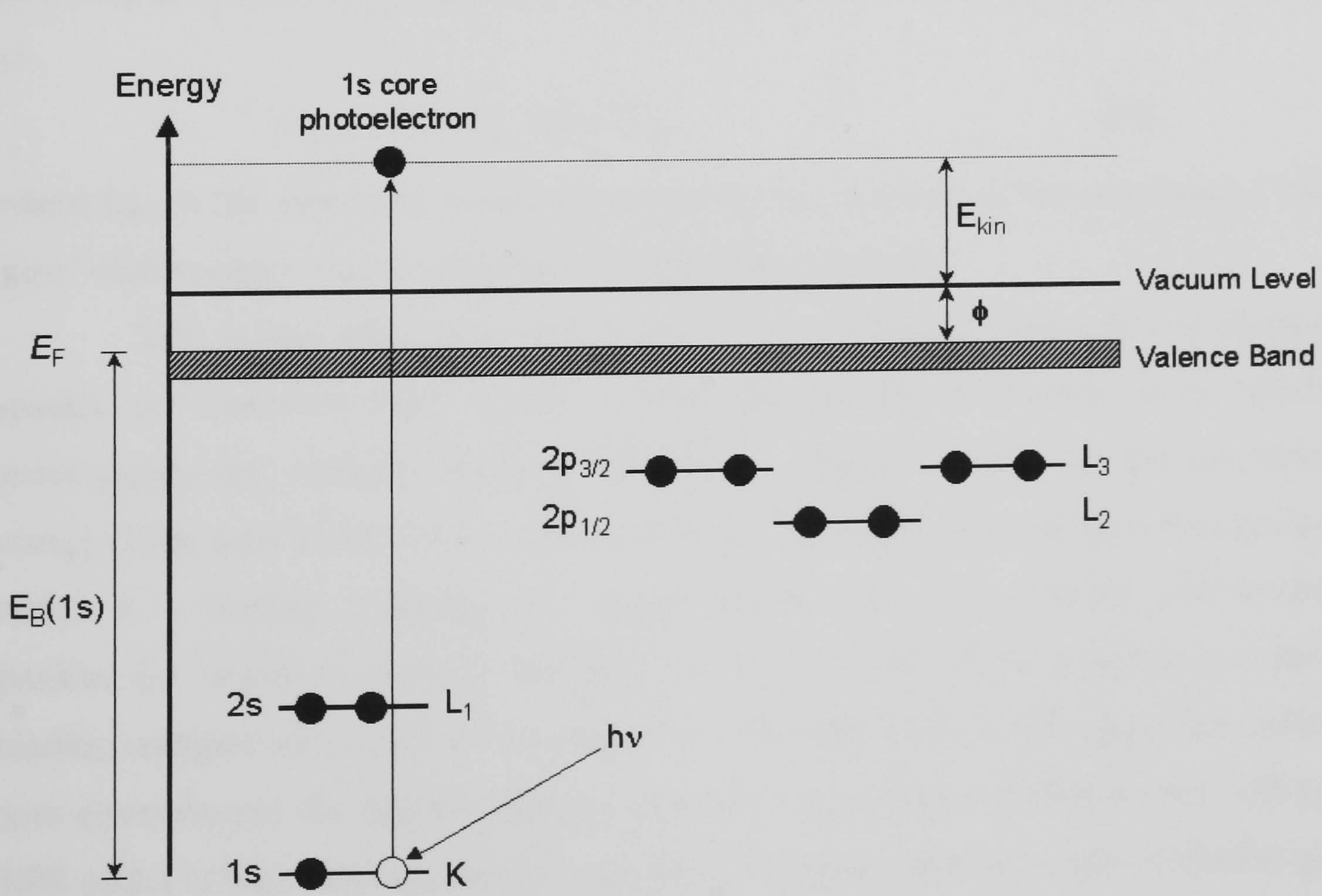

The XPS process produces photoemission from both core and valence levels of surface atoms into the vacuum, however emission from the valence band is most effectively probed by UPS (X-ray photons are unsuitable for valence level studies as their inherent energy spread of 1 eV leads to poor resolution of valence peaks and the probability of emitting valence electrons with X-rays is small). The key to chemical identification is that the core electrons deep inside atoms are largely insensitive to their surroundings when condensed into the solid phase and retain binding energies E_B that are signatures of the atom type.

Unlike the Auger electrons, the kinetic energy of an X-ray photoemitted electrons is dependent on the kinetic energy of the incident X-rays. It should also be noted here that Equation 28 is only valid if the electronic states of the system under study are the same after ionisation of the electron as they were before. This approximation is known as the Koopman's theorem. However, in reality, the electronic states after ionisation are different to those before the ionisation event, and the remaining electron relaxes to a different energy state after the ionisation event in order to screen the core hole that has been created (so-called "final-state shift"). This gives the emitted photoelectron slightly more energy and the Einstein Equation can now be stated as:

$$E_{Kin} = h\nu - E_B - \phi + E_{Rel} \qquad (29)$$

where E_{Rel} is the electronic energy generated by the creation of the core holes ("final-state" shift energy). E_{Rel} is generally no more than a few eV.

XPS is also often used as a probe of the chemical environment of elemental species or "oxidation state" of the surface species, and is referred to as "electron spectroscopy for chemical analysis" or ESCA. This is because the precise binding energy of the core levels of an atom or molecule is critically dependent on the species to which it is bonded. Consequently charge transfer may leave atoms with partially positive (or negative) charges, leading to a shift in core levels to higher (or lower) binding energies associated with increased (or decreased) Coulombic attraction between core electrons and the nucleus. Hence, atoms in a high formal oxidation state will yield XPS peaks at high binding energy relative to the same atom in a low oxidation state. The local environment surrounding the atom in question influences the magnitude of this so-called chemical shift.

2.6 Ultraviolet Photoemission Spectroscopy (UPS)

UPS is a particularly well suited technique for studying a wide range of properties controlled by the loosely bound valence electrons of surface atoms and molecules. UPS is related to XPS but, whereas XPS is employed to investigate the strongly bound core electrons, the UPS technique allows one to study the weakly bound valence levels and is particularly well suited for investigating the electronic structure of adsorbates on solid surface.

An illustration of the photoemission from the valence band of a solid and from an adsorbate with a single valence level using monochromatic UV photons of energy hν is given in Fig. 7. Superimposed on the emission from the substrate valence band are photoemitted electrons from the weakly bound valence level of the adsorbate. To a first approximation, the binding energy of this level can be measured by UPS using the Einstein equation in an analogous manner to XPS:

$$E_B = h\nu - E_{Kin} - \phi \qquad (30)$$

Fig.7. *Schematic diagram of the energetics of an ultraviolet photoemission experiment. From "Surface", by Attard and Barnes, Oxford University Press, 1998.*[1]

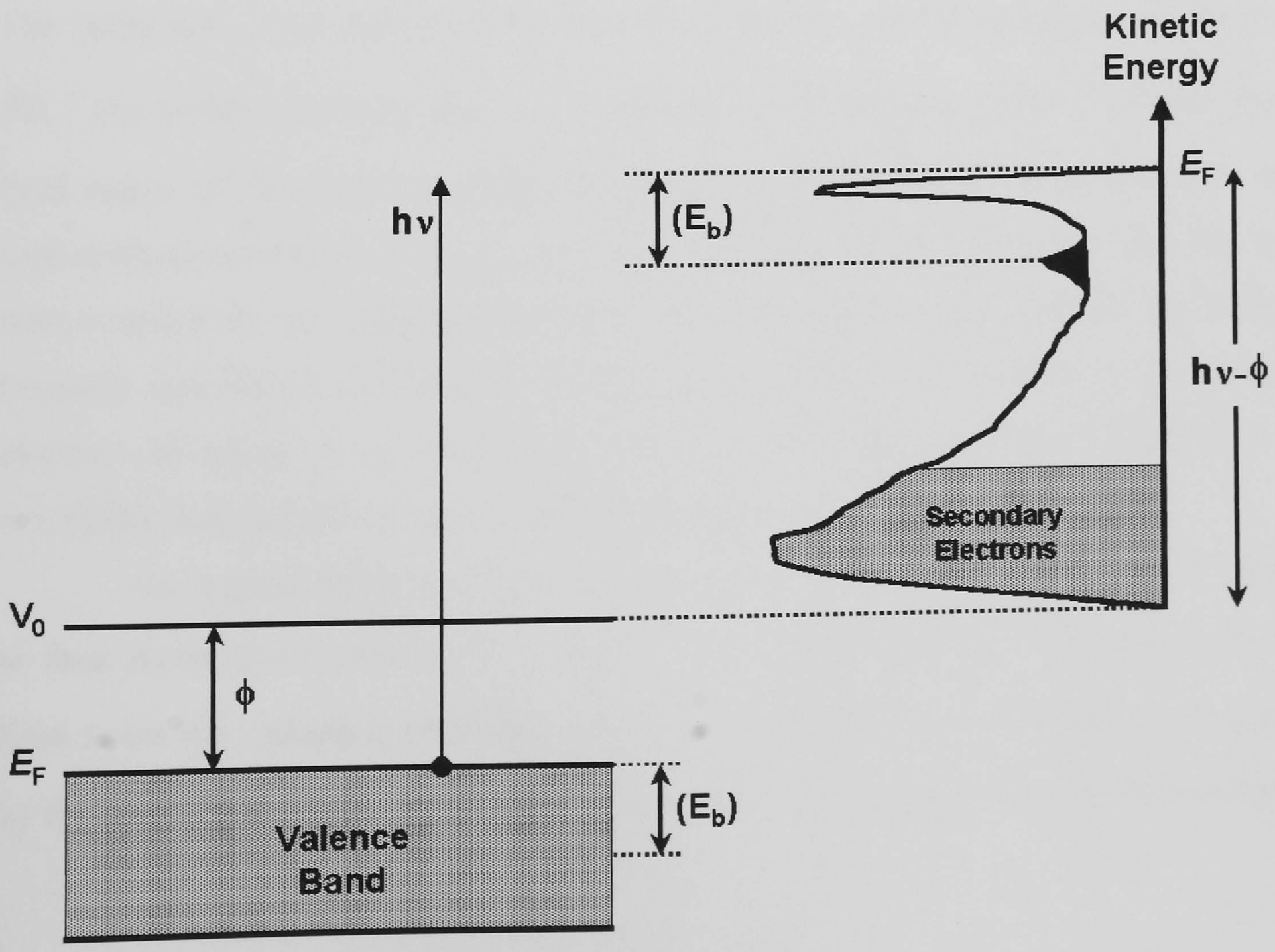

Information on the molecular states of an adsorbate can be gained in UPS by using a technique known as "fingerprinting". By comparing the energetic positions of the electronic levels of the molecule in the gas phase to the corresponding values for the adsorbed species, modifications induced by the physical and/or chemical bond formed between the adsorbate and the substrate can be deduced. As for the XPS technique, one need to be careful in rigidly assigning the relative shifts in UPS peaks from adsorbates purely to changes in bonding (so-called 'initial state effects'). Relaxation of the electronic energies of valence orbitals associated with the presence of a core hole state (created as a result of photoemission) also plays an important role (so-called 'final state effects'). Assuming that E_{Rel} is the relaxation in orbital energy associated with the creation of the core hole, the Einstein equation now becomes:

$$E_B = h\nu - E_{Kin} - \phi - E_{Rel} \qquad (31)$$

A further application of UPS is in the determination of molecular orientation and symmetry of the adsorbate on the single crystal surface.[2] By using the polarisation and angular dependence of the emission from valence levels, specific conclusions about the orientation of the adsorbed molecule can be drawn. This method is based on the use of the differential cross section formula given by Fermi's Golden Rule:

$$\frac{d\sigma}{d\Omega} \approx \left|\langle \Phi_f |\mu| \Phi_i \rangle\right|^2 \delta(E_f - E_i - \hbar\omega) \qquad (32)$$

The initial state $|\Phi_i\rangle$ represents the bound electron in a particular orbital, the final state $\langle\Phi_f|$ the emitted electron, and $\mu = E \bullet p$ the dipole operator (where E is the electric field vector of the incoming photon beam). Knowing that an adsorbed molecule has a well-defined orientation with respect to the substrate, it can be shown that the initial state is given by the particular orbital of the oriented molecule and the final state is uniquely specified by the kinetic energy E_{Kin} and the momentum k of the outgoing electron. By using the so-called symmetry selection rules, detailed information on the orientation and symmetry of adsorbed molecules can be obtained.

For a given polarisation E, excitations from an initial state Φ_i are only allowed to final states Φ_f of particular symmetry. Using group theory, the symmetry of those final states (i.e. outgoing electrons) that fulfil the requirement $\langle \Phi_f |\mu| \Phi_i \rangle \neq 0$ is given by the direct product of the representations of the initial state and the dipole operator:

$$\Phi_i \otimes E = \Phi_f \qquad (33)$$

Using symmetry selection rules, one can therefore predict whether emission from a specific orbital Φ_i is allowed or forbidden for a particular detector position and a given polarisation. These rules are especially powerful if the detector is positioned in a high-symmetry direction, such as the surface normal or mirror planes of the system. The application of symmetry selection rules in many cases allows the assignment of peaks in the UPS spectra to orbitals or bands. Conversely, using a plausible peak assignment, symmetry selection rules allow one to obtain the orientation and symmetry of the adsorbate.

2.7 Normal Incidence X-ray Standing Wavefield (NIXSW) Absorption

The technique of normal incidence X-ray standing wavefield absorption is in theory a relatively simple method for determining the local registry of an atom adsorb on a single crystal surface. In a NIXSW experiment, X-ray radiation with the required energy to generate a Bragg reflection at normal incidence strikes the surface of a single crystal. A standing wavefield is generated within the crystal by the interference of the incident and backscattered waves. The nodal planes of the standing wavefield lie parallel to the Bragg scattering planes, and their separation is equal to that of the scattering planes. The XSW can penetrate up to one μm into the surface of the crystal and extends as a coherent XSW outside the crystal over a distance comparable to the distance of a typical bonded adsorbate. As the nodes of the XSW are related to the scatterer plane distance, the XSW can be viewed as creating hypothetical lattice planes above the surface from which the position of an adsorbate can be determined.

When the photon energy is scanned through a range of reflectivity associated with the standing wavefield, its phase changes in a way that can be modelled. By monitoring the absorption of the X-rays by the absorbed atom as this standing wavefield shifts, the resulting profile obtained can be used to determine its location relative to the bulk scattering planes. In practice this is achieved by monitoring the Auger electron emission, photoemission or X-ray fluorescence. However, in NIXSW experiments involving light elements such as oxygen, there is an intrinsic problem in obtaining X - ray absorption profiles with sufficient Signal to Noise Ratio (SNR) due to the small cross-section for 1s ionisation at the energy of the XSW (typically 2–5 keV). Therefore only the oxygen 1s photoemitted electrons were monitored in the current work because they provided X-ray absorption profiles with the best possible Signal to Noise Ratio (SNR). For the heavier sulfur atom, the $KL_{2,3}L_{2,3}$ Auger electrons were collected and provided adequate XSW profiles.

The basic equation governing an NIXSW experiment is that which defines the intensity I of the XSW at a particular point in space:[3-5]

$$I = \left| 1 + \left(\frac{E_H}{E_0} \right) \exp\left(- \frac{2\pi i z}{d_H} \right) \right|^2 \qquad (34)$$

where E_H and E_0 are the amplitudes of the reflected and incident X-rays respectively, z is the perpendicular distance of the adsorber atom from the surface and d_H is the

scattering plane distance. The amplitude of the scattered wave relative to the incident wave is the square root of the reflectivity R multiplied by a phase factor φ:

$$\frac{E_H}{E_0} = \sqrt{R}\exp(i\varphi) \tag{35}$$

which means that:

$$I = 1 + R + 2\sqrt{R}\cos\left(\varphi - \frac{2\pi z}{d_H}\right) \tag{36}$$

This analysis is strictly true for a single adsorbate position on a rigid lattice. In reality there may be a distribution of adsorption sites due to vibrational or static disorder. This can be represented by a distribution of z-values such that:

$$\int_0^{d_H} f(z)dz = 1 \tag{37}$$

In this case the adsorption profile is given by:

$$I = 1 + R + 2\sqrt{R}\int_0^{d_H} f(z)\cos\left(\varphi - \frac{2\pi z}{d_H}\right)dz \tag{38}$$

which can also be written as:

$$I = 1 + R + 2f_{co}\sqrt{R}\cos\left(\varphi - \frac{2\pi D(hkl)}{d_H}\right)dz \tag{39}$$

in terms of two parameters, the coherent fraction f_{co} and the coherent position D(hkl). The coherent fraction f_{co} relates to how well defined the atoms' positions are with respect to the reflecting plane. The f_{co} can take values between 0 and 1, a value of 1 represents a completely well defined position, and low values arise from dynamic (vibrational motion) or static (occupation of multiple sites) disorder. For an atom that occupies a single type of adsorption site, the D(hkl) value is a measure in Å of the perpendicular distance of the atoms from a reflecting plane. This scattering plane may or may not go through the surface and the coherent position extracted from the analysis of NIXSW profiles may be with respect to the hypothetical lattice planes that are formed in the formation of an XSW.

It is well known that the four principal adsorption sites on a (111) surface are Atop, Bridge, Face Centred Cubic (FCC) and Hexagonal Close Packed (HCP) (Fig. 8). In order to unambiguously assign the local registry of an element, NIXSW experiments are generally performed with respect to two different sets of reflecting planes (both (111) and ($\bar{1}$11) planes were used in the current work). This results in two sets of

coherent fractions and coherent positions for the same adsorbate. Using a process of real space triangulation of the coherent positions using the equations derived from Fig. 8, this gives:

$$\text{Atop:} \qquad D\left(\bar{1}11\right) = \frac{D(111)}{3} \tag{40}$$

$$\text{Bridge:} \qquad D\left(\bar{1}11\right) = \frac{D(111)}{3} + \frac{d(111)}{2} \tag{41}$$

$$\text{FCC:} \qquad D\left(\bar{1}11\right) = \frac{D(111) + 2d(111)}{3} \tag{42}$$

$$\text{HCP:} \qquad D\left(\bar{1}11\right) = \frac{D(111) + d(111)}{3} \tag{43}$$

and it is possible to assign the adsorption sites. In effect these equations allow the calculation of D($\bar{1}$11) for each of the four adsorption sites mentioned and it is then a case of matching the experimental D($\bar{1}$11) value from the ($\bar{1}$11) NIXSW experiment to assign the adsorption site.

Fig.8. *Diagram showing the principal adsorption sites on a (111) surface and the two different planes (111) and ($\bar{1}$11) that are used in NIXSW experiments. From Ref. (3).*

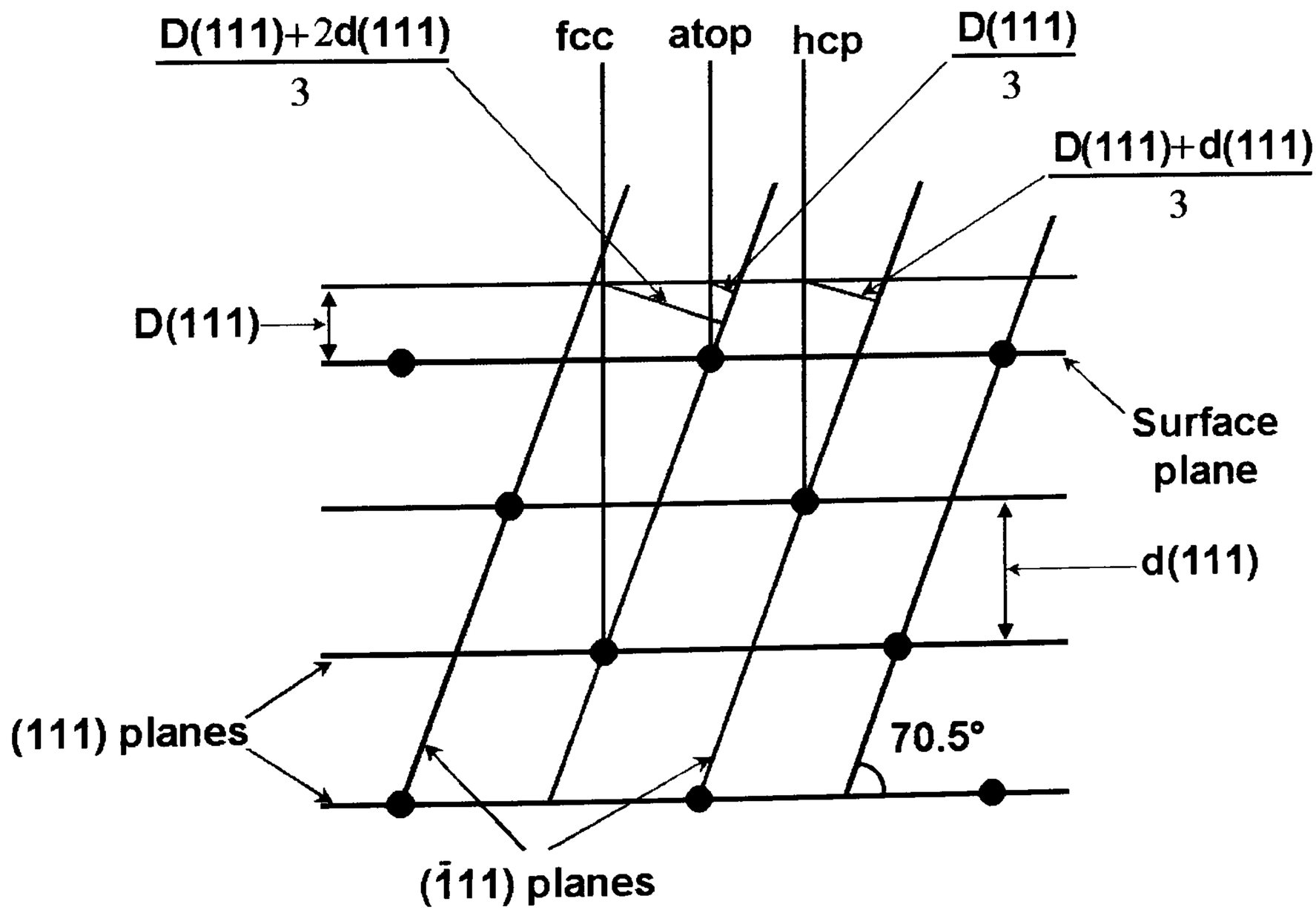

Furthermore, non-dipole effects in the angular distribution have been shown to have a substantial influence on the interpretation of NIXSW data obtained by monitoring core level photoemission. The origin of the strong effects observed in NIXSW experiments is due to the asymmetry of the photoelectron distribution about the photon propagation direction for non-dipole excitation. Naturally, in NIXSW experiments the photoelectrons are by necessity detected in a direction "backwards" to the direction of propagation of the incident X-rays, but conversely the detector is in the "forward" direction with respect to the reflected beam. Consequently, if there is a backward/forward asymmetry in the photoemission due to non-dipole excitation, the measurement detects the incident and reflected components of the standing wave with different efficiency, leading to a variance from a pure dipole absorption profile.

The net effect of these non-dipole effects is that the analysis of the photoemission XSW profiles leads to coherent fractions that are too high, sometimes superior to 1. Recent NIXSW studies have attempted to compensate this problem by introducing a dimensionless "Q-factor"[6] and a further Δ term[7] in order to correctly fit the NIXSW data. This expression is given in Equation 44. Further, it was recently found by Lee and co-workers[8] that the Δ term has a negligible effect on the values of D(hkl) and f_{co}, consequently this term was ignored in our treatment of results. From previous work performed by our group, it was determined that the Q value for oxygen is 0.25[9-11] and 0 for sulfur.[12-14]

$$\frac{\partial\sigma}{\partial\Omega} \propto R\frac{(1+Q)}{(1-Q)} + 2\sqrt{Rf_{co}}\frac{\left(1+Q^2\tan^2\Delta\right)}{(1-Q)} \times \cos\left(\Phi + \tan^{-1}(Q\tan\Delta) + 2\pi D/d_H\right) \qquad (44)$$

2.8 Near Edge X-ray Absorption Fine Structure (NEXAFS)

When an X-ray beam strikes an adsorbate–substrate complex, a proportion of the radiation is absorbed by the adsorbed molecule. If the X-ray has sufficient energy to excite the electrons within the adsorbate, the measurement of the amount of absorption with increasing X-ray photon energy reveals the so-called edge structure, where the level of absorption suddenly increases. Usually oscillations can be seen superimposed on the edge step. These oscillations, which occur within about 40 eV of the edge and gradually die away as the photon energy increases, are known as NEXAFS.

Close inspection of these oscillations in a NEXAFS spectrum can lead to the determination of the geometry of the molecule adsorbed on the surface. Indeed, information on the orientation of an adsorbate are normally inferred from the polarisation dependence of the $1s \rightarrow \pi^*$ and/or $1s \rightarrow \sigma^*$ transitions. The excitation of the 1s core level into the unoccupied π^* and σ^* orbitals or resonances is governed by dipole selection rules. Therefore the use of polarised synchrotron radiation light results in preferential excitations into the π^* or σ^* final states depending on the orientation of the molecule relative to the electric field vector E. Since the antibonding π^* and σ^* orbitals are localised with a definitive fixed orientation with respect to the molecular geometry it is possible to determine the orientation of the molecular axis or plane relative to the substrate. In other words, by using polarised X-rays, the presence or absence of π^* and σ^* orbitals in NEXAFS spectra can provide information on the geometry of the adsorbed species. Furthermore, the absorption of the X-ray radiation can be experimentally measured by monitoring the emission of Auger electrons that are created by the resonant excitations of the core levels as the photon energy is scanned through the edge.

In the case of thiophene, the π^* and σ^* molecular orbitals can be viewed as consisting of "vectors" and "planes", respectively (Fig. 9). The atoms in the aromatic ring of the thiophene molecule are σ-bonded to one another and can be described as a planar arrangement of σ^* orbitals in the plane of the ring. On the other hand, the π^* orbitals are perpendicular to the aromatic ring and can be viewed as a set of vectors. In simple terms, when the molecule is oriented in a flat orientation in the x-y plane, there is a maximum overlap between the π^* orbitals and the polarisation of the incoming X-ray beam when the beam is at grazing incidence. On the other hand, when the

incoming X-radiation is at normal incidence, there is a maximum overlap between the σ* orbitals and the electric field vector E of the beam in a flat orientation. Conversely, if the molecule is oriented in an upright orientation, there is maximum overlap between the σ* orbitals and the polarisation of the beam at grazing incidence and maximum overlap between the π* orbital and the polarisation of the beam at normal incidence.

Fig.9. *Diagram showing how the σ-bonds in thiophene can be represented by a circle and the π-bonds can be depicted by a vector perpendicular to the aromatic ring of the molecule.*

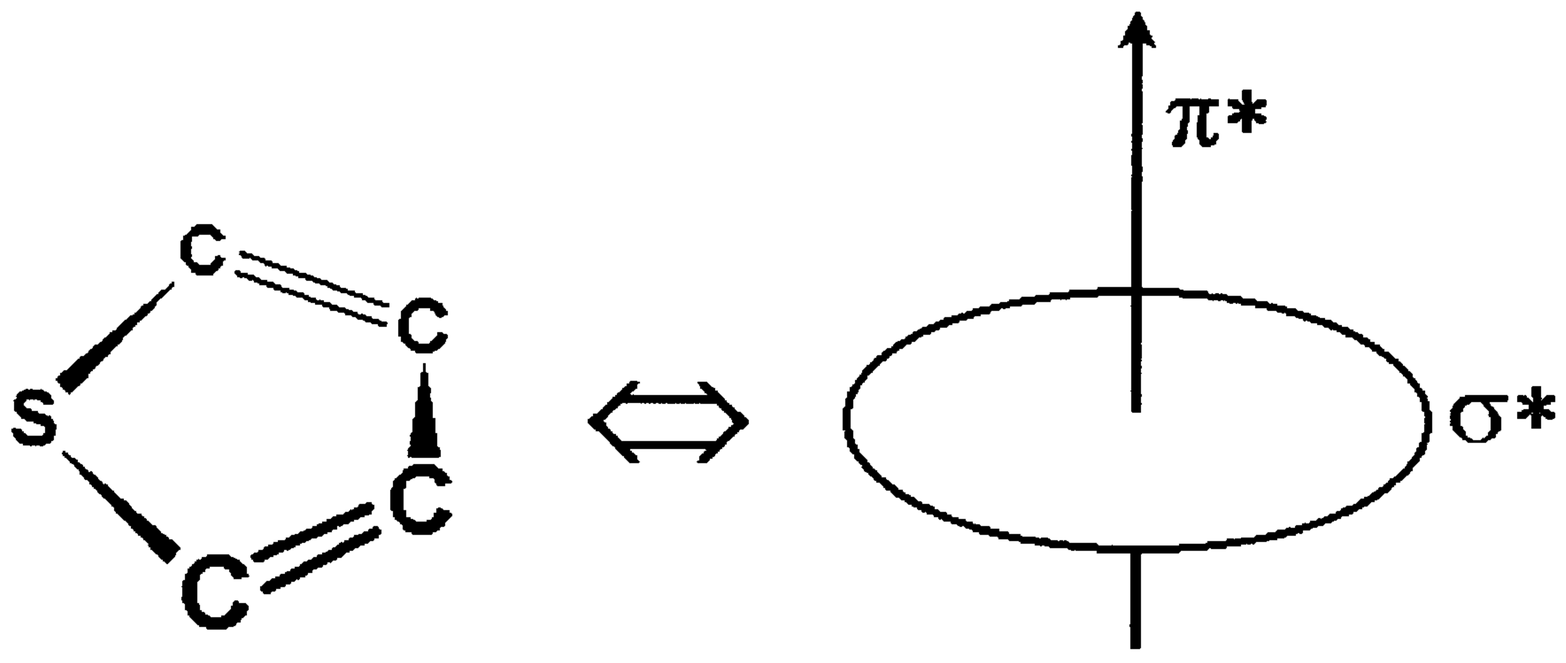

Fig. 10 depicts the basic selection rules that can be used in assigning the orientation of the thiophene molecule on the surface. However, the actual angle can be calculated by analysis of the relative areas under the peaks attributed to the π* and σ* resonances in NEXAFS spectra. By using the π* resonances, it can be shown[15] that the angle of orientation can be calculated from:

$$I(\theta) \propto \frac{1}{3}P\left[1+\frac{1}{2}(3\cos^2\theta-1)(3\cos^2\alpha-1)\right] \qquad (45)$$

and by using the σ* resonances, the angle of orientation can be calculated from:

$$I(\theta) = \frac{2}{3}\left[1-\frac{1}{4}(3\cos^2\theta-1)(3\cos^2\gamma-1)\right] \qquad (46)$$

where P is the degree of polarisation of the X-ray beam (0.85),[16] θ is the angle of X-ray incidence (19.5° for grazing incidence, 90° for normal), and α and γ represent the angle that the molecules makes with the surface.

Fig.10. *Hypothetical thiophene molecule adsorbed on the surface of a single crystal in a flat (a) and upright (b) orientations. This diagram also shows how the orbitals overlap with the polarisation vector (electric field vector* $\vec{E}$ *represented by the red arrow) of the incoming X-ray beam.*

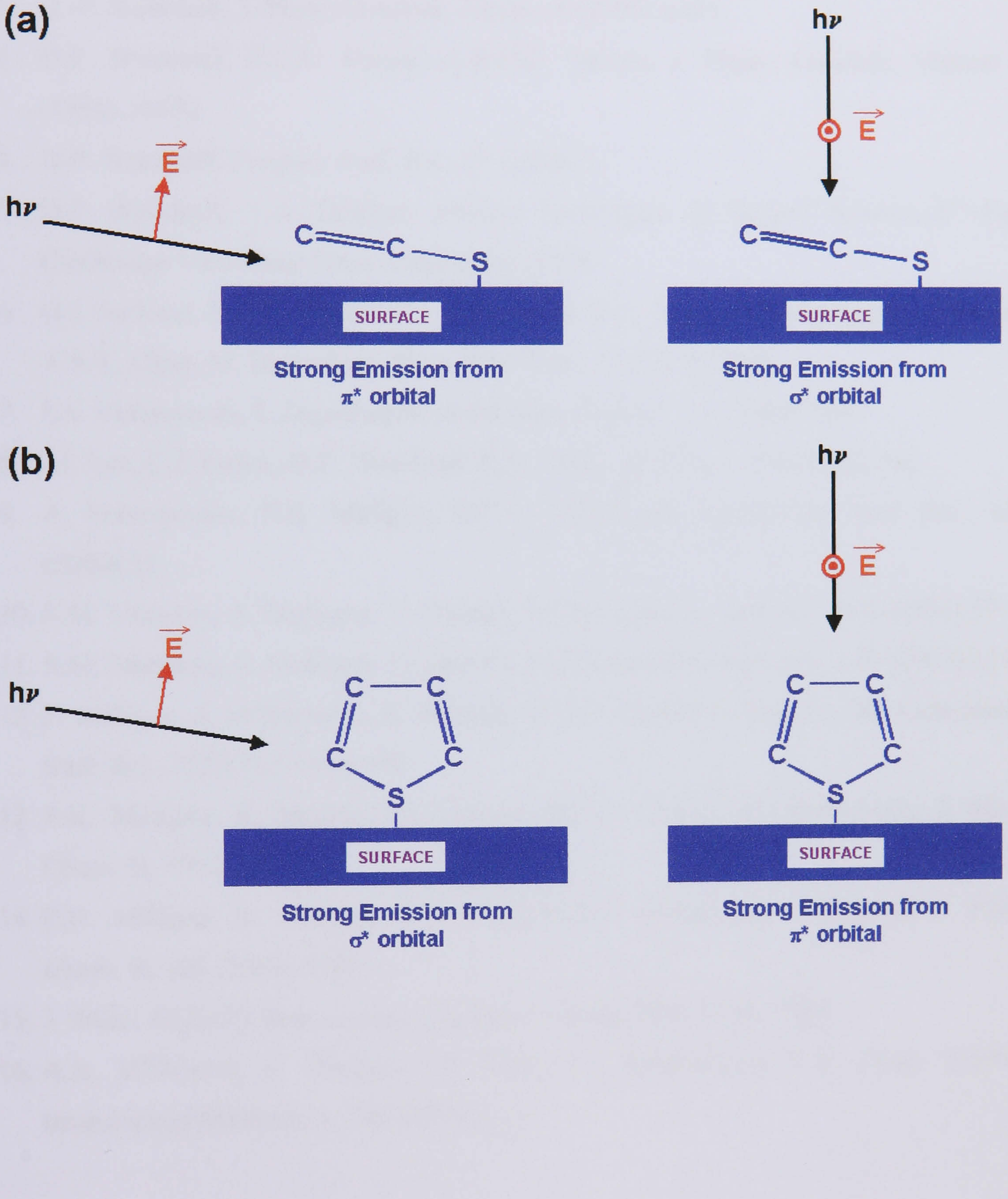

2.9 References

1. G. Attard, C. Barnes, *Surfaces*, Oxford Chemistry Premiers, Oxford University Press, Oxford, 1998
2. H.-P. Steinrück, J. Phys.: Condens. Matter, 8 (1996) 6465
3. D.P. Woodruff, B.C.C. Cowie, A.R.H.F. Ettema, J. Phys.: Condens. Matter, 6 (1994) 10633
4. D.P. Woodruff, Progres. Surf. Sci., 57 (1998) 1
5. D.P. Woodruff, T.A. Delchar, *Modern Techniques of Surface Science*, 2nd Ed., Cambridge University Press, Cambridge, 1994
6. G.J. Jackson, B.C.C. Cowie, D.P. Woodruff, R.G. Jones, M.S. Kariapper, C.Fisher, A.S.Y. Chan, M. Butterfield, Phys. Rev. Lett., 84 (2000) 2346
7. I.A. Vartanyants, J. Zegenhagen, Solid State Comm., 113 (2000) 299
8. J.J. Lee, C.J. Fisher, D.P. Woodruff, R.G. Jones, Surf. Sci., 494 (2001) 166
9. A. Sotiropoulos, P.K. Milligan, B.C.C. Cowie, M. Kadodwala, Surf. Sci., 444 (2000) 52
10. S.M. Johnston, A. Mulligan, V. Dhanak, M. Kadodwala, Surf. Sci., 519 (2002) 57
11. S.M. Johnston, A. Mulligan, V. Dhanak, M. Kadodwala, Surf. Sci., 530 (2003) 111
12. P. Milligan, J. McNamarra, B. Murphy, B.C.C. Cowie, D. Lennon, M. Kadodwala, Surf. Sci., 412/413 (1998) 166
13. P.K. Milligan, B. Murphy, D. Lennon, B.C.C. Cowie, M. Kadodwala, J. Phys. Chem. B, 105 (2001) 140
14. P.K. Milligan, B. Murphy, D. Lennon, B.C.C. Cowie, M. Kadodwala, J. Phys. Chem. B, 105 (2001) 5231
15. J. Stöhr, *NEXAFS Spectroscopy*, Springer-Verlag, New York, 1996
16. A.A. McDowell, D. Norman, J.B. West, J.C. Campuzano, R.G. Jones, Nuclear Instrumental Methods A, 246 (1986) 131

Chapter 3: Experimental

3.1 Introduction

Surface science studies are most commonly carried out at low pressure and this involves the use of high vacuum (HV) and ultra high vacuum (UHV) systems. The experiments described in the current work were performed using four different systems: two UHV chambers in the Surface Science Laboratory of the Department of Chemistry at the University of Glasgow, and two other UHV chambers at the Synchrotron Radiation Source (SRS) of the Daresbury Laboratory.

3.2 Experimental (Glasgow)

3.2.1 EELS Chamber

3.2.1.1 System Design

The EELS chamber is described in Fig. 1 and is so-called after being equipped with an Electron Energy Loss Spectrometer (not used in this project). This chamber enables TPD, AES and LEED experiments to be carried out and it is equipped with three different types of pumps (Fig. 2). In order to obtain UHV conditions, the pumping of the system was normally achieved in several stages. First, a pressure of 1×10^{-3} mbar could be acquired by using a rotary pump (Edwards Ltd). Once this pressure was achieved, a turbomolecular pump (V-250 – Varian Ltd) and an ion pump (Vac-Ion Plus 300 Triode – Varian Ltd) were switched on and a pressure as low as 10^{-8} mbar could be reached.

However UHV conditions could not be completed without baking the system in order to drive residual gases off the wall of the chamber and from the different components located inside the chamber. For this, two portable covers wide enough to encase the chamber and three ceramic heaters were employed to increase the temperature of the system to 150°C generally for a period of 16 hours. UHV pressure was finally attained after de-gassing the QMS (RC RGA – Hiden Analytical Ltd), ion gun (PSP Vacuum Technology Ltd), sample, ion gauge (VIG18 – Vacuum Generators

Ltd), LEED/Auger optics (RVL – VG Microtech Ltd) and ion pump which finally resulted in a pressure of 1×10^{-10} mbar.

Fig.1 *Schematic diagram of the EELS chamber.*

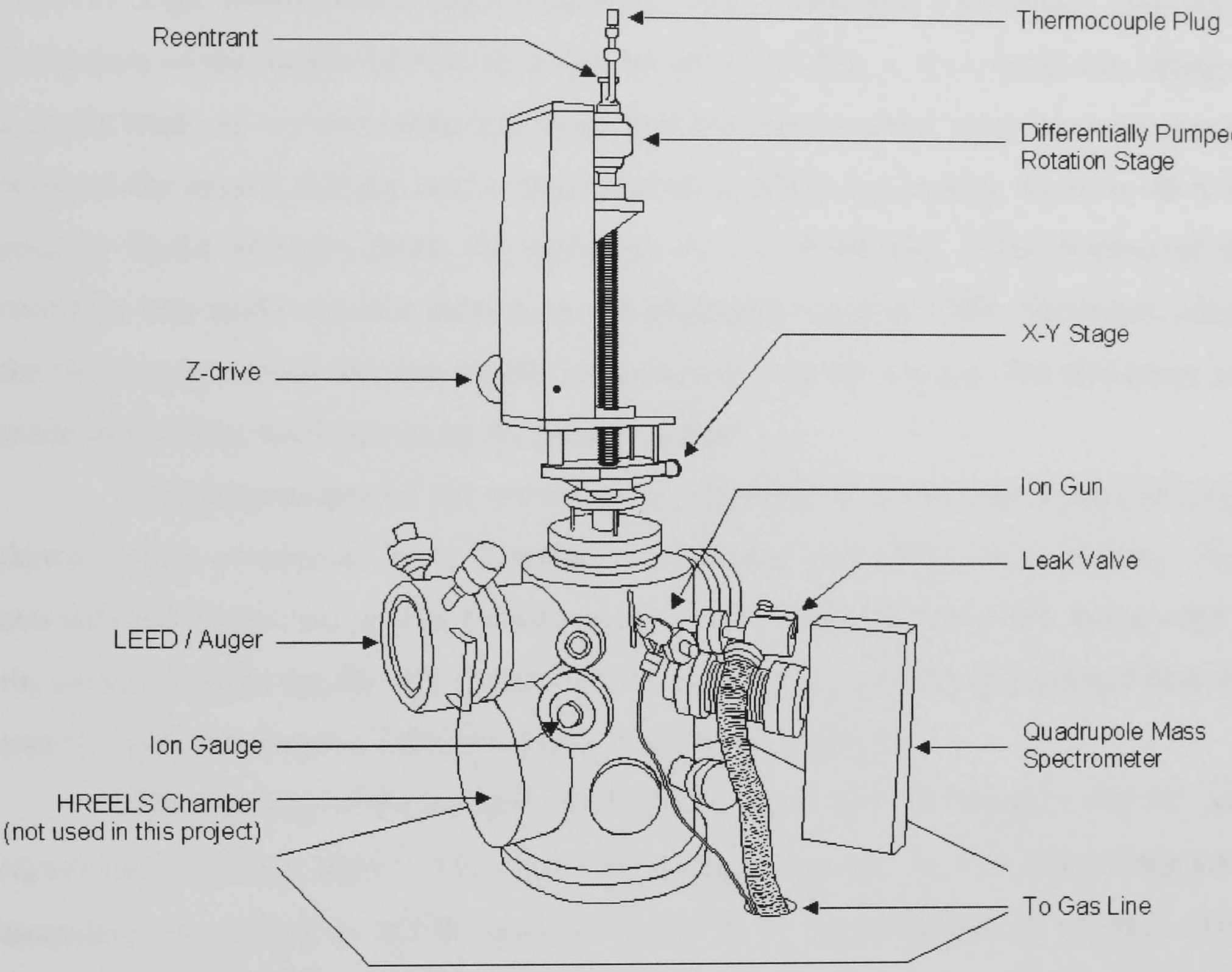

Fig.2 *Schematic diagram of the pumping design of the EELS system.*

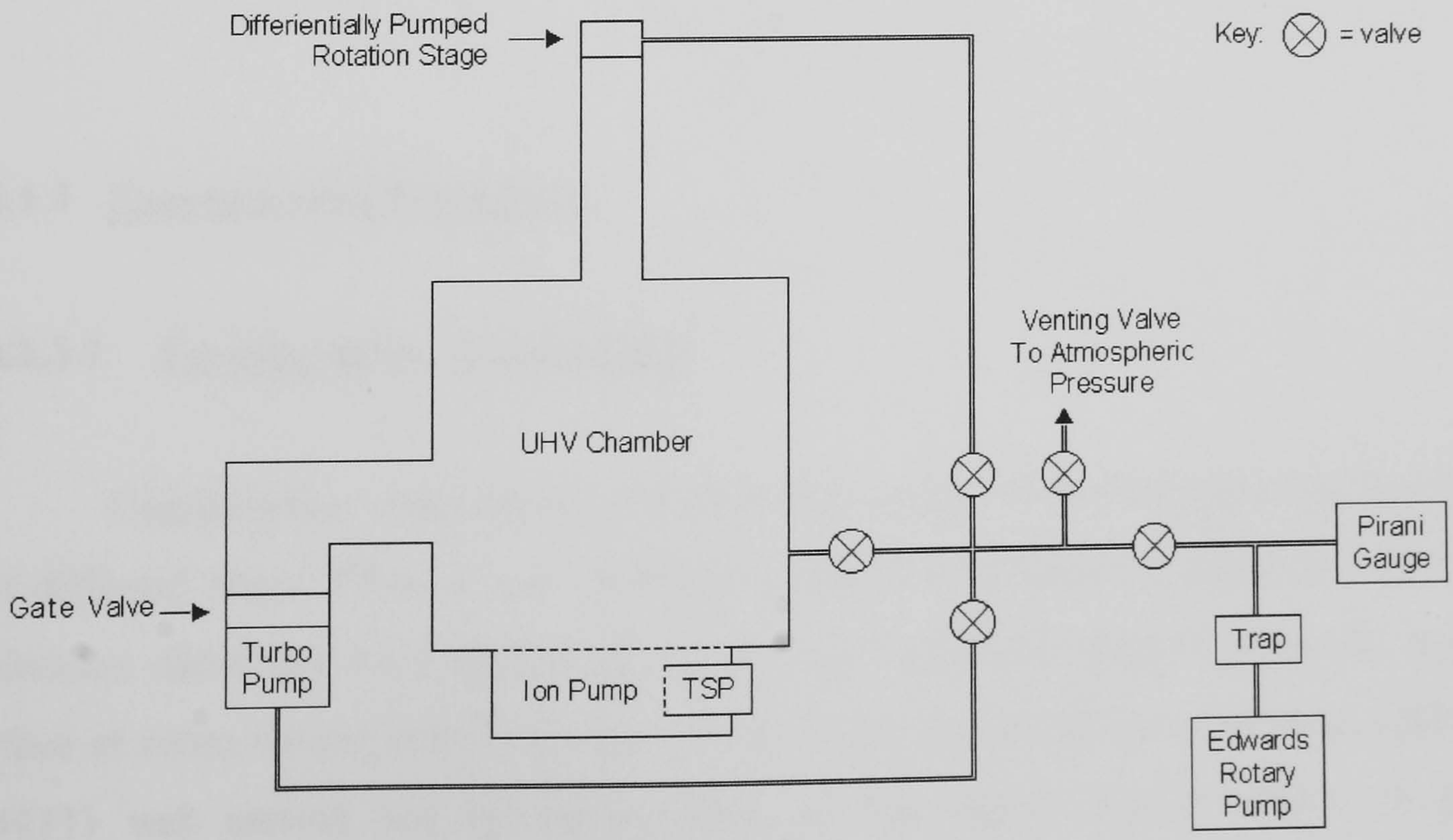

3.2.1.2 Sample Preparation

The design of the sample holder was made in such a way that it must withstand and enable both cooling (down to 90 – 100 K) and heating (up to 800 - 900 K) of the Cu(111) single crystal under UHV conditions. Fig. 3 illustrates a schematic diagram of the bottom of the sample holder. As it can be seen from Fig. 3, the crystal was sitting in a cradle made of tantalum strip and wires spot-welded together. Good thermal contact between the crystal and the cradle was required to allow for cooling down to 98 K by pouring liquid nitrogen down the reentrant. It was found that if the bottom of the reentrant was made out of a glass it would physically support UHV conditions, clamp the two tungsten rods and also enable to resistively heat the crystal. The re-entrant was made of stainless steel further up the sample holder.

The temperature of the crystal was measured by a chromel-alumel (K type) thermocouple connected to a Eurotherm controller for temperature display. Both chromel and alumel wires were twisted together and inserted inside a hole in the edge of the crystal. Further up, the two thermocouple wires were separated and isolated from the sample holder by means of ceramic pipes and plastic sheathing.

The cleaning of the sample involved first sputtering the sample with Ar^+ ions (accelerating voltage used: 1 keV) for 1 hour (target current: 10 μA) and subsequently annealing the crystal to 823 K (current used: 25 A) for a further 20 minutes. After cleaning, Both surface cleanliness and crystallographic order were finally checked by AES and LEED, respectively.

3.2.1.3 Experimental Procedure

3.2.1.3.1 Co-adsorption Experiments

Coadsorption experiments of sulfur and carbon monoxide were performed in two different ways. First, it was previously shown by Campbell and Koel that H_2S molecules dissociate on Cu(111) at 200 K and hydrogen desorbs from the copper surface at room temperature.[1] In the current work, the formation of atomic sulfur on Cu(111) was carried out by dosing H_2S on the single crystal surface at room

temperature (*ca.* 300 K), which was subsequently annealed to 623 K. Knowing that the Cu(111)($\sqrt{7}\times\sqrt{7}$)R±19°–S structure corresponds to a sulfur coverage of 0.43 ML,[(2)] by using the AES and LEED techniques it was therefore possible to establish the amount of sulfur present on the surface by determination of the S to Cu peak-to-peak AES ratio. LEED was also employed to detect the formation of ordered structures on the surface. In the case of carbon monoxide, it has been shown that CO desorbs from Cu(111) surface below 195 K.[(3)] Cooling the crystal down to 98 K using liquid nitrogen turned out to be therefore necessary.

Both H_2S and CO gases were available commercially in lecture bottles. These bottles were attached to a gas-line described in Fig. 4. This gas line had a base pressure of 8×10^{-2} mbar. Introduction of the gases into the chamber was simply performed by firstly closing the appropriate valves to isolate the line to the pumps, filling up the line with the gas and finally opening the suitable valves to introduce the chemical compound into the chamber.

Fig.3 *The bottom of the sample holder*

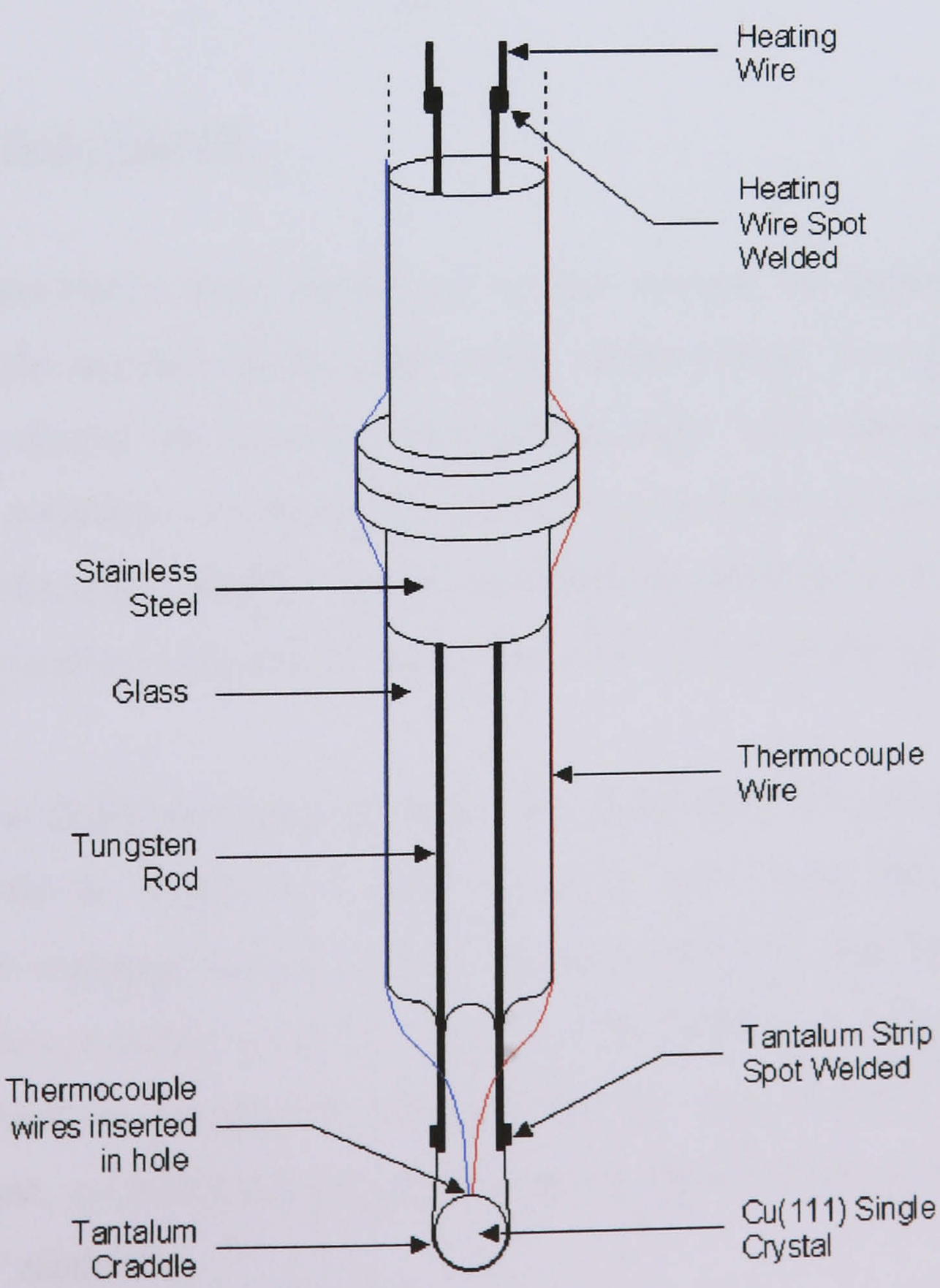

Fig.4 *Schematic diagram of the EELS gas-line*

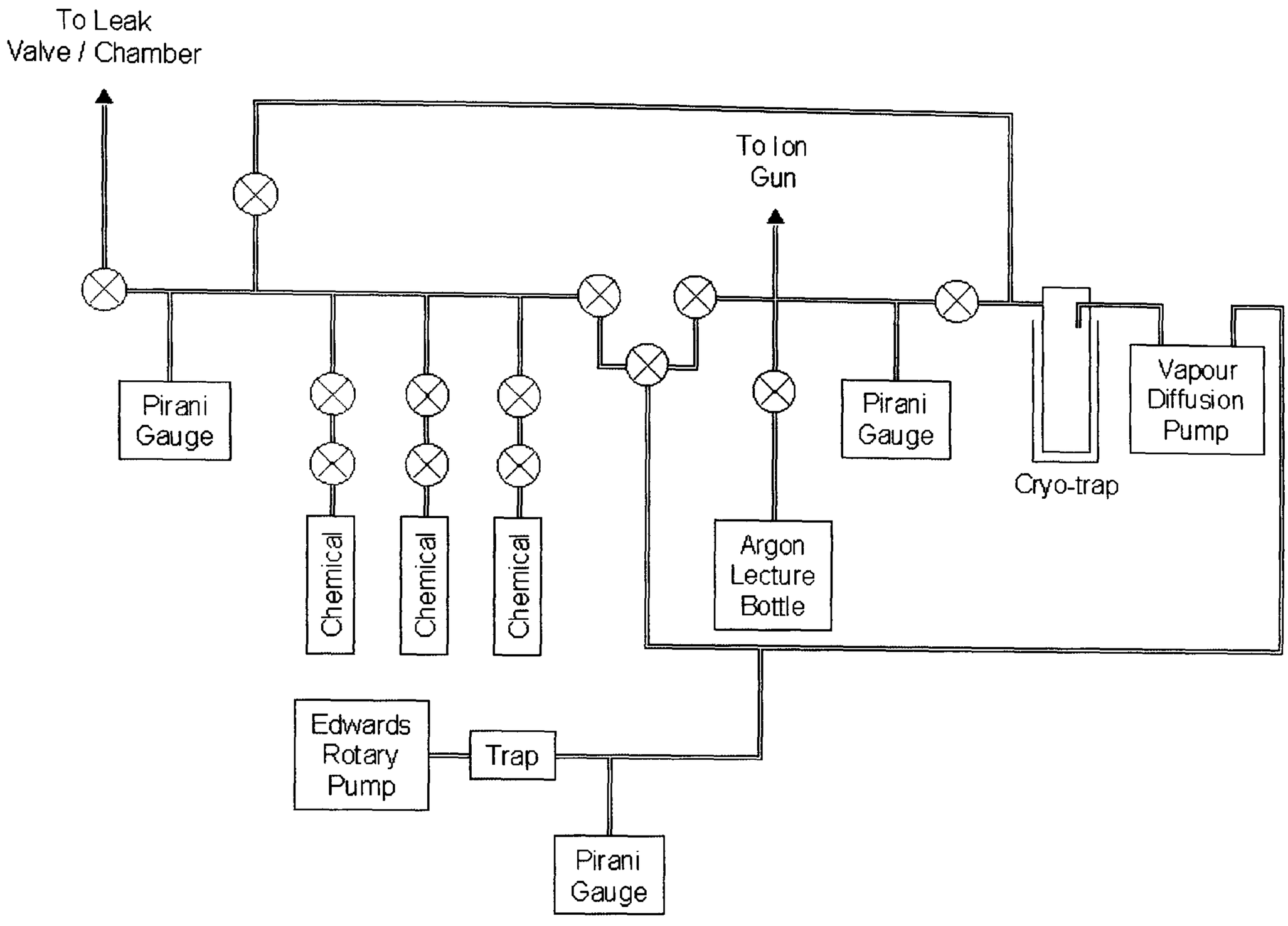

3.2.1.3.2 TPD Experiments

TPD experiments were carried out by first cooling the crystal down to 98 K and then dosing the material on the cold surface of the crystal. Two different methods were used while dosing the crystal: "line-of-sight" and "back filling". The "line-of-sight" technique consisted of placing the surface of the crystal 30 mm in front of the stainless steel dosing pipe, whereas in the "back filling" method the crystal was located 50 mm above the dosing tube and its face rotated by 180° so it did not face the dosing tube.

The main difference between these two techniques was the large amount of material that could be dosed in a short period of time using the "line-of- sight" technique without exposing the rest of the chamber to excessive quantities. In the "back filling" method less material could be dosed on the surface in a more accurate way. Only CO was dosed in the present project using the "line-of-sight" technique. H_2S, thiophene, benzene, cyclohexene and cyclohexane (Aldrich 99%) were all dosed using the "back filling" method.

The chemicals of interest were attached to the EELS gas line (Fig. 4), their vapour was allowed in the gas line and then into the chamber. Any impurity was removed by applying three freeze-pump-thaw cycles. The purity of the chemicals was further checked by using the QMS and comparing the recorded scan with their respective cracking patterns.

After dosing the crystal was brought down and positioned within a few millimetres of the front of the QMS. In order to analyse material that only desorbed from the surface of the crystal and not the sample holder, a shield with a 3mm diameter entrance aperture was placed over the head of the QMS. A heating rate of 0.5 K/s was used to collect all TPD spectra.

3.2.1.3.3 LEED/AES Analysis

LEED and AES experiments used both a retarding field analyser (RFA) which is a relatively simple detector. In the LEED mode, a series of concentric meshes (Fig. 5) were used as a high pass filter to pass only elastically scattered electrons. By applying a potential slightly lower than the primary electron potential V_p on the mesh M_1 (closest to the screen S), only diffracted electron beams could reach the phosphor screen and enabled us to physically see the symmetry and crystalline order of the surface under study. In the AUGER mode, the connections of the mesh at the back of the control unit were changed (M1 earthed and M2 connected to the retarding potential) and this time the retarding potential was modulated sinusoidally ($V_0 + \Delta V \sin \omega t$).

In general the Auger peaks are small and superimposed on a large secondary electron background, making their identification difficult. However, it is possible to electronically overcome this difficulty by using a phase sensitive detector which permits the derivation of the measured signal and the dN(E)/dE curve to be directly obtained. Differentiation removed the constant background and allowed increased amplification of the original signal.

Two modulation voltages were employed in collecting the AES spectra. During the CO coadsorption investigation, a modulation voltage of 20 V_{p-p} was used. However, an alternative voltage of 3.192 V_{p-p} was utilised during the sulfur studies where a higher resolution was required for S coverage (θ_S) determination. A higher resolution also

involved a lower signal N(E) and this signal could be subject to a poor signal-to-noise ratio.

Fig.5 *The LEED apparatus.*

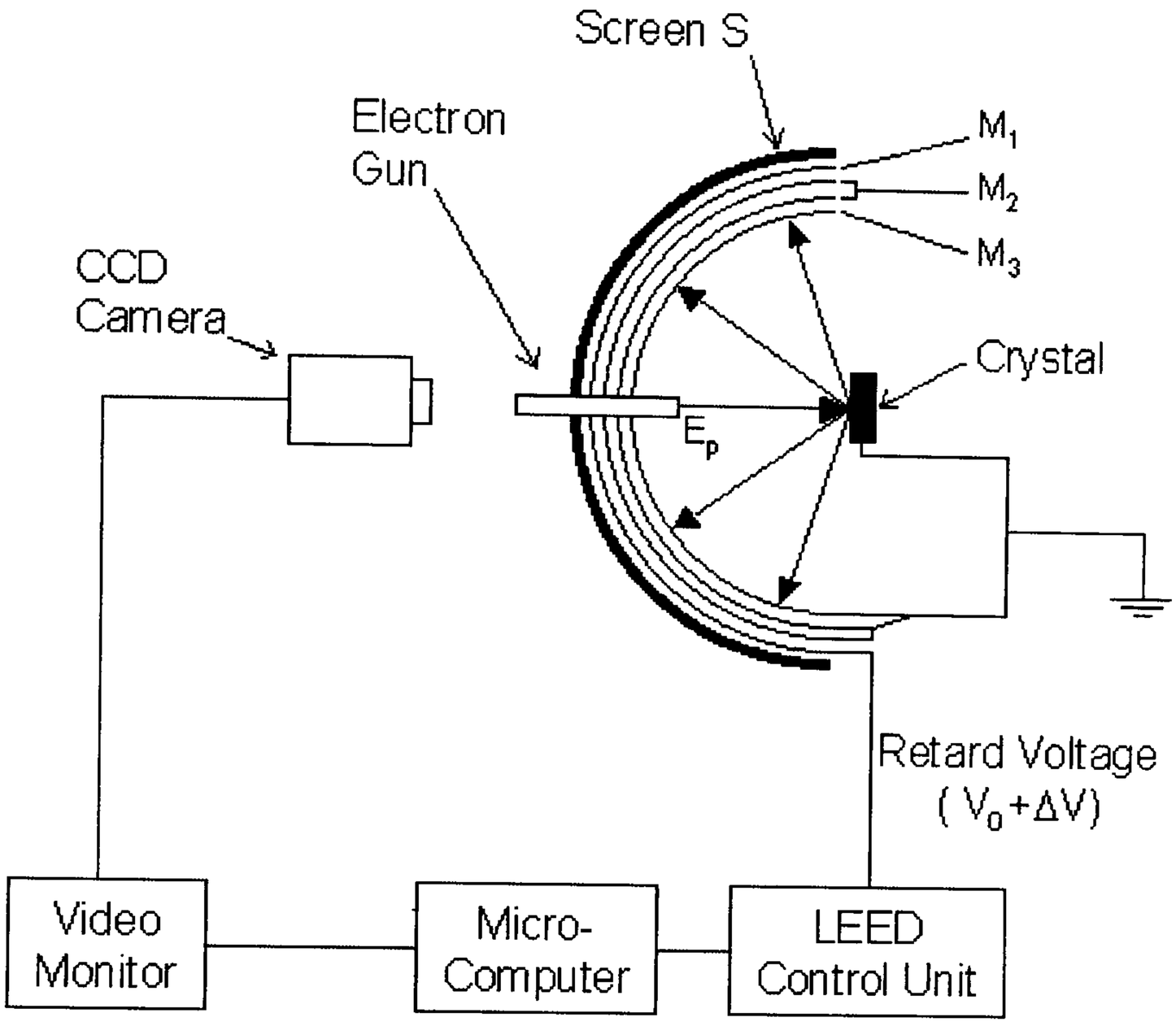

3.2.2 UPS Chamber

3.2.2.1 System Design

The UPS chamber (Fig. 6) was equipped with a LEED spectrometer (RFA detection), a helium UV-source, a twin anode (Mg and Al) X-ray gun and a CLAM-2 electron energy analyser. It enabled LEED, XPS and UPS experiments to be performed.

As with the EELS chamber, the pumping of the UPS chamber was carried out in several stages (Fig. 7). Initial pumping was done by a rotary pump (Edwards Ltd) down to 1×10^{-3} mbar. Once this pressure was achieved, a diffusion pump (E04K – Edwards Ltd) was utilised to obtain pressure as low as 10^{-8} mbar. Finally a TSP (ST22 – Vacuum Generators Ltd) was employed to pump low gas loads.

However, as was the case with the EELS chamber, the entire system had to be baked at 150°C to remove any atmospheric molecules, mainly water, adsorbed on the wall of the chamber. The bake-out was normally switched off after 15 hours once a pressure of 1×10^{-7} mbar was achieved.

After de-gassing the TSP, electron bombardment sample heater (ZEBH – Vacuum Generators Ltd), QMS (Smart-IQ^{+} – VG Gas Analysis System Ltd), Ion gun (EX03 – VG Microtech Ltd), X-ray source (Twin Anode XR3E2 – VG Microtech Ltd), Ion gauge (VIG18 – Vacuum Generators Ltd) and LEED optics (RVL – VG Microtech Ltd), a final pressure as low as 1×10^{-10} mbar was normally acquired.

Fig.6 *The UPS Chamber.*

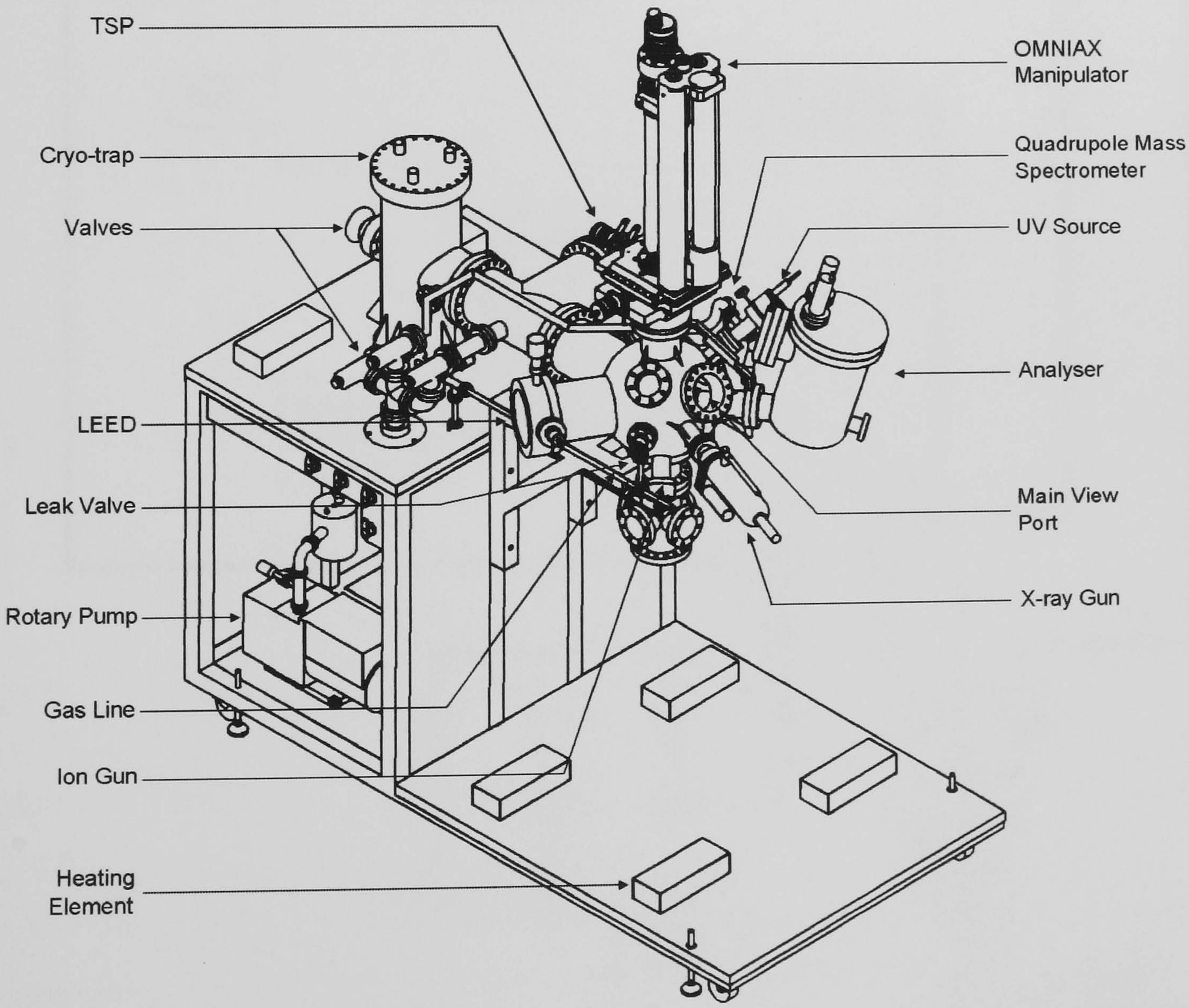

Fig.7 *Schematic diagram of the pumping arrangement of the UPS Chamber.*

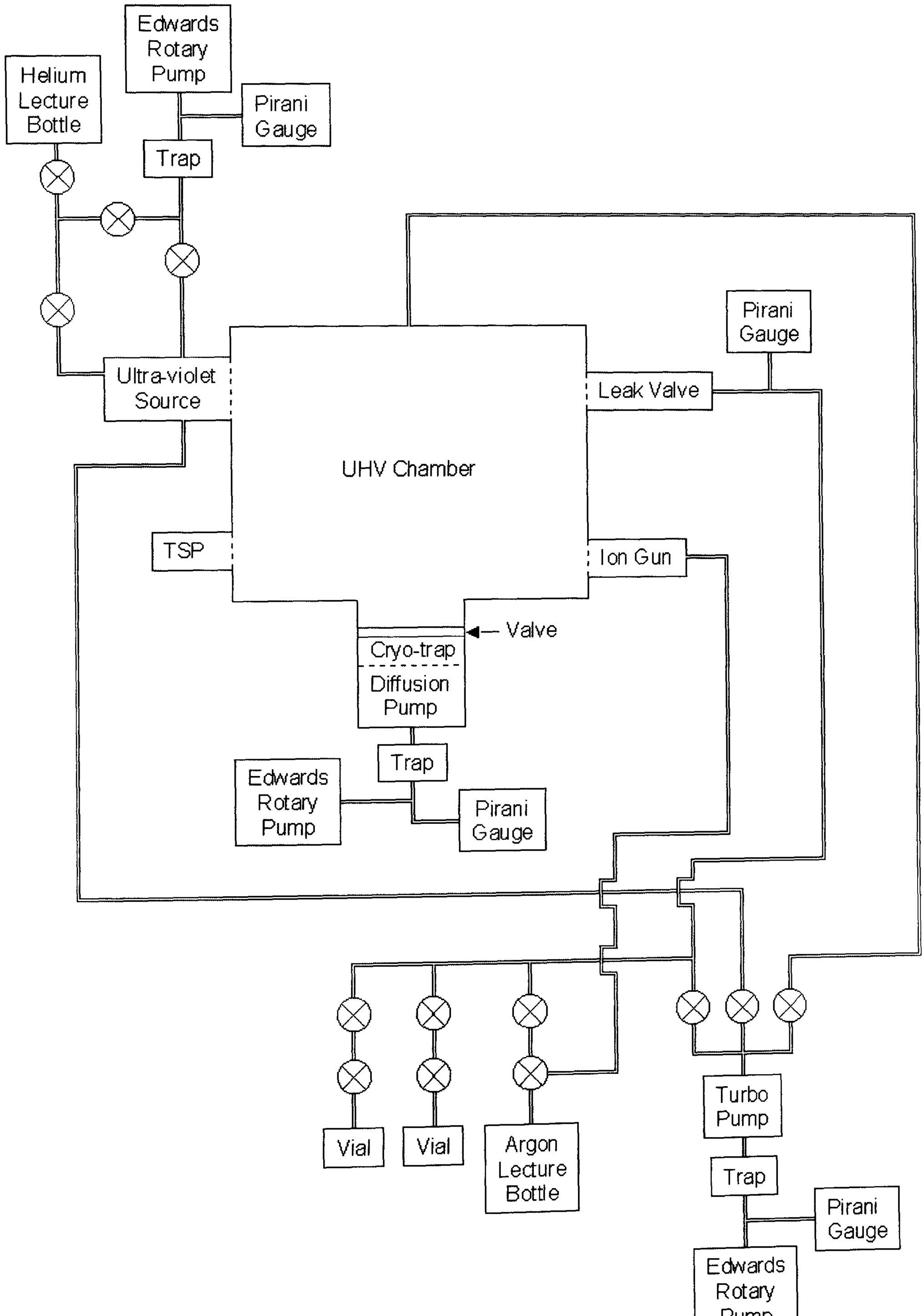

3.2.2.2 Sample Preparation

The manipulator and sample holder were both designed and manufactured by the Vacuum Generators company. The Omniax manipulator (MX series) is a high precision, high rigidity and UHV translator. Two micrometers ensured the X and Y horizontal motions, whereas a stepper motor drive system (McLennan Servo Supply Ltd) was used to move the Cu(111) crystal along the vertical Z-axis. The specific design of the sample holder (Fig. 8) allowed rotation of the crystal around the Z-axis and also adjustment of its azimuthal angle. Motions around the crystal polar and azimuthal angles were driven by two separate stepper motors. This sample holder also provided a means of heating the crystal up to 1200°C and cooling it down to 123 K under UHV conditions.

The electron bombardment apparatus, shown in Fig. 9, was used to heat the crystal. As it can be seen in Fig. 9, the Cu(111) crystal was clamped on the anode plate, and at the back of this plate a thoria-coated iridium filament was located in the middle of the cathode support tray. These different parts were electrically insulated to each other and also to the supporting system by means of ceramic supports, spacers and sapphire balls. By only passing a current through the filament, the temperature of the crystal could be increased to 473 K. However, in order to obtain a temperature of 873 K, it was necessary to anneal the crystal. This could be achieved by applying a potential difference of 650 V between the anode and the cathode plates. This voltage accelerated the electrons emitted from the filament towards the back of the anode plate providing more energy and subsequently more heat.

The cooling of the crystal was done by using liquid nitrogen from condensed dry gas. Liquid N_2 reached the sample holder through a capillary tube, and a highly conductive braid and copper reservoir were thermally connected to the anode plate where the crystal sat. Good thermal contact was essential to obtain low temperature (123 K). A thermocouple (K-type), which was attached to the anode plate next to the crystal and connected to a Eurotherm controller, was used to monitor the crystal temperature during the heating and cooling process.

Many problems were encountered with the initial design of the electron beam heater, especially during bombarding. Sputtered material from the assembly plates was deposited on the ceramic supports and spacers creating short circuits and made the

heater unusable. Modifications were therefore made. The Vacuum Generators thoria-coated iridium W-shaped filament was replaced by a home made thoriated tungsten U - shaped filament. The rigidity of this new filament gave the opportunity to remove the ceramic spacers. Also a shield made of tantalum spot-welded on either sides of the too narrow anode plate brought additional protection to the filament underneath.

It was finally decided to bombard the crystal with the anode plate in the horizontal position with respect the azimuthal, and this minimised the amount of sputtered materials on the ceramic supports. Cleaning the crystal consisted first of bombarding the crystal with Ar^+ ions for 30 minutes (target current: 30 μA) and annealing the crystal at 873 K for 20 minutes. Finally surface order and cleanliness were monitored by LEED and XPS.

Fig.8 *Sample holder of the UPS chamber (side view).*

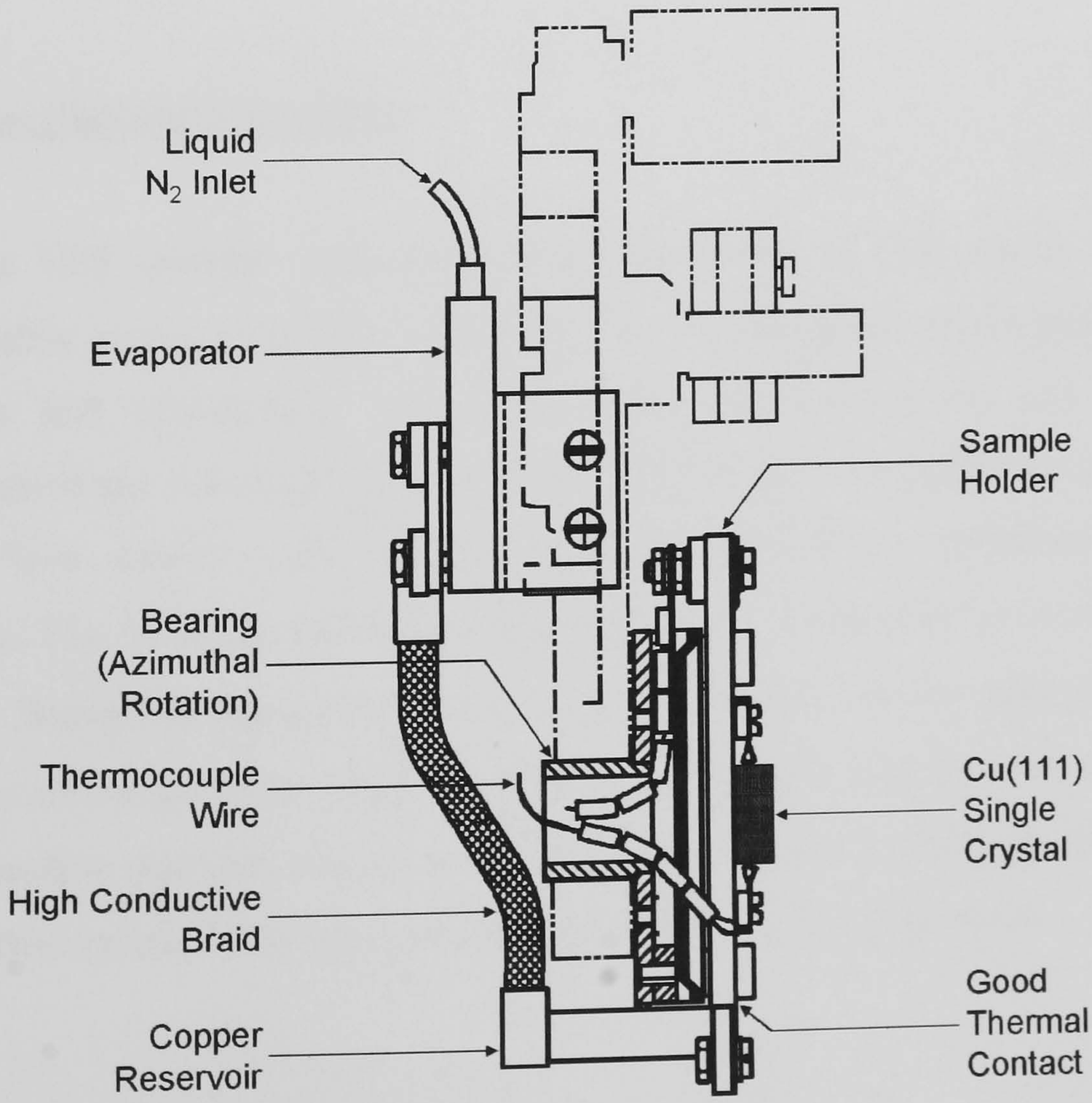

Fig.9 *The electron bombardment sample heater (side view).*

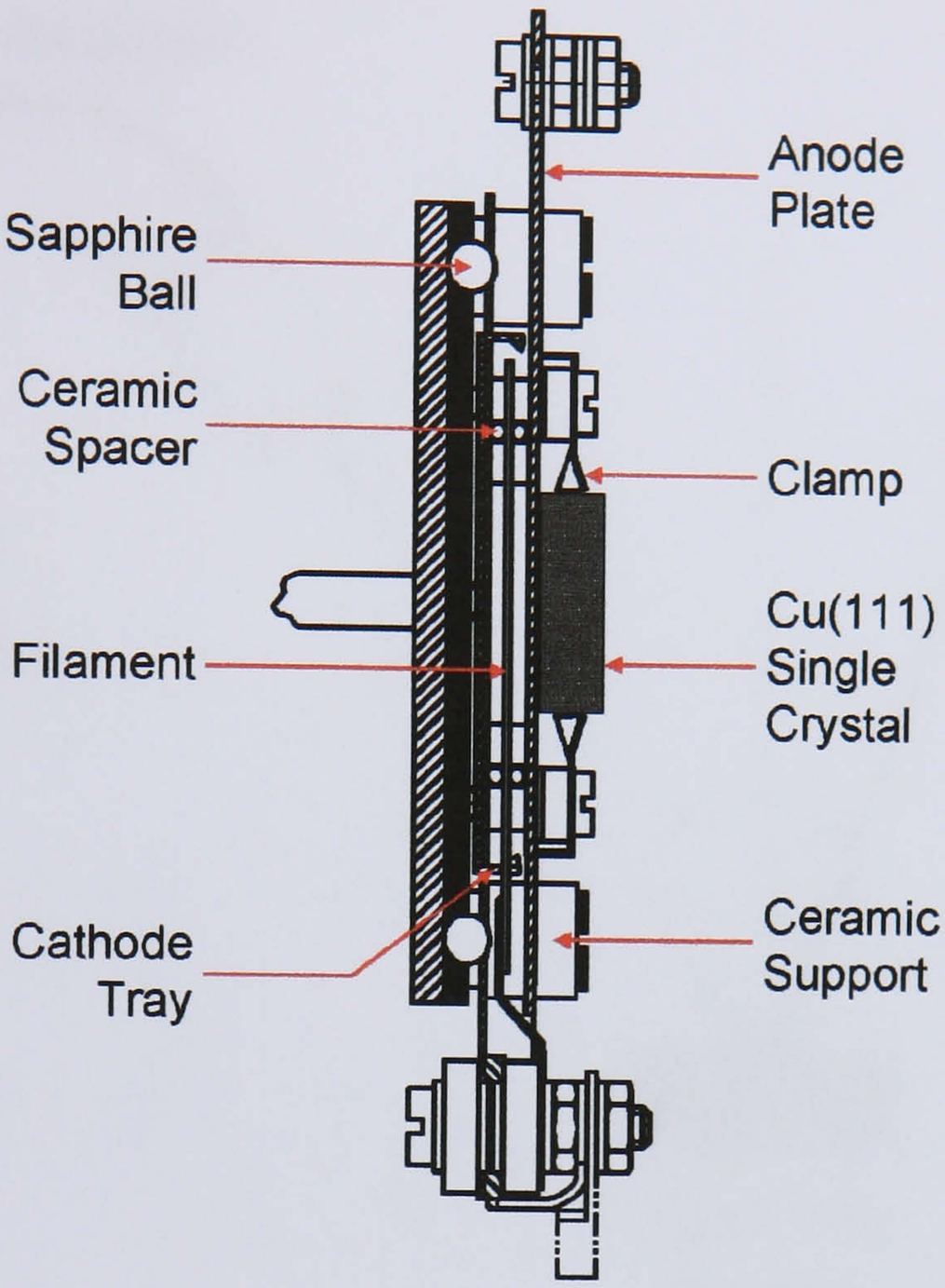

3.2.2.3 Experimental Procedure

The UPS chamber was used during the course of this project to study the effects of sulfur precovered Cu(111) surfaces on the adsorption of thiophene, benzene, cyclohexene and cyclohexane molecules at an electronic level. The quantitative determination of the amount of sulfur present on the crystal was achieved using the XPS technique. Two anodes were available and provided X-ray radiation at different wavelengths. The Al anode which provided light at hν = 1486.6 eV was not used during this project. Instead the Mg anode was utilised (hν = 1253.6 eV) because it was suitable for the range of energy under study. During an XPS experiment, the pass energy of the CLAM-2 electron analyser was set at 50 eV. Fig. 10 shows a schematic diagram of the position of the crystal, X-ray gun and analyser during a XPS experiment.

Fig.10 *Schematic diagram of the crystal positioning during a XPS experiment.*

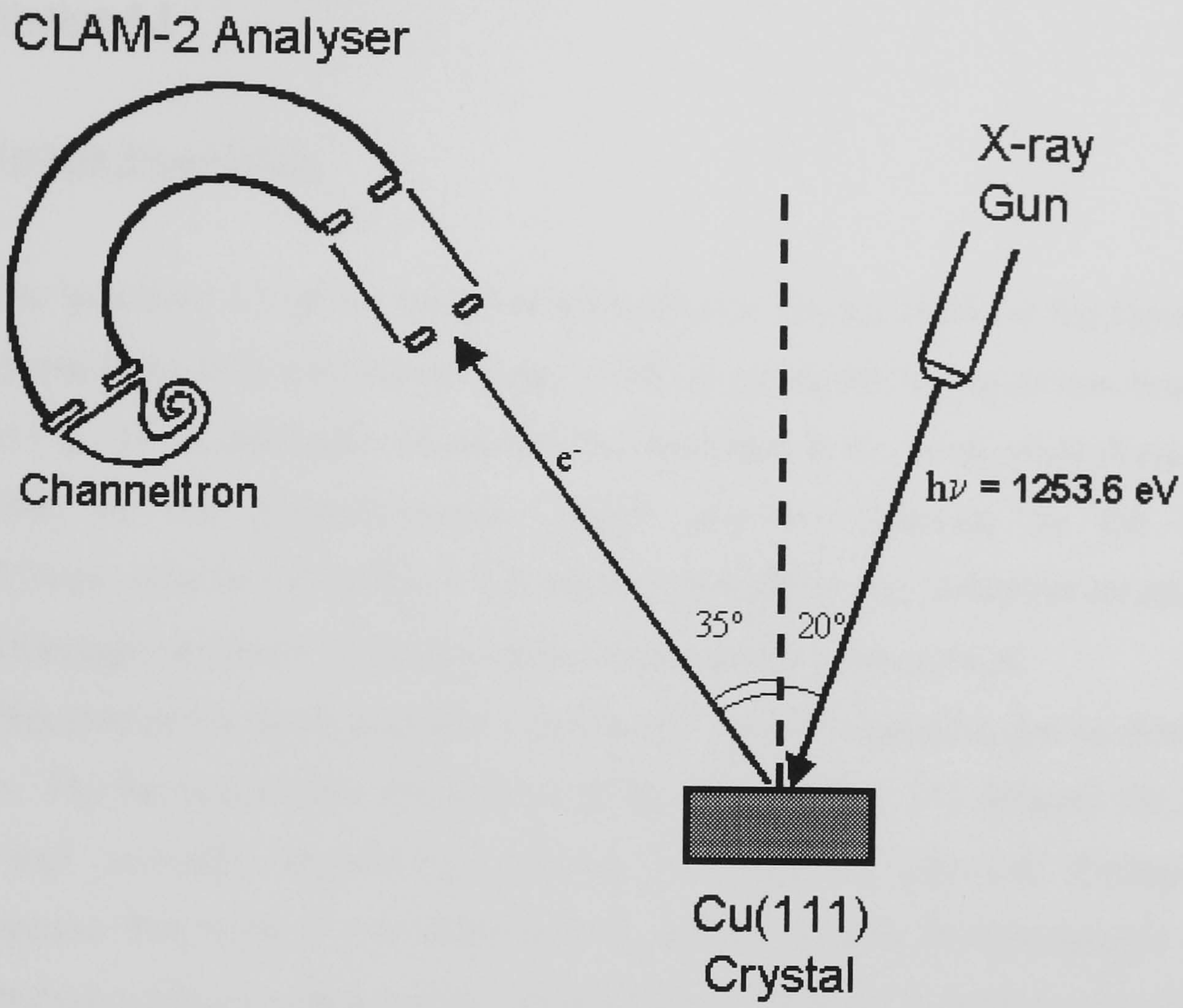

The UPS experiments, as described in Chapter 2, provides information on the electronic properties of the system under study. Also mentioned in Chapter 2, the symmetry selection rules in photoemission spectroscopy, which enable one to predict whether emission from a specific MO is allowed or forbidden for a particular detector position and a given polarisation, are especially powerful if the detector is positioned in a high-symmetry direction, such as the surface normal or mirror planes of the system.[4] For this reason, our UPS measurements were performed at normal emission where the surface of the crystal was facing the electron analyser. During scanning, the pass energy of the electron analyser was set at 10 eV in the UPS mode.

UPS experiments of sulfur adsorbed on clean copper surfaces were performed at room temperature. However, photoemission measurements involving thiophene, benzene, cyclohexene and cyclohexane molecules on clean and S pre-covered Cu(111) surfaces were carried out at cryogenic temperature (123 K). All four chemicals (Aldrich 99%) were attached and stored in the gas line (Fig. 7), purified using the freeze-pump-thaw technique and their purity compared against their cracking pattern. Finally the LEED apparatus was used to detect any surface ordering.

3.3 Experimental (Daresbury)

3.3.1 Station 4.1

3.3.1.1 System Description

The beamline 4.1 of the Synchrotron Radiation Source (SRS) at the Daresbury Laboratory has been fully operational since 1995. A schematic layout of this beamline is given in Fig. 11. A particular feature of this beamline is the conceptual design and characteristic of the monochromator which provides photons in the range $15 \leq h\nu \leq 170\,eV$ (within the visible – UV region) and allows the electronic structure to be probed through excitation of shallow core levels and the valence band.

This station has been described elsewhere[5,6] and its operation can be described as follows. The horizontal and vertical focusing mirrors (Fig. 11) deflects the beam sideways and vertically respectively towards the entrance slits and through the monochromator. The beam is then diffracted by one of the three interchangeable gold-coated spherical gratings which can be translated into the beam by means of a manual linear drive. The first grating covers the energy range 15 – 45 eV; the second one the energy range 45 – 130 eV and the highest energy range, 130 – 170 eV, is achieved by the third grating. Finally a post-focusing ellipsoidal mirror direct the beam towards the end-station UHV chamber.

Fig.11 *Schematic layout of the branch line 4.1 showing the optical path lengths.*

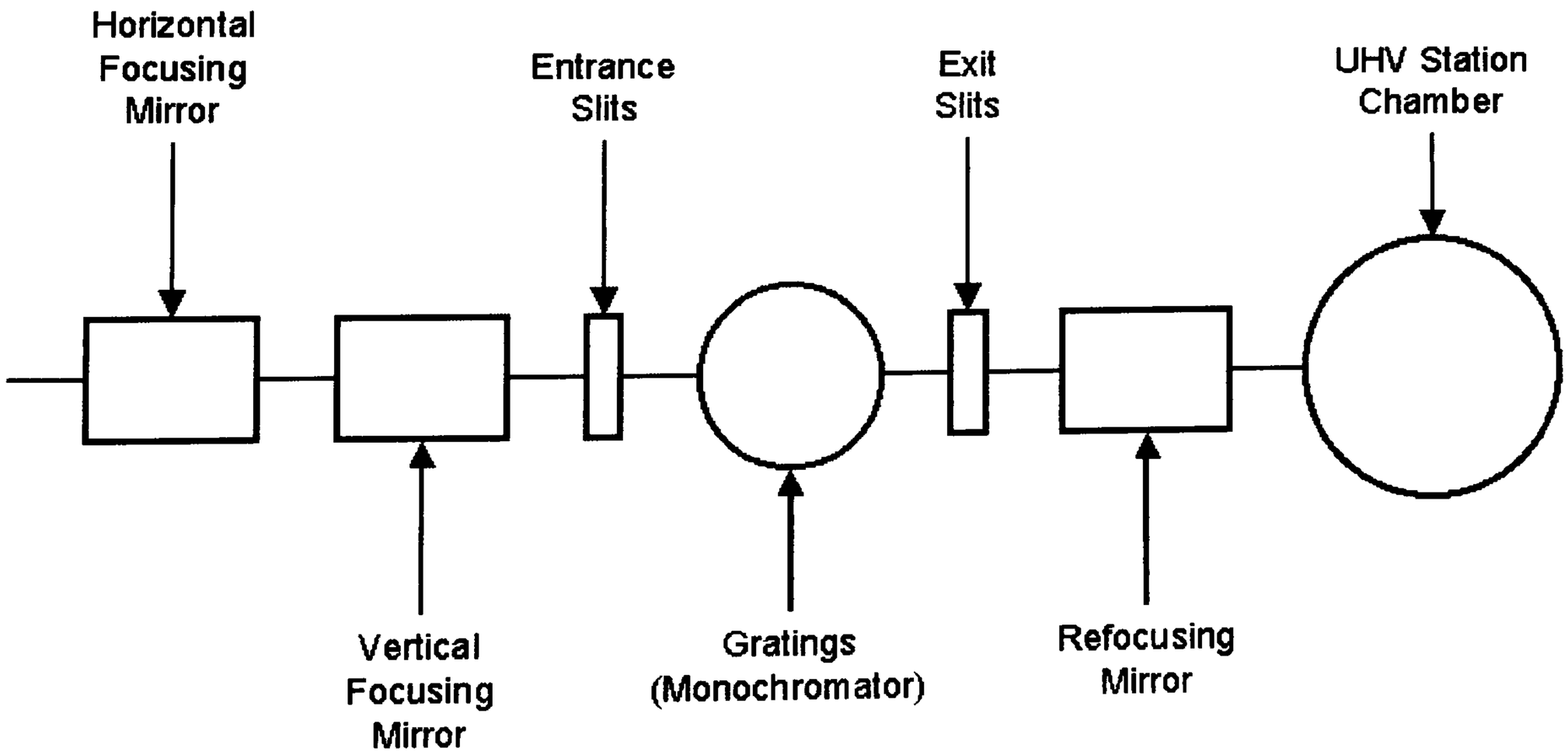

The end-station UHV surface science chamber was equipped with a QMS (Vacuum Generators Ltd), a LEED (Omicron Ltd) and a Scienta SES 200 hemispherical electron energy analyser which combined with the performance of the photon beam constituted a very powerful tool for surface science studies. Although a helium UV-source and X-ray gun were available, those were not used during this project.

3.3.1.2 Sample Preparation

The three semiconductor crystals were mounted on a VG Omniax manipulator which also provided means of liquid nitrogen cooling and resistive heating as standard although cooling the samples was not used during this project

The Si(100) (double domain) and Si(111) samples were first outgassed at 723 K for 12 hours. Cleaning was performed by several flashing cycles to 1473 K. A chromel-alumel thermocouple attached to the sample holder and an optical pyrometer were available, however it was found that the pyrometer was more reliable to measure the temperature of the samples. During the flashing process, as well as monitoring the temperature, the pressure was kept below 1×10^{-9} mbar in order to avoid any contamination. A different method was used for cleaning the Ge(100) (double domain) sample. This involved sputtering the surface with Ar^+ ions (acceleration potential: +500V) for 15 minutes subsequently followed by annealing the sample to 873-973 K for 10 minutes.

The surface cleanliness of all three crystals was checked by photoemission. The presence of characteristic surface states in the valence band spectra of Si(100)-(2×1), Si(111)-(7×7) and Ge(100)-(2×1) were used to assess the cleanliness of the surfaces after flashing. Further, for Si(100)-(2×1) cleanliness and surface quality were also monitored by collecting core level Si 2p spectra. These core level spectra resulted in high surface sensitivity and high photoelectron signal. Surface cleanliness of the three semiconductor surfaces was also confirmed by the sharpness of their LEED patterns.

3.3.1.3 Experimental Procedure

Thiophene, benzene, and benzonitrile (Aldrich 99%) were stored in a stainless steel gas handling line and also purified using the conventional freeze-pump-thaw method. Dosing of the three molecules was performed at room temperature.

Photoemission experiments were carried out at photon energies of 40 eV for valence band structure and 140 eV for core level measurements. The Fermi level E_F, from which the binding energies (BE) were referred to, was determined from the tantalum backplate.

All three samples were positioned in two particular orientations during measurement:

- normal emission where the surface of the semiconductors was facing the electron energy analyser and the photon beam was incident at 55° with respect to the surface normal;
- off-normal (or grazing) emission where the surface normal of the crystal was parallel to the beam line and photoelectrons detected by the analyser at 55°.

3.3.2 Station 6.3

3.3.2.1 System Description

Station 6.3 of the Daresbury SRS has been described elsewhere.[7,8] It is a soft X-ray UHV beam line which provides monochromatic photons in the energy ranges 1780 – 7000 eV suitable for XPS, NEXAFS and NIXSW experiments. Its beam line concept is shown on Fig. 12.

Its operation can be described as follows. First, a set of carbon stripper foils removed any radiation in the visible-UV region that might interfere with the monochromatic operation. The light was then deflected by a gold-coated toroidal pre-mirror which focused the X-ray radiation horizontally and vertically through a double crystal monochromator. The three crystal pairs in use, InSb(111), Ge(111) and Si(111), had photons energy ranges of 1780 – 5200 eV, 2010 – 6000 eV and 2800 – 7000 eV respectively and could be interchanged under UHV conditions. The monochromatic

beam then passed through the I_0' monitor used to measure the decrease in intensity of the X-ray beam with time. The raw data collected from each experiment were divided by this current value for comparison. The exit jaws and the design of the monochromator where the rotation and translation mechanism of the crystals ensured that a horizontally and vertically focused beam always hit the sample. This assembly also produced the highest photon resolution required for NIXSW and NEXAFS experiments.

The end-station UHV chamber station was equipped with a LEED front view (Vacuum generators Ltd) used to set up NIXSW experiments for reflection which were not normal to the sample surface, a sample electron beam heater and liquid nitrogen cooling, and a CHA HA-100 (VSW Ltd) utilised for photons stimulated Auger electrons and XPS experiments.

Fig.12 *Schematic diagram of the beamline 6.3 showing the optical path lengths.*

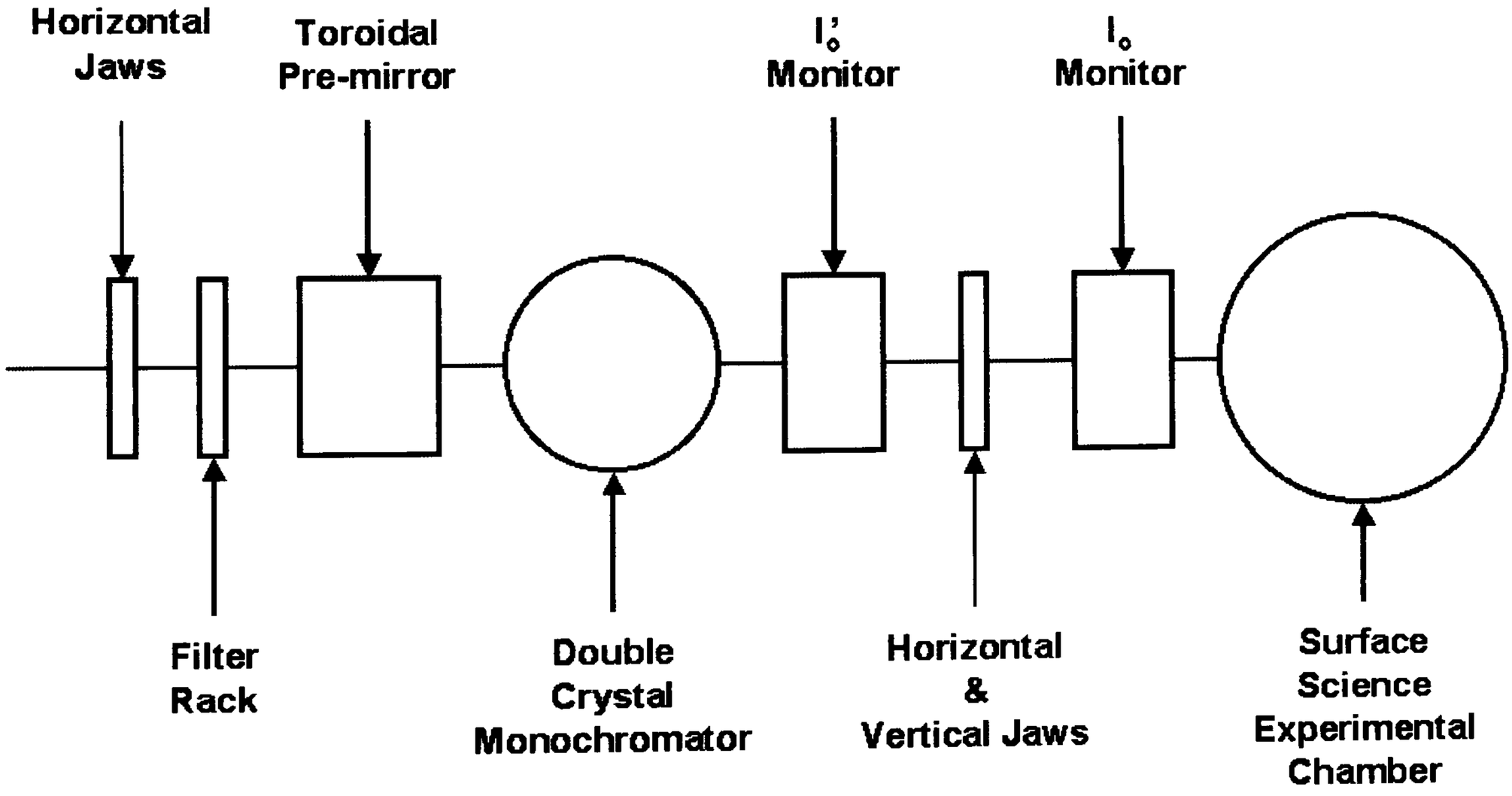

3.3.2.2 Sample Preparation & Experimental Procedure

The Cu(111) sample was mounted onto a HPLT manipulator (Vacuum Generators Ltd) incorporating polar and azimuthal rotation. The crystal was cleaned by Ar^+ bombardment followed by annealing to 823 K. Surface cleanliness was then verified with XPS and surface quality by LEED.

Thiophene, CO and H_2S (Aldrich 99%) were stored in a stainless steel gas dosing line. Thiophene was purified following the freeze-pump-thaw method. H_2S was dosed at room temperature by back filling of the UHV chamber, whereas CO and thiophene molecules were dosed on a cold surface (120 K).

NEXAFS experiments were performed with light incident at normal and 19.5° (grazing) emission from the surface while monitoring the yield of $S(KL_{2,3}L_{2,3})$ Auger electrons as the photon energy was scanned through the S K-edge.

NIXSW experiments were carried out in the (111) and (111) planes. NIXSW Profile were obtained by monitoring the yields of the O(1s) photoemitted electrons and $S(KL_{2,3}L_{2,3})$ Auger electrons.

3.4 References

1. C.T. Campbell, B.E Koel, Surf. Sci. 183 (1987) 100
2. J.L. Domange, J. Oudar, Surf. Sci., 11 (1968) 124
3. W. Kirsten, B. Kruger, F. Thieme, Surf. Sci. 176 (1987) 505
4. H.-P. Steinrück, J. Phys.: Condens. Matter, 8 (1996) 6465
5. V.R. Dhanak, A.W. Robinson, G. van der Laan and G Thornton, Rev. Sci. Instrum. 63 (1992) 1342
6. V.R. Dhanak, A.G. Shard, C.A. Muryn, P.L. Wincott and G. Thornton, J. Synchrotron Rad. 569 (1998) 569
7. A.A. MacDowell, D. Norman, J.B. West, J.C. Campuzano and R.G. Jones, Nuc. Instr. Meth. A 246 (1986) 131
8. A.A. MacDowell, D. Norman and J.B. West, Rev. Sci. Instrum. 57 (1986) 2667

Chapter 4. The Structure of a Coadsorbed Layer of Thiophene and CO on Cu(111)

4.1 Introduction

The influence of coadsorbed carbon monoxide on the structure and bonding of thiophene on Cu(111) has been characterised using a combination of LEED, AES, XPS, TPD, NEXAFS and NIXSW. The AES, XPS and TPD techniques indicate that both molecules are reversibly adsorbed and desorb molecularly. Contrary to benzene, where the coadsorption of CO induces ordering of the disordered layers, the LEED analysis in the present study establishes that no ordering occurs in the disordered chemisorbed thiophene layer. Our NIXSW results show that both CO and thiophene adopt atop adsorption sites within the coadsorbed overlayers and the same site (atop) is adopted by both molecules in pure layers. Moreover, our NEXAFS measurements imply that the orientation of C_4H_4S within the coadsorbed layers is also similar to the one adopted in a pure layer. When coadsorbed with thiophene, however, the CO molecules are in a more inclined orientation as suggested by our NIXSW data, which contrasts with the linear geometry observed in pure CO layers of a similar coverage. We attribute the lack of any significant co-operative effects between the CO and thiophene within the coadsorbed overlayers to be due to the relatively weak thiophene– and CO–substrate interactions.

4.2 Results

4.2.1 Initial Characterisations

Prior to the performance of synchrotron-based structural measurements, the initial characterisation of the coadsorption of thiophene and CO on Cu(111) was performed at the Glasgow laboratory using the EELS chamber. This UHV system, which has been described in Chapter 3, is equipped with the AES, LEED and TPD capabilities.

The TPD spectra of thiophene adsorbed on Cu(111) depicted in Fig 1(a) (black line) was previously studied by our group.[1,2] It was established that the adsorption structure of chemisorbed thiophene is coverage dependent. In the low coverage α-phase, thiophene is initially adsorbed with its sulfur atom in an atop site and with the aromatic ring at 26° to the surface. With increasing coverage (above 0.1 ML), a phase transition occurs. The new phase, referred to as the β-phase, involves an increase in the inclination of the aromatic ring to 44° and an elongation (weakening) of the Cu – S bond from 2.62 to 2.83 Å.[2] If we follow the assignment made in the previous investigation,[2] the peaks centred at 144, 163, 202 and 275 K in Fig.1(a) (black line) correspond to the desorption of thiophene condensed layers, thiophene molecules in the β-phase, thiophene molecules in the α-phase and desorption of thiophene from the defect sites, respectively.

The TPD spectrum collected from the pure CO overlayer depicted in Fig.1(b) (blue line) is in very good agreement to those obtained by Thieme *et al.*[3] Their spectra showed three desorption maxima labelled by the authors α, β_1 and β_2, centred at approximately 130, 152 and 170 K. Here, those three peaks are also present in Fig.1(b) at 123, 145 and 163 K, in addition to two other peaks at lower temperatures (100 and 115 K). The difference in 7 K observed between the two studies may be due to either the different temperature rates used (0.7 $K.s^{-1}$ in Thieme work and 0.5 $K.s^{-1}$ in the present study) although this should normally have a small effect, or this could also be due to the different calibration and/or position of the thermocouple employed. We also explain the appearance of the two extra peaks in the current work by the lower deposition temperature (CO deposited at 105 K in Thieme work; 95 K here).

The current work was only concerned with the effect of coadsorbed CO on thiophene in the α-phase. The formation of this phase was made possible by condensing layers of C_4H_4S at 95 K and annealing to a temperature high enough to desorb multilayers and thiophene in the β-phase. Subsequently, the α-phase layer was exposed to 30 L of CO at 95 K. The TPD spectra which show the desorption of thiophene (red line) and CO (magenta line) from coadsorbed layers are also pictured in Fig. 1, along those collected from the pure overlayers for comparison. As can be seen, thiophene desorbs from the coadsorbed overlayer in an identical manner to that observed for pure layers. However, differences exist in the desorption behaviour of CO from pure and coadsorbed layers. Although there are some differences in the spectra, CO desorbs over similar temperature ranges from both pure and coadsorbed overlayers. The spectrum from the coadsorbed overlayer has three main desorption peaks at 97, 129 and 159 K, and in contrast to the pure overlayer there is no peak at 208 K which is associated with desorption of CO from defect sites.

Finally, the TPD and AES results indicate that both molecules in pure and coadsorbed overlayers are associatively adsorbed and desorb molecularly, as neither surface carbon nor H_2 and C_xH_y species were detected. The LEED analysis also suggests that the coadsorption of CO does not induce ordering of the disordered chemisorbed thiophene layer.

Fig.1. *TPD spectra showing the desorption of thiophene and CO from pure and coadsorbed layers. (a) Desorption of 1.2 L of thiophene adsorbed on Cu(111) in "line-of-sight" (black line) and thiophene in α-phase coadsorbed with CO (red line). (b) Desorption of CO from a pure overlayer, formed by dosing 30 L at 95 K using the "back filling" method (blue line) and CO coadsorbed with thiophene (magenta line).*

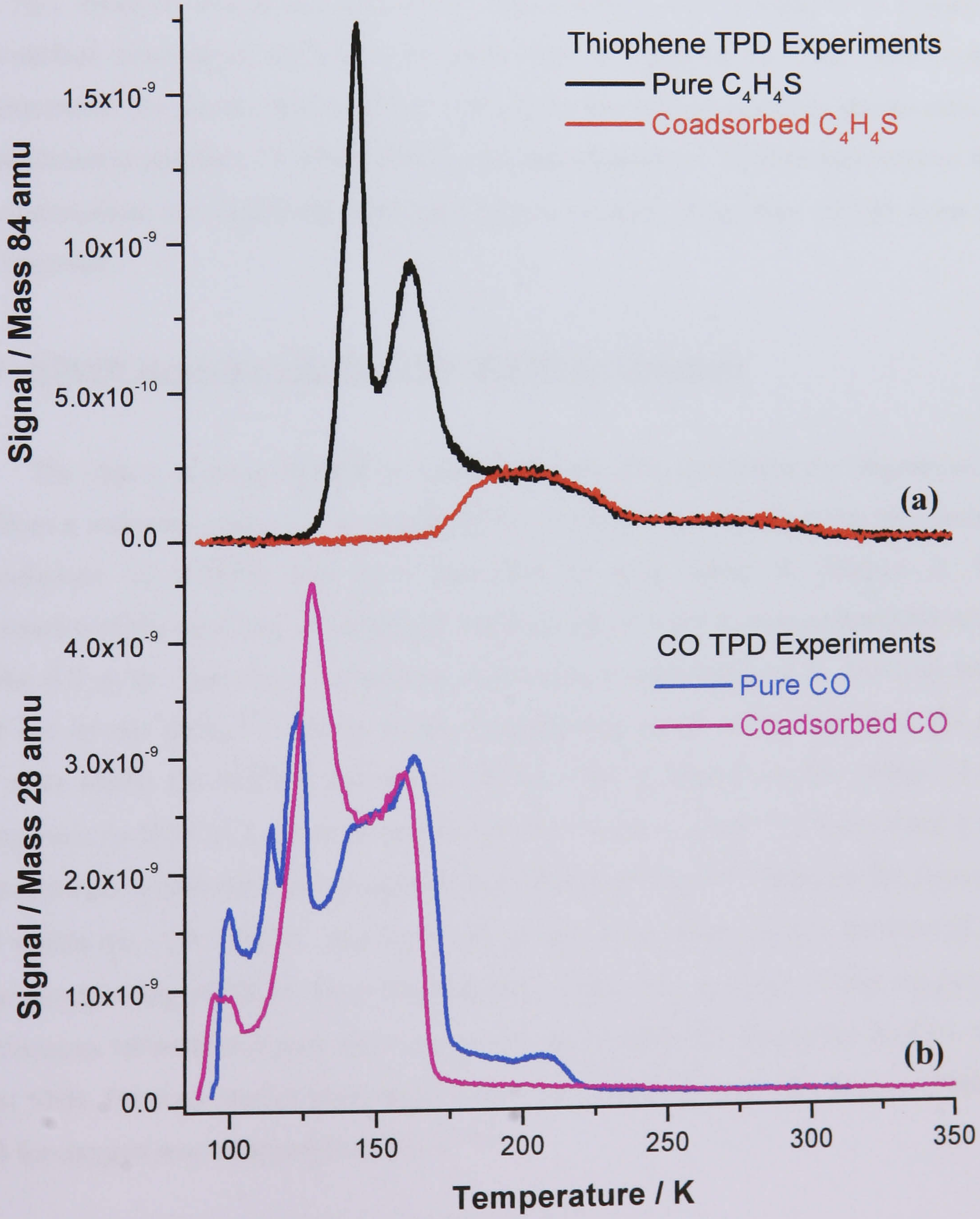

4.2.2 Structure of (√3×√3)R30°-CO

4.2.2.1 LEED Analysis

The formation of pure CO overlayers was carried out by exposing the Cu(111) surface, cooled to 120 K, to 30 L of CO using the "backfilling" method. The LEED analysis displayed a (√3×√3)R30°-CO structure directly after dosing, which gradually faded. This structure, which was previously observed by several groups,[3-6] is known to have a surface coverage of 0.33 ML. To check that the electrons from the LEED optics were responsible for the desorption of CO, the crystal was moved vertically downwards by a few millimetres and the (√3×√3)R30°-CO structure reappeared. We therefore believe that these observations are consistent with the electron induced desorption of CO from the Cu(111) surface.

4.2.2.2 NIXSW Analysis of the Pure (√3×√3)R30°-CO Structure

The object of using NIXSW in Surface Science is to determine the distance of an atom from a reflecting plane and to establish the adsorption site occupied by this atom.[7] The technique of NIXSW has been described in more detail in Chapter 2. The determination of the positions of oxygen atoms using the NIXSW technique available at the beamline 6.3 at the Daresbury Laboratory is possible as demonstrated by previous work carried out by our group.[8,9] However, the experimental set-up of this beamline did not allow us to obtain the NIXSW profiles of carbon. This is because at the energy of the standing wave (≈ 2972 eV), the cross-section for the ionisation of the C (1s) electrons is too small to produce a detectable photoelectron flux (SNR insufficient). Therefore the structure of CO within the (√3×√3)R30° overlayer was probed by determining the position of the oxygen atoms using NIXSW. This involved monitoring the intensity of the oxygen 1s photoelectrons rather than Auger electrons which provided X-ray absorption profiles with the best SNR. Previous studies performed by our group also showed that using a Q-factor of 0.25 for oxygen was an appropriate value.[8,9]

Prior to collecting oxygen data, copper profiles were obtained from the clean substrate. Collecting substrate NIXSW profiles has two functions, firstly from them the energy spread (ΔE) of the incident X-rays and Bragg energy of the standing wavefield can be determined. Both of these values are then used as non-adjustable parameters in the fitting of adsorbate profiles. The values for ΔE and Bragg energy can also be determined from the reflectivity (the incoherent standing wavefield) which is measured in conjunction with the profile. The second purpose of collecting substrate profiles is to confirm crystal quality, the profiles collected were fitted to a distance D = 0.00 Å and a coherent fraction f_{co} = 0.85, values expected for a well ordered surface.

Fig. 2 shows the experimental NIXSW data of the oxygen 1s photoelectron collected in the (111) and ($\bar{1}$11) reflecting plane (black lines). Also plotted are the fits for the profile (red lines). The coherent fraction and coherent position, derived from the modelling of the experimental profiles, are provided in Table 1. The fitted (111) profile gives D = 0.94 ± 0.05 Å and f_{co} = 0.79 ± 0.05. The relative high coherent value f_{co} indicates that CO adopts on Cu(111) one distinct adsorption site. However, a D value of 0.94 Å is clearly too short to be the height of oxygen above the (111) plane which passes through the unrelaxed surface, considering that CO normally bonds to transition metal surfaces C end down. In NIXSW experiments, hypothetical scattering planes are formed by the standing wave propagating outwards from the bulk crystal, as the periodicity of a standing wave is equal to a lattice spacing (2.08 Å in the case of Cu(111)). If a distance of 2.08 Å is added to the current D value, the oxygen atom would be in a more realistic 3.02 ± 0.05 Å above the surface. Moreover, by assuming that the oxygen is 3.02 Å above the (111) plane, the expected D($\bar{1}$11) values for O occupying an atop, bridge and three fold hollow sites (FCC and HCP) can be determined. Table 2 provides the calculated expected values, compared with the experimental one. The comparison clearly shows that the experimental ($\bar{1}$11) D of 0.79 ± 0.05 Å and f_{co} of 0.90 ± 0.05 Å are closest to the values expected for the occupancy of atop sites (D = 1.01 Å and f_{co} = 0.79). It may appear counter-intuitive that the ($\bar{1}$11) f_{co} is larger than that observed with the (111) planes, since it would be expected that the low frequency frustrated rotational mode of the CO molecule would cause a greater reduction in the ($\bar{1}$11) f_{co} than for the (111) value. However we do not believe that the apparent

difference is significant, since the observed ($\bar{1}11$) f_{co} value of 0.90 ± 0.05 is just outside experimental error of the value predicted (0.79 ± 0.05) from the (111) data. To summarise, the NIXSW data collected for the (√3×√3)R30°-CO structure formed on Cu(111) is consistent with an atop adsorption site for CO and a Cu–O separation of 3.02 Å.

Table 1. *Values for D and f_{co} obtained from fitting the oxygen NIXSW (111) and ($\bar{1}11$) profiles for CO in pure overlayers.*

Reflecting Plane	D / Å	f_{co}
(111)	0.94 ± 0.05	0.79 ± 0.05
($\bar{1}11$)	0.79 ± 0.05	0.90 ± 0.05

Table 2. *Comparison made between the experimental ($\bar{1}11$) D and f_{co} values for CO in pure overlayers and those that would be expected for atop, bridge and threefold hollow (FCC and HCP) sites for the molecules, given the observed (111) values.*

	Atop	Bridge	FCC	HCP	Experimental
D($\bar{1}11$) / Å	1.01	2.07	2.39 (0.31)	1.70	0.79
f_{co}	0.79	0.26	0.79	0.79	0.90

Fig.2. *Oxygen NIXSW (111) and ($\bar{1}11$) profiles (black lines) collected from pure ($\sqrt{3}\times\sqrt{3}$)R30°-CO surface. The fits for the profile are also shown (red lines).*

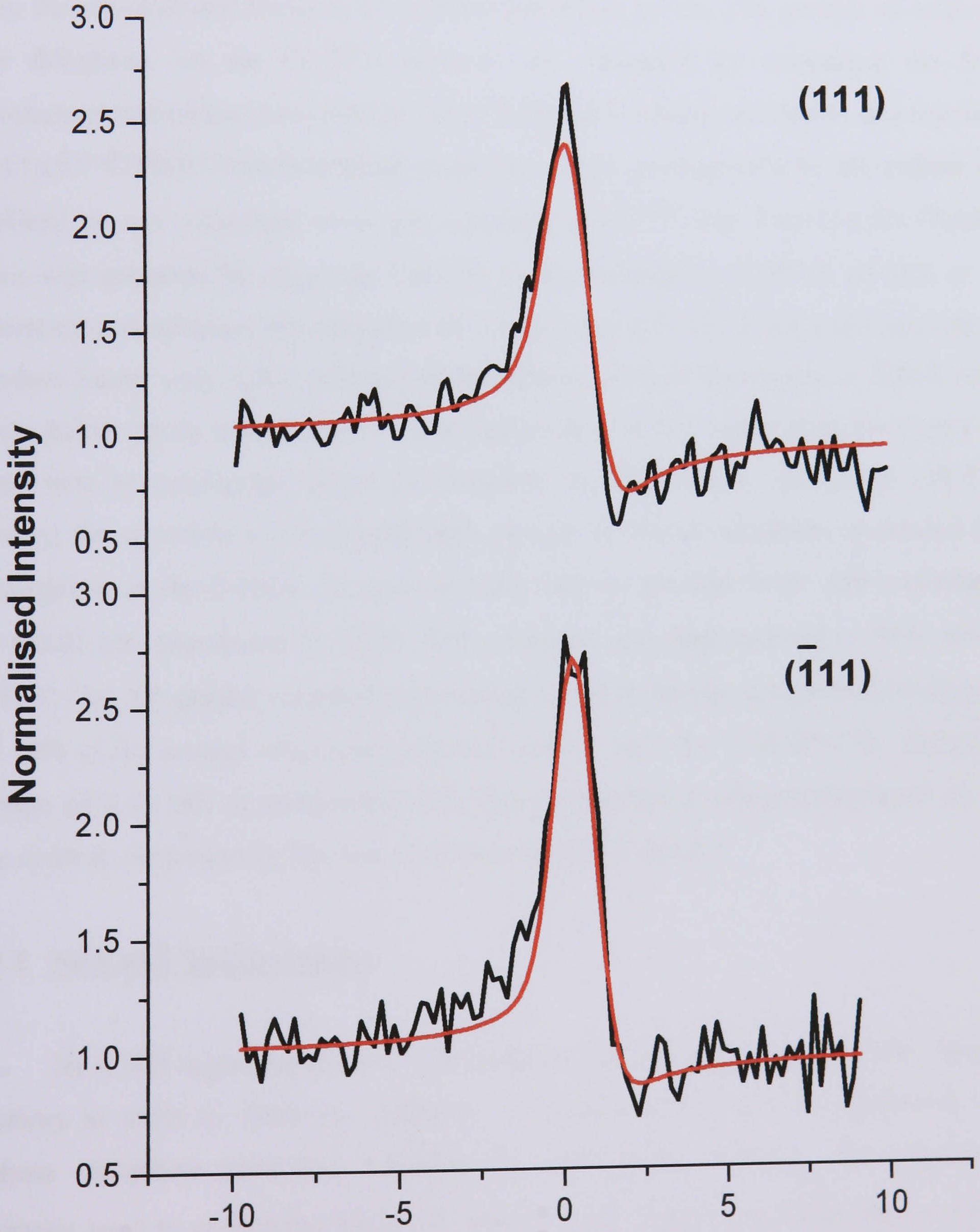

4.2.3 Structural Studies of Coadsorbed Overlayers

4.2.3.1 Preparation of CO and Thiophene Coadsorbed Overlayers

In the present study, we have been concerned only with the effects of coadsorbed CO on the structure and bonding of α-phase thiophene layers. The amount of sulfur, and hence thiophene, on the Cu(111) surface was calibrated by comparing the S (1s) photoelectron intensities (measured by XPS) from the thiophene overlayers and that from a Cu(111)($\sqrt{7}\times\sqrt{7}$)R19°-S surface which possesses a total coverage of 0.43 ML (where 1 ML is defined as one adsorbate atom per substrate atom).[10] The Cu(111)($\sqrt{7}\times\sqrt{7}$)R19°–S surface was prepared by exposing Cu(111) to approximately 18,000 L of H_2S at room temperature and subsequently annealing the single crystal to 623 K for a few seconds. This procedure leaves only sulfur adatom on the surface, as H_2S dissociates at 200 K and H_2 desorbs below room temperature.[11] The thiophene and CO coadsorbed overlayers were formed first by condensing layers of thiophene on the Cu(111) surface at 120 K and annealing the crystal to a temperature high enough to desorb thiophene condensed layers and thiophene in the β-phase, in order to leave only an α-phase layer with a coverage of 0.10 ± 0.01 ML (monitored by XPS). This overlayer was then exposed to 30 L of CO at 120 K. O (1s) XP spectra collected post-dosing revealed that the coadsorbed overlayer has 56 ± 10% of the amount of oxygen contained within the ($\sqrt{3}\times\sqrt{3}$)R30°–CO , indicating a coverage of 0.19 ML of coadsorbed CO. The coadsorbed overlayers displayed no long-range order as evidenced by the lack of an ordered LEED pattern.

4.2.3.2 NEXAFS Measurements

NEXAFS experiments were also performed at the beamline 6.3 of the Daresbury laboratory in order to study the influence of coadsorbed CO on the orientation of the α-phase thiophene molecules adsorbed on the Cu(111) surface. The experimental geometries used to collect the NEXAFS spectra were identical to those used in NIXSW experiments. Grazing (19.5°) NEXAFS were collected in the ($\bar{1}$11) NIXSW geometry, while normal (90°) NEXAFS spectra were collected using the (111) geometry. Prior to CO

dosing, NEXAFS experiments were carried out on the pure α-phase thiophene overlayer. The NEXAFS measurements, which are based on the monitoring of the yield of the S($KL_{2,3}L_{2,3}$) Auger electrons as the energy of the incoming photons is scanned through the S K-edge, are displayed in Fig. 3(a). The results of these measurements are similar to those obtained in previous investigations of thiophene on Cu(111) by our group.[1,2] In this earlier work it was established that thiophene NEXAFS spectra can be deconvoluted into six peaks, which are pre-π*, π*, σ* and three other resonances (labelled a, b and c and corresponding to S(1s) → S(4s), S(1s) → S(4p) and S(1s) → S(5s) transitions respectively).[2] If we follow the assignment previously made, the dominant bands present in Fig. 3(a) at photon energies of 2468.3 eV at grazing incidence and 2469.2 eV at normal incidence are due to S(1s) → π* and S(1s) → σ* (C-S) transitions, respectively. The dependencies of the σ* and π* resonances on the polarisation of the incoming X-ray, by application of the selection rules for NEXAFS experiments,[12] are indicative of thiophene adopting a flat geometry on the Cu(111) surface. As can be seen in Fig. 3(a), the π* resonance, which is most enhanced at grazing X-ray incidence and absent at normal incidence, and the σ* resonance, which shows a complete opposite dependency, confirm the flat orientation of C_4H_4S on Cu(111). Furthermore, the NEXAFS spectra collected from the coadsorbed layers are similar and display the same polarisation dependence as those collected from pure α-phase thiophene overlayers. In Fig 3(b), the most intense feature at 2468.4 eV in the grazing spectrum is dominated by a contribution from the π* resonance, whereas the most intense band situated at 2469.3 eV in the normal incidence spectrum is dominated by the σ* contribution. The polarisation dependence of the π* and σ* resonances are again consistent with thiophene adopting a flat geometry on the Cu(111) surface. In summary, the orientation of the thiophene ring is not significantly affected by the presence of coadsorbed CO.

Fig.3. *Grazing (black and blue lines) and normal incidence (red and magenta lines) sulfur K-edge NEXAFS spectra collected from (**a**) pure α-phase thiophene overlayer and (**b**) thiophene coadsorbed with CO. Also shown are the two dominant π* and σ* resonances.*

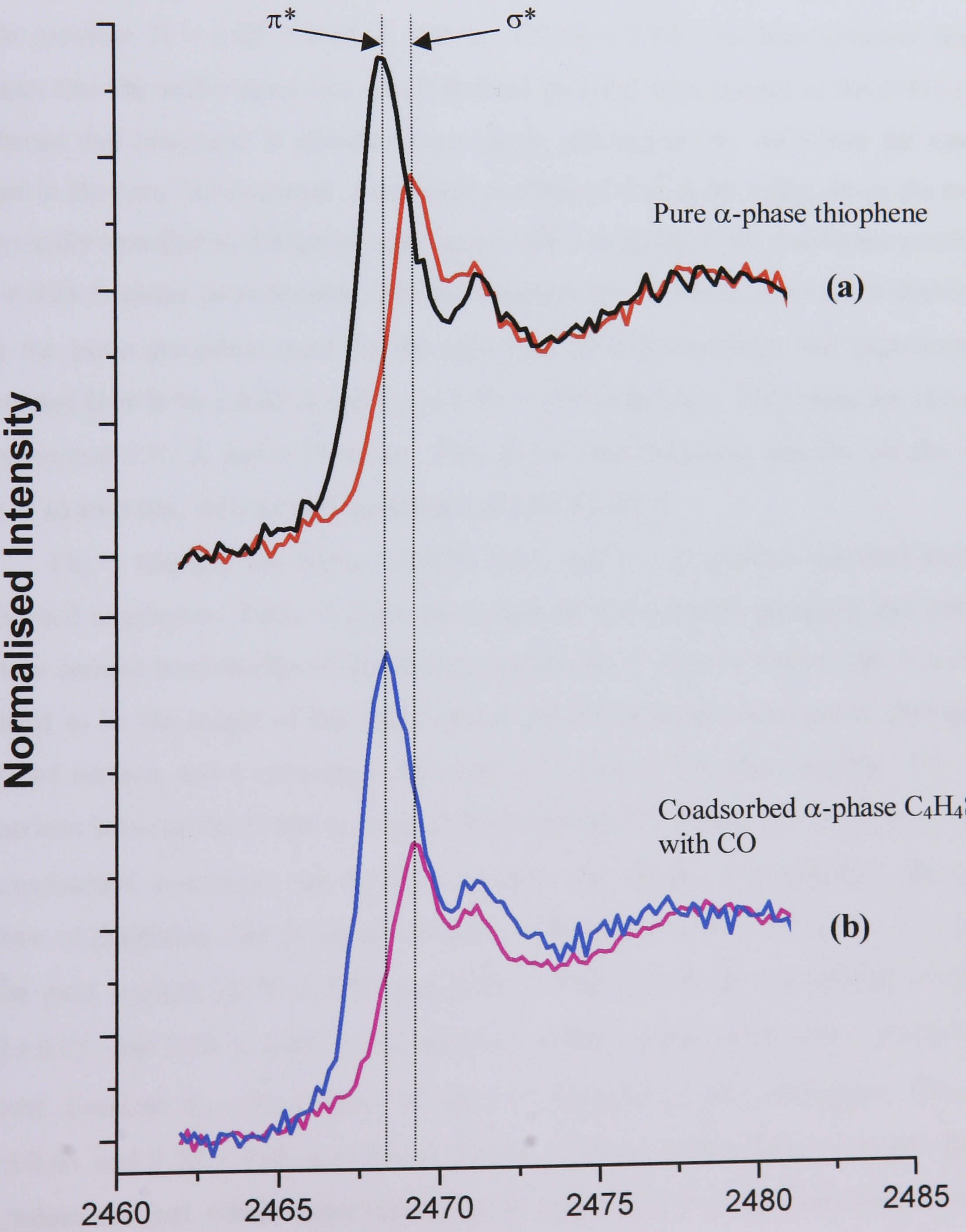

4.2.3.3 NIXSW Measurements

The NIXSW measurements of the S($KL_{2,3}L_{2,3}$) Auger electrons performed in the (111) and ($\bar{1}$11) reflecting planes on the pure α-phase thiophene overlayer are depicted in Fig. 4. The results of these measurements are in good agreement to those obtained in previous studies of thiophene on Cu(111) by our group.[1,2] The coherent position and coherent fraction for sulfur in the current study are tabulated in Table 3. The fit of the (111) profile provides D = 0.62 ± 0.05 Å and f_{co} = 0.79 ± 0.05. The high coherent fraction indicates that the sulfur atom has a well defined position with respect to the (111) plane, and hence that thiophene is adsorbed on a single adsorption site. As it was the case for oxygen in the pure CO overlayer, a coherent position of 0.62 Å for sulfur above the surface is physically unrealistic. If a lattice spacing of 2.08 Å is added to D, a coherent position of 2.70 ± 0.05 Å seems more feasible. The local registry of the sulfur atom can be determined using the same procedure used for the (√3×√3)R30°-CO overlayer. The experimentally determined D of 0.94 ± 0.05 Å and f_{co} of 0.74 ± 0.05 Å for the ($\bar{1}$11) plane are closest to the respective 0.90 Å and 0.79 values. This shows that thiophene adsorbs via the sulfur atom in an atop site, with a Cu–S separation of 2.70 ± 0.05 Å.

Fig. 5 displays the sulfur NIXSW (111) and ($\bar{1}$11) profiles obtained from the coadsorbed overlayers. Table 5 gives the values of the coherent positions and coherent fractions derived from the fits of the profiles. Again, the D value of 0.64 ± 0.05 Å is clearly too short to be the height of the sulfur above the (111) plane which passes through the unrelaxed surface, and a coherent position of 2.72 ± 0.05 Å is more realistic. The direct comparison between the D and f_{co} derived from the NIXSW profiles for the pure α-phase and coadsorbed overlayers can be used to study the effects of coadsorbed CO on the structure of thiophene. The D values obtained with respect to the (111) and ($\bar{1}$11) planes for the pure α-phase (2.70 ± 0.05 and 0.94 ± 0.05 Å) and the coadsorbed overlayers (2.72 ± 0.05 and 0.70 ± 0.05 Å) are identical within experimental error. Similarly, the coherent fractions f_{co} with respect to the (111) planes remain unchanged. These are 0.79 ± 0.05 and 0.70 ± 0.05 respectively for the pure and coadsorbed overlayers. Clearly, both values are just within experimental error, although the coadsorbed value is at the

lowest end of the range. However, the adsorption of CO does affect the observed f_{co} values in the case of the ($\bar{1}$11) reflecting plane. The coadsorbed value of 0.51 is significantly lower than that found for the pure overlayer (0.74). This is indicative of a greater uncertainty in the position of the thiophene parallel to the surface for the coadsorbed layer than there is in the pure overlayer. Dynamic motions or a wider distribution in the static positions of the atoms parallel to the surface can be at the origin of this uncertainty in position, brought about by the coadsorption of CO. To summarise, the D values and the high (111) f_{co} for the coadsorbed overlayers suggest that the sulfur still resides in atop sites, although the decrease in the f_{co} value with respect to the ($\bar{1}$11) reflecting plane indicates a slightly greater degree of uncertainty in the position of the S atom parallel to the surface in the presence of coadsorbed CO.

In Fig. 6 are oxygen (1s) NIXSW profiles collected from coadsorbed overlayers. The (111) D value of 0.79 ± 0.05 Å, presented in Table 7, is again too small to be the height of the oxygen atom above the (111) plane. The addition of a lattice spacing (2.08 Å) gives a more realistic D = 2.87 ± 0.05 Å. This height for the oxygen in the coadsorbed layer is less than the 3.02 ± 0.05 Å obtained for the (√3×√3)R30°-CO surface. The (111) f_{co} of 0.90 ± 0.05 determined for the oxygen in the coadsorbed layer indicates that CO adopts a single well defined adsorption site. However, the D and f_{co} with respect to the ($\bar{1}$11) plane of 0.94 ± 0.05 Å and 0.29 ± 0.05, respectively, are also different to the values obtained for the pure CO overlayer. The ($\bar{1}$11) f_{co} appears to be considerably lower than the value for the pure layer (0.90). Table 8 provides the height expected in the ($\bar{1}$11) plane for the oxygen atom in various high symmetry sites, calculated from (111) data. The experimental ($\bar{1}$11) D value of 0.94 ± 0.05 Å is close to the value expected for atop occupancy (0.96 Å), however, the observed ($\bar{1}$11) f_{co} of 0.29 is significantly lower than the expected value of 0.90. The small ($\bar{1}$11) f_{co} is clear evidence of significant uncertainty in the position of the oxygen atom with respect to the ($\bar{1}$11) planes. This increase in uncertainty can once again be ascribed to greater degrees of either static disorder or vibrational motion. We believe that an increase in static disorder with respect to the ($\bar{1}$11) plane is at the origin for the reduction in ($\bar{1}$11) f_{co}. This disorder could either stem from the occupancy of multiple adsorption sites by CO, or through the slight lateral displacement of the oxygen atom from

a "perfect" atop position probably due to adsorbate-adsorbate interactions within the coadsorbed overlayers. However, based on the high experimental (111) f_{co}, it would appear unlikely that CO resides in more than a single site. In theory, the occupancy of multiple adsorption sites would result in a greater distribution of height with respect to the (111) plane and would lead to a decrease in the (111) f_{co}. This is clearly not observed in the present case (f_{co} = 0.90). Consequently we assign the low ($\bar{1}11$) f_{co} value to a displacement of the oxygen atom away from a "perfect" atop position.

Table 3. *Values for D and f_{co} obtained from fitting the sulfur NIXSW (111) and ($\bar{1}11$) profiles for thiophene in pure overlayers.*

Reflecting Plane	D / Å	f_{co}
(111)	0.62 ± 0.05	0.79 ± 0.05
($\bar{1}11$)	0.94 ± 0.05	0.74 ± 0.05

Table 4. *Comparison made between the experimental ($\bar{1}11$) D and f_{co} values for thiophene in pure overlayers and those that would be expected for atop, bridge and threefold hollow (FCC and HCP) sites for the molecules, given the observed (111) values.*

	Atop	Bridge	FCC	HCP	Experimental
D($\bar{1}11$) / Å	0.90	1.94	2.29 (0.21)	1.59	0.94
f_{co}	0.79	0.26	0.79	0.79	0.74

Table 5. *Values for D and f_{co} obtained from fitting the sulfur NIXSW (111) and ($\bar{1}11$) profiles for thiophene in coadsorbed overlayers.*

Reflecting Plane	D / Å	f_{co}
(111)	0.64 ± 0.05	0.70 ± 0.05
($\bar{1}11$)	0.87 ± 0.05	0.51 ± 0.05

Table 6. *Comparison made between the experimental ($\bar{1}11$) D and f_{co} values for thiophene in coadsorbed overlayers and those that would be expected for atop, bridge and threefold hollow (FCC and HCP) sites for the molecules, given the observed (111) values.*

	Atop	Bridge	FCC	HCP	Experimental
D($\bar{1}11$) / Å	0.91	1.95	2.29 (0.21)	1.60	0.87
f_{co}	0.70	0.23	0.70	0.70	0.51

Table 7. *Values for D and f_{co} obtained from fitting the oxygen NIXSW (111) and ($\bar{1}11$) profiles for CO in coadsorbed overlayers.*

Reflecting Plane	D / Å	f_{co}
(111)	0.79 ± 0.05	0.90 ± 0.05
($\bar{1}11$)	0.94 ± 0.05	0.29 ± 0.05

Table 8. *Comparison made between the experimental ($\bar{1}11$) D and f_{co} values for CO in coadsorbed overlayers and those that would be expected for atop, bridge and threefold hollow (FCC and HCP) sites for the molecules, given the observed (111) values.*

	Atop	Bridge	FCC	HCP	Experimental
D($\bar{1}11$) / Å	0.96	2.00	2.34 (0.26)	1.65	0.94
F_{co}	0.90	0.30	0.90	0.90	0.29

Fig.4. *Sulfur NIXSW (111) and ($\bar{1}11$) profiles (black lines) collected from a pure α - phase thiophene surface. The fits for the profile are also shown (red lines).*

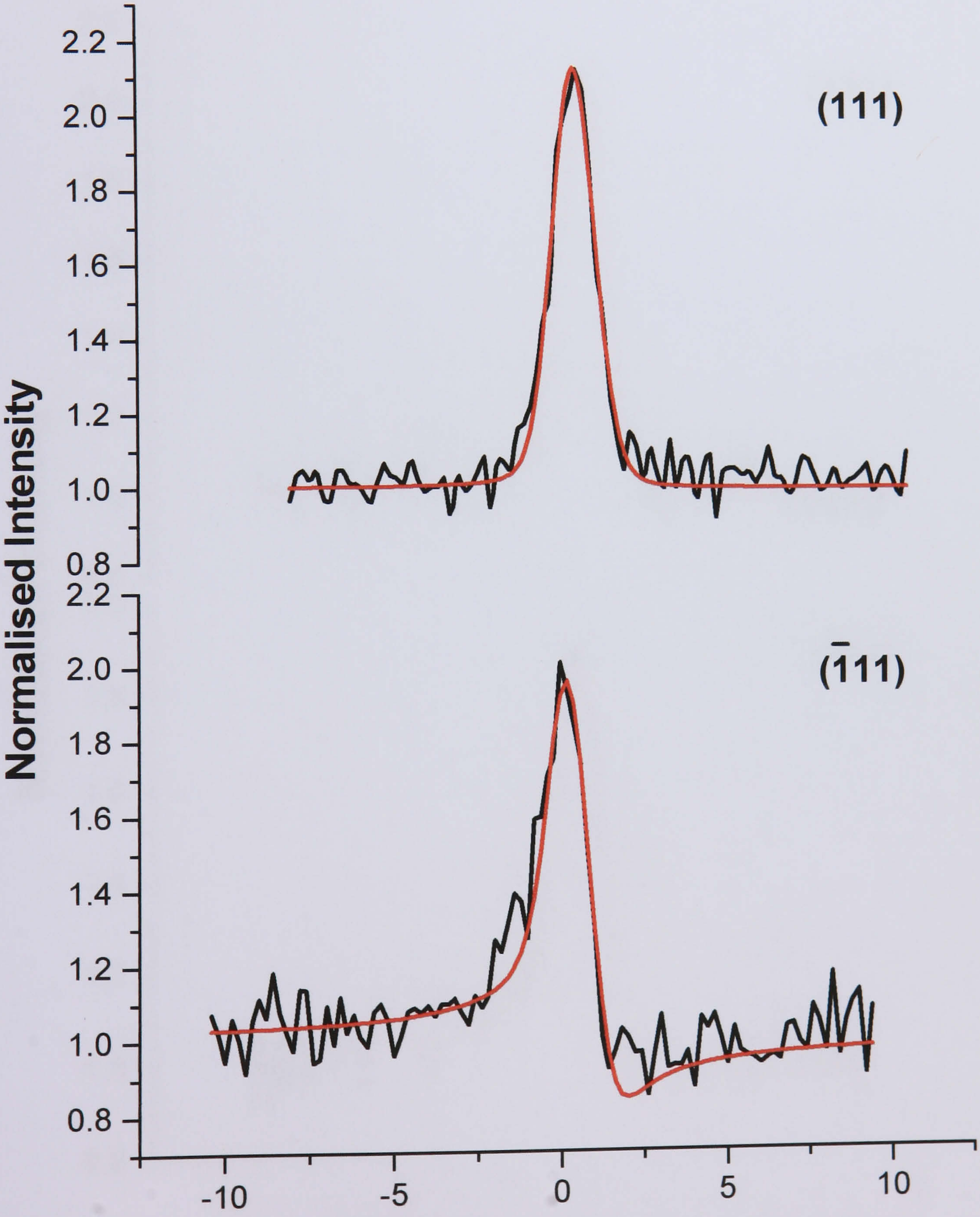

Fig.5. *Sulfur NIXSW (111) and ($\bar{1}11$) profiles (black lines) collected from a coadsorbed thiophene overlayer. The fits for the profile are also shown (red lines).*

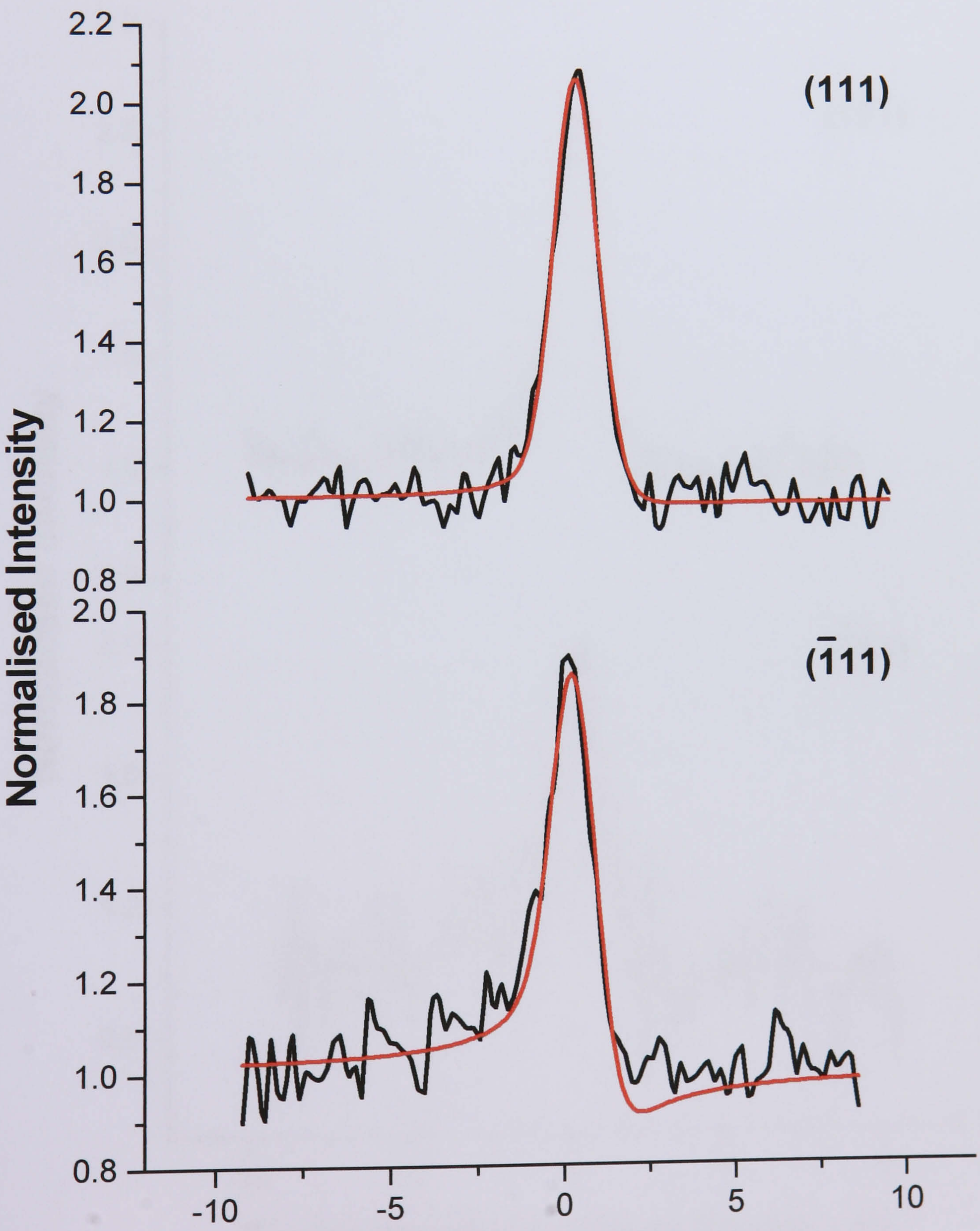

Fig.6. *Oxygen NIXSW (111) and ($\bar{1}11$) profiles (black lines) collected from a coadsorbed CO overlayer. The fits for the profile are also shown (red lines).*

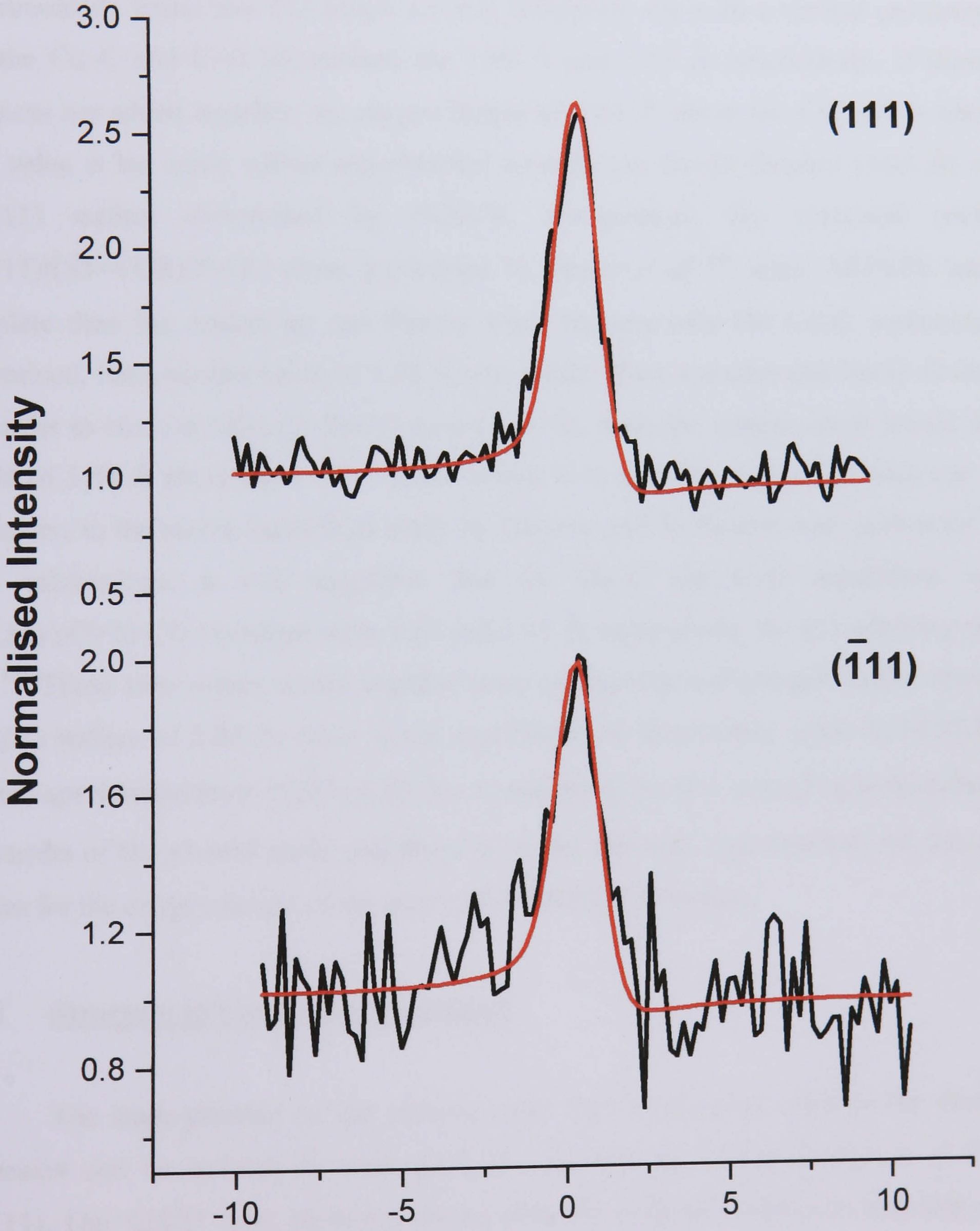

4.3 Discussion

4.3.1 Structure of (√3×√3)R30°–CO

Our results on the pure (√3×√3)R30°–CO surface are in excellent agreement with previous structural studies of CO on copper surfaces.[13–15] In the quantitative LEED analysis of the Cu(100)/c(2×2)-CO structure by Andersson and Pendry,[13] it was experimentally found that CO adopts an atop adsorption site with a vertical geometry, and that the Cu–C and C–O separations are 1.90 Å and 1.13 Å, respectively. If those two distances are added together, an oxygen height of 3.03 Å above the Cu(100) is obtained. This value is the same within experimental error to our Cu–O distance (3.02 Å) on the Cu(111) surface determined by NIXSW. Furthermore, the structural study of Cu(111)/(√3×√3)R30°-CO phase performed by Moler *et al.*[14] using ARPEFS was less complete than the Andersson and Pendry work because only the Cu–C separation was determined, but a similar value of 1.91 Å was found. If we consider that the C–O distance is similar to the Cu(100)/c(2×2)-CO case (1.13 Å), then the oxygen atom would have a height of 3.04 Å above the (111) surface which is in excellent agreement with our work. Moreover, in the recent theoretical study by Glassey and Hoffmann who performed some DFT calculations, it was suggested that the Cu–C and C–O separations of the Cu(111)/p(2×2)-CO overlayer were 1.82 and 1.13 Å, respectively, for CO adopting on atop site.[15] These two values added together give an hypothetical oxygen height above the Cu(111) surface of 2.95 Å, close to our experimentally determined value by NIXSW and within experimental error (3.02 ± 0.05 Å) . In summary, there is a good agreement between the results of the present study and those from the previous experimental and theoretical studies for the oxygen height of the pure (√3×√3)R30°-CO surface.

4.3.2 Structure of Coadsorbed Overlayer

The main purpose of the present study was to discover whether the thiophene molecules can be induced to form ordered structures by the coadsorption of CO on Cu(111). Our LEED data, however, shows that CO does not induce an ordering of the

disordered thiophene overlayer, which clearly differentiates the thiophene/CO system from coadsorption systems involving benzene and CO on other transition metal surfaces (Ni, Pt, Pd, Rh and Ru).[16–23] Several mechanisms have been proposed to explain the reordering of benzene overlayers in the presence of coadsorbed CO. In the so-called coadsorption induced ordering (CIO) model,[16] it was suggested that charge transfer from the electron donating species (benzene) to the substrate, and from the substrate to the electron withdrawing (CO) species causes the formation of anti-parallel dipoles which interact attractively and induce ordering. However, in a more recent work, Neuber *et al.* suggested that although anti-parallel induced surface dipoles may determine the structure of an ordered coadsorbate system, they may not be exclusively necessary to produce ordered structures.[17] The authors subsequently proposed that based on simple packing considerations, tightly packed repulsive bodies will naturally order to minimise their total energy. It is clear that in the current study the CO/thiophene/Cu(111) system does not form an ordered structure, and these two effects when combined are not sufficient to induce ordering within the adlayers.

The lack of CO induced ordering could be explained differently, i.e. the strain introduced into the overlayer by CO increasing the packing density could be relieved through another route. In contrast to benzene, thiophene can undergo a compression induced phase transition which involves an increase in the tilt of the thiophene ring from 26° (α-phase) to 44° (β-phase), and a lengthening of the Cu–S separation by 0.2 Å.[2] The possibility of the induction of a thiophene phase transition by CO can be readily dismissed based on the NEXAFS spectra depicted in Fig. 3. Our data clearly indicate that there is no re-orientation of the thiophene ring. Therefore the strain within the overlayers introduced by the higher degree of packing caused by the coadsorbed CO is not reduced by a compressional induced phase transition of the thiophene. Our TPD spectra presented in Fig.1(a) also show that the presence of coadsorbed CO does not drastically affect the bonding of thiophene in the α-phase to Cu(111). This argument is reinforced by our NIXSW data which indicate that the bonding of C_4H_4S to the copper surface is not perturbed, in that the small increase in the Cu–S bond length from 2.70 Å (pure layer) to 2.72 Å (coadsorbed overlayer) is not significant. Furthermore, although the greater packing caused by the coadsorbed CO does not induce a phase transition, evidence provided by

NIXSW suggests that there is some coadsorbate induced stress within the overlayer. The displacement of the sulfur atom within the coadsorbed layer from a "perfect" atop position could be readily understood in terms of relieving stress caused by the greater packing density.

The TPD spectra of CO displayed in Fig. 1(b) indicate that the strength of the CO interaction with the Cu(111) surface is not significantly affected as the desorption of CO from the coadsorbed layers occurs at a similar temperature to that observed for pure layers. The lack of change in the strength of the Cu–CO interaction is consistent with the behaviour of thiophene. If a co-operative effect was in operation between CO and thiophene one would expect that the bonding of both molecules would be influenced. It would appear unlikely that the bonding of CO would be altered and not that of thiophene. So, from the data available it would appear that there are no significant coadsorbate induced changes in the bonding of the adsorbed species. From our NIXSW data, it is apparent that the local registry of CO is affected by coadsorption to a greater extent than that of thiophene. Although the NIXSW data are still consistent with CO adopting an atop site, the small ($\bar{1}11$) f_{co} (0.29) and the smaller Cu–O separation of the coadsorbed layer (2.87 ± 0.05 Å) compared to the pure layer (3.02 ± 0.05 Å) indicate that the oxygen atom is significantly displaced from an atop position. Although the comparison made between the experimental and theoretical ($\bar{1}11$) f_{co} values for CO presented in Table 8 suggests a bridge site, we believe that the displacement of the oxygen atom could actually occur in two ways; either the CO maintains a linear geometry and is displaced significantly from an atop position, or it still adopts an atop site but has a tilted rather than linear geometry. The latter possibility is preferred based on the evidence provided by previous studies. Roke *et al.* found that coadsorbed butane can force adsorbed CO to adopt a tilted, rather than linear, geometry on Pt(533),[24] and the CO molecule was believed to be tilted by up to 42° with respect to the surface normal in this previous work. In the present study we cannot precisely determine the tilt of the CO molecule because the actual C–O bond length for the coadsorbed molecule is not known. However, a minimum angle of tilt can be calculated if we assume that the C–O bond length for the coadsorbed species is the same in the pure overlayer (1.13 Å). This value is likely to be a minimum value for the C–O separation because any charge transfer into the CO bond ($2\pi^*$) induced by coadsorption is likely to

cause a slight lengthening of the bond. Using these assumptions with simple geometry we can calculate that the CO molecule is tilted by at least by 32° (see schematic diagram in Fig. 7). An upper limit for the degree of tilt can be calculated if we assume that all known copper carbonyl complexes have a CO maximum bond length of 1.23 Å.[25] So with this unfeasible CO bond length the molecule would be tilted by 39° with respect to the surface normal. A tilted geometry for CO would also be consistent with the behaviour of high coverage ($\theta_{CO} > 0.33$ ML) pure layers. Raval *et al.* found evidence for tilted atop bound CO molecules in pure CO overlayers with coverages $0.33 < \theta_{CO} < 0.44$ ML, formed by adsorption at 95 K.[5] Against this background it would seem reasonable to summarise that the higher packing density induced by the presence of coadsorbed thiophene could cause the tilting of atop bound CO.

Fig.7. *Schematic diagram of (a) thiophene and CO in pure and (b) coadsorbed layers used to calculate the tilt angle of the CO molecules within the coadsorbed overlayers.*

(a) *Pure Thiophene and CO overlayers*

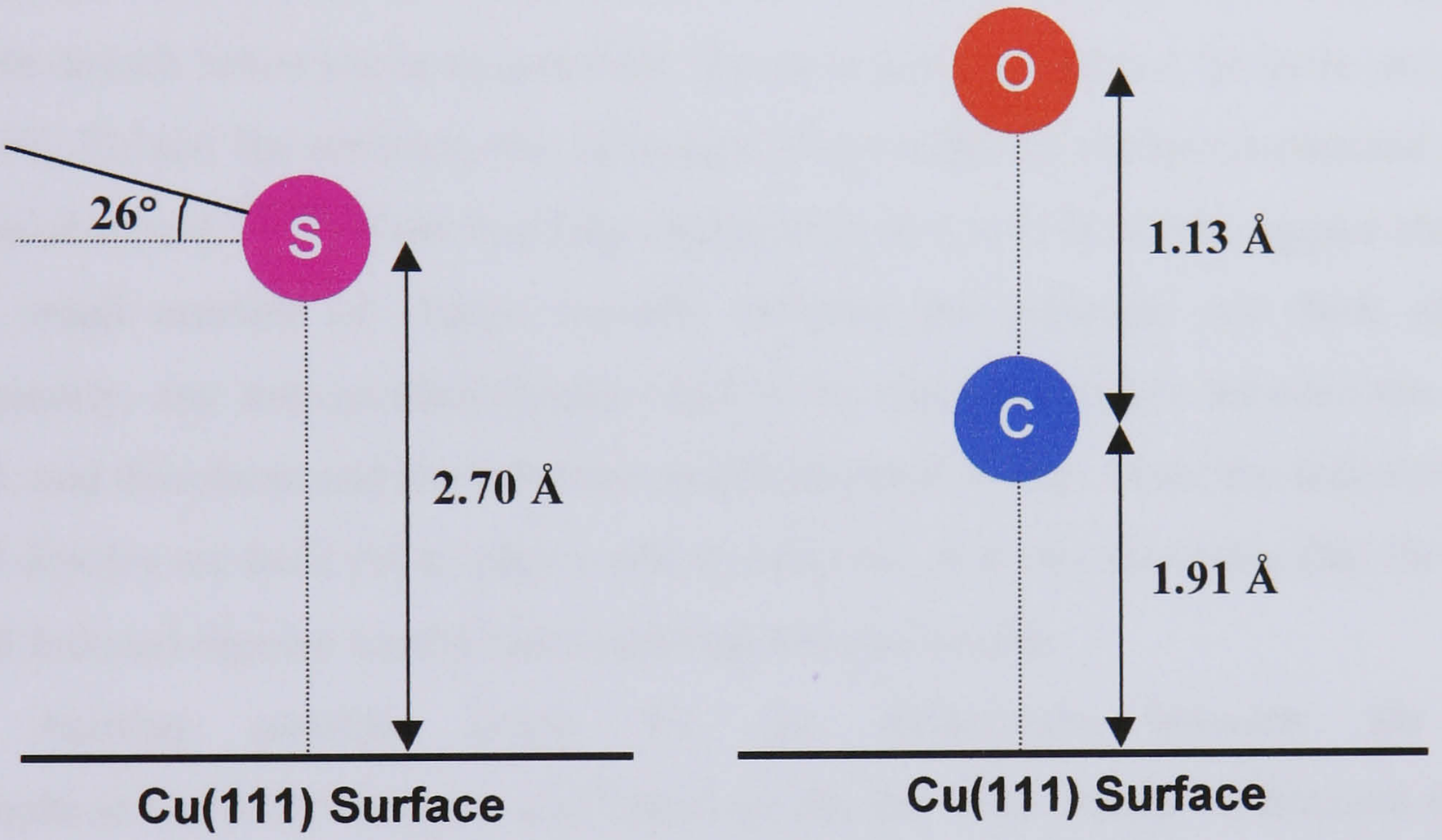

(b) *Thiophene and CO coadsorbed overlayers*

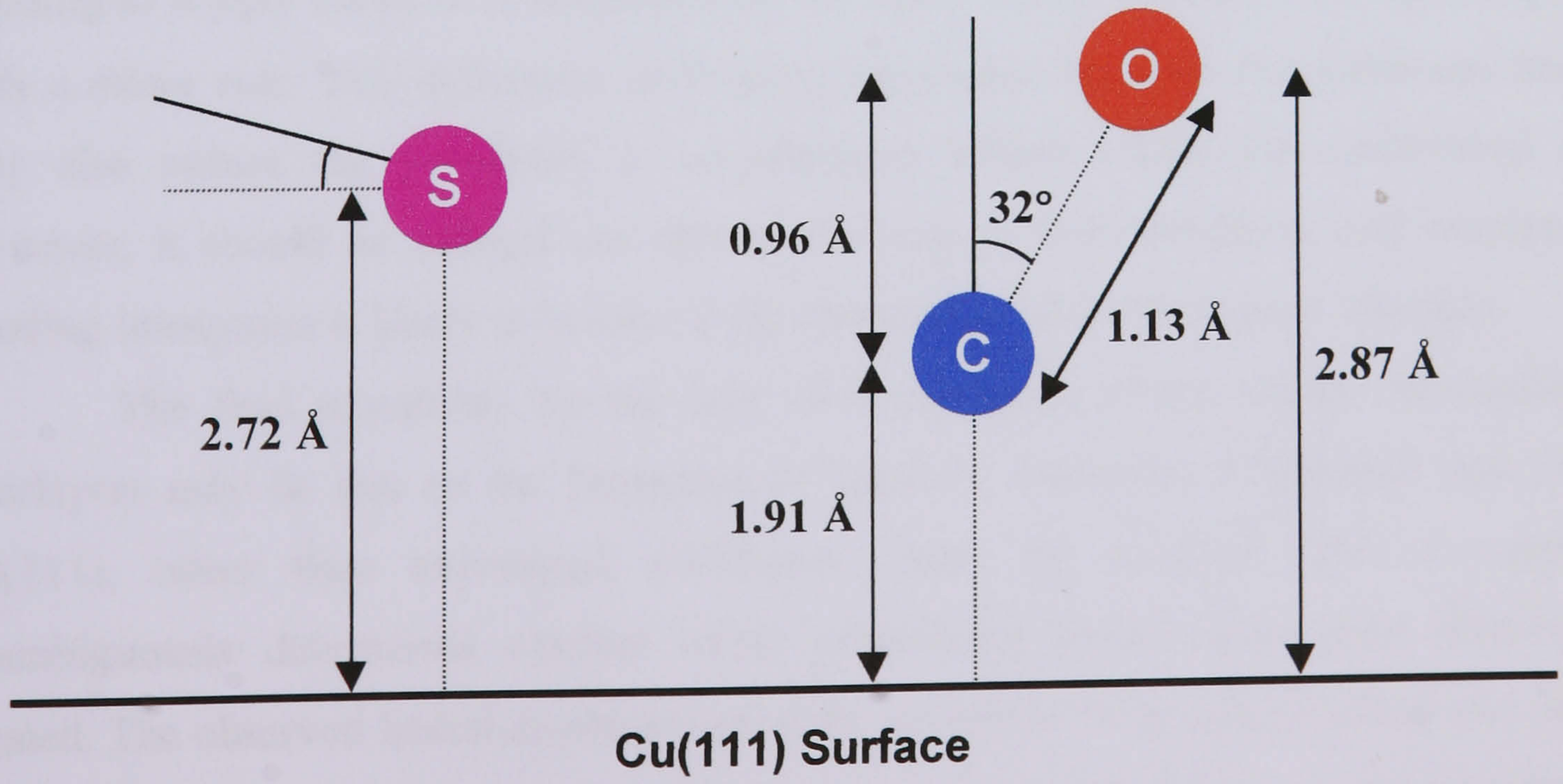

Clearly, the apparent lack of any observable co-operative effects within the thiophene/CO/Cu(111) overlayer distinguishes it from the benzene/CO coadsorbed layers observed on other transition metal surfaces. It would therefore be useful to discuss what properties of the present overlayer could be the origin for the inhibition of these co-operative effects. One possible explanation for this apparent lack of significant co-operative effects is the relatively weak bonding of thiophene and CO on Cu(111). Both CO and thiophene are only weakly chemisorbed on Cu(111), which is demonstrated by the fact that they both desorb below room temperature. Benzene and CO interact far more strongly with Ni, Pt, Pd, Rh and Ru surfaces, the substrates where ordering within coadsorbed overlayer has been observed.[16–23] Weak bonding interactions on Cu(111) would suggest that there is only a small amount of charge transfer between the substrate and both adsorbates. Consequently, any anti-parallel dipoles induced by charge transfers between the substrate and CO, and thiophene and the substrate would be small in size. Since the induction of anti-parallel dipoles are believed to play a role in ordering, it is not surprising that the presence of small induced dipoles would make ordering less favourable.

Another possible cause for the differences between the current CO/thiophene/Cu(111) overlayer and based on the previous studies of benzene systems is the different ways that thiophene and benzene bond. The bonding of benzene towards metal surfaces is dominated by the interactions of its π-system. Although thiophene is also an aromatic molecule, it has been demonstrated theoretically[26] and by our group[2] that its bonding to copper surfaces is dominated by the sulfur atom, with the π interaction playing only a minor role. This difference in bonding interaction between thiophene and benzene may also reduce the possibility of co-operative effects within the coadsorbed layer. However, it should be pointed out that in the case of both thiophene and benzene any bonding interaction is likely to involve a net charge transfer to the copper substrate.

The final possibility for the lack of co-operative effects within the coadsorbed overlayers may be due to the formation of separate domains of thiophene and CO on Cu(111), rather than intermixed overlayers. From the available data it cannot be unambiguously determined whether either intermixing occurs or separate domains are formed. The observed lateral displacement of the thiophene from a perfect atop site, and the tilting of the CO could be consistent with either an intermixed surface, or separate domains.

This is because both possible structures have greater packing densities, which we believe is the origin of the displacement of the thiophene and tilting of the CO, than the two pure overlayers separately. Although we cannot unambiguously say which of the two possible models is correct, LEED evidence tends to support the occurrence of an intermixed layer. In previous studies of coadsorbed overlayers where separate domains were believed to be formed, LEED patterns were observed and they were a combination of those displayed by pure layers of the two coadsorbates. So, if there are domains of tilted CO molecules in the current overlayer one might expect to observe a (1.5×1.5)R18° pattern, which is the structure of a pure CO overlayer which contains tilted molecules.[5] Since this pattern is not observed this suggests an intermixed overlayer rather than separate domains of CO and thiophene.

4.4 Conclusion

The most significant findings of the current study are outlined below:

1. The CO/thiophene/Cu(111) overlayer displays no coadsorbate induced ordering and both CO and thiophene desorb at temperatures similar to those observed for their pure overlayers.

2. The local registries of both thiophene and CO are not affected significantly by coadsorption. Both molecules retain atop adsorption sites within the coadsorbed overlayers, however thiophene is displaced from a "perfect" atop site and the axis of the CO molecule is tilted. Both of these effects have been assigned to higher packing densities within the coadsorbed layer than in the two separate pure overlayers.

3. It is suggested that the lack of ordering is associated with the weak bonding of the CO and thiophene to the Cu(111) surface. Such weak bonding is likely to induce only small anti-parallel dipoles within the coadsorbed species. Since these dipoles are believed to be the driving force for coadsorbate induced ordering, smaller induced dipoles are likely to make ordering less favourable.

4.5 References

1. P. Milligan, J. M°Namarra, B. Murphy, B.C.C. Cowie, D. Lennon, M. Kadodwala, Surf. Sci., 413 (1998) 166
2. P. Milligan, B. Murphy, B.C.C. Cowie, D. Lennon, M. Kadodwala, J. Phys. Chem.B, 105 (2001) 140
3. W. Kirstein, B. Krüger, F. Thieme, Surf. Sci., 176 (1986) 505
4. P. Hollins, J. Pritchard, Surf. Sci., 99 (1980) L389
5. R. Raval, S.F. Parker, M.E Pemble, P. Hollins, J. Pritchard, M.A. Chesters, Surf. Sci., 203 (1988) 353
6. B.E. Hayden, K. Kretzchmar, A.M. Bradshaw, Surf. Sci., 155 (1985) 553
7. D.P Woodruff, Progress in Surface Science, 57 (1998) 1
8. A. Sotiropoulos, P.K. Milligan, B.C.C. Cowie, M. Kadodwala, Surf. Sci., 444 (2000) 52
9. S.M. Johnston, G. Rousseau, V. Dhanak, M. Kadodwala, Surf. Sci., 447 (2001) 163
10. J.L. Domange, J. Oudar, Surf. Sci., 11 (1968) 124
11. C.T. Campbell, B.E. Koel, Surf. Sci., 183 (1987) 100
12. A.P. Hitchcock, J.A. Horsley, J. Stohr, J. Chem. Phys., 85 (1986) 4835
13. S. Andersson, J.B. Pendry, J. Phys. C Solid St. Phys., 13 (1980) 3547
14. E.J. Moler, S.A. Kellar, W.R.A. Huff, Z. Hussain, Y. Chen, D.A. Shirley, Phys. Rev. B, 54 (1996) 10862
15. W.V. Glassey, R. Hoffmann, J. Phys. Chem. B, 105 (2001) 3245
16. C.M. Mate, C.T. Kao, G.A. Somorjai, Surf. Sci., 206 (1988) 145
17. M. Neuber, F. Schneider, C. Zubrägel, M. Neumann, J. Phys. Chem., 99 (1995) 9160
18. C.M. Mate. G.A. Somorjai, Surf. Sci., 160 (1985) 543
19. H. Ohtani, M.A. Van Hove, G.A. Somorjai, J. Chem. Phys., 92 (1988) 3974
20. W. Huber, H.P. Steinrück, T. Pache, D. Menzel, Surf. Sci., 217 (1989) 103
21. E. Bertel, G. Rosina, F.P. Netzer, Surf. Sci., 172 (1986) L515
22. M.A. Van Hove, R.F. Lin, G.A. Somorjai, J. Am. Chem. Soc., 108 (1986) 2532
23. P.A. Heimann, P. Jakob, T. Pache, H.P. Steinrück, D. Menzel, Surf. Sci., 210 (1989) 282

24. S. Roke, J.M. Coquel, A.W. Kleyn, J. Chem. Phys., 113 (2000) 6376
25. Cambridge Crystallography Database
26. J.A. Rodriguez, Surf. Sci., 234 (1990) 421

Chapter 5. The Effects of Sulfur Pre-covered Cu(111) Surfaces on Saturated and Unsaturated Organic Molecules

5.1 Introduction

The adsorption of thiophene, benzene, cyclohexene and cyclohexane on clean and preadsorbed sulfur Cu(111) surfaces has been characterised by means of TPD, AES, LEED, XPS and UPS techniques. The AES, TPD and XPS analysis established that the molecules are reversibly adsorbed on all four surfaces studied. More importantly, our experimental results clearly show that the co-adsorption of sulfur influenced the bonding of each of the probe molecules to Cu(111) in particular ways. At a pre-coverage of 0.12 ML of sulfur, the desorption of thiophene and benzene in our TPD experiments is shifted to higher temperatures, clearly showing that coadsorbed sulfur at this precise coverage stabilises the adsorption of the aromatic molecules. With increasing S pre-coverage, the stabilising effects of sulfur on these two molecules diminish, and by 0.33 ML of sulfur, destabilisation of the adsorption of the aromatic molecules takes place. The stabilisation of cyclohexene was also effective but occurred at higher sulfur coverages (up to $\theta_S = 0.33\,\mathrm{ML}$). We believe that steric blocking by sulfur adatoms is responsible for the destabilisation of thiophene, benzene and cyclohexene. For the saturated cyclohexane molecule, however, stabilisation does not occur and the appearance of a new desorption peak in our TPD spectra indicates the formation of a less stable adsorption state at all sulfur coverages studied.

We postulate that the stabilisation of thiophene, benzene and cyclohexene on Cu(111) in presence of sulfur can be explained in terms of a simple electrostatic model. The formation of induced anti-parallel dipoles, which is caused by the charge transfer from the unsaturated molecules to the substrate and from the substrate to sulfur adatoms, provokes an increase of charge donation from the π-levels of the unsaturated molecules into unoccupied levels of the substrate and results in the reinforcement of the chemisorption bond strength of the π-bonded species. A similar electrostatic model can also be used to describe the destabilisation of the cyclohexane. The electrostatic field set up by sulfur, which results in the formation of induced parallel dipoles, reduces the charge transfer from the substrate to the saturated molecule (back-donation being the

principal mode of interaction between C_6H_{12} and Cu(111)) and thus destabilises the adsorption of the saturated molecule.

5.2 Results

5.2.1 Initial Characterisations: AES, LEED and UPS Studies of the S/Cu(111) System

An initial investigation of the adsorption behaviour of H_2S on Cu(111) was performed using the AES, LEED and UPS capabilities. First, AES data were collected after exposing the Cu(111) single crystal to H_2S at 300 K and subsequent annealing to 623 K. The graph depicted in Fig. 1 consists of the S(LVV)/Cu(LVV) AES peak-to-peak heights ratio as a function of H_2S exposure. As can be seen in this figure, the uptake of H_2S is rapid between 0 – 20 L and then saturates at higher H_2S exposures. The linear trend on this graph suggests a constant sticking probability below 20 L. With further H_2S adsorption, an apparent saturation of the surface occurs at approximately 100 L. Our AES data is in very good agreement with the study carried out by Campbell and Koel on the same system.[1] The authors suggested in this previous work that the adsorption of H_2S was associative below 200 K but dissociative above this temperature, with the subsequent desorption of gaseous H_2 taking place at room temperature and leaving only atomic sulfur on the Cu(111) surface. We believe that the same mechanism takes place in the current study.

LEED experiments performed in the range $0 \leq \theta_S \leq 0.33$ ML at 300 K did not show any well defined patterns which suggests that at this temperature and coverage range sulfur adatoms do not form any ordered structures on Cu(111). However, at saturation coverage, a sharp and well defined LEED pattern appears as shown in Fig. 2(b). By comparing this image with the results obtained by Domange and Oudar in the original study on the adsorption of sulfur on copper single crystal surfaces,[2] we identify this sharp LEED pattern as a Cu(111)($\sqrt{7}\times\sqrt{7}$)R19°–S structure. The use of ^{35}S radioactive tracer enabled these authors to quantify the amount of sulfur present on the surface, and it was found that at saturation there were three sulfur atoms for every seven copper atoms (or $\theta_S = 0.43$ ML). The analysis of the S/Cu AES ratio therefore enables

us to calculate the absolute coverage in ML of sulfur in further experiments involving the adsorption of S on Cu(111) from H_2S exposure.

Fig. 3 shows nested UP spectra of clean and sulfur adsorbed Cu(111) surfaces using an He(I) UV source collected at normal emission. The UPS data were taken after exposure to H_2S at room temperature and subsequent annealing to 623 K. The sulfur coverages were determined by XPS and are 0.09 ± 0.02, 0.18 ± 0.01, 0.25 ± 0.02, 0.32 ± 0.01 and 0.43 ML. The UP spectrum of the clean Cu(111) shows the copper surface state (Cu_{ss}) at 0.4 eV binding energy (BE), and two surface resonances (Cu_{res}) at 2.8 and 4.0 eV BE. The origin of these characteristic bands have been discussed elsewhere.[3] Fig. 3 also shows that the adsorption of sulfur induces noticeable changes in the region of the copper valence band. First, upon sulfur adsorption, a small decrease in intensity of the Cu_{ss} and a more pronounced decrease in intensity of both Cu_{res} occur. Second, an increase in emission in the region 4.1 - 6.0 eV BE takes place. A similar observation was previously reported by Ling *et al.*[4] and Leschik and co-workers[5] in the investigations of the p(2×2)-S structure on Cu(100) using the ARPES technique. These authors ascribed the emission peaks located at 4.7 and 5.4 eV below the Fermi level to $3p_z$- and $3p_{x,y}$-orbitals respectively. The broad feature detected in the range 4.1 – 6.0 eV BE in Fig. 3 can therefore be attributed to emission from the 3p orbitals of sulfur adsorbed on the Cu(111) surface. Third, the comparison between the clean and S - covered spectra indicates another sulfur-induced feature above the copper d-band. The feature in the region 1.4 – 1.8 eV BE was also detected by Ling *et al.*[4] and Leschik and co-workers[5] for S adsorbed on Cu(100) and was attributed to antibonding orbitals arising from the interaction between Cu 3d and S 3p electrons. A similar assignment can be made here for the S/Cu(111) complex. Finally, at a coverage of θ_S = 0.43 ML, a feature centred at *ca.* 1.3 eV BE appears in Fig. 3 and this feature coincides with the development of the $(\sqrt{7}\times\sqrt{7})R19°$–S structure. A peak at similar BE was observed by Ling *et al.* in their ARPES investigation of the p(2×2)-S phase on Cu(100),[4] and there is a general agreement that the sulfur atoms in the p(2×2) structure occupy the fourfold hollow sites of the Cu(100) surface.[6-8] Our UPS data may therefore support the structure model proposed by Foss *et al.*[10] and Jackson and co-workers[11] who suggested that in the $(\sqrt{7}\times\sqrt{7})R19°$-S phase, sulfur reconstructs the Cu(111) surface by forming one Cu_4S tetramer per surface unit mesh (see Fig. 1 of Chapter 1).

Fig.1 *Sulfur uptake on Cu(111) after H_2S exposures as monitored by the S(152eV)/Cu(918eV) AES peak-to-peak height ratio. The crystal was flashed to 623 K prior to measurement.*

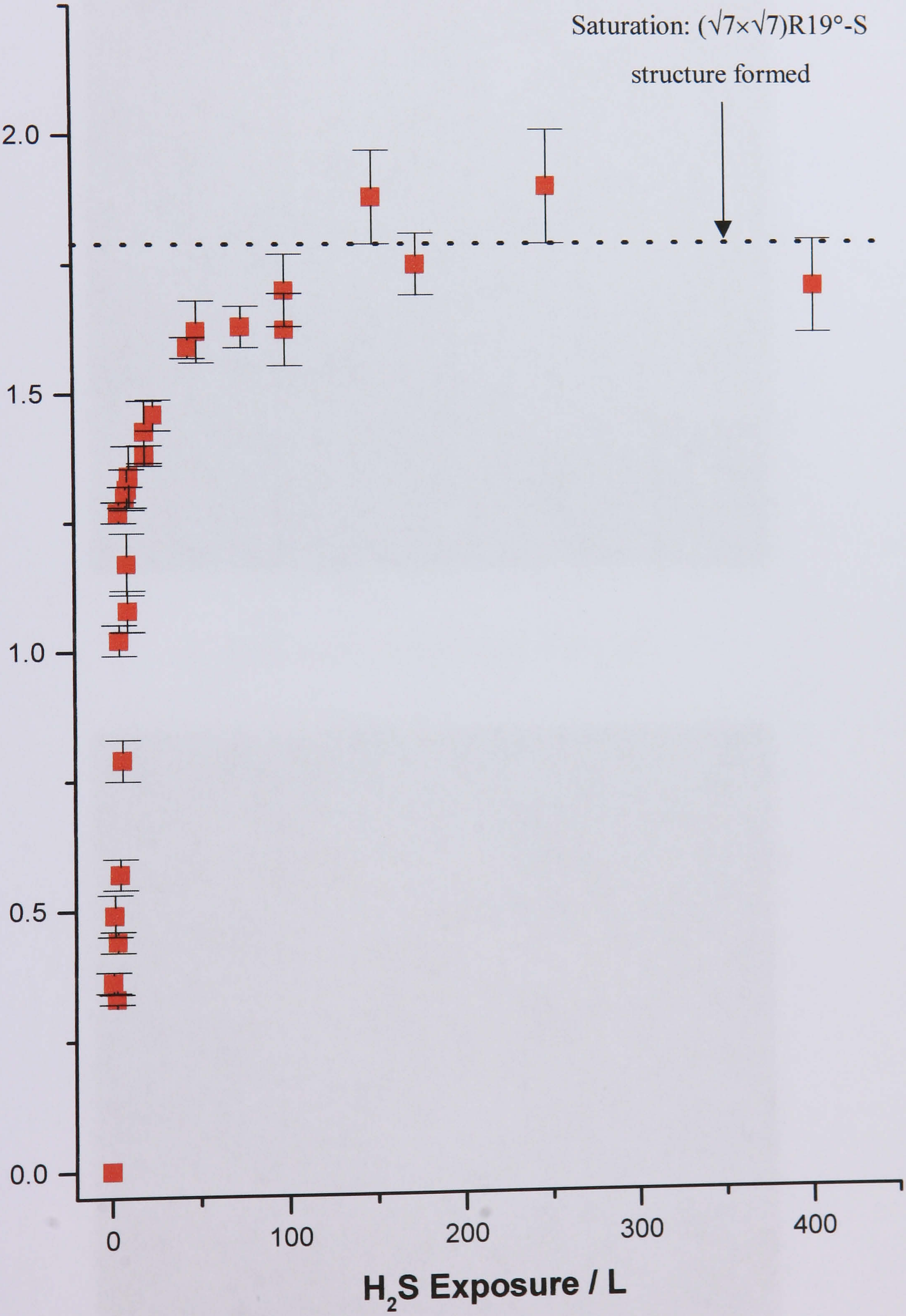

Fig.2 *LEED pattern showing (a) clean (1×1) and (b) (√7×√7)R19°-S structure.*

a) Cu(111)(1×1) (E_P = 143 eV)

b) Cu(111)(√7×√7)R19°-S (E_P = 101 eV)

Fig.3 *Normal emission UP spectra taken after H_2S exposure on Cu(111) at 300 K and subsequently flashed to 623 K. The sulfur coverages were determined by XPS; (a) 0.0 – 8.0 eV BE range; (b) expansion, 0.0 – 2.5 eV BE range.*

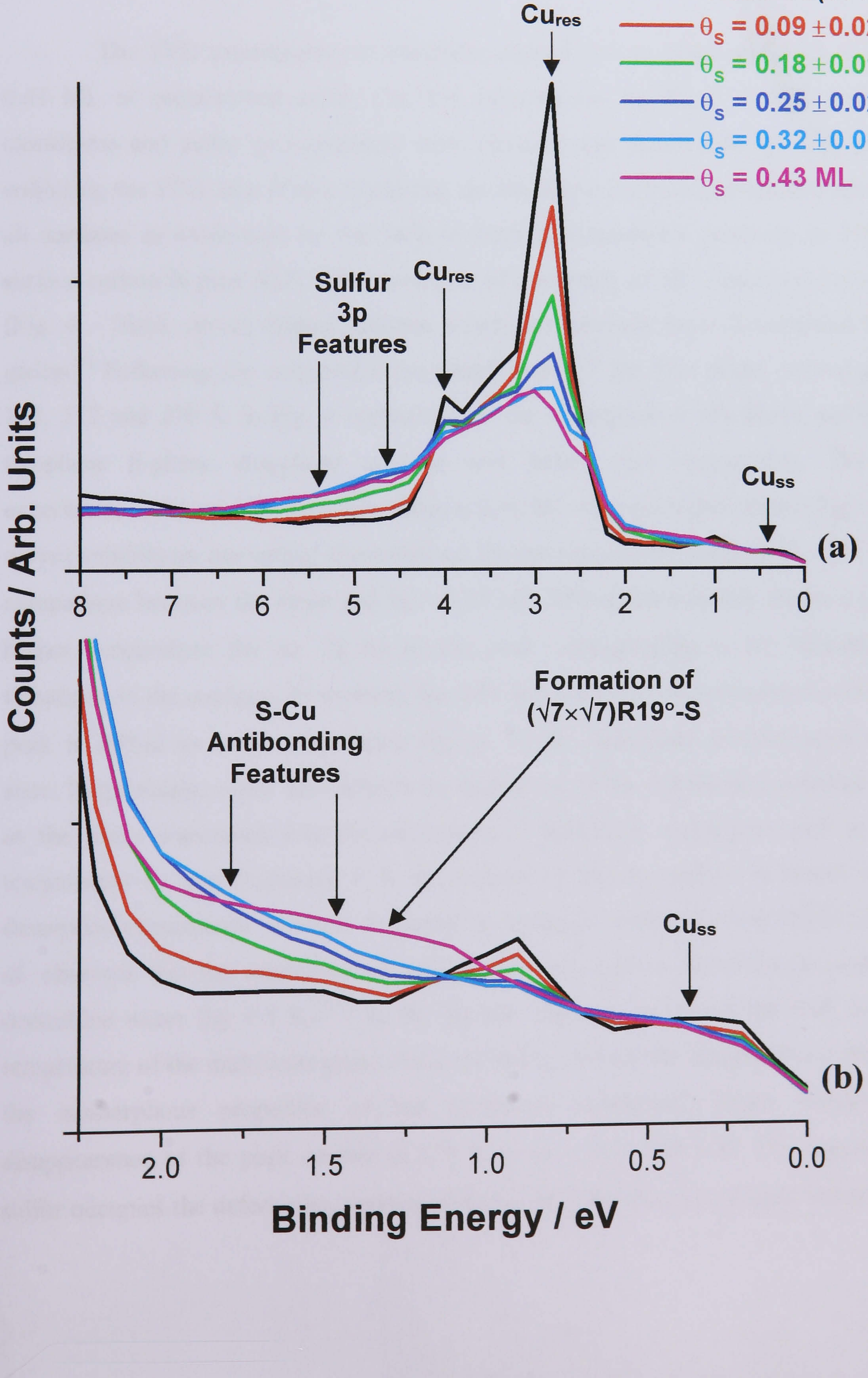

5.2.2 Influence of S on the bonding of Thiophene, Benzene, Cyclohexene and Cyclohexane

5.2.2.1 TPD Measurements

5.2.2.1.1 Thiophene TPD Experiments

The TPD experiments of thiophene carried out on clean and 0.12, 0.33 and 0.43 ML of preadsorbed sulfur Cu(111) surfaces are displayed in Fig. 4. Surface cleanliness and sulfur pre-coverages were checked and determined by AES prior to collecting the TPD data. It was found that the thiophene molecules reversibly adsorb on all surfaces as evidenced by the lack of both decomposition products in TPD and surface carbon in post AES. The adsorption of thiophene on the clean Cu(111) surface (Fig. 4 – black curve) display features which have already been investigated by our group.[9] Following the assignment previously made,[9] the four peaks centred at 145, 163, 212 and 279 K in Fig. 4 correspond to the desorption of thiophene multilayers, thiophene β-phase, thiophene α-phase and defect sites respectively. The TPD experiment of 8 L of thiophene adsorbed on 0.12 ML of preadsorbed sulfur (Fig. 4 – red curve) exhibits an interesting characteristic. In the temperature range 216 – 281 K, the comparison between the clean and θ_S = 0.12 ML TPD spectra clearly shows a shift to higher temperature (by *ca.* 22 K) of the peak corresponding to the desorption of thiophene in the α-phase. In contrast, for 0.33 and 0.43 ML of preadsorbed sulfur, this peak is shifted to lower temperature (by *ca.* 21 K), indicating destabilisation of this state. Surprisingly, sulfur also affects the formation of the thiophene condensed layers as the peaks associated with the desorption of thiophene multilayers shift to lower temperature by approximately 4 K in presence of atomic sulfur. In recent thermal desorption experiments of water deposited at cryogenic temperature on Pt(111), Kay *et al.* observed that the desorption of amorphous water occurs below the desorption of crystalline water (by 4.5 K).[12] In the present case, the origin of the shift to lower temperature of the multilayer peaks observed in Fig. 4 could be attributed to a change in the isomorphous properties of the thiophene condensed layers. Further, the disappearance of the peak centred at 279 K at θ_S = 0.33 and 0.43 ML suggests that sulfur occupies the defect sites, and the presence of sulfur does not greatly influence the

thiophene β-phase as the positions of the corresponding peaks are only shifted by ±5 K.

5.2.2.1.2 Benzene TPD Experiments

TPD experiments of benzene adsorbed on clean and 0.12, 0.33 and 0.43 ML of preadsorbed sulfur on Cu(111) were also carried out in the present study. Previous TPD experiments of benzene adsorbed on a Cu(111) surface performed by Bent *et al.*[13] showed features centred at 152, 157, 200 and 270 K, and these four desorption peaks corresponded to desorption of condensed bulk-like benzene multilayers, second physisorbed benzene layer, first weakly chemisorbed π-bonded benzene layer and desorption from surface defect sites respectively. A recent thermal desorption study of benzene adsorbed on a pseudomorphic Cu monolayer on Ni(111) by Koschel and co-workers[14] provided similar results. The TPD data of benzene adsorbed on the clean Cu(111) surface collected in our UHV system and depicted in Fig. 5 (black curve) are in excellent agreement with the two previous studies. Using the assignment previously made,[13,14] we attribute the desorption peaks centred at 153 and 201 K in Fig. 5 to desorption of benzene from the condensed and π-bonded chemisorbed benzene layers, respectively. The broadness of the features corresponding to the desorption of the first chemisorbed benzene layers was previously attributed to repulsive lateral interactions among the adsorbates bound to the surface.[13] We further assign the broad tail centred at 275 K to desorption of benzene molecules adsorbed on the defect sites. In comparison to the TPD data published by Bent *et al.*,[13] and Koschel and co-workers,[14] we are unable to differentiate the second physisorbed benzene layer peak from that of the multilayer one. As for thiophene, the TPD experiment of benzene adsorbed on 0.12 ML of preadsorbed sulfur (Fig. 5 – red curve) exhibits a shift in the desorption of first benzene chemisorbed layer to higher temperature (by 19 K). For benzene adsorbed on 0.33 and 0.43 ML of preadsorbed S, the presence of sulfur destabilises the adsorption of the benzene molecules, resulting in the desorption of the chemisorbed benzene layer shifted to lower temperatures by *ca* 35 K. The surface defect sites are also occupied by sulfur adatoms as the peak centred at 275 K progressively disappears with increasing sulfur coverage. The presence of preadsorbed sulfur leads to complicated features in the

temperature range 125 – 170 K, where both condensed and second physisorbed benzene layers could be involved. Desorption features situated *ca* 17 K below the clean surface multilayer peak for the θ_S = 0.33 and 0.43 ML spectra can be observed in Fig. 5 and could again be attributed to a change in the isomorphous properties of benzene condensed layers. From the absence of H_2 desorption signals in our TPD experiments, it was concluded that benzene does not dissociate on the four surfaces investigated.

5.2.2.1.3 Cyclohexene TPD Experiments

Similar experiments were carried out using the non-aromatic and unsaturated cyclohexene molecule. To the best of our knowledge, the temperature programmed desorption of cyclohexene adsorbed on clean Cu(111) has not been reported in the literature yet. However, the spectrum in Fig. 6 (black curve) can be compared to the recent investigation of the adsorption of cyclohexene on Au(111) by Koel and Syomin.[15] Both TPD spectra display a peak at low temperature (144 K in the current work, 143 K on Au(111))[15] which corresponds to the desorption of cyclohexene multilayers, and a second peak attributed to the desorption of cyclohexene monolayer (189 K on Cu(111), 213 K on the (111) face of Au).[15] Our TPD data shows a third broad peak centred at 260 K (not mentioned by Koel and Syomin) that we assign to the desorption from surface defects (steps, kinks, cracks, edge and screw dislocations, and terrace vacancies). The stabilising effects of 0.12 ML of preadsorbed sulfur on the adsorption of cyclohexene on Cu(111) can be observed in Fig. 6 as the peak attributed to the desorption of cyclohexene monolayer is shifted by 29 K to higher temperature. In contrast to thiophene (Fig. 4) and benzene (Fig. 5), the peak corresponding to the desorption of cyclohexene monolayer is also shifted to higher temperature (by 29 K) at θ_S = 0.33 ML (Fig. 6 – green curve). This indicates that the promotional effect of sulfur is bigger for cyclohexene, as the promotion extends to higher sulfur coverage. At a saturation coverage of 0.43 ML (blue curve), sulfur destabilises the adsorption of cyclohexene on the Cu(111) surface as cyclohexene monolayer peak is shifted to lower temperature (by 19 K when compared to the peaks of the stabilised state), and a new desorption peak centred at 175 K appears. As it was the case for thiophene and benzene,

preadsorbed S affects the adsorption of the cyclohexene multilayers and prevents the C_6H_{10} molecules from occupying to the defect sites.

5.2.2.1.4 Cyclohexane TPD Experiments

The TPD spectra for the saturated cyclohexane molecule adsorbed on clean, 0.12, 0.33 and 0.43 ML of preadsorbed S on Cu(111) are displayed in Fig. 7. For cyclohexane adsorbed on the clean surface (black curve), the position of the desorption peaks centred at 141 and 176 K are in good agreement with previous TPD studies of the same system carried out by Bent and co-workers.[16] In this previous investigation, the authors observed TPD peaks at 140 and 180 K which were attributed to desorption of multilayer and monolayer, respectively. We therefore assign the two peaks at 141 and 176 K in the present work to the desorption of cyclohexane multilayers and monolayer respectively. We also attribute the small tail in the temperature range 180 - 196 K as being the result of the desorption of C_6H_{12} from the Cu(111) defect sites. More importantly, in contrast to the three other unsaturated probe molecules, the four TPD spectra in Fig. 7 clearly show that sulfur does not have any stabilising effects on the bonding of the saturated cyclohexane molecules, as no shifts in desorption of the cyclohexane monolayer to higher temperature can be observed. However, the formation of new desorption peaks in the temperature range 151 - 172 K can be observed in Fig. 7. These new features are situated below the clean surface monolayer desorption peak and therefore suggest that a less stable adsorption state is formed for cyclohexane adsorbed on the three pre-covered sulfur Cu(111) surfaces. Fig. 7 also shows that at $\theta_S = 0.33$ and 0.43 ML sulfur quenches the defect sites as the feature centred at 188 K disappears, and once again S affects the isomorphous properties of the cyclohexane multilayer.

5.2.2.1.5 Information Obtained from Integrated Areas under TPD Spectra

The determination of the integrated areas under the TPD spectra, which are a direct representation of the number of molecules adsorbed on a surface, also provides some useful information. Tables 1 to 4 display the values of the areas under the TPD

spectra of thiophene (α-phase only), benzene, cyclohexene and cyclohexane in the temperature regions which correspond to the desorption of the first chemisorbed layers. First, Tables 1 and 2 show that the number of thiophene and benzene molecules adsorbed on Cu(111) increases from 0 to 0.12 ML of preadsorbed sulfur. This suggests that the packing density within the thiophene and benzene overlayers increases in this sulfur coverage range, and may indicate a change in the orientation of both aromatic molecules to a more upright orientation. Tables 1 and 2 also indicate that the number of adsorbed thiophene and benzene molecules reaches a maximum at 0.12 ML of preadsorbed sulfur, and for $\theta_S > 0.12$ ML, however, the number of C_4H_4S and C_6H_6 molecules present on the surface decreases. These observations are in good agreement with our TPD data which showed that $\theta_S = 0.12$ ML stabilises the adsorption of thiophene and benzene on Cu(111), and that 0.33 and 0.43 ML of preadsorbed sulfur destabilise the adsorption of the two aromatic molecules. For cyclohexene, Table 3 indicates that an increase in packing density within the cyclohexene overlayer occurs from 0 to 0.33 ML of sulfur, and also reveals that destabilisation only occurs at a sulfur pre-coverage of 0.44 ML, confirming that sulfur promotes the bonding of cyclohexene up to 0.33 ML of sulfur and destabilises the adsorption of cyclohexene at the saturation coverage. In contrast, Table 4 shows that the number of cyclohexane molecules adsorbed on the surface increases with increasing sulfur coverage. This also implies that the packing density within the cyclohexane monolayer increases with increasing sulfur coverages and may suggest that the cyclohexane molecules desorbing in the temperature range 151 – 172 K (corresponding to the destabilised state in our TPD spectra depicted in Fig. 7) are adsorbed on Cu(111) in a tilted orientation.

Table 1.*Areas under the TPD spectra of thiophene on clean and sulfur pre-covered Cu(111) surfaces in the temperature range 194 – 278 K.*

Sulfur Coverage θ_S / ML	Area under TPD ($\times 10^{-8}$) / Arb. Units
0	1.05 ± 0.02
0.12	1.31 ± 0.03
0.33	1.12 ± 0.05
0.43	0.88 ± 0.03

Table 2.*Areas under the TPD spectra of benzene on clean and sulfur pre-covered Cu(111) surfaces in the temperature range 191 – 258 K.*

Sulfur Coverage θ_S / ML	Area under TPD ($\times 10^{-8}$) / Arb. Units
0	1.18 ± 0.04
0.12	1.28 ± 0.03
0.33	0.78 ± 0.03
0.43	0.72 ± 0.02

Table 3.*Areas under the TPD spectra of cyclohexene on clean and sulfur pre-covered Cu(111) surfaces in the temperature range 153 – 236 K.*

Sulfur Coverage θ_S / ML	Area under TPD ($\times 10^{-8}$) / Arb. Units
0	0.84 ± 0.01
0.12	0.99 ± 0.02
0.33	1.01 ± 0.02
0.43	0.92 ± 0.02

Table 4. *Areas under the TPD spectra of cyclohexane on clean and sulfur pre-covered Cu(111) surfaces in the temperature range 150 – 194 K.*

Sulfur Coverage θ_S / ML	Area under TPD ($\times 10^{-8}$) / Arb. Units
0	0.92 ± 0.01
0.12	1.01 ± 0.01
0.33	1.15 ± 0.01
0.43	1.14 ± 0.02

Fig.4 *TPD spectra of 8 L of* ***thiophene*** *adsorbed on a clean Cu(111) surface and 0.12, 0.33 and 0.43 ML of preadsorbed sulfur on Cu(111); (a) 90 – 360 K temperature range; (b) expansion, 120 – 350 K temperature range.*

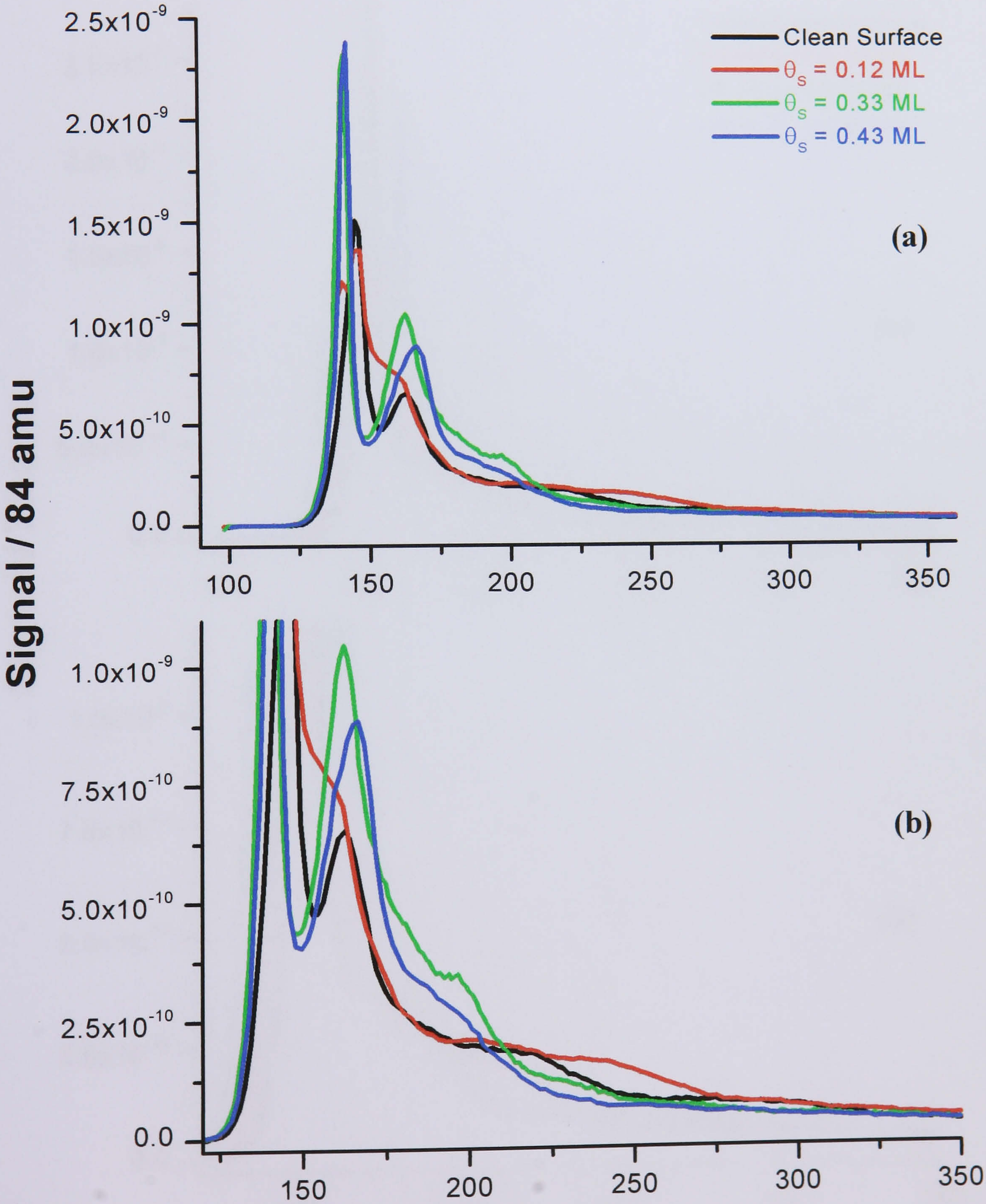

Fig.5 *TPD spectra of 6 L of* ***benzene*** *adsorbed on a clean Cu(111) surface, and 0.12, 0.33 and 0.43 ML of preadsorbed sulfur on Cu(111); (a) 90 – 360 K temperature range; (b) expansion, 120 – 350 K temperature range.*

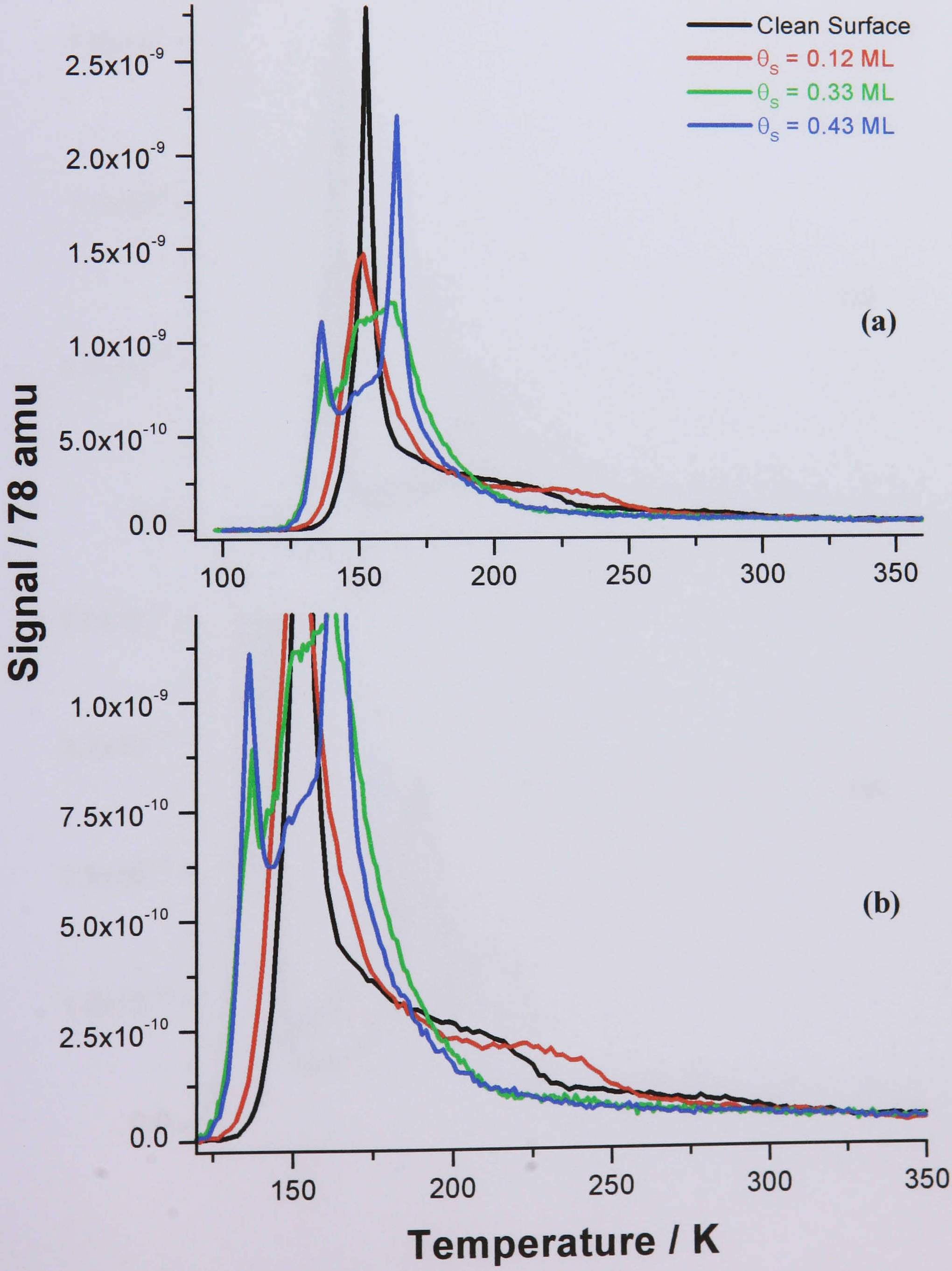

Fig.6 *TPD spectra of 12 L of* ***cyclohexene*** *adsorbed on a clean Cu(111) surface, and 0.12, 0.33 and 0.43 ML of preadsorbed sulfur on Cu(111); (a) 90 - 360 K temperature range; (b) expansion, 120 – 350 K temperature range.*

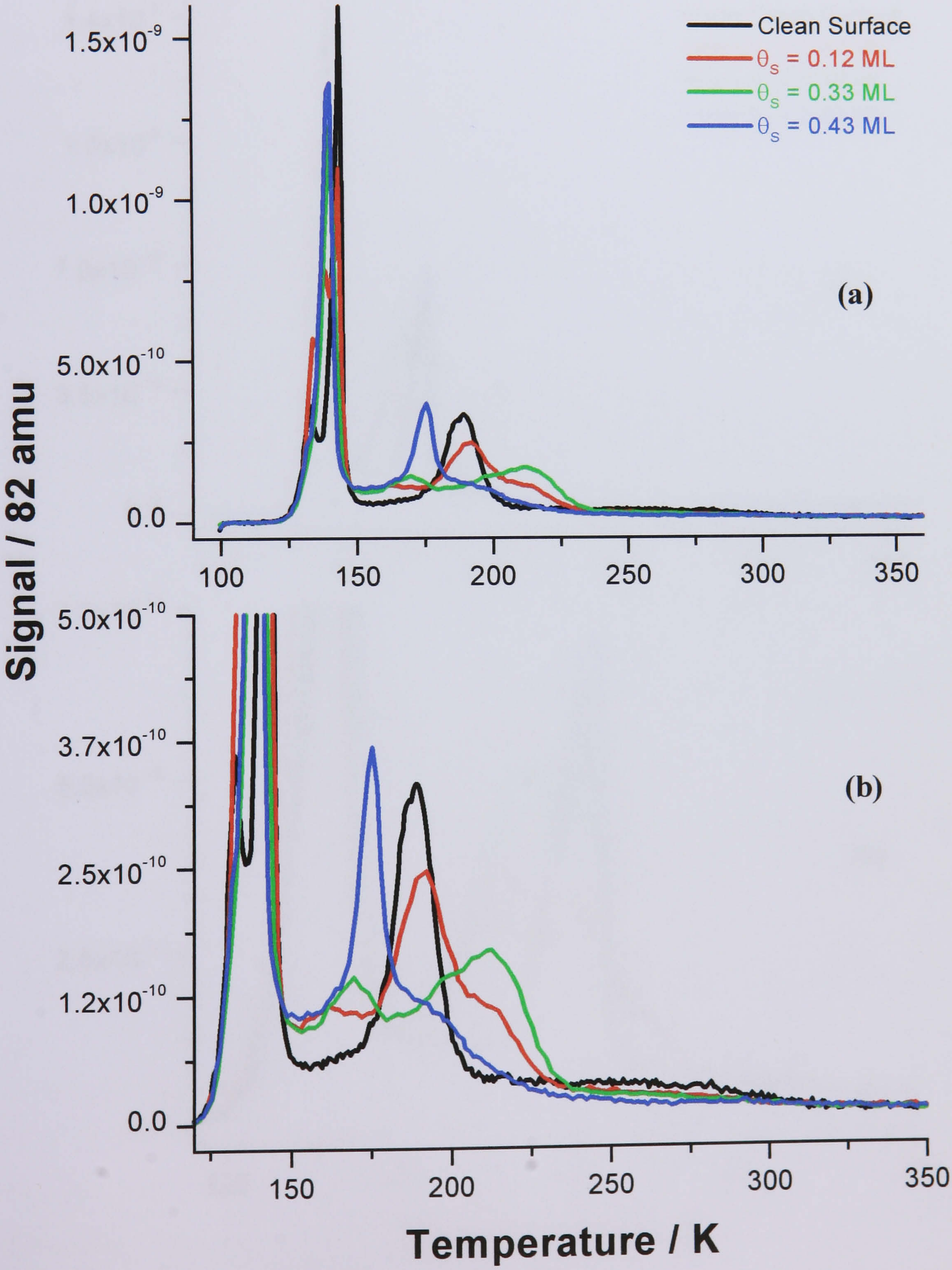

Fig.7 *TPD spectra of 12 L of* ***cyclohexane*** *adsorbed on a clean Cu(111) surface, and 0.12, 0.33 and 0.43 ML of preadsorbed sulfur on Cu(111); (a) 90 - 360 K temperature range; (b) expansion, 120 – 225 K temperature range.*

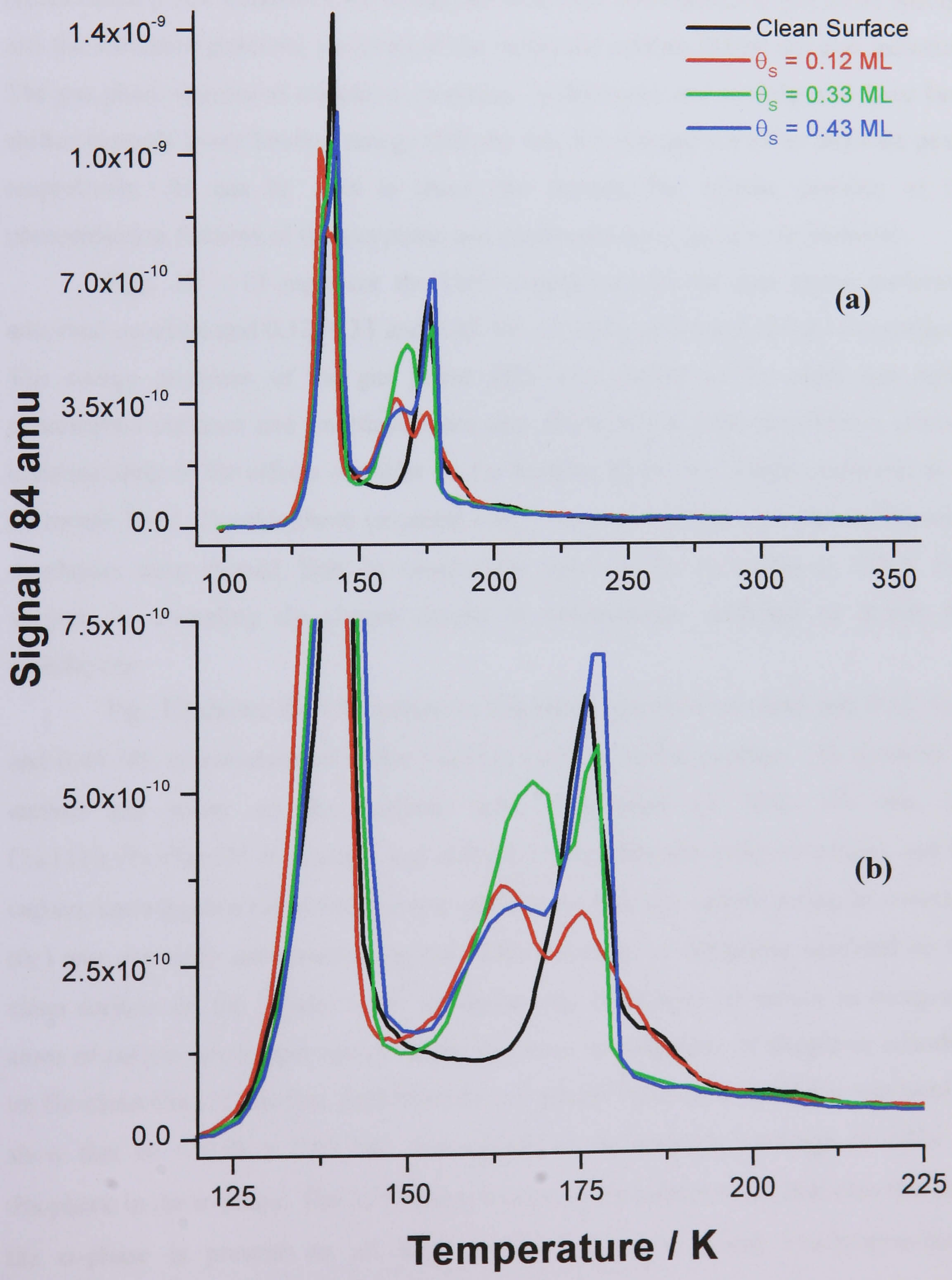

5.2.2.2 UPS Measurements

Figs. 8 and 9 show the UP spectra of thiophene, benzene, cyclohexene and cyclohexane multilayers on clean Cu(111) surfaces collected at normal emission with a photon energy of hν = 21.2 eV (He I source). The four UP spectra of the condensed layers of the probe molecules are compared with their corresponding gas phase spectra, and the ionisation potential positions of the molecular orbitals (MOs) are also indicated. The gas phase spectra of thiophene, benzene, cyclohexene and cyclohexane have been shifted towards lower binding energy (BE) by 4.8, 5.3, 4.6 and 5.8 eV to align the peaks respectively. As can be seen in these two figures, the relative position of the photoemission features of the gas phase and condensed layer spectra are identical.

Figs. 10 – 13 represent the UPS experiments of the four probe molecules adsorbed on clean and 0.12, 0.33 and 0.43 ML of sulfur preadsorbed Cu(111) surfaces. The energy positions of the gas phase MOs and spectra of the clean and sulfur preadsorbed surfaces and multilayers are also displayed in order to obtain a detailed understanding of the effects of sulfur on the bonding of the four probe molecules at an electronic level. The thiophene (α-phase only), benzene, cyclohexene and cyclohexane overlayers were formed, first, by condensing layers of the molecules at 123 K and, second, by annealing the copper crystal to temperatures sufficient to desorb the multilayers.

Fig. 10 shows the UP spectra of thiophene adsorbed on clean and 0.12, 0.33 and 0.43 ML of preadsorbed sulfur Cu(111) surfaces in the α-phase. The amounts of carbon and sulfur on the surfaces were determined by XPS. For this, the Cu(111)($\sqrt{7}\times\sqrt{7}$)±19°–S structure was utilised to determine the sulfur coverages, and for carbon, knowing that thiophene has one sulfur atom and four carbon atoms, its coverage (θ_C) was primarily calibrated using the sulfur coverage of thiophene adsorbed on the clean surface (in the present work we define one monolayer of carbon as being one atom of carbon per copper atom). In the previous investigation of thiophene adsorbed on the clean Cu(111) surface performed by our group,[9] the AES technique was used to show that θ_S = 0.08 ± 0.03 ML corresponds to the absolute coverage of sulfur of thiophene in the α-phase. The XPS data collected in the current work indicates that only the α-phase is present on all four surfaces. Also, in recent synchrotron-based investigations of the thiophene/Cu(111) complex performed at cryogenic temperature

by Imanishi *et al.*[17] and our group,[9,18] it was found that in the low coverage phase the thiophene molecule forms a π-bonded species. In the original angle-resolved photoemission study of the same system carried out at room temperature, Richardson and Campuzano[19] observed that the π-levels ($1a_2$ and $2b_1$ MOs) of the molecule experienced a bonding shift to higher binding energy. The same conclusion can be drawn in the present study. For thiophene adsorbed on the clean Cu(111) surface, the comparison between the positions of the $1a_2$ and $2b_1$ orbitals for the multilayer and overlayer spectra in Fig. 10 clearly shows that the π - levels of the adsorbed molecule are shifted to higher binding energy (by 0.5 ± 0.1 eV). The UPS experiment of thiophene adsorbed on 0.12 ML of preadsorbed sulfur also display a shift of the π – levels to higher BE, however this bonding shift corresponds to 1.0 ± 0.1 eV (see drawing in Fig. 10(b)). This indicates that the π-system of the thiophene molecules in the α-phase interacts more strongly with the Cu(111) surface in the presence of 0.12 ML of preadsorbed sulfur, in excellent agreement with our TPD data. In contrast, from the comparison of the shapes of the clean and θ_S = 0.33 and 0.43 ML spectra, no shifts in energy of the $1a_2$ and $2b_1$ π – levels are observable when compared to the condensed phase (see Fig. 10(b)). This suggests that at these pre-coverages, the presence of sulfur destabilises the adsorption of thiophene in the α-phase and significantly reduces the interaction between the π system and the substrate. Table 5 summarises the various conclusions drawn from our UPS experiments, along with the observations made in our TPD experiments, for thiophene in the α-phase adsorbed on the clean and sulfur pre-covered Cu(111) surfaces. This table illustrates the consistency between the two surface sensitive techniques employed in this work, as the stabilisation of the thiophene molecules observed in our TPD experiments is consistent with a shift to higher binding energy of the π-levels in our UP spectra, and no shift in energy coincides with the destabilisation of the adsorption of the thiophene molecules.

The normal emission UP spectra of 16 L of benzene adsorbed on clean and sulfur preadsorbed Cu(111) surfaces and annealed to 183 K in order to obtain one layer of benzene on the surfaces are shown in Fig. 11. To the best of our knowledge there have been no previous UPS studies of benzene adsorption on the clean (111) face of copper. In Fig. 11, the bar graphs, which represent the positions of the ionisation potentials of the gas phase benzene MOs, and the spectra of condensed benzene layers have been shifted by 0.4 eV towards lower binding energy in order to line up the low

lying $2a_{1g}$ levels with those of the overlayer benzene spectra. The detailed analysis of the peak positions for benzene adsorbed on clean Cu(111) reveals that the $1e_{1g}$ π-level is shifted by 0.9 ± 0.1 eV to higher binding energy. This result agrees with the previous NEXAFS and HREELS data collected by Bent *et al.* which indicated that the benzene molecules in the first layer are π-bonded to the surface.[13] The same conclusion was drawn by Koschel *et al.* for a submonolayer of benzene ($\theta_{C_6H_6}$ = 0.55 ML) adsorbed on the pseudomorphic Cu monolayer on Ni(111) using the ARUPS technique.[14] These authors observed a small bonding shift of the π-levels by 0.2 - 0.3 eV to higher BE, which also indicated that the first layer of benzene molecules were weakly π-bonded on this specific surface. Bent and co-workers[13] also suggested that the maximum surface coverage expected for a layer of coplanar benzene molecules was approximately 1.5×10^{14} molecules.cm^{-2}. The Cu-Cu nearest bond length on Cu(111) is 2.55 Å, therefore the area of the unit cell is 5.63×10^{-16} cm^2, and the coverage corresponding to one layer of flat benzene is equal to θ_C = 0.8 ML. The amounts of carbon present on the surface determined by XPS for benzene adsorbed on 0, 0.12, 0.33 and 0.43 ML of preadsorbed sulfur were $\theta_C = 0.45 \pm 0.02$, 0.51 ± 0.03, 0.35 ± 0.02 and 0.33 ± 0.04 ML, respectively. These values indicate that all the UPS experiments were performed at submonolayer coverages. More importantly, the analysis of the peak locations for benzene adsorbed on the 0.12 ML of preadsorbed sulfur Cu(111) surface in Fig. 11 shows that the $1e_{1g}$ π-level is shifted to higher binding energy, but this time by 1.1 ± 0.1 eV. As for thiophene, this specific sulfur pre-coverage induces stabilisation of the adsorption of the aromatic benzene molecules on the Cu(111) substrate. Close inspections of the benzene submonolayer spectra for θ_S = 0.33 and 0.43 in Fig. 11 demonstrate the destabilising effects of sulfur as no shifts of the $1e_{1g}$ π-levels are observable, in good agreement with TPD experiments displayed in Fig. 5. Table 6 summarises the conclusions drawn from our UPS and TPD experiments of benzene adsorbed on the clean and sulfur pre-covered Cu(111) surfaces. This table shows the correlation between the changes in desorption temperature observed in our TPD spectra and the shifts in binding energy of $1e_{1g}$ π-state deduced from our UP data.

Fig. 12 shows the UPS experiments of 16 L of cyclohexene adsorbed at 123 K on clean and 0.12, 0.33 and 0.43 ML of sulfur pre-covered Cu(111) surfaces and subsequently annealed to 178 K to leave approximately one monolayer of carbon on the

surface as monitored by the XPS technique. To our knowledge no UPS studies of the C_6H_{10}/Cu(111) system have been reported in the literature. In Fig. 12, the multilayer spectra and bar graphs, which indicate the positions of the ionisation potentials of the MOs of cyclohexene in the gas phase, have been shifted by 0.5 eV to lower BE in order to align the lowest lying nonbonding level (7a). For cyclohexene adsorbed on the clean Cu(111) surface, the comparison between the energetic positions of the 11b orbital (corresponding to $\pi_{C=C}$) of the multilayer and overlayer spectra does not show any detectable shifts to higher binding energy, which indicates that the interaction between the π-electrons of cyclohexene and the clean surface is extremely weak. However, for cyclohexene adsorbed on 0.12, 0.33 and 0.43 ML of preadsorbed sulfur, although some of the π-levels are still not shifted, we observe a shift by 0.8 ± 0.1 eV to higher BE of the same π-levels. This analysis reveals that the interactions of the π electrons with the substrate are stronger in presence of preadsorbed sulfur, and this extra bonding mechanism could explain the shift to higher temperature observed in the TPD spectra of cyclohexene, as the molecule becomes more strongly π-bonded to the surface. This results is surprising for the $\theta_S = 0.43$ ML UP spectrum, but close inspection of the TPD spectra in the region 199 - 217 K in Fig. 6 reveals that some of the cyclohexene molecules on the sulfur saturated surface (blue curve) are more strongly bonded to Cu(111) than the ones on the clean substrate (black curve). Table 7 illustrates the consistency between our UPS and TPD data, as the stabilisation of cyclohexene is consistent with a shift to higher binding energy of the 11b π-level, and no shift in energy coincides with the destabilisation of the adsorption cyclohexene. The comparison between the benzene, thiophene and cyclohexene TPD and UPS data when stabilisation occurs is also given in Table 8 and the values in this table further demonstrate the consistency between the results obtained using these two surface sensitive techniques, as the difference in BE shift is proportional to the shift in temperature.

Finally, the normal emission UP spectra of cyclohexane adsorbed on clean and 0.12, 0.33 and 0.43 ML of preadsorbed sulfur on Cu(111) are displayed in Fig. 13. 16 L of C_6H_{12} were deposited on the four surfaces at 123 K and the crystal was subsequently annealed in order to desorb the multilayers and to leave one layer of cyclohexane on the surface. The relative carbon coverages are indicated in Fig. 13 and one layer of C_6H_{12} molecules corresponds to approximately one monolayer of carbon as determined by

XPS. The annealing temperatures used to obtain $\theta_C \approx 1$ ML on the single crystal were 158 K for the clean surface and 173 K for all sulfur pre-covered Cu(111) surface. Because the annealing temperatures had to be increased by 15 K for the three S preadsorbed surfaces, this indicates that more cyclohexane molecules were adsorbed on the surface in presence of sulfur. As already suggested by the analysis of the areas under our TPD spectra (Table 8), our XPS results confirm the increase in the packing density within the first cyclohexane layer in presence of preadsorbed sulfur. In the previous EELS, RAIRS and LEED investigation of cyclohexane adsorbed on clean Cu(111) at cryogenic temperature, Raval *et al.*[20] suggested that for one monolayer of cyclohexane on the clean surface, the molecules are adsorbed in C_{3v} symmetry with the carbon skeleton of the molecule parallel to the surface and the three axial H atoms pointing directly at the substrate underneath. Because our UP spectra of all four surfaces do not show any drastic changes in the relative intensities of the photoemission peaks in the BE range 4.0 – 10.5 eV, this indicates that the UPS data collected and displayed in Fig 13 corresponds to photoemitted electrons of cyclohexane molecules adsorbed in a flat orientation following the conclusions drawn by Raval and co-workers.[20] This would mean that the peaks centred at 177 K in the four TPD spectra of cyclohexane depicted in Fig. 7 may coincide with the desorption of cyclohexane molecules adsorbed in a flat orientation. Raval *et al.*[20] also observed that with increasing cyclohexane coverage ($\theta_{C_6H_{12}} > 1$ ML) the symmetry of the molecule was subsequently reduced to C_S which was attributed to an orientational change with the cyclohexane molecules tilted towards the surface axis. Because an increase in packing density may occur with preadsorbed sulfur on the Cu(111) surfaces which would indicate a possible change in the geometry of cyclohexane to a more upright orientation, the TPD peaks observed in the region between 151 and 172 K in Fig. 7 may be due to the desorption of tilted cyclohexane molecules. Not surprisingly, Fig. 13 reveals that no stabilisation effects occur as no shifts of the MO levels to higher binding energy are observable, in good agreement with our TPD results. Interestingly, the analysis of the position of the ionisation potentials of the molecular orbitals of cyclohexane in the gas phase which have been carefully shifted to line up the nonbonding low-lying levels ($3e_g$, $3a_{2u}$) with those of the experimental UP spectra collected in the present work reveals that a difference of 0.4 eV exists between the photoemission peak positions of cyclohexane adsorbed on the clean Cu(111) surface and the C_6H_{12} molecules adsorbed on the

preadsorbed sulfur surfaces at all three sulfur pre-coverages. Because the energetic positions of all MOs change at the same time, this indicates that a change in relaxation shift in presence of preadsorbed sulfur occurs.

Fig.8 *UP spectra of (**a**) **thiophene** and (**b**) **benzene** multilayers adsorbed on clean Cu(111). The spectra were collected with photon energy of 21.2 eV (He I) and are compared with the gas phase spectra of thiophene[16] and benzene[17]. The positions of the molecular orbitals are also indicated.*

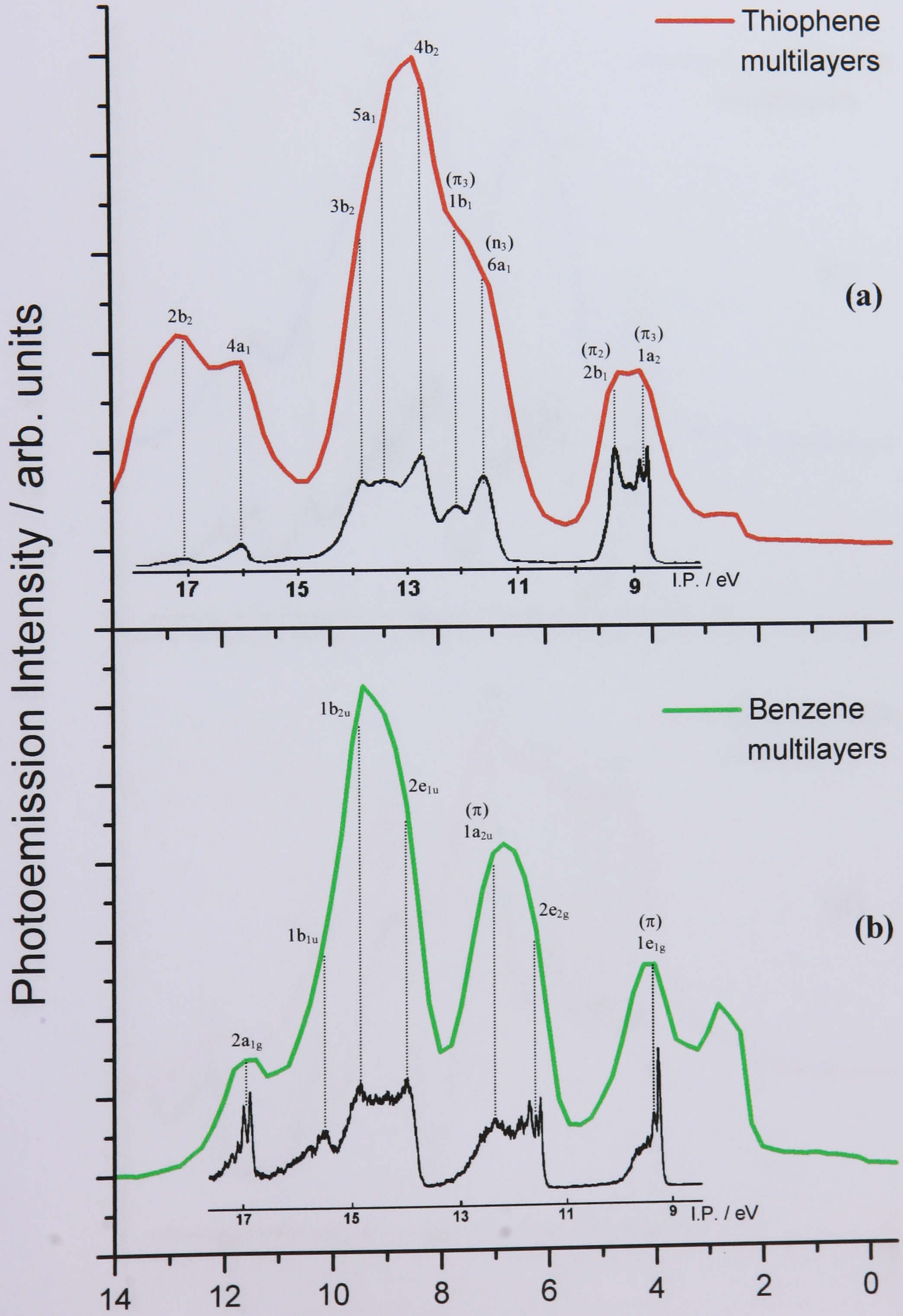

Fig.9 *UP spectra of (c)* ***cyclohexene*** *and (d)* ***cyclohexane*** *multilayers adsorbed on clean Cu(111). The spectra were collected with photon energy of 21.2 eV (He I) and are compared with the gas phase spectra of cyclohexene*[17] *and cyclohexane*[17]*. The positions of the molecular orbitals are also indicated.*

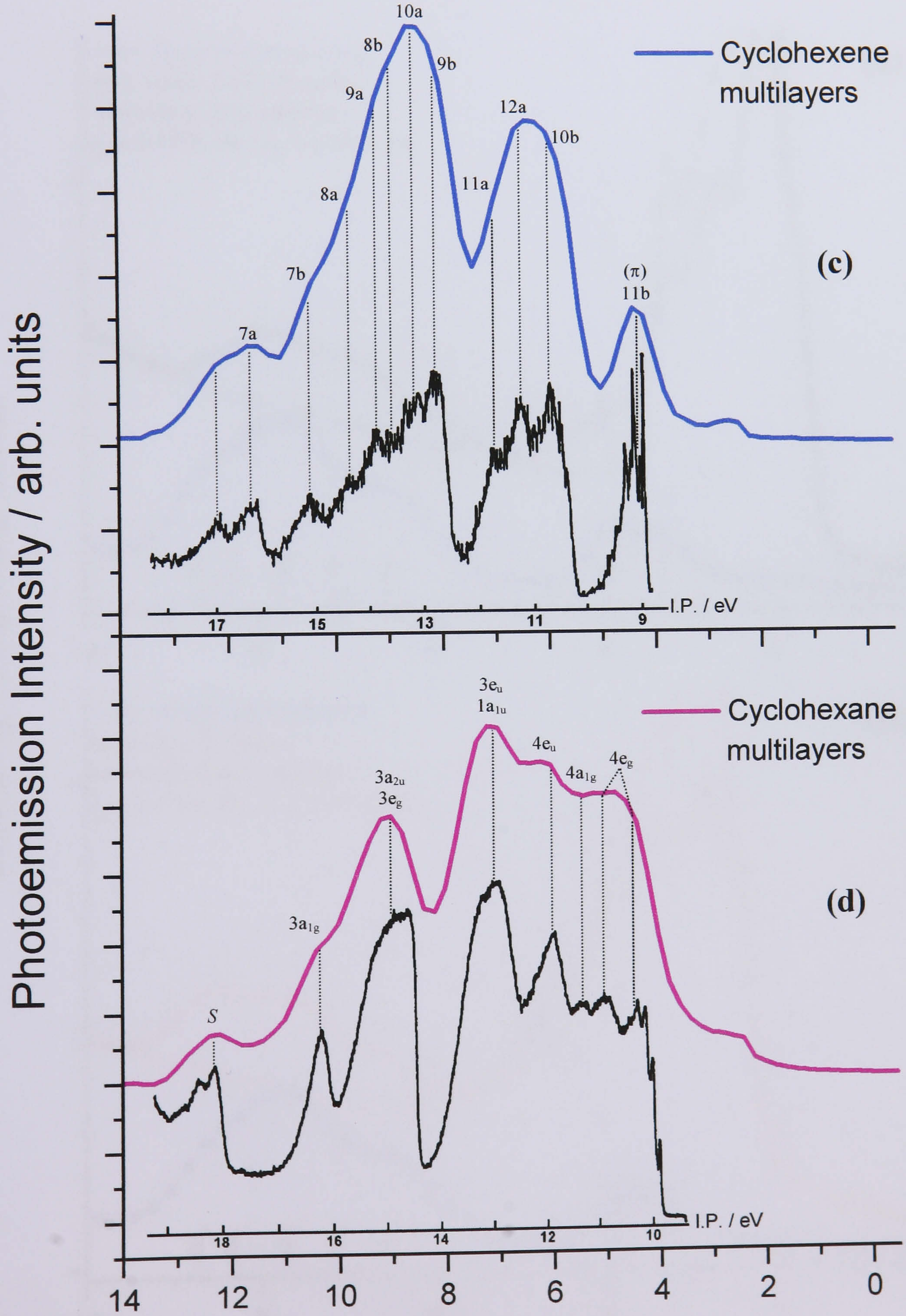

Fig.10a. *UP spectra He I ($h\nu$ = 21.2 eV) at normal emission of* ***thiophene*** *overlayer (α - phase) adsorbed on (**a**) clean and (**b**) 0.12 ML of S on Cu(111). Thiophene multilayer spectra, plotted on a different scale, are also displayed for comparison. Figures in brackets are estimated errors.*

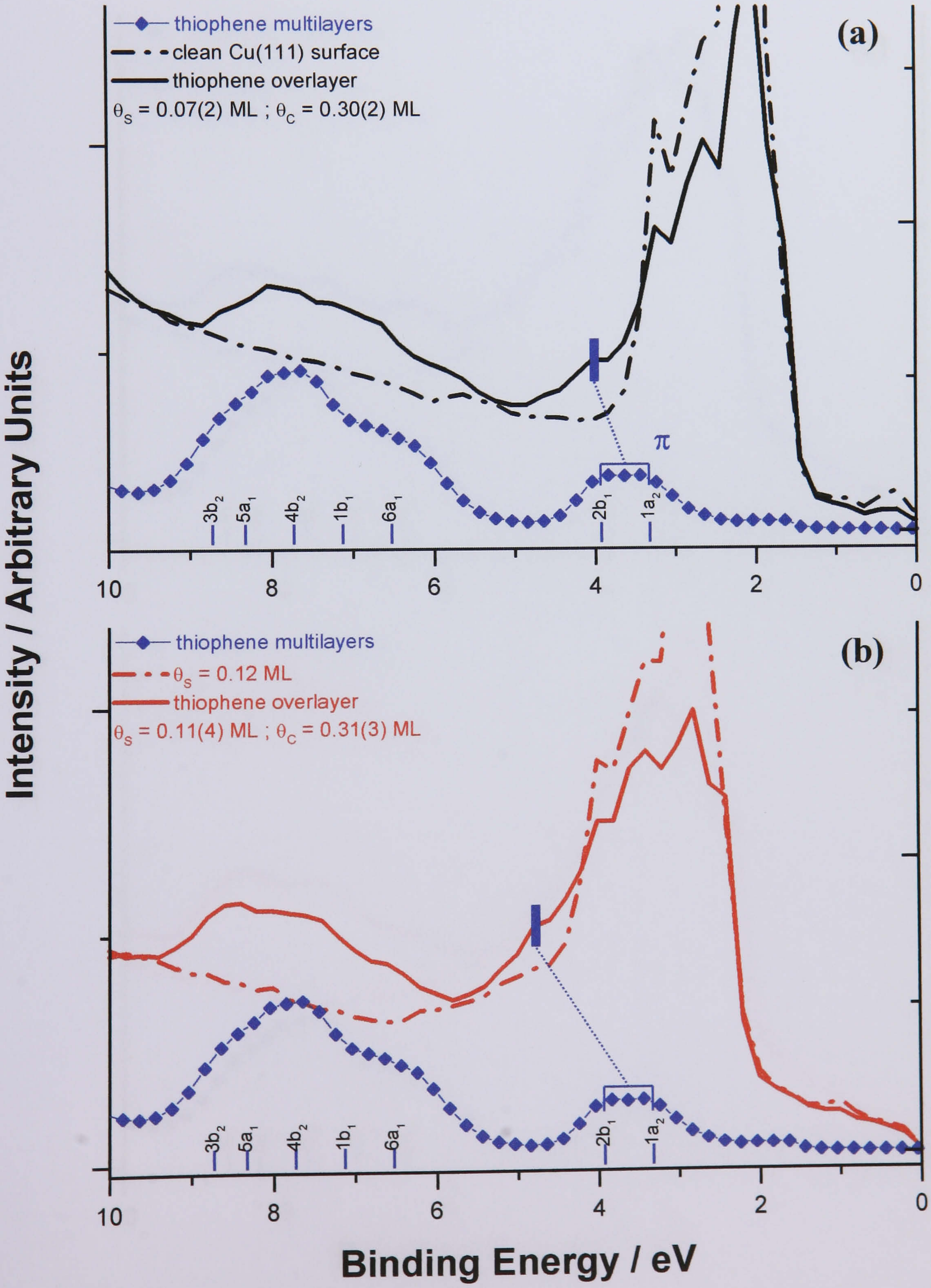

Fig.10b *UP spectra He I (hν = 21.2 eV) at normal emission of* ***thiophene*** *overlayer (α - phase) adsorbed on* (**c**) *0.33 and* (**d**) *0.43 ML of S on Cu(111). Thiophene multilayer spectra, plotted on a different scale, are also displayed for comparison. Figures in brackets are estimated errors.*

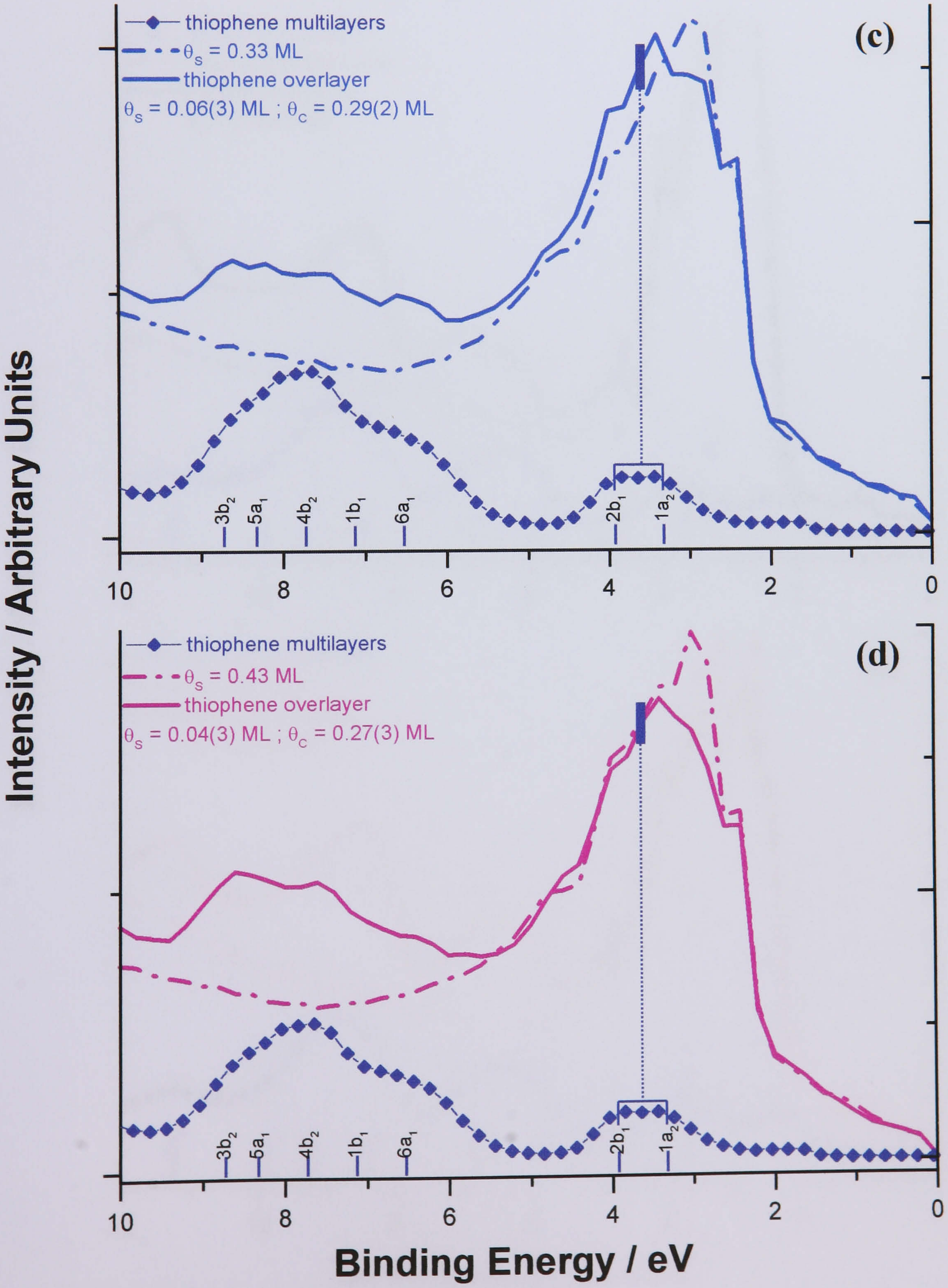

Fig.11a *UP spectra He I ($h\nu$ = 21.2 eV) at normal emission of* ***benzene*** *overlayer adsorbed on* ***(a)*** *clean and* ***(b)*** *0.12 ML of S on Cu(111). Benzene multilayer spectra, plotted on a different scale, are also displayed for comparison. Figures in brackets are estimated errors.*

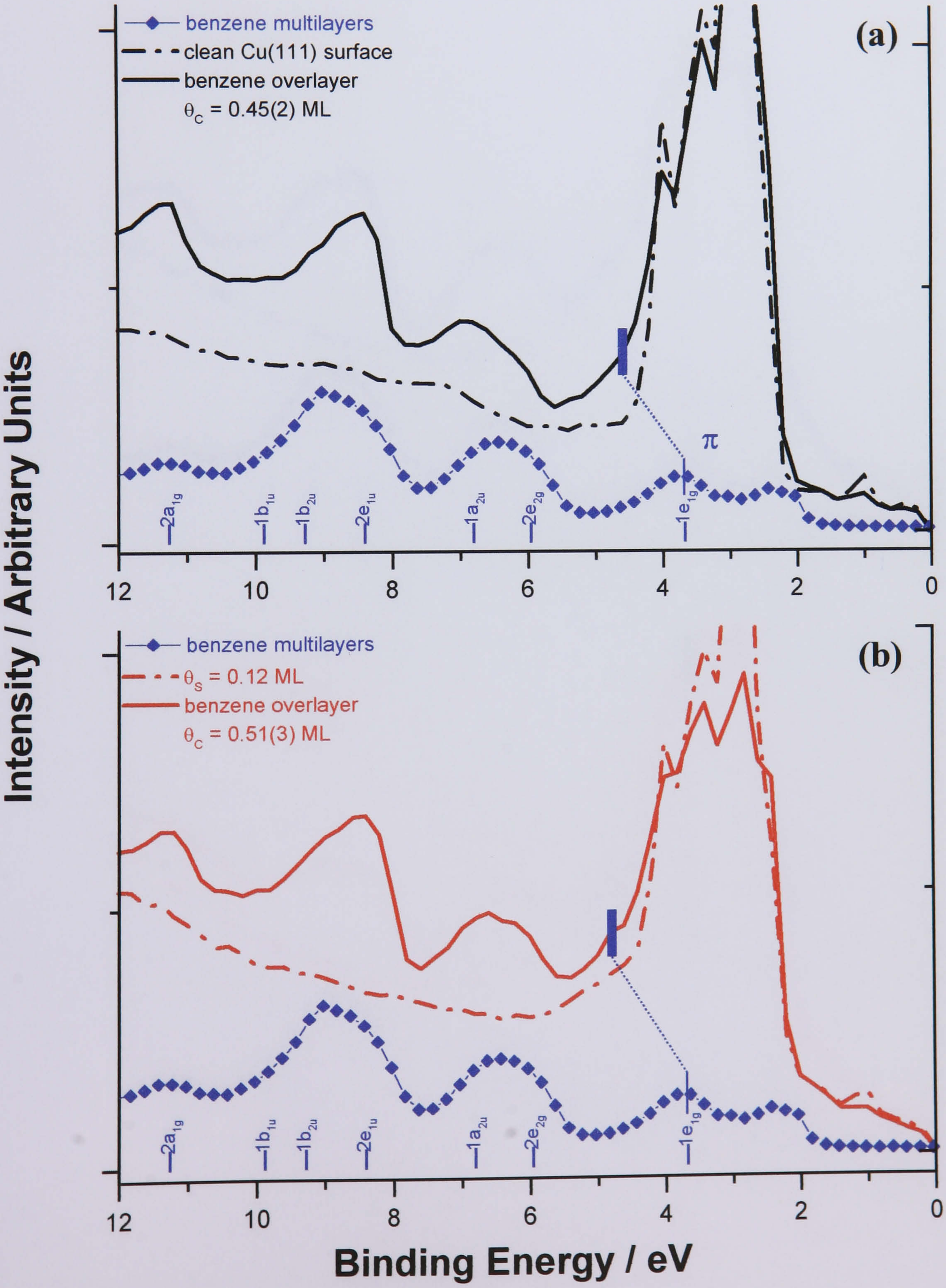

Fig.11b *UP spectra He I (hν = 21.2 eV) at normal emission of* ***benzene*** *overlayer adsorbed on* (**c**) *0.33 and* (**d**) *0.43 ML of S on Cu(111). Benzene multilayer spectra, plotted on a different scale, are also displayed for comparison. Figures in brackets are estimated errors.*

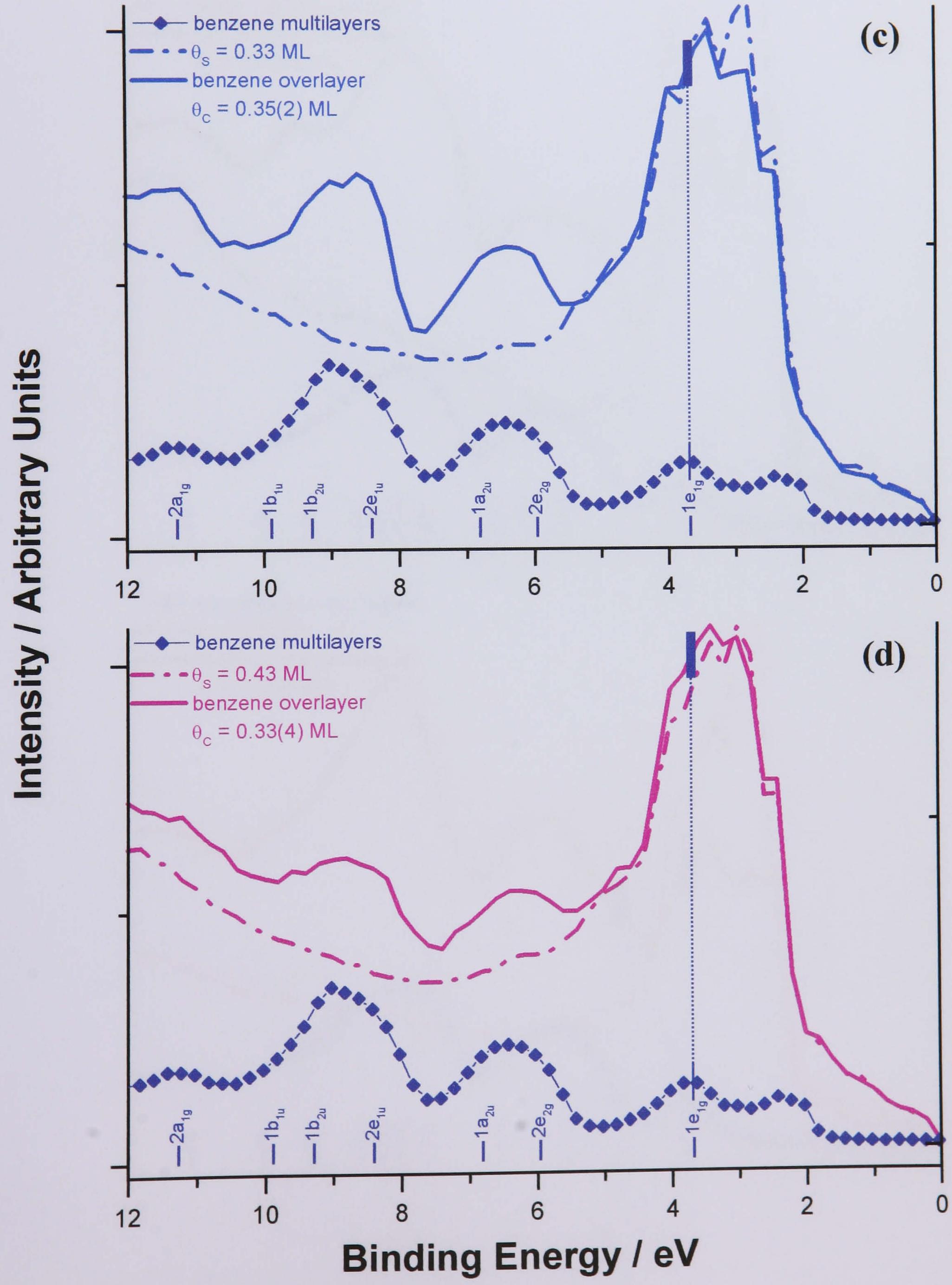

Fig.12a *UP spectra He I ($h\nu$ = 21.2 eV) at normal emission of* ***cyclohexene*** *overlayer adsorbed on* ***(a)*** *clean and* ***(b)*** *0.12 ML of S on Cu(111). Cyclohexene multilayer spectra, plotted on a different scale, are also displayed for comparison. Figures in brackets are estimated errors.*

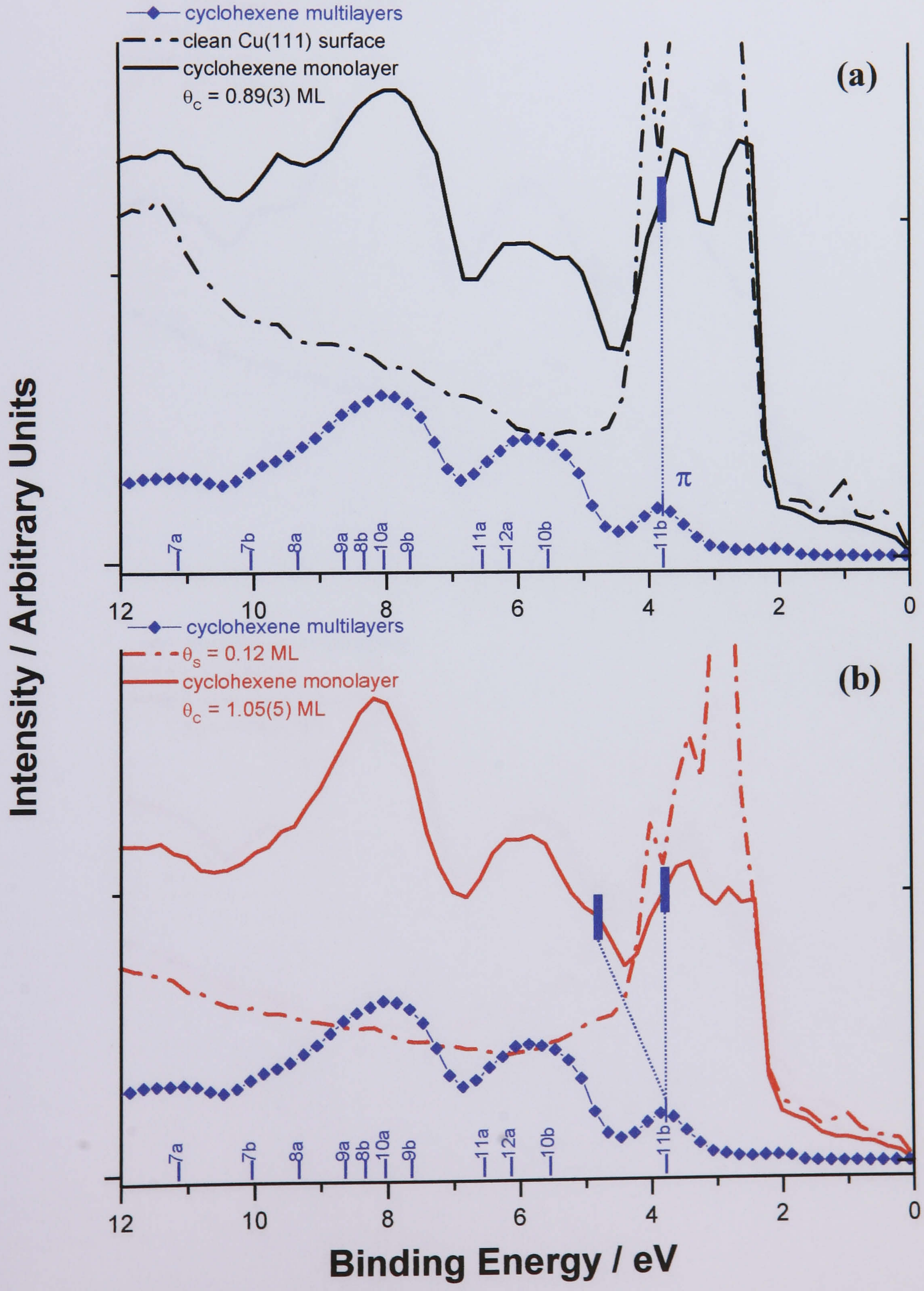

Fig.12b *UP spectra He I (hν = 21.2 eV) at normal emission of* ***cyclohexene*** *overlayer adsorbed on (**c**) 0.33 and (**d**) 0.43 ML of S on Cu(111). Cyclohexene multilayer spectra, plotted on a different scale, are also displayed for comparison. Figures in brackets are estimated errors.*

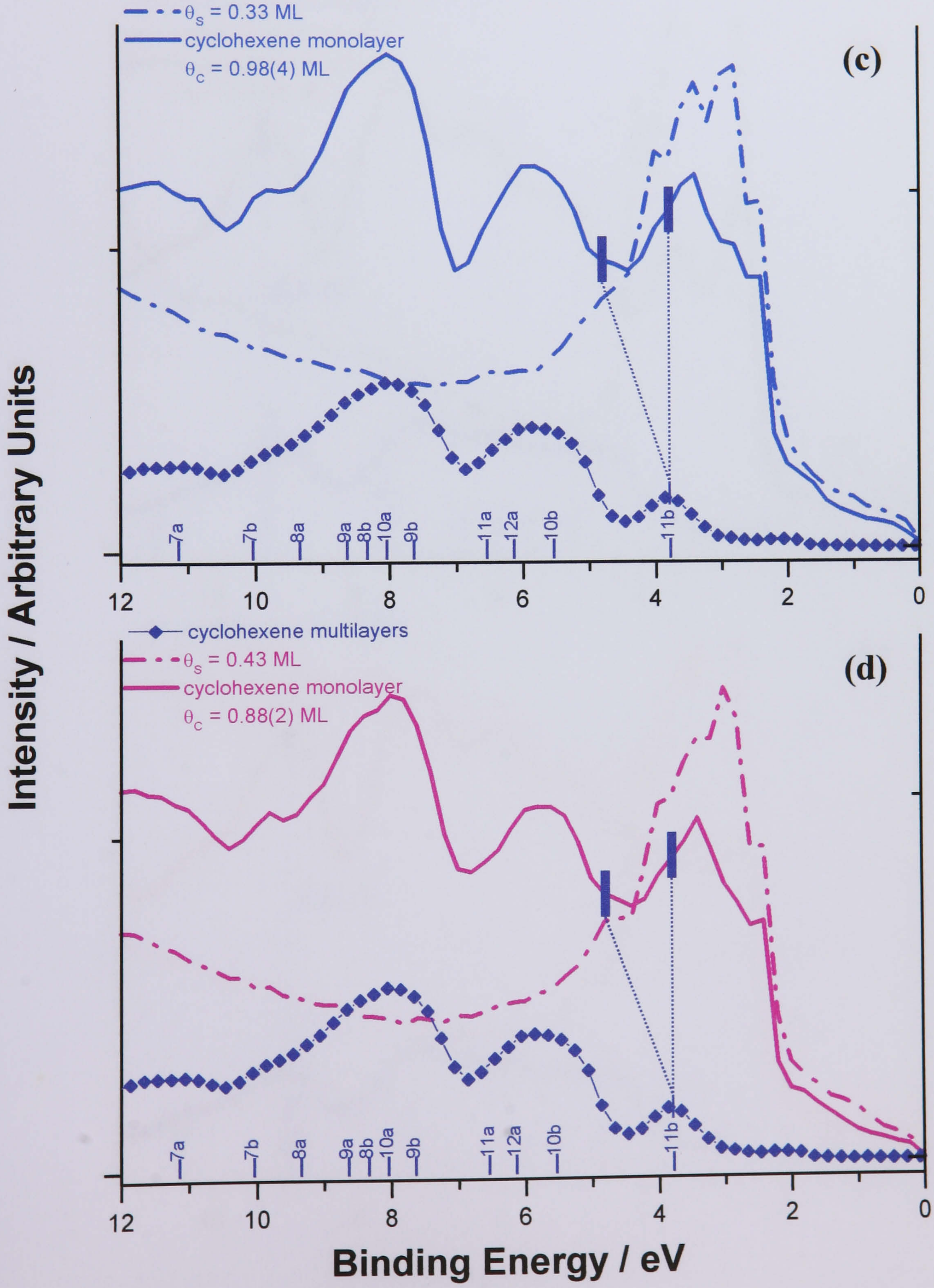

Fig.13a *UP spectra He I ($h\nu$ = 21.2 eV) at normal emission of* ***cyclohexane*** *overlayer adsorbed on* ***(a)*** *clean and* ***(b)*** *0.12 ML of S on Cu(111). Cyclohexane multilayer spectra, plotted on a different scale, are also displayed for comparison. Figures in brackets are estimated errors.*

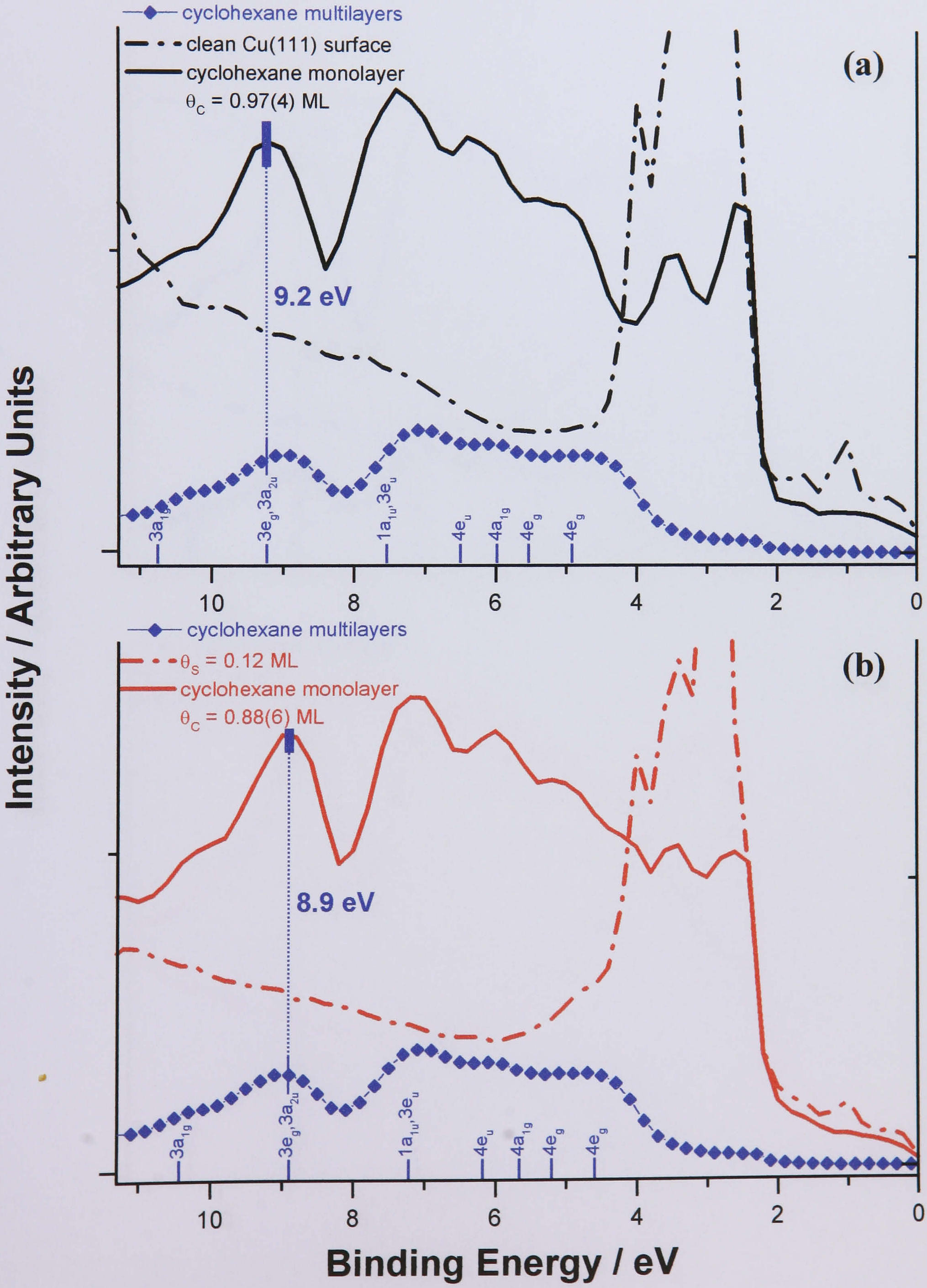

Fig.13b *UP spectra He I ($h\nu$ = 21.2 eV) at normal emission of* ***cyclohexane*** *overlayer adsorbed on* ***(c)*** *0.33 ML and* ***(d)*** *0.43 ML of S on Cu(111). Cyclohexane multilayer spectra, plotted on a different scale, are also displayed for comparison. Figures in brackets are estimated errors.*

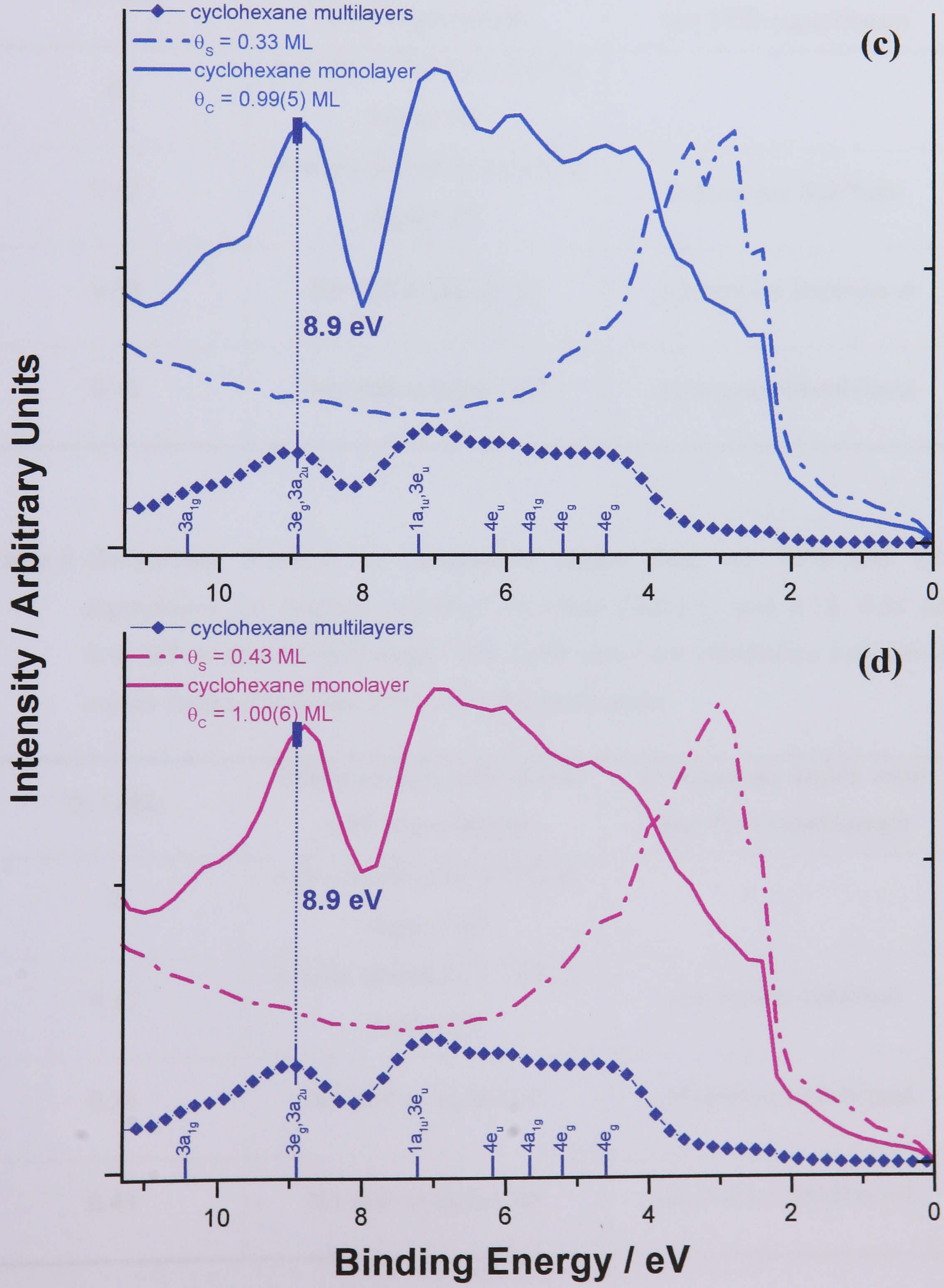

Table 5. *Comparison between the conclusions drawn from our UPS and TPD experiments of thiophene (α-phase) adsorbed on clean Cu(111), and 0.12, 0.33 and 0.43 ML of preadsorbed sulfur. This table shows the consistency between the two techniques employed.*

θ_S / ML	Observations made in our UPS experiments	Conclusions drawn from our TPD experiments
0	π-levels shifted by 0.5 eV to higher BE	–
0.12	π-levels shifted by 1.0 eV to higher BE	Adsorption stabilised
0.33	No shift to higher BE	Adsorption destabilised
0.43	No shift to higher BE	Adsorption destabilised

Table 6. *Comparison between the conclusions drawn from our UPS and TPD experiments for benzene adsorbed on clean Cu(111), and 0.12, 0.33 and 0.43 ML of preadsorbed sulfur. This Table shows the consistency between the results deduced from our TPD and UPS experiments.*

θ_S / ML	Observations made in our UPS experiments	Conclusions drawn from our TPD experiments
0	π-level shifted by 0.9 eV to higher BE	–
0.12	π-level shifted by 1.1 eV to higher BE	Adsorption stabilised
0.33	No shift to higher BE	Adsorption destabilised
0.43	No shift to higher BE	Adsorption destabilised

Table 7. *Comparison between the conclusions drawn from our UPS and TPD experiments for cyclohexene adsorbed on clean Cu(111), and 0.12, 0.33 and 0.43 ML of preadsorbed sulfur.*

θ_S / ML	Observations made in our UPS experiments	Conclusions drawn from our TPD experiments
0	No shift to higher BE	–
0.12	π-level shifted by 0.8 eV to higher BE	Adsorption stabilised
	No shift to higher BE	Adsorption destabilised
0.33	π-level shifted by 0.8 eV to higher BE	Adsorption stabilised
	No shift to higher BE	Adsorption destabilised
0.43	π-level shifted by 0.8 eV to higher BE	Adsorption stabilised
	No shift to higher BE	Adsorption destabilised

Table 8. *A comparison is made between the experimentally observed UPS and TPD values for the benzene, thiophene and cyclohexene molecules adsorbed on clean and preadsorbed sulfur Cu(111) surfaces when stabilisation occurs.*

Molecule and MO of interest	Shift in BE of π-levels for molecule adsorbed on clean Cu(111)	Shift in BE of π-levels for stabilised species / eV	Difference in BE Shift / eV	Shift in temperature from TPD Experiments / K
Benzene $1e_{1g}$	0.9 ± 0.1	1.1 ± 0.1	0.2 ± 0.1	19 ± 2
Thiophene $2b_1$, $1a_1$	0.5 ± 0.1	1.0 ± 0.1	0.5 ± 0.1	22 ± 2
Cyclohexene 11b	0	0.8 ± 0.1	0.8 ± 0.1	29 ± 2

5.3 Discussion

The TPD results of thiophene, benzene and cyclohexene adsorbed on the clean Cu(111) surfaces are in excellent agreement with the previous thermal desorption studies of the similar systems performed by our group,[9] Bent *et al.*[13] and Xi and co-workers,[16] respectively. Although we are unable to detect the desorption from the benzene bilayer (in Ref. [13] the separation between the multilayer and second layer peaks was only 5 K) and no desorption of cyclohexane adsorbed on the defect sites was reported in Ref. [16], the spectra present in Figs. 4, 5 and 7 (black curves) match the features depicted in these three previous investigations.

More importantly, the results from the present studies are particularly interesting considering the well-known poisoning behaviour of sulfur on transition metal surfaces. For instance, various studies have shown the poisonous effects of preadsorbed sulfur on the reactivity of benzene on Pt(111)[21] and thiophene adsorbed on Mo(110),[22] W(211),[23] Ni(111),[24] Ru(0001)[25] and sulfide-modified molybdenum (MoS_x[26,27] and MoS_2(0002))[28,29] surfaces at all S coverages. However, the TPD experiments depicted in Figs. 4, 5 and 6 clearly illustrate the promotional effects of sulfur on the bonding of the three unsaturated molecules to Cu(111), as the peaks attributed to the desorption of the first layers of thiophene (α-phase), benzene and cyclohexene molecules are shifted to higher temperatures.

The promotional effects of sulfur on supported coinage metal catalysts have also been reported by Hutchings *et al.*[30-35] These authors demonstrated that partial poisoning of supported copper catalysts using sulfur could be a viable approach for the design of selective catalysts.[30–32] The modification of Cu/Al_2O_3 by very low levels of thiophene significantly enhanced the selectivity of the formation of but - 2 - en - 1 - ol from the hydrogenation of but-2-enal. Detailed analyses of their results showed that sulfur acted as a promoter for this selective hydrogenation reaction, rather than a poison as would have been expected.[30] Similar promotional effects by sulfur were also observed with Au/ZnO for the same reaction.[33-35]

The UPS data collected in the present work provides strong evidence that the origin of the stabilisation observed in our TPD experiments is due to an electronic effect. Indeed, the analyses of the UP spectra in Figs. 10, 11 and 12 reveal that the π - levels of thiophene, benzene and cyclohexene are shifted to higher BE in the

presence of preadsorbed sulfur, indicating that S enhances the interaction of π-states of these three adsorbates with the substrate and explains the increase in bond strength of the molecules adsorbed on the sulfur pre-covered Cu(111) surfaces. Further, Table 8 shows that the degree of shift of the π-levels is proportional to the difference of desorption temperature.

The stabilisation of benzene on Cu(110) by low coverages of atomic Cl was observed by Lambert *et al.*[36] In their TPD experiments, this stabilisation was characterised by an upward shift of ≤ 70 K in the desorption temperature of chemisorbed benzene (which was dependent on the initial Cl coverage) and corresponded to an increase of 0.2 eV in the interaction energy of benzene with the Cu(110) substrate. In view of the values displayed in Table 8, one would expect this increase in BE to be bigger, considering that in the current work a shift by 19 ± 2 K to higher desorption temperature of the benzene molecules corresponds to an increase in binding energy of 0.2 ± 0.1 eV as determined by UPS. Further, the enhancement in the chemisorption bond strength of benzene on Cu(110) in the presence of coadsorbed Cl was also theoretically studied by Lomas and Pacchioni using ab initio cluster model wavefunctions.[37] The authors found that the increase in bond strength of chemisorbed benzene could be explained by a simple electrostatic model, where Cl adatoms create a surface dipole-layer which induces an increase in charge donation from benzene to the Cu substrate.

A similar electrostatic model can also be employed here to explain the promotion effects of sulfur on the bonding of thiophene, benzene and cyclohexene. The bonding of unsaturated hydrocarbons to metal surfaces is commonly described in a frontier orbital approach which was developed by Dewar, Chatt and Duncanson fifty years ago.[38,39] In this model the bonding is described as a donation of molecular π-electrons into unoccupied levels of the metal while the molecular antibonding π* orbital becomes occupied through back-donation. For the unsaturated thiophene, benzene and cyclohexene molecules on Cu(111), charge donation from the π systems to the substrate is more important than back-donation from the Cu(4s,4p) band into the π*-levels. This larger charge donation is represented by the dipole moment μ_I in Fig.14. With the adsorption of electronegative sulfur elements on Cu(111), charge transfer from the substrate to the anionic species occurs which leads to the formation of the dipole moment μ_S as depicted in Fig. 14, with μ_S anti-parallel to μ_I. We have seen in

the previous chapter that in the so-called Coadsorption Induced Ordering (CIO) model,[40] it was suggested that charge transfer from benzene to Pt(111) and from Pt(111) to CO causes the formation of anti-parallel dipoles which interact attractively and induce ordering of the disordered benzene layer. In the present case, we believe that the anti-parallel μ_S and μ_1 dipoles interact attractively, and the direct results of this interaction is an increase in charge donation from the π species to the Cu(111) substrate, with μ_1 becoming μ_2 and $\mu_2 > \mu_1$. We should mention that in the previous chapter, it was suggested that the lack of any significant cooperative effects between the CO and thiophene within the coadsorbed overlayers was due to the relatively weak adsorbate – substrate interactions. However, it is well known that S is more strongly bonded to Cu(111) than CO, as CO desorbs molecularly from the copper surface below room temperature (see Fig. 1 Chapter 4) and sulfur adatoms do not desorb from Cu(111). The value of the dipole moment μ_S would thus be bigger than the one of μ_{CO}. In summary, we believe that a simple electrostatic model can be used to explain the observed enhancement of the chemisorption bond strength of the π-bonded thiophene, benzene and cyclohexene molecules to Cu(111), as the presence of coadsorbed sulfur provokes an increase in charge donation from the adsorbates to the substrate.

It should be noted that this electrostatic model is only valid for complexes where charge donation from the adsorbates to the substrate is significantly more important than back donation, and Cu, Ag and Au are the only transition metals which satisfy this condition. For unsaturated molecules adsorbed on other transition metal surfaces such as Pt, Pd or Rh, back-donation from the metal d-band to the molecular anti-bonding levels is the predominant mode of interaction and no promotional effect by coadsorption of sulfur on these three metal surfaces has ever been reported in the literature. Instead, sulfur acts as a poison for these metal surfaces and Rodriguez and Hrbek were able to demonstrate that the origin of this poisoning is electronic, as their UPS data showed that sulfur perturbs the electronic properties of Pt, Pd and Rh by reducing the density of states (DOS) near the Fermi level and by withdrawing charges from the metal d-band,[41] charges which are required for adsorption and/or reactivity to occur. Further proofs that this electronic model is only applicable to coinage metals are provided in studies by Hutchings *et al.* and Lomas and Pacchioni. First, in a recent investigation by Hutchings and co-workers,[35] the beneficial effects of sulfur on the selective hydrogenation of crotonaldehyde to crotyl alcohol was not observed on Co, Ni

and Ru supported catalysts, which indicates the sulfur promotion is only valid for copper and gold supported catalysts. Second, in their theoretical investigation of the promotional effect of Cl on the adsorption of benzene,[37] Lomas and Pacchioni suggested that on Pd(111) the stabilisation effect of Cl was not observed because the back-donation contribution of Pd to the overall bonding is more important than on Cu, and any increase in charge donation from benzene to Pd is not sufficient to overcompensate any decrease in back donation. The reinforcement of the chemisorption bond strength of unsaturated molecules in presence of electronegative Cl or S is therefore only effective on coinage metal surfaces.

The TPD spectra depicted in Figs. 4 and 5 show that 0.12 ML of preadsorbed sulfur has a stabilisation effect on the bonding of thiophene (α-phase only) and benzene. At higher sulfur pre-coverages (θ_S = 0.33 and 0.43 ML), both molecules are destabilised as the peaks corresponding to desorption of the first layers are shifted to lower temperature. However, our TPD data displayed in Fig. 6 indicates the biggest promotional effects of preadsorbed sulfur on the adsorption of cyclohexene, as the promotion extends to higher sulfur pre-coverages. It appears that the bonding mechanism between the unsaturated molecules and the surface may play an important role in the stabilising / destabilising effects observed. The bonding of thiophene and benzene molecules, whose π-electrons are delocalised around the rings, requires a large number of free copper sites. On the other hand, the adsorption of cyclohexene, whose mode of interactions with the surface involves the π electrons which are localised around the olefinic portion of the C_6H_{10} molecule, necessitates less free Cu sites. Further, we believe that the destabilisation of the three unsaturated molecules is due to a steric effect, i.e. sulfur blocks the sites required for adsorption. Steric blocking was also observed by Garfunkel *et al.*[21] for benzene adsorbed on sulfur pre-covered Pt(111) surfaces, and Campbell and Koel attributed the decrease of the rate of the water-gas shift reaction to steric blocking by the sulfur adatoms of the sites required for dissociative water adsorption.[1]

Finally, we believe that the destabilisation of cyclohexane in presence of sulfur can also be rationalised in terms of an electrostatic model. In a previous investigation of cyclohexane adsorbed on Cu(111), Raval *et al.* suggested that the "softening" of the C – H stretching mode observed in their vibrational data was thought to arise from the C – H ···Metal interaction, and the bonding of the molecule to the surface involved a net

transfer of electrons in this interaction from the metal Cu(4s,4p) band into the σ* C–H antibonding orbitals.[20] More recently, Fosser *et al.*[41] performed an ab initio calculation of the same system and it was also proposed that there is a significant transfer of charge from the Cu substrate into the adsorbed cyclohexane molecule, however the charge is back-donated into empty Rydberg orbitals and not into the orbital of C–H σ* character. The bonding mechanism of cyclohexane on Cu(111) is illustrated in Fig. 15 and μ_3 represents the dipole moment stemming from charge back-donation from the copper substrate to the adsorbate. The adsorption of S on Cu(111) induces the formation of the dipole moment μ_S which is parallel to μ_3 and interacts repulsively with this dipole moment. Consequently, μ_3 becomes μ_4 with $\mu_4 < \mu_3$, and the presence of sulfur provokes a diminution of charge donation from the Cu(4s,4p) band into the Rydberg or σ* C–H molecular orbitals. Because the charge back-donation is now reduced, the bond strength of cyclohexane on Cu(111) decreases and therefore destabilisation occurs.

Fig.14 *Diagrams showing that (a) on the clean Cu(111) surface the charge donation from the adsorbate π system to the substrate is more important than the back-donation from the substrate to π^*; and (b), with the adsorption of sulfur, charge transfer from the substrate to the anionic species occurs which leads to the formation of the anti-parallel dipole moment μ_S. μ_S and μ_1 interact attractively, with μ_1 becoming μ_2 and $\mu_2 > \mu_1$ and provoke an increase in the charge donation from the π-bonded species to the substrate.*

(a)

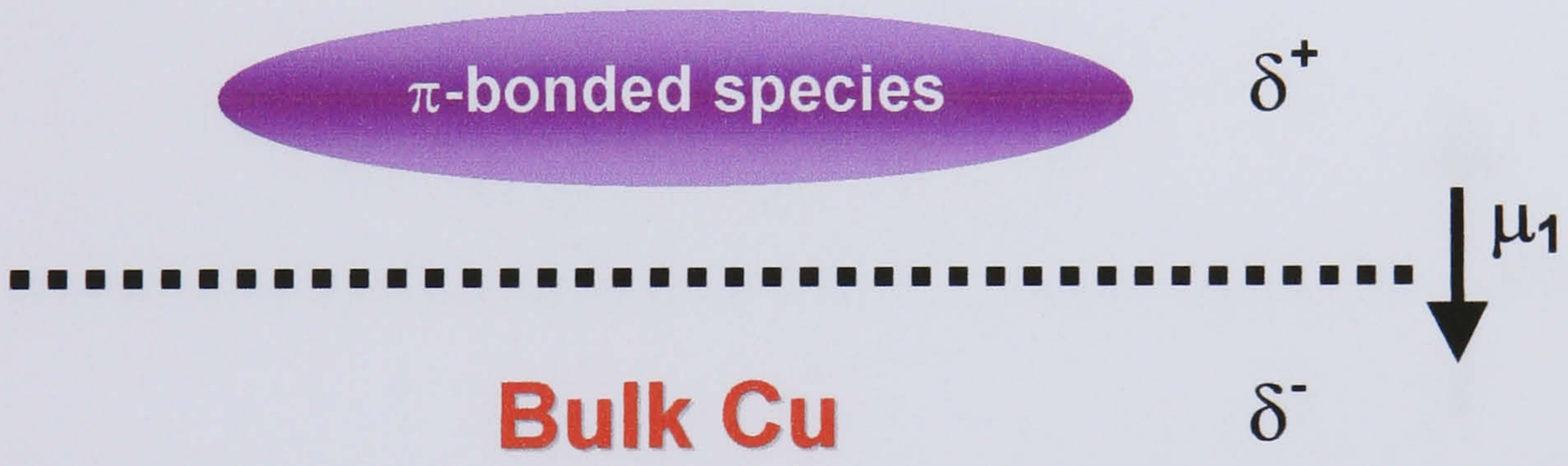

(b)

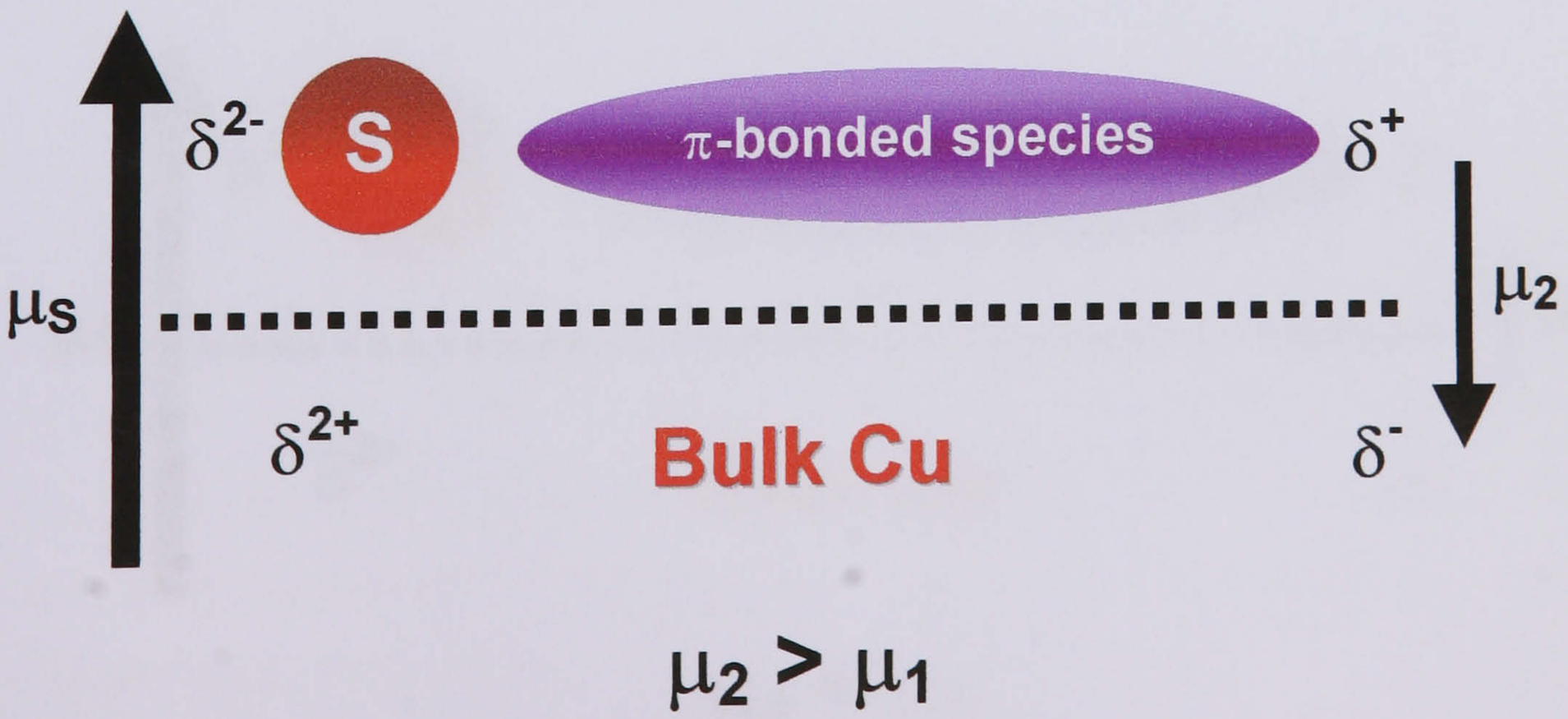

Fig.15 *Diagrams showing that (a) the adsorption of cyclohexane on the clean Cu(111) surface is dominated by the back-donation from the substrate to the adsorbate;*[20,42] *and (b) the presence of S on Cu(111) induces the formation of* μ_S *which is parallel to* μ_3 *and interacts repulsively with* μ_3 *(with* μ_3 *becoming* μ_4 *with* $\mu_4 < \mu_3$*). Consequently, the back-donation from the substrate to the adsorbate is reduced and destabilises the adsorption of cyclohexane on Cu(111) occurs.*

(a)

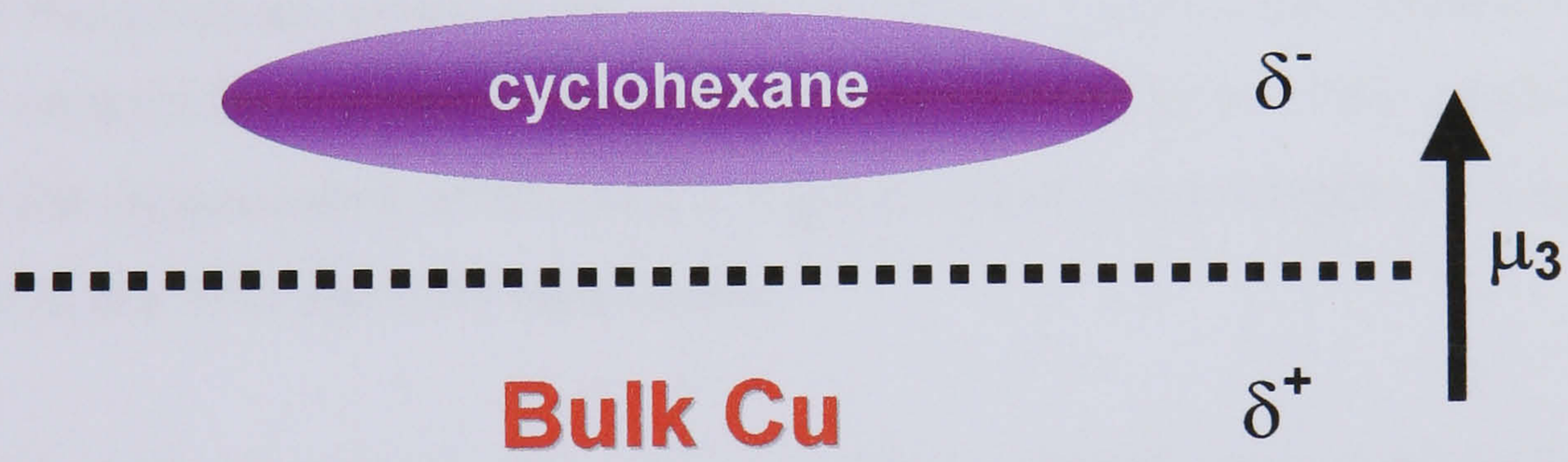

(b)

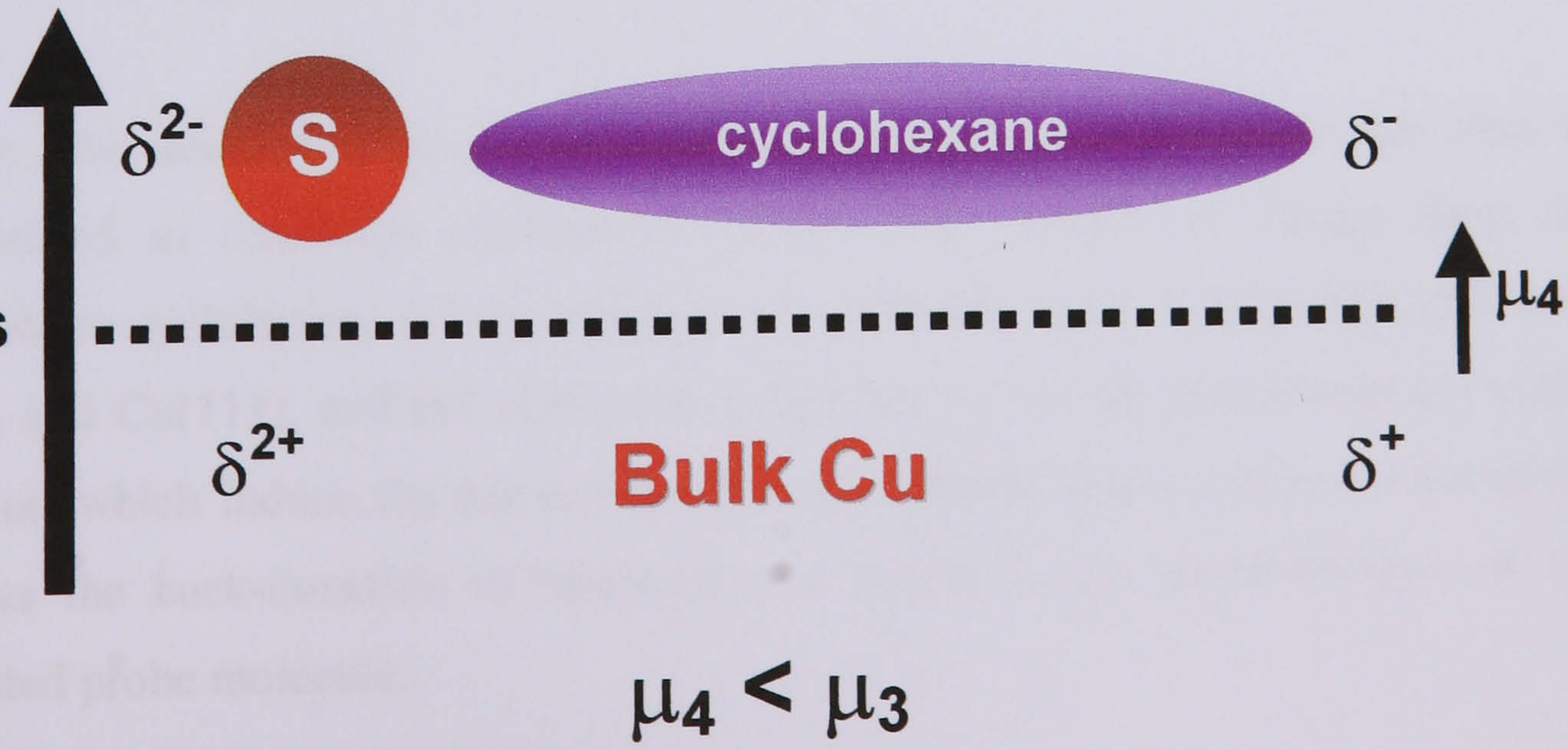

5.4 Conclusion

The most significant findings of the current study are outlined below:

1. In contrast to the well-known poisoning behaviour of sulfur on transition metal surfaces, the results from the current study show that sulfur promotes the bonding of unsaturated molecules to Cu(111), in excellent agreement with the recent findings by Hutchings and co-workers.[30-35]

2. We believe that the stabilisation brought about by sulfur on the adsorption of thiophene, benzene and cyclohexene is due to an electronic effect. An increase of charge donation from the π-levels of the unsaturated molecules into unoccupied levels of the substrate, which is due to the formation of anti-parallel dipoles which interact attractively, occurs in presence of coadsorbed sulfur. This mechanism explains the enhancement of the bond strength of the π-bonded species to Cu(111) observed in our TPD and UPS experiments.

3. This electrostatic model for sulfur promotion is only valid for coinage metals, as for Cu, Ag and Au surfaces charge donation from the adsorbates to the substrate is significantly more important than back-donation.

4. Steric blocking by sulfur adatoms is believed to be responsible for the destabilisation of thiophene, benzene and cyclohexene, and steric effects are limited to sulfur coverages to which promotion extends.

5. Finally, the destabilisation of the saturated cyclohexane molecules can also be rationalised in terms an electrostatic model. The transfer of charge from the substrate to cyclohexane is believed to be the principle mode of interaction between C_6H_{12} and Cu(111), and the electrostatic field set up by the electronegative sulfur element, which induce the formation of parallel dipole which interact repulsively, reduces the back-donation of electrons and results in the destabilisation of the saturated probe molecule.

5.5 References

1. C.T. Campbell, B.E. Koel, Surf. Sci., 183 (1987) 100
2. J.L. Domange, J. Oudar, Surf. Sci., 11 (1968) 124
3. D. Westphal, A. Goldmann, Surf. Sci., 131 (1983) 113
4. D.T. Ling, J.N. Miller, D.L. Weissman, P. Pianetta, P.M. Stefan, I. Lindau, W.E. Spicer, Surf. Sci., 124 (1983) 175
5. G. Leschik, R. Courths, H. Wern H, Surf. Sci., 294 (1993) 355
6. H.C. Zeng, R.A. McFarlane, K.A.R. Mitchell, Phys. Rev. B, 39 (1989) 8000
7. E. Vlieg, I.K. Robinson, R. McGrath, Phys. Rev. B, 41 (1990) 7896
8. A.E.S. von Wittenau, Z. Hussain, L.Q. Wang, Z.Q. Huang, Z.G. Ji, D.A. Shirley, Phys. Rev. B, 45 (1992) 13614
9. P. Milligan, B. Murphy, B.C.C. Cowie, D. Lennon, M. Kadodwala, J. Phys. Chem.B, 105 (2001) 140
10. M. Foss, R. Feidenhans'l, M. Nielsen, E. Findeisen, T. Buslaps, R.L. Johnson, F. Besenbacher, Surf. Sci., 388 (1997) 5
11. G.J. Jackson, S.M. Driver, D.P. Woodruff, B.C.C. Cowie, R.G. Jones, Surf. Sci., 453 (2000) 183
12. Z. Dohnalek, G.A. Kimmel, R.L. Ciollo, K.P. Stevenson, R.S. Smith, B.D Kay, J. Chem. Phys., 112 (2000) 5932
13. M. Xi, M.X. Yang, S.K. Jo, B.E. Bent, J. Chem. Phys., 101 (1994) 9122
14. H. Koschel, G. Held, P. Trischberger, W. Widdra, H.P. Steinruck, Surf. Sci., 437 (1999) 125
15. D. Syomin, B.E.Koel, Surf. Sci., 498 (2002) 61
16. M. Xi, B.E. bent, J. Phys. Chem., 97 (1993) 4167
17. A. Imanishi, T. Yokoyama,Y. Kitajima, T. Ohta, Bull. Chem. Soc. Jap., 71 (1998) 831
18. P. Milligan, J. McNamarra, B. Murphy, B.C.C. Cowie, D. Lennon, M. Kadodwala, Surf. Sci., 412/413 (1998) 166
19. N.V. Richardson, J.C. Campuzano, Vacuum, 31 (1981) 449
20. R. Raval, S.F. Parker, M.A. Chesters, Surf. Sci., 289 (1993) 227
21. E.L. Garfunkel, M.H. Farias, G.A. Somorjai, J. Am. Chem. Soc., 107 (1985) 349
22. J.T. Roberts, C.M. Friend, Surf. Sci., 186 (1987) 201
23. R.E. Preston, J.B. Benziger, J. Phys. Chem., 89 (1985) 5010

24. G.R. Schoofs, R.E. Preston, J.B. Benziger, Langmuir, 1 (1985) 313
25. R.A. Cocco, B.J. Tatarchuk, Surf. Sci., 218 (1989) 127
26. J.A. Rodriguez, J. Dvorak, T. Jirsak, Surf. Sci. Lett., 457 (2000) L413
27. M. Salmeron, G.A. Somorjai, A. Wold, R. Chianelli, K.S. Liang, Chem. Phys. Lett., 90 (1982) 105
28. S.L. Petterson, K. Shultz, Langmuir, 12 (1996) 941
29. M. Salmeron, G.A. Somorjai, A. Wold, R. Chianelli, K.S. Liang, Chem. Phys. Lett., 90 (1982) 105
30. G.J. Hutchings, F. King, I.P. Okoye, M.B. Padley, C.H. Rochester, J. Catal. 148 (1994) 453
31. G.J. Hutchings, F. King, I.P. Okoye, M.B. Padley, C.H. Rochester, J. Catal. 148 (1994) 464
32. M.B. Padley, C.H. Rochester, G.J. Hutchings, F. King, J. Catal. 148 (1994) 438
33. J.E. Bailie, G.J. Hutchings, Chem. Commun., (1999) 2151
34. J.E. Bailie, H.A. Abdullah, J.A. Anderson, C.H. Rochester, N.V. Richardson, N. Hodge, J.-G. Zhang, A. Burrows, C.J. Kiely, G.J. Hutchings, Phys. Chem. Chem. Phys., 3 (2001) 4113
35. J.E. Bailie, G.J. Hutchings, J. Mol. Catal. A: Chem., 177 (2002) 209
36. J.R. Lomas, C.J. Baddeley, M.S. Tikhov, R.M. Lambert, Langmuir, 11 (1995) 3048
37. J.R. Lomas, G. Pacchioni, Surf. Sci., 365 (1996) 297
38. M.J.S. Dewar, Bull. Soc. Chim. France, 18 (1951) C79
39. J. Chatt, L.A. Duncanson, J. Chem. Soc., (1953) 2939
40. C.M. Mates, C.T. Kao, G.A. Somorjai, Surf. Sci., 206 (1988) 145
41. J.A. Rodriguez, J. Hrbek, Acc. Chem. Res., 32 (1999) 719
42. K.A. Fosser, R.G. Nuzzo, P.S. Bagus, C.Wöll, Angew. Chem. Int. Ed., 41 (2002) 1735

Summary 1. Coadsorption Studies

The results from these two coadsorption studies, which at first sight appear different, are in fact connected.

In contrast to previous co-adsorption studies involving benzene and CO on Ni, Pt, Rh and Ru single crystal surfaces, we have observed that the CO/thiophene/Cu(111) system displays no coadsorbate induced ordering, and we believe that this lack of ordering is associated with the weak bonding of the CO and thiophene to the Cu(111) surface. Indeed, such a weak bonding induces only small anti-parallel dipoles within the coadsorbed species, and since these dipoles are believed to be the driving force for coadsorbate induced ordering, smaller induced dipoles are likely to make ordering less favourable.

In the second study, we have observed the promotional effects of pre-adsorbed sulfur on the adsorption of thiophene, benzene and cyclohexene on Cu(111). In contrast to CO, sulfur is more strongly bonded to the copper surfaces, and we propose that the formation of anti-parallel dipoles formed by the transfer of charge from the unsaturated molecule to the Cu(111) surface and from the copper substrate to adsorbed sulfur is the driving force for the observed promotional effects. Further evidence for the role of anti-parallel dipoles in the stabilisation of co-adsorbed molecules comes from the study of cyclohexane/S/Cu(111). In this system, where the induced dipoles are parallel, stabilisation of the C_6H_{12} molecules does not occur.

Chapter 6. Photoemission Studies of the Adsorption of Thiophene on Si(100)-(2×1), Si(111)-(7×7) and Ge(100)-(2×1)

6.1 Introduction

The adsorption of thiophene on Si(100)-(2×1), Si(111)-(7×7) and Ge(100)-(2×1) at room temperature has been investigated in order to develop an improved understanding of the relationship between the structural/electronic properties and chemical activity of all three surfaces studied. Recent work has shown that the π - bonded dimers of the (2×1) reconstructed Si(100) and Ge(100) surfaces can undergo cycloaddition reactions with dienes,[9] however the main interest of the current work was to find out whether the absence of π-bonded dimers on Si(111)-(7×7) had a significant effect on its reactivity towards a diene such as thiophene. The synchrotron-based valence band photoemission data collected at the station 4.1 of the Daresbury Laboratory clearly show that the adsorption of thiophene on all three surfaces leads to the formation of the same surface species, and the direct comparisons of the photoemission data with gas phase spectra suggest that this moiety is a 2,5-dihydrothiophene-like species. The formation of the 2,5-dihydrothiophene-like species on Si(100)-(2×1) and Ge(100)-(2×1) is consistent with a [4+2] cycloaddition mechanism, and the relative reactivities of these two surfaces towards thiophene are also consistent with a Diels-Alder reaction. On the other hand, the formation of a 2,5-dihydrothiophene-like moiety on the Si(111)-(7×7) surface cannot occur *via* a Diels-Alder mechanism due to the absence of the required π-bonded silicon dimers. This implies that although the reaction mechanism is dependent upon the electronic and structural properties of the three surfaces, the actual product formed in the reaction between the aromatic molecule and the silicon or germanium surfaces is not.

6.2 Results

6.2.1 Thiophene/Si(100)-(2×1)

Fig. 1 shows the normal (surface of the crystal facing the analyser and photons incident at 55° with respect to the surface normal) and off-normal (surface facing the incoming photons and photoelectron detected at 55° with respect to the surface normal) photoemission spectra collected from the clean Si(100)-(2×1) using a photon energy of 40 eV. The exact structure of the (2×1) reconstructed Si(100) surface is still discussed, however after numerous experimental and theoretical studies it is believed that this surface is made of rows of buckled silicon dimers.[1-3] These silicon dimers consist of a strong σ bond and a weaker π linkage and can be considered to have a double bond, with a π overlap which is significantly less than the one found for the analogous C=C double bond. The spectra depicted in Fig. 1 are in good agreement with previous experimental[4-6] and theoretical[5,7] studies of the clean Si(100)-(2×1) surface. The bands observed with binding energy (BE) from 2 to 13 eV originate from bulk derived states, and the surface electronic states, which originate from the unoccupied dangling bonds of the Si surface atoms are located at 1 eV (most pronounced in normal emission) and 1.5 eV (most pronounced in off-normal emission). Calculations carried out by Chadi predict that the surface state at 1.5 eV is associated with the π character of the asymmetric silicon dimers.[7] In summary, the similarity of the spectra in Fig. 1 to those obtained in previous work suggests that the surfaces are clean and well ordered, as also double checked by using the LEED technique.

The cleanliness and surface quality of the Si(100)-(2×1) surface was also assessed by collecting core level Si 2p spectra with photons of hν = 140 eV, shown in Fig. 2. The Si 2p spectrum of the clean surface (blue curve) displays a surface state at +0.5 eV from the bulk signal, which was previously assigned by Landemark *et al.* to the up atom of the silicon dimer.[8] This surface state is highly sensitive to both contamination and surface order, and its presence was used as another criteria for surface quality. For instance, as can be seen in Fig. 2, the adsorption of 36 L of thiophene (magenta curve) quenches the Si 2p surface state. This extra check of surface quality for Si(100)-(2×1) was taken as a precaution because of the highly reactive nature of the substrate.

Fig.1. *Normal and off-normal emission valence band photoemission spectra ($h\nu = 40\ eV$) collected from a clean Si(100)-(2×1) surface. The surface states observed in the clean surface spectra have been labelled.*

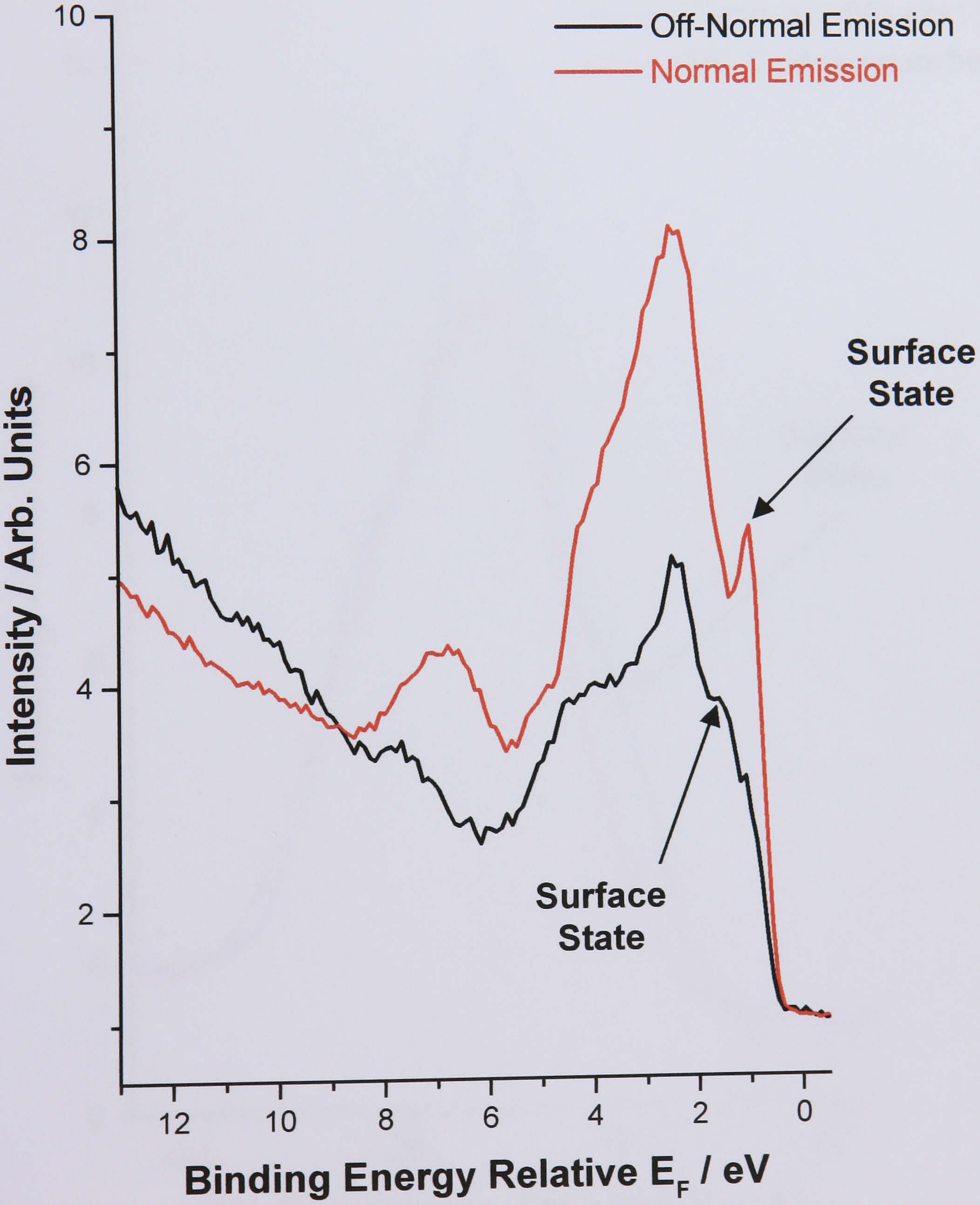

Fig.2. *Si 2p core level spectra (hν = 140 eV), from clean Si(100)-(2×1) and a surface dosed with 36 L of thiophene. The surface state observed in the clean surface spectrum has been labelled.*

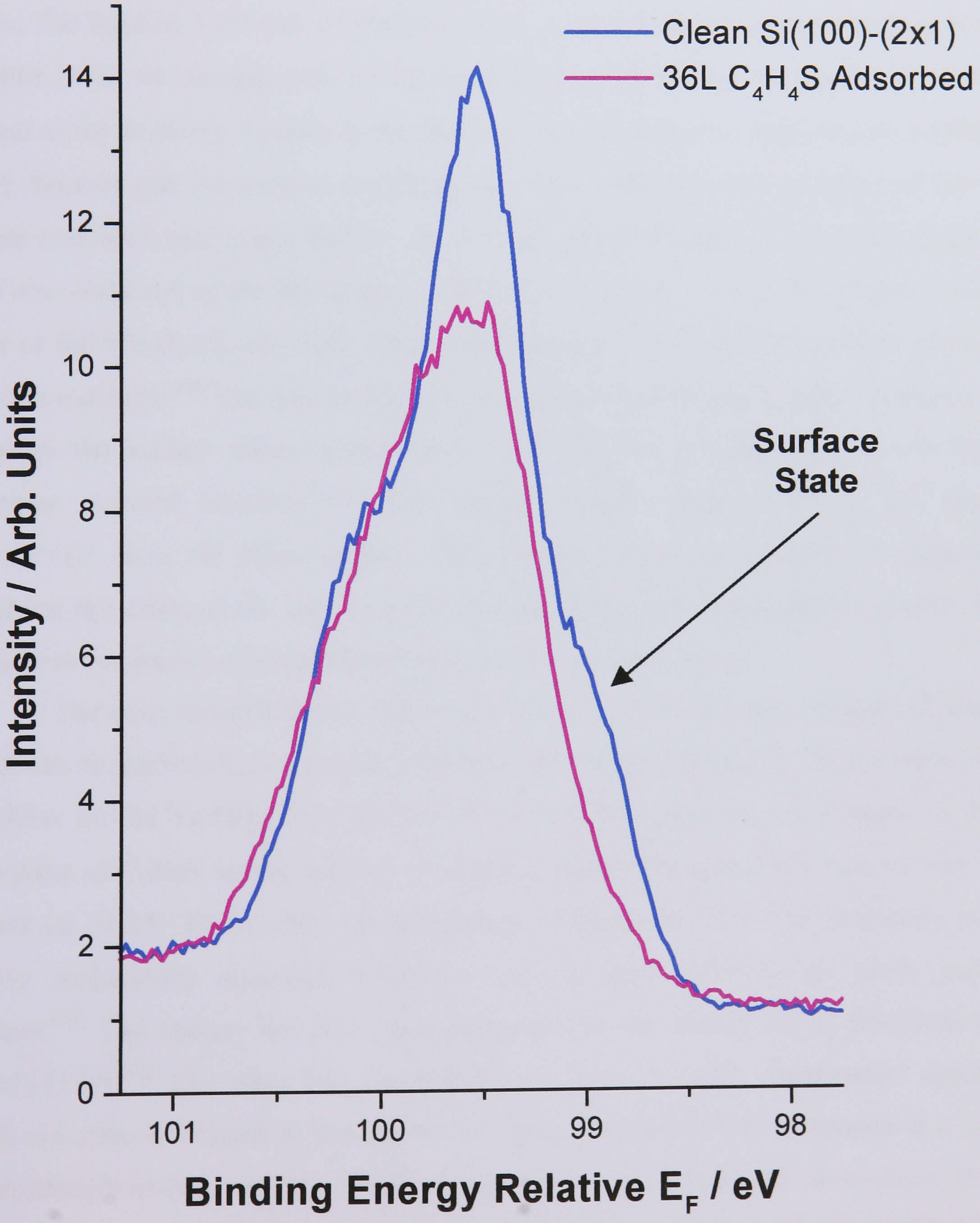

Fig. 4 depicts the normal and off-normal valence band photoemission spectra of 60 L of thiophene adsorbed on Si(100)-(2×1) at room temperature. Both spectra have four broad features in the BE region 0 – 5 eV, 5 – 9 eV, 9 – 14 eV and 14 - 18 eV which have different relative intensities in the normal and off-normal orientation and also consist of individual bands. In the 0 – 5 eV BE region, three discernible bands at 1.0, 2.5 and 3.8 eV can be observed for the normal and off-normal spectra. We believe that these three bands can be attributed to the emission of photoelectrons from the Si surface atoms. The band at 1 eV can be assigned to the remnants of the silicon dangling bond (π) state, while we strongly believe that the features at 2.5 and 3.8 eV originate from the σ bond of the Si dimer. Indeed, in the study of organic molecules adsorbed on Si(100)-(2×1), Hamers and co-workers suggested that after adsorption the structure of the Si dimers remained, and hence the Si – Si σ bond was still intact.[9] Electronic features were also observed in the BE range 2 – 4 eV by Uhrberg *et al.* in the photoemission study of Si(100)-(2×1), and these states were assigned by the authors to the σ bond of the silicon dimers.[10] The plot in Fig. 5 clearly shows that the adsorption of thiophene quenches the surface states centred at 1.0 eV BE, but the spectra collected from thiophene covered Si(100)-(2×1) also display greater intensity in the BE range 2.0 – 4.5 eV than the clean surface. This indicates that the presence of adsorbed thiophene has changed the nature of the bonding within the silicon dimers, due to the increase in the density of states observed in the 2 – 4 eV BE region.

The three broad features observed in the 5 – 18 eV BE region consist of bands which can be attributed to molecular orbitals of the moiety formed by the adsorption of thiophene on the Si(100)-(2×1) surface. If we consider previous work based on the adsorption of C_4H_4S on the surface of single crystals, three different species can be formed on Si(100)-(2×1) upon the adsorption of thiophene. The first possibility is a weakly molecularly adsorbed thiophene species, also observed on noble metal surfaces.[11] This moiety has also been suggested for the adsorption of thiophene on Si(111)-(7×7).[12] The other two possibilities are more strongly chemisorbed species which are directly bonded to the surface Si atoms. The first of these species is a 2,3-dihydrothiophene-like moiety, which was proposed by Jeong and co-workers in a previous study of thiophene adsorbed on the Si(100)-(2×1) surface.[13] Their UPS data, collected using a He(I) UV source, and semiempirical PM3 calculations provided the evidence for the assignment of the 2,3-dihydrothiophene-like moiety.[13] The second

possible chemisorbed moiety is a 2,5-dihydrothiophene-like species, which has been suggested as the moiety formed by thiophene on Si(100)-(2×1) by Qiao *et al.* [14] Their HREELS data revealed that the chemisorbed thiophene was a 2,5-dihydrothiophene-like moiety, which was consistent with a [4+2] cycloaddition reaction between C_4H_4S and the Si dimers.

The comparison between the gas phase spectra of thiophene,[15] 2,3-dihydrothiophene[16] and 2,5-dihydrothiophene,[17] and the difference UP spectra is made and displayed in Fig. 6 in order to determine which of the three possible moieties is formed after thiophene adsorption on Si(100)-(2×1). The normal and off-normal difference spectra are obtained by subtracting the corresponding clean surface spectrum from the one obtained after thiophene adsorption, and this type of spectrum emphasises the states produced by the adsorbate. The validity of using gas phase UP spectra to fingerprint the 2,3- and 2,5-dihydrothiophene-like surface moieties is provided by an ARUPS study of benzene on Si(100)-(2×1) by Gokhale and co-workers.[18] In this study it was found that benzene adsorption leads to the formation of a 1,4-cyclohexadiene-like moiety. The ARUP spectra of the benzene derived surface species displayed strong similarities with a spectrum collected from condensed multilayers of 1,4-cyclohexadiene and look different to the one of benzene.

The arguments that could help us to analyse the UPS data are given as follows. If a weakly perturbed thiophene species was formed after adsorption the observed UP spectrum would be expected to be very similar to the gas phase spectrum of the molecule apart from a possible shift in the band associated with the π-system of the aromatic ring. However it is clear in Fig. 6 that the thiophene gas phase spectrum does not match very well the difference UP spectra of thiophene adsorbed on Si(100)-(2×1), which rules out the possible thiophene-like structure of the moiety under study. Furthermore, it would also appear at first sight that the simple comparison with gas phase of 2,3- and 2,5-dihydrothiophene would not be justified for the two other possible moieties. This is because unlike their gas phase analogues the 2,3- and 2,5-dihydrothiophene-like surface moieties have C-Si instead of C-H bonds. However, this difference between the gas phase species and the surface moieties does not prevent meaningful comparison of photoemission spectra. Evidence to support this assumption comes from previous work carried out by Kuhn and co-workers who showed that the presence of side groups on a 2,3- or 2,5-dihydrothiophene ring in the gas phase does not

cause significant changes to photoemission spectra.[19] Gas phase photoemission spectra from derivatives of 2,3- and 2,5-dihydrothiophene are very similar to those of the parent molecules, with the same number of bands being observed. The only significant difference is that for the derivatives all the bands are shifted by a similar amount to either lower or higher BE from the positions of the parent molecules.

From the comparison between the gas phase photoelectron spectra of the three possible moieties depicted in Fig. 6, we believe that the gas phase of the 2,5-dihydrothiophene spectrum is the best match with the UP spectra of thiophene adsorbed on Si(100)-(2×1) at room temperature. This implies that the 2,5-dihydrothiophene-like moiety is formed on the surface with the carbon atoms at the 2 and 5 positions being bonded to the silicon atoms of the surface dimers, as shown in Fig. 3. Based upon the observations made in a previous study by Hamers and co-workers,[9] we suggest that the silicon dimer remains intact and unbuckles when the 2,5-dihydrothiophene-like moiety is formed. This assignment contradicts the work of Jeong *et al.*[13] but agrees with the work of Qiao and co-workers.[14] We also propose that the adsorption geometry of the moiety would have C_s symmetry with its symmetric plane perpendicular to the Si–Si dimer bond and the C=C double bond between two β-carbons while passing through the sulfur atom. This defines the plane formed by C(2)–Si–Si–C(5) to be close to normal to the surface, as can be seen in the schematic diagram of Fig. 3. These conclusions are consistent with a [4+2] cycloaddition reaction between C_4H_4S and the Si dimers of the Si(100)-(2×1) surface and is consistent with a Diels-Alder mechanism.

Fig.3. *The probable bonding geometry of the 2,5-dihydrothiophene-like moiety formed on Si(100)-(2×1) upon thiophene adsorption is shown schematically.*

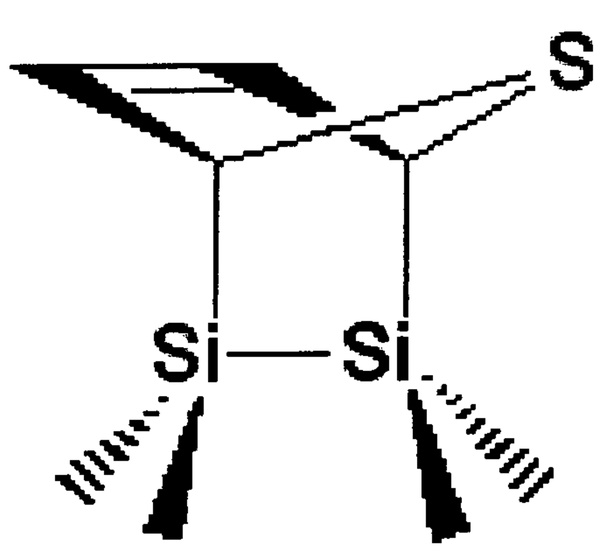

Fig.4. *Normal and off-normal emission valence band photoemission spectra ($h\nu = 40\ eV$) collected from a Si(100)-(2×1) surface that had been exposed to 60 L of thiophene at room temperature.*

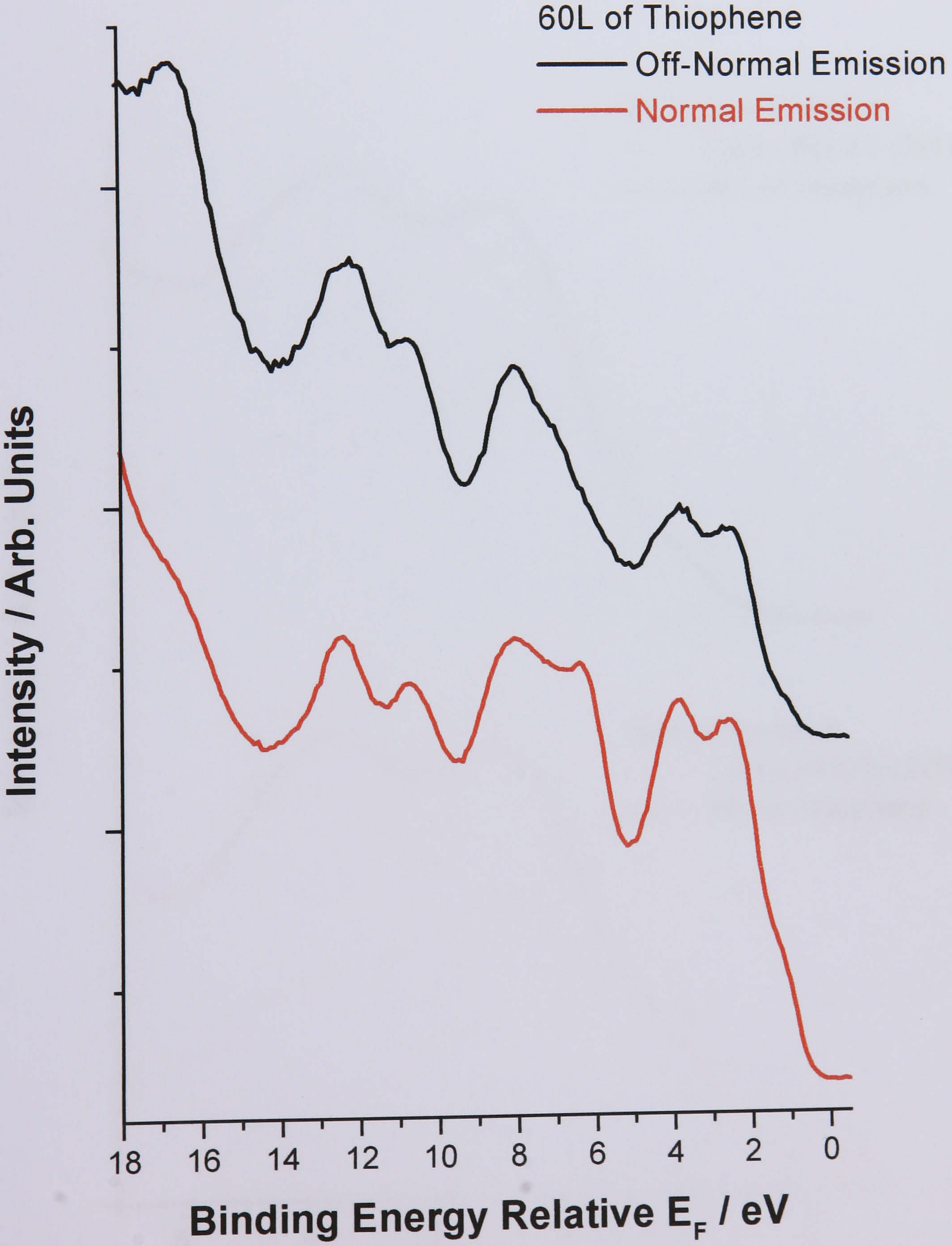

Fig.5. *Comparison between the off-normal and normal emission valence band photoemission spectra ($h\nu$ = 40 eV) of the clean Si(100)-(2×1) surface and the same surface exposed to 60 L of thiophene at room temperature. This plot shows the quenching of the surface states centred at 1.0 eV and the increase in the bands at 2.5 and 3.8 eV BE.*

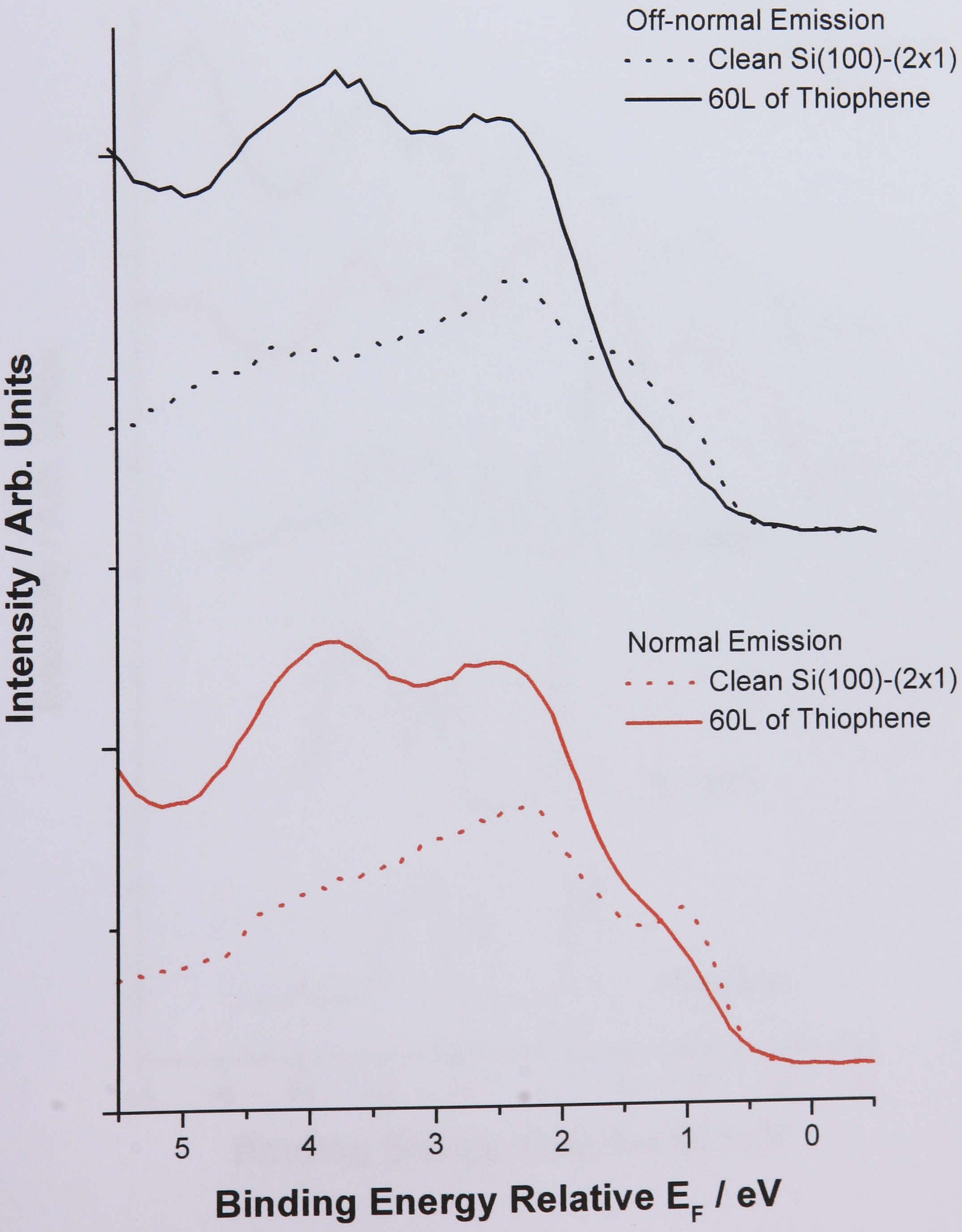

Fig.6. *Normal and off-normal difference spectra (hν = 40 eV) collected from Si(100)-(2×1) which had been exposed to 60 L of thiophene and is compared with gas phase spectra of thiophene[40], 2,5-dihydrothiophene (2,5-DHT)[35] and 2,3-dihydrothiophene (2,3-DHT).[24] The gas phase spectra have been shifted by 2 eV to lower BE.*

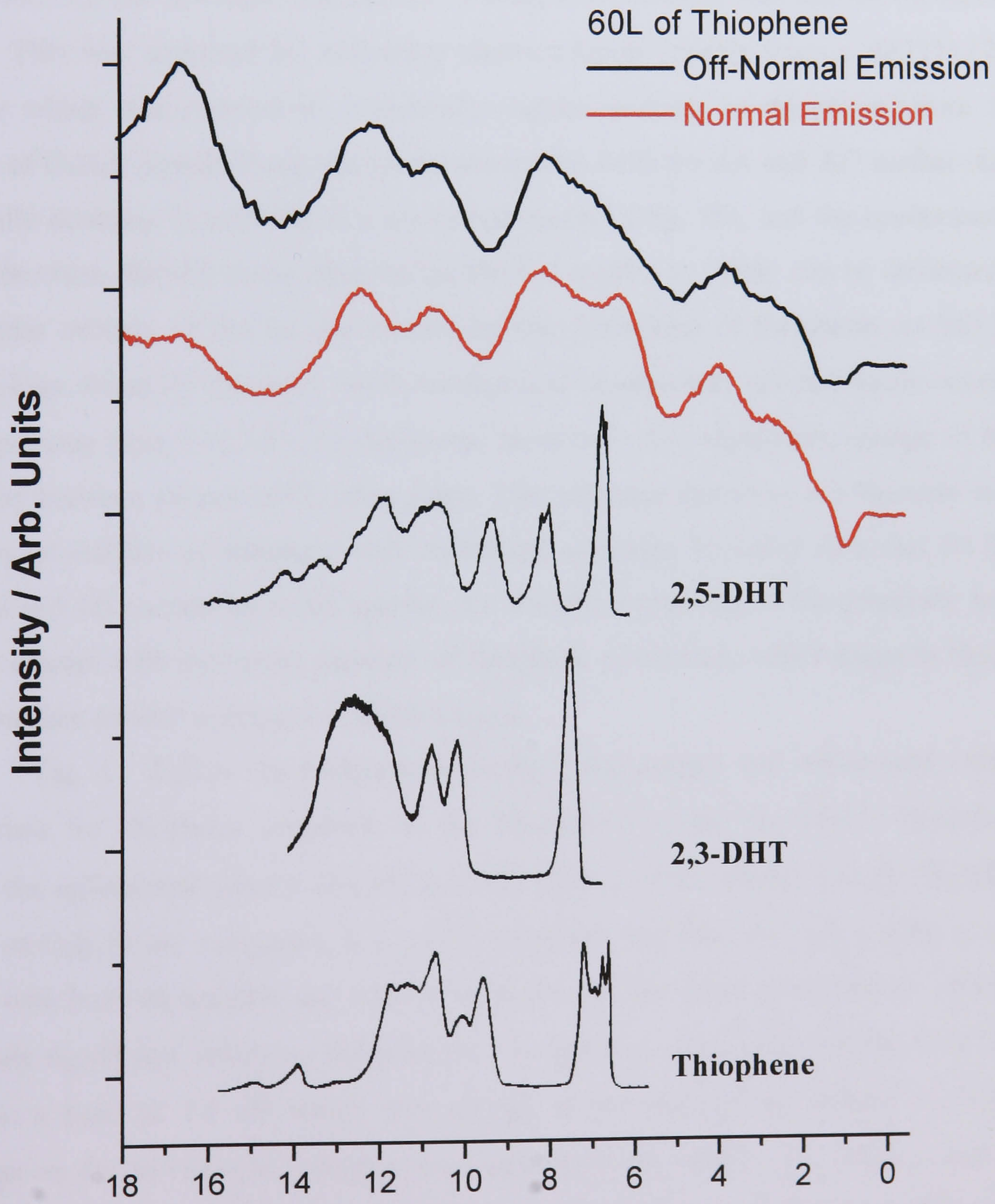

6.2.2 Thiophene/Si(111)-(7×7)

The clean surface UP spectra of the Si(111)-(7×7) surface displayed in Fig. 7 are in excellent agreement with previous work of the same system.[3,5,20] The two features centred at 0.5 and 1.1 eV are attributed to the rest atom (RA) and adatom (AD) surface states respectively. The presence of these two surface states, which confirm the cleanliness of Si(111)-(7×7), and the sharp (7×7) LEED pattern observed emphasise the good quality and high crystallographic order of the Si(111) surface used. In contrast to Si(100)-(2×1), the coverage dependence of thiophene bonding was studied on Si(111)-(7×7). This was achieved by collecting photoemission spectra from a Si(111)-(7×7) surface which was exposed to sequentially higher amounts of thiophene (from 1 to 300 L of C_4H_4S dosed). Upon thiophene adsorption both the RA and AD surface states gradually decrease in intensity in a concerted manner (Fig. 10), and the appearance of new adsorbate derived bands observed in the BE region 5 - 18 eV can be attributed to molecular orbitals of the moiety formed by the adsorption of thiophene on Si(111)-(7×7) (Figs. 8 and 9). The most rapid development of adsorbate induced bands occurred for exposures from 1 to 16 L of thiophene, however a less significant change in band intensity between 16 and 300 L takes place. This indicates that there is a decrease in the sticking probability of thiophene with increasing coverage. It is also clear that for both normal and off-normal emission spectra, the relative intensities of the adsorbate bands do not change with increasing amounts of thiophene adsorption, which suggests that the same surface moiety is present at all coverages.

Fig. 11 depicts the comparison between the normal and off-normal valence band data for thiophene adsorbed on the Si(100)-(2×1) and Si(111)-(7×7) surfaces. When the ***off-normal*** spectra of Si(111)-(7×7) (300 L of thiophene) and Si(100)-(2×1) (60 L of C_4H_4S) are compared, it is readily apparent that they are very similar to each other, with both the position and relative intensities of the bands being almost identical. The only significant difference between the two spectra is that in the Si(100)-(2×1) case there is a band at 1.0 eV which corresponds to the state of the unused Si dimers, whereas on the Si(111)-(7×7) surface the remnant of the metallic RA surface state can be observed at 0.5 eV BE (Fig. 11). On the other hand, there are significant differences between the UPS data of Si(111)-(7×7) and Si(100)-(2×1) at ***normal*** emission. Although the bands in the BE region 5 – 18 eV, which correspond to the molecular

orbitals of the thiophene derived moiety, appear in the same positions for both silicon surfaces, the relative intensities of the UP spectra differ. However the observation of bands with similar positions in photoemission spectra in Fig. 11 is a good evidence that the adsorption of thiophene leads to the formation of a 2,5-dihydrothiophene-like moiety on both Si(100)-(2×1) and Si(111)-(7×7) surfaces. Also given in Fig. 12 is the comparison between the gas phase spectra of 2,5-dihydrothiophene and the UP difference spectra of thiophene adsorbed on Si(111)-(7×7) and Si(100)-(2×1). As can be seen in this graph, there is a very good match between the gas phase and experimental UP spectra. This provides further evidence for the formation of 2,5-dihydrothiophene-like moieties upon thiophene adsorption on both silicon surfaces.

The normal emission data may initially appear to suggest that the moiety adopts significantly different geometries on the two surfaces because in UPS the relative intensities of the orbitals are correlated to the geometry of the surface moiety. However, in contrast to the normal emission data, the off-normal emission data for both surfaces display almost identical relative intensities, implying similar bonding geometries. This inconsistency between the normal and off-normal spectra can be resolved when the overall symmetry of the adsorbate–substrate complex is considered. If spectra are collected in a normal emission orientation (surface of the single crystal faces the analyser), constraints are placed on the allowed symmetries of the initial electronic states, and only states which have even symmetry with respect to reflection in planes that pass through the surface normal can be observed.[21] However, in the off-normal collection geometry there are no constraints on the symmetry of the initial state for which photoemission is allowed. This has some important consequences in the present case because the symmetry of the 2,5-dihydrothiophene-like moiety will be strongly influenced by the symmetries of Si(100)-(2×1) and Si(111)-(7×7) surfaces. For the adsorption geometry proposed for the 2,5-dihydrothiophene-like moiety on Si(100)-(2×1) the overall symmetry is C_S (the two surface Si atoms to which the molecule is bonded are symmetric – see Fig. 3). On the other hand, on the Si(111)-(7×7) surface, the overall symmetry of the adsorbate–substrate complex is likely to be reduced to C_1 (the molecule is likely to be attached to two asymmetric surface Si atoms). Therefore the difference in relative intensities in the normal emission spectra reflect the difference in the overall symmetry of the 2,5-dihydrothiophene/Si(100)-(2×1) and 2,5-dihydro-thiophene/Si(111)-(7×7) complexes.

To summarise, although differences in relative intensities of peaks in photoemission spectra generally indicate that the moiety adopts a different orientation with respect to the polarisation vector of the incident radiation, in the present case the similar relative peak intensities in photoemission spectra from the Si(100)-(2×1) and Si(111)-(7×7) suggest that on both surfaces the 2,5-dihydrothiophene-like moiety adopts a very similar geometry. The differing relative intensities of the normal emission data reflects the difference of the overall symmetry of the adsorbate – substrate complex on the two surfaces, as would be expected from the symmetry properties of the clean substrate. The two most important conclusions that can be drawn from the photoemission data are that firstly a 2,5-dihydrothiophene-like moiety is formed by the adsorption of thiophene on Si(111)-(7×7), and secondly the orientation of the moiety on the Si(111)-(7×7) surface is not significantly different to that adopted on the Si(100)-(2×1) surface.

Fig.7. *Normal and off-normal emission valence band photoemission spectra ($h\nu = 40\ eV$) collected from a clean Si(111)-(7×7) surface. The surface states corresponding to the Rest Atoms (RA) and Adatoms (AD) observed in the clean surface spectra have been labelled.*

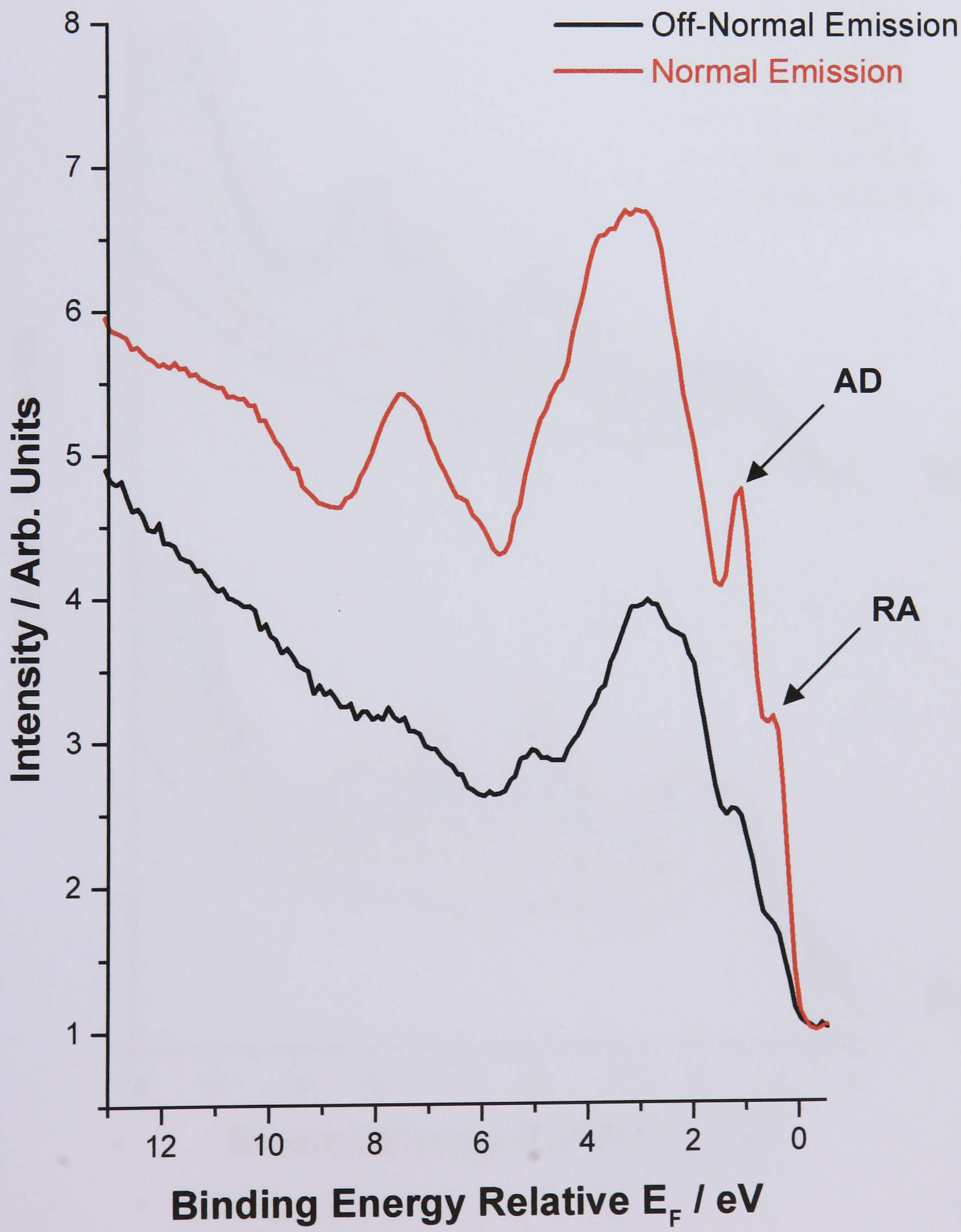

Fig.8. *Off-normal (a) and normal emission (b) valence band spectra (hν = 40 eV) collected from clean Si(111)-(7×7) and surfaces which had been exposed to 1, 2, 4, 8, 16 and 300 L of thiophene at room temperature.*

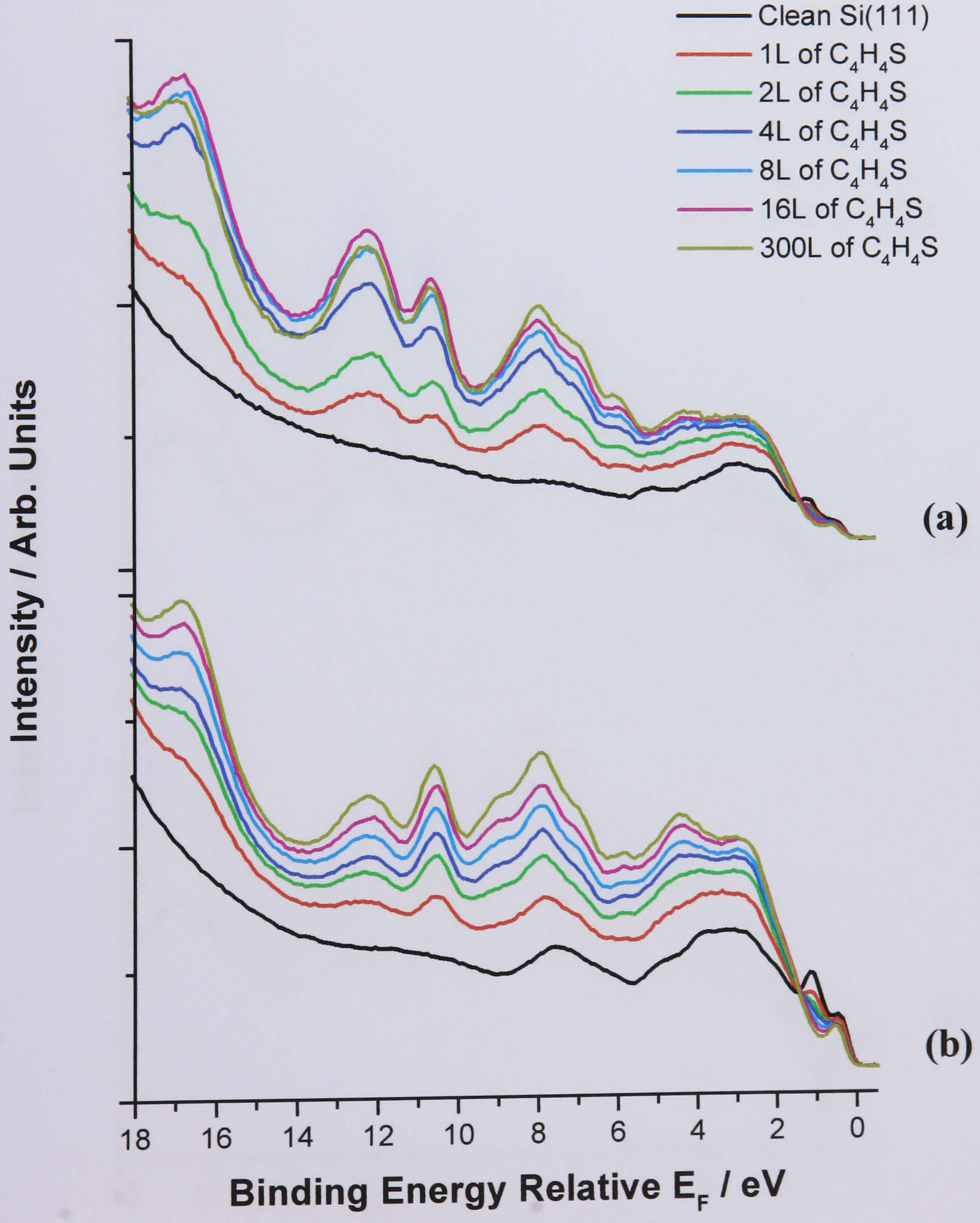

Fig.9. *Off-normal (a) and normal (b) emission difference UP spectra ($h\nu$ = 40 eV) produced by subtracting clean surface spectrum from those taken after exposing the Si(111)-(7×7) surface with 1, 2, 4, 8, 16 and 300 L of thiophene.*

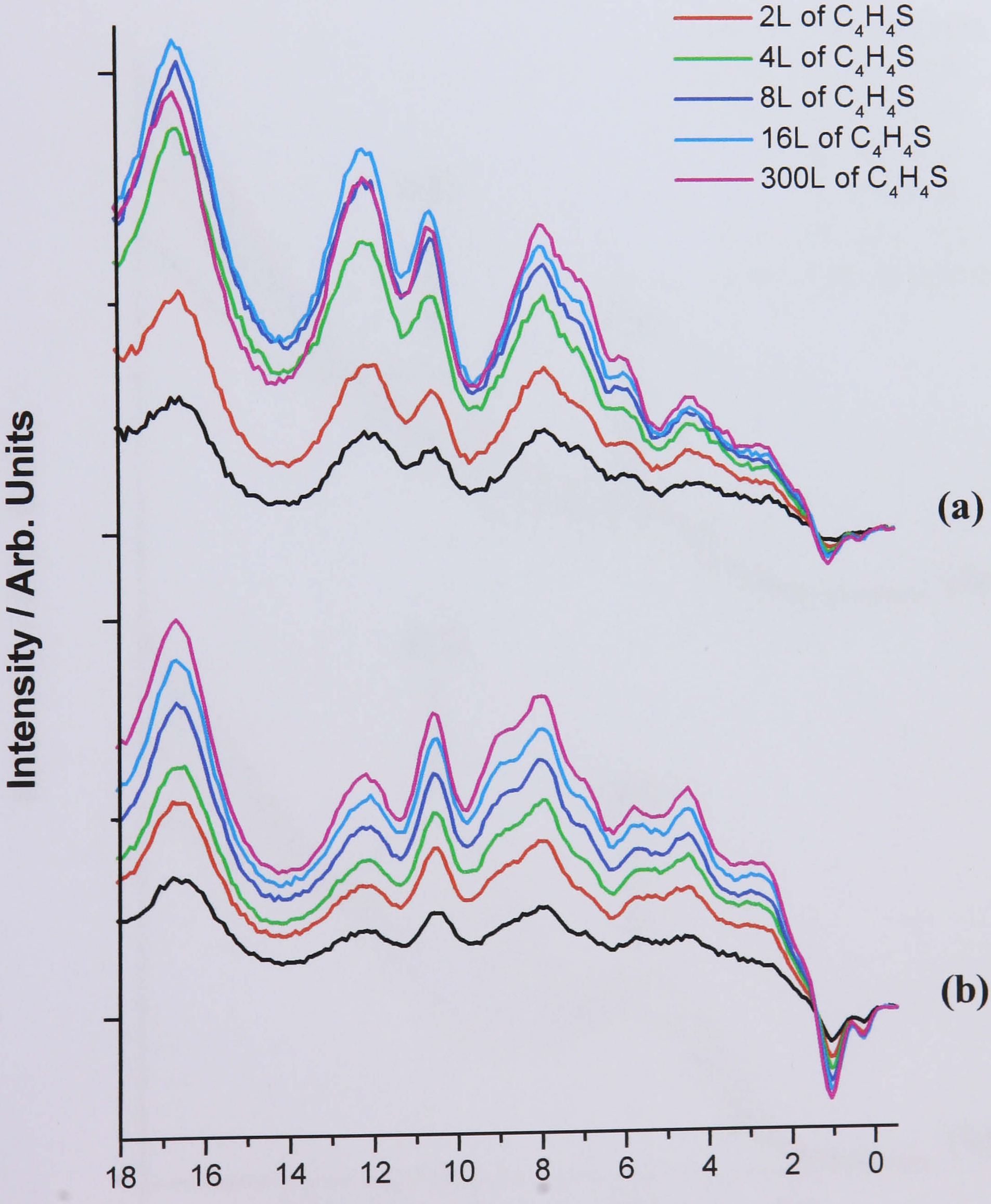

Fig.10. *Off-normal (a) and normal (b) emission valence band spectra (hν = 40 eV) collected from clean Si(111)-(7×7) and surfaces which had been exposed to 1, 2, 4, 8, 16 and 300 L of thiophene at room temperature which shows the gradual decrease in intensity of the RA and AD surface states upon increasing thiophene exposure*

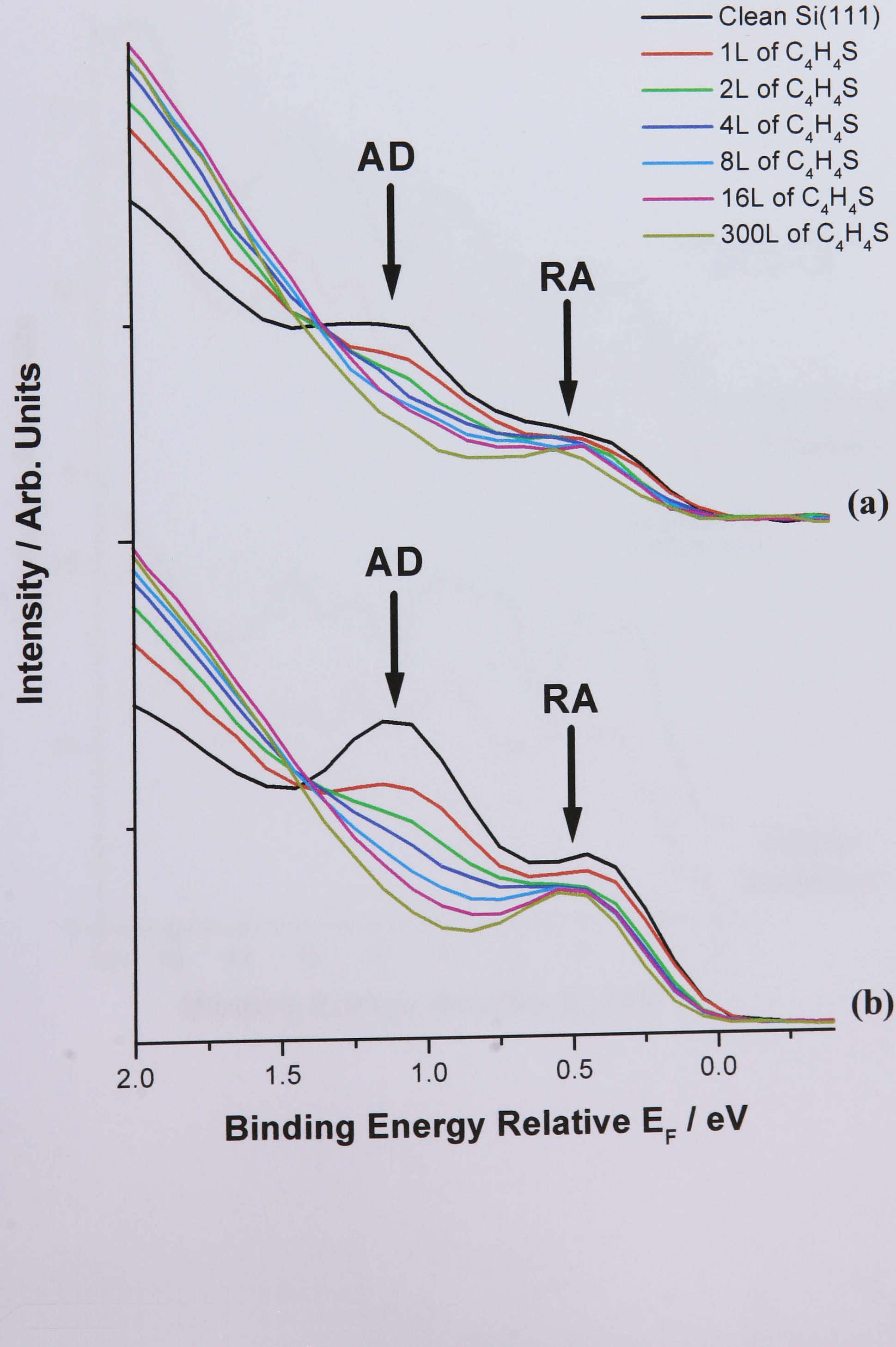

Fig.11. *Off-normal and normal emission valence band spectra (hν = 40 eV) collected from the Si(100)-(2×1) and Si(111)-(7×7) surfaces which had been exposed to 60 and 300 L of thiophene at room temperature respectively.*

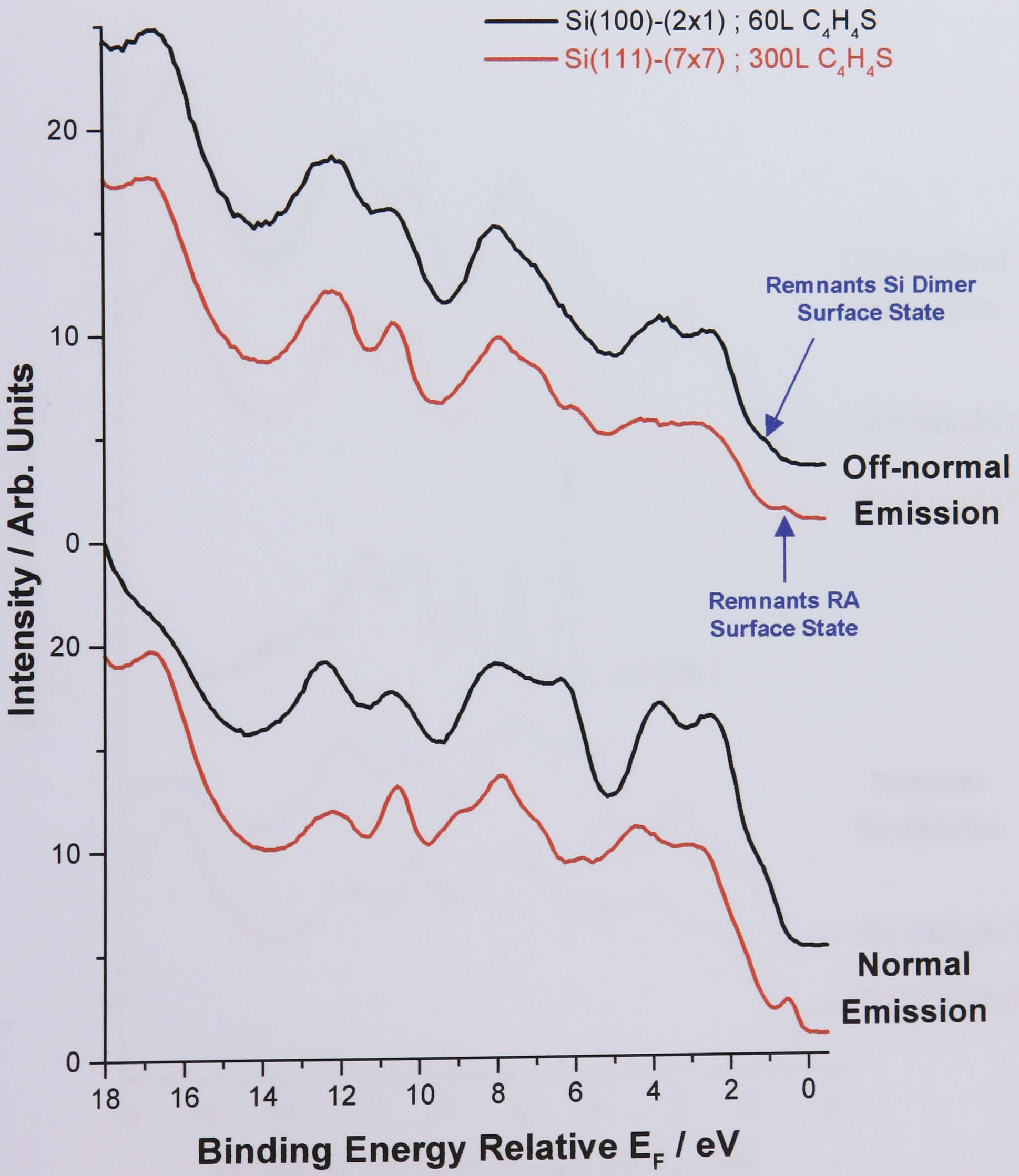

Fig.12. *Off-normal and normal difference spectra (hν = 40 eV) collected from the Si(100)-(2×1) and Si(111)-(7×7) surfaces, which had been exposed to 60 and 300 L of thiophene respectively, are compared with gas phase spectrum of 2,5-dihydrothiophene (2,5-DHT). The gas phase spectrum has been shifted by 2 eV to lower BE.*

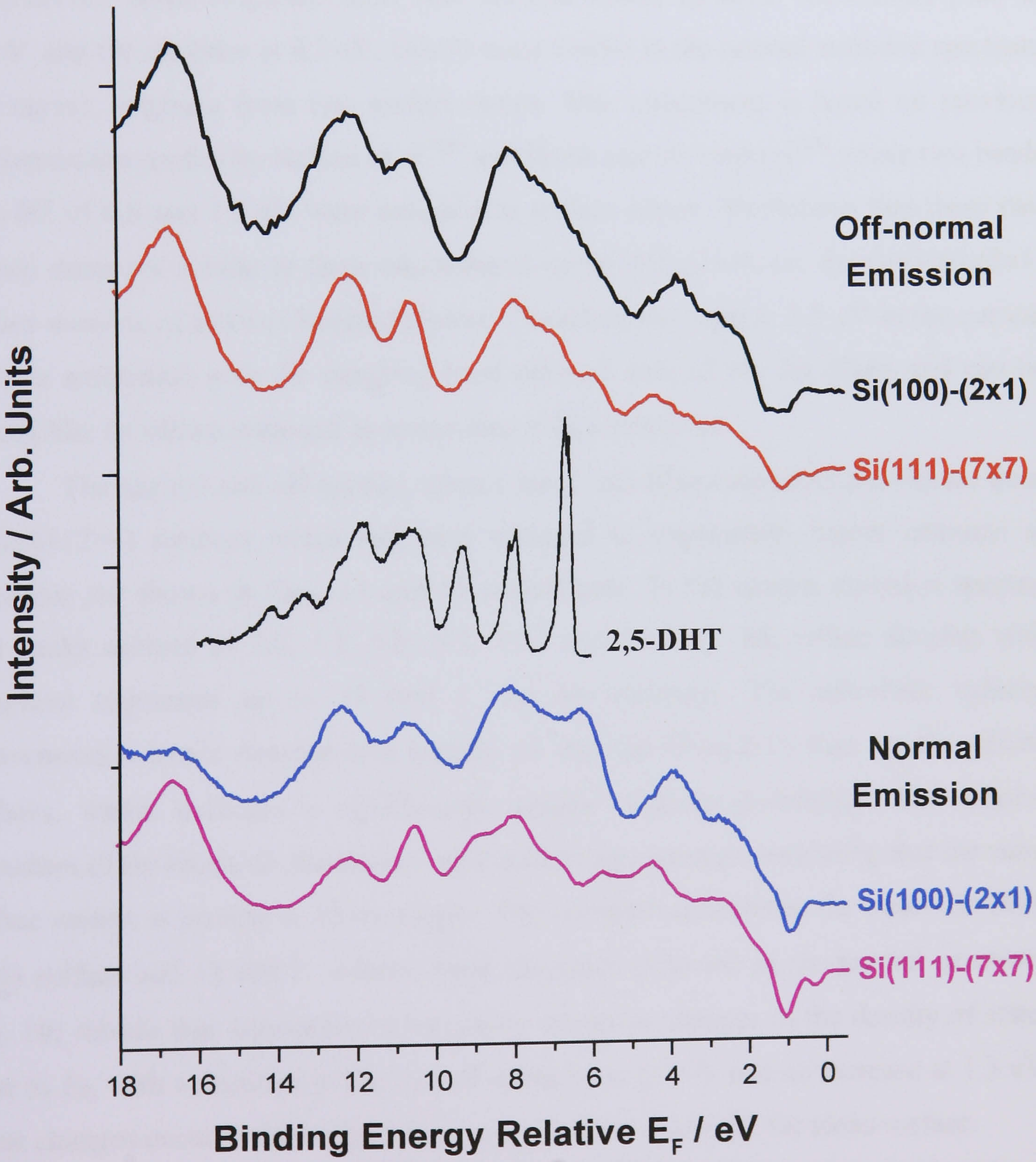

6.2.3 Thiophene/Ge(100)-(2×1)

Fig. 13 shows the photoemission data taken from the clean Ge(100)-(2×1) surface. These spectra are in good agreement with previous experimental and theoretical work,[22-24] in particular the normal emission spectrum which is very similar to the one collected by Hsieh and co-worker who used the same emission geometry and photon energy.[24] As can be seen in Fig. 13, both the normal and off-normal spectra of the clean surface present a series of bands with BE between 0 and 12 eV. The majority of the observed bands originate from bulk derived states, however the intense peak at 1.5 eV and the shoulder at 0.7 eV, clearly most visible in the normal emission spectrum (red curve), originate from two surface states. This assignment is based on previous photoemission studies by Nelson *et al.*[23] and Hsieh and co-workers[24] where two bands with BE of 0.6 and 1.3 eV were assigned to surface states. We believe that these two surface states are similar to those encountered on Si(100)-(2×1), i.e. the Ge(100)-(2×1) surface consists of rows of buckled dimers. Therefore the band at 1.5 eV in the current study is associated with the dangling bond derived state of the Ge dimer and can be viewed like its silicon analogue as possessing π-like character.

The normal and off-normal valence band and difference spectra collected from Ge(100)-(2×1) surfaces which had been exposed to sequentially higher amounts of thiophene are shown in Figs. 14 and 15 respectively. In the normal emission spectra, four peaks centred at 2.0, 3.7, 5.9, 8.3, 10.1 and 11.9 eV BE which develop with thiophene exposures up to 13 000 L can be observed. The adsorbate induced photoemission bands develop less rapidly on the Ge(100)-(2×1) than on the silicon surfaces, which indicates a significantly smaller sticking probability. The relative intensities of the bands do not change with increasing exposure, indicating that the same surface moiety is present at all coverages. The comparison between the clean Ge(100)-(2×1) surface and 13 000 L valence band spectrum collected in the normal geometry (Fig. 16) reveals that adsorption of thiophene results in changes in the density of states close to E_F, with a decrease in the overall intensity at 0.6 eV and an increase at 1.3 eV. These changes occur in the region where surface states occur for the clean surface.

Like the normal emission data there are no changes in the relative intensities of bands observed in off-normal emission with increasing exposures of thiophene, which indicates that the bonding of the surface moiety does not significantly alter with

increasing coverage. The positions and relative intensities of the bands in the off-normal spectra of thiophene adsorbed on Ge(100)-(2×1) are almost identical to those found for Si(100)-(2×1) and Si(111)-(7×7), as shown in Fig. 17. Also displayed in this graph is the gas phase spectrum of 2,5-dihydrothiophene and from the comparison made, it is clear that a 2,5-dihydrothiophene-like moiety is formed by the adsorption of thiophene on the Ge(100)-(2×1) surface. We therefore suggest that the bonding of the 2,5-dihydrothiophene-like moiety to Ge(100)-(2×1) is identical to that proposed for Si(100)-(2×1), with the moiety bonding to an unbuckled germanium dimer. The same assignment was proposed by Hamers *et al.*,[9] where the authors showed that the surface chemistry of alkenes with Ge(100)-(2×1) is very similar to the one observed on Si(100)-(2×1).On both Si(100)-(2×1) and Ge(100)-(2×1) the strong σ back bone between the dimer atoms remains intact after adsorption of the alkene. Applying similar arguments to those used for Si(100)-(2×1), the reactions of alkenes and dienes with Ge(100)-(2×1) have been viewed as [2+2] and [4+2] cycloadditions.

In conclusion, the photoemission data clearly shows that the moiety formed by the adsorption of thiophene on Ge(100)-(2×1) is the same as that produced on both Si surfaces. From the similar relative peak intensities in the off-normal emission spectra we believe that the adsorption geometry of the moiety is not significantly different on the three surfaces. The most striking difference revealed by the photoemission data is that the sticking probability of thiophene on Ge(100)-(2×1) is significantly smaller than on the silicon surfaces.

Fig.13. *Normal and off-normal emission valence band photoemission spectra ($h\nu = 40\ eV$) collected from a clean Ge(100)-(2×1) surface. The surface states observed in the clean surface spectra have been labelled.*

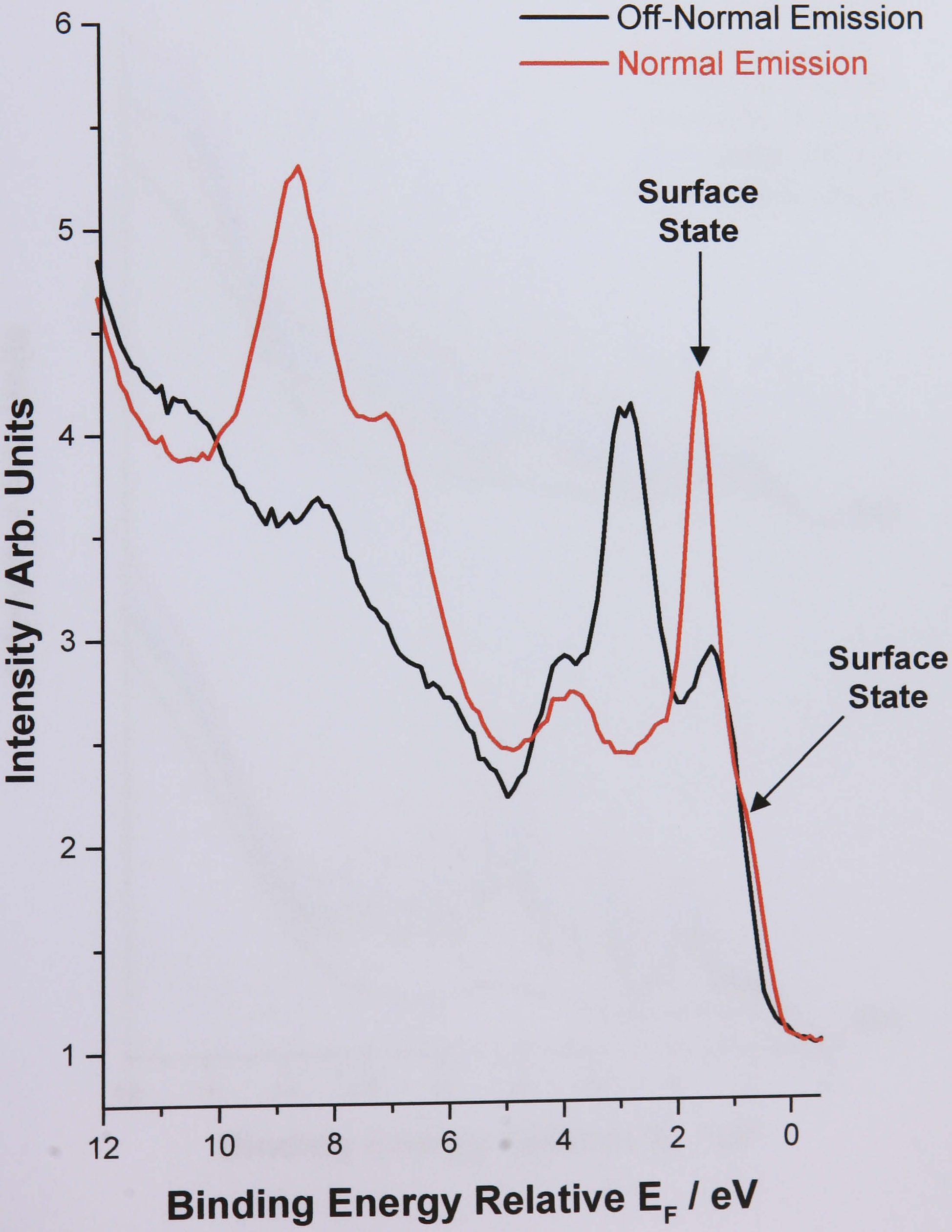

Fig.14. *Off-normal (a) and normal emission (b) valence band spectra (hν = 40 eV) collected from clean Ge(100)-(2×1) and surfaces which had been exposed to 30, 100, 300, 3000 and 13 000 L of thiophene at room temperature.*

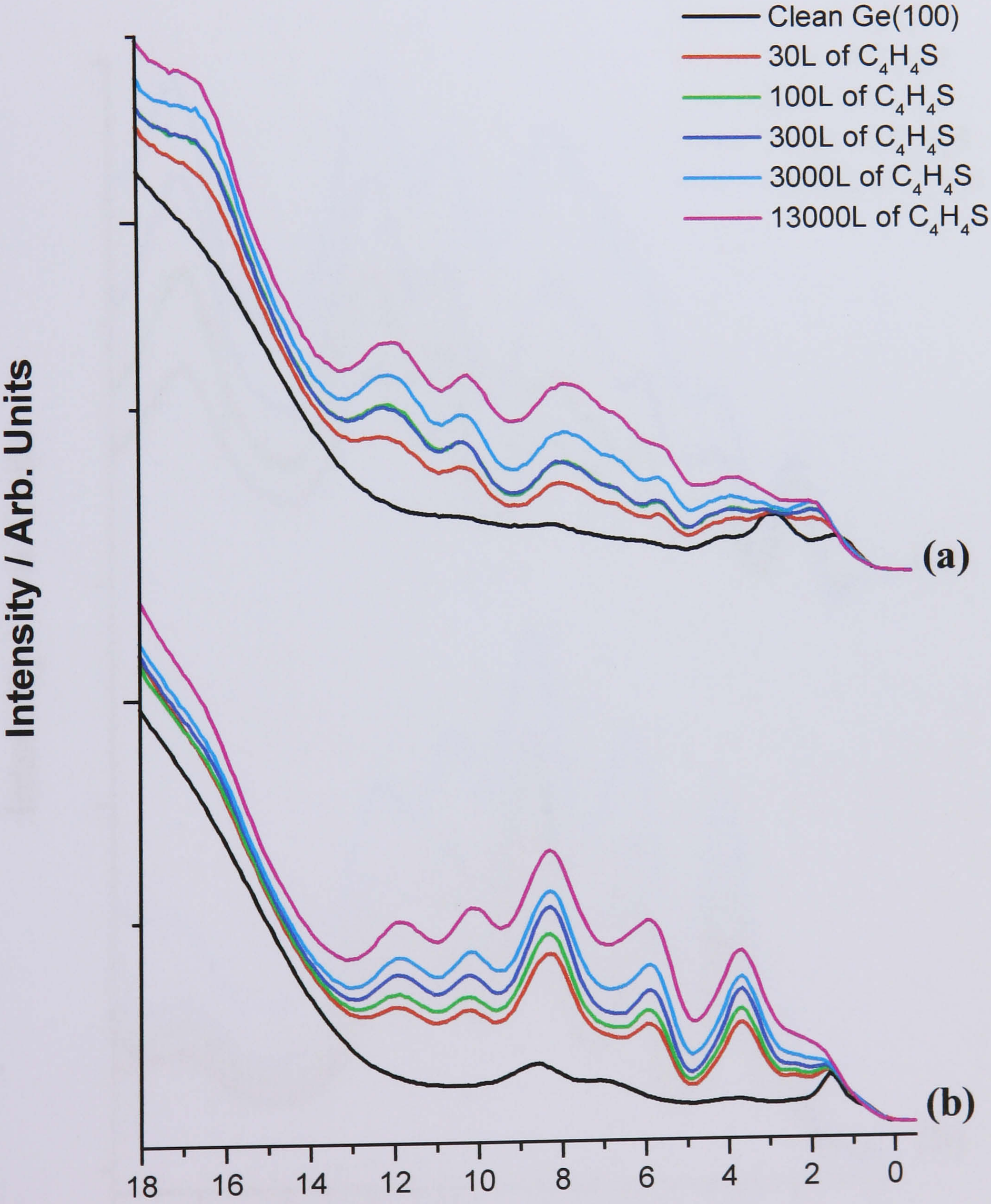

Fig.15. *Off-normal (a) and normal (b) emission difference spectra (hν = 40 eV) produced by subtracting clean surface spectrum from those taken after exposing the Ge(100)-(2×1) surface with 30, 100, 300, 3000 and 13 000 L of thiophene at room temperature.*

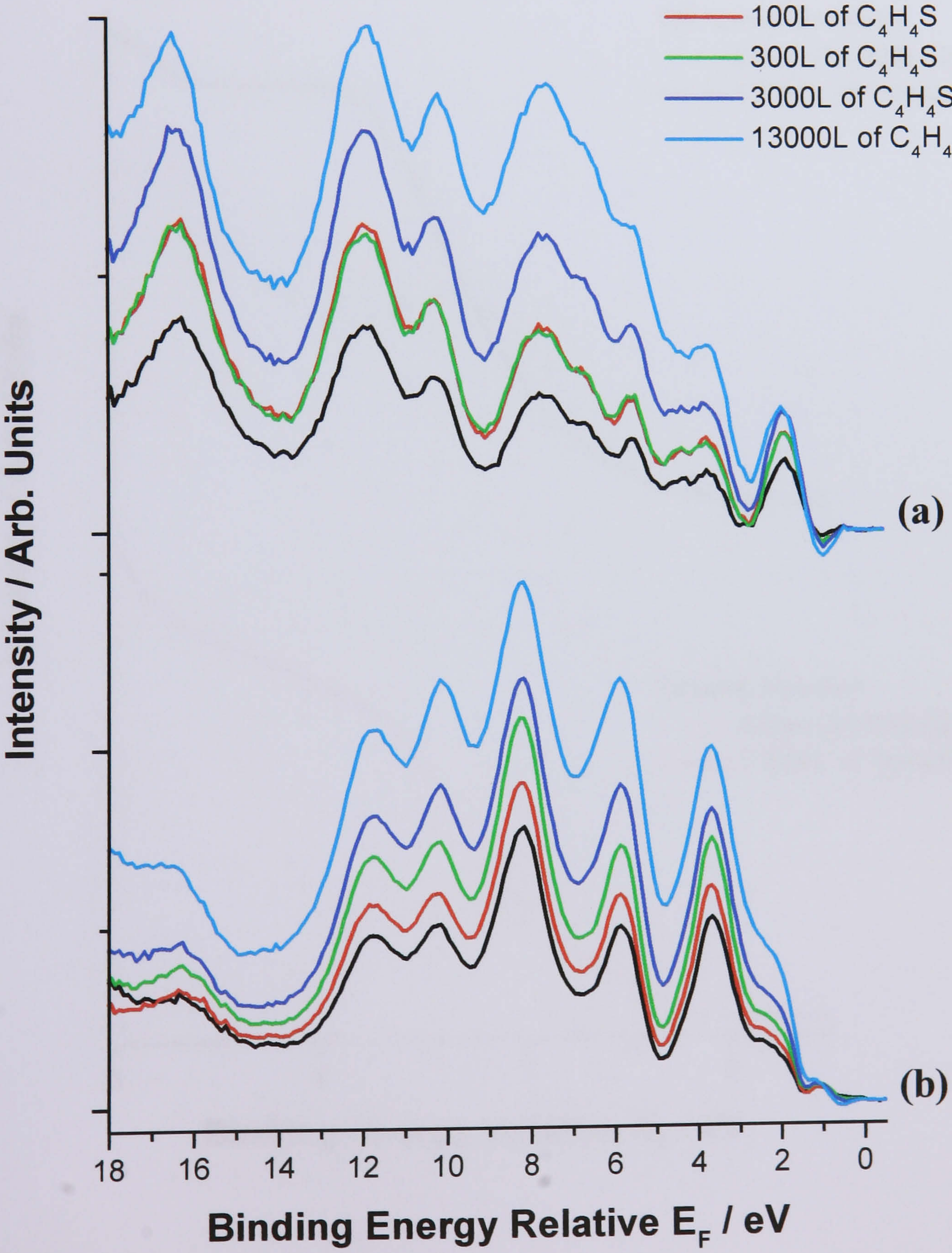

Fig.16. *Comparison between the off-normal and normal emission valence band photoemission spectra (hν = 40 eV) of the clean Ge(100)-(2×1) surface and the same surface exposed to 13 000L of thiophene at room temperature.*

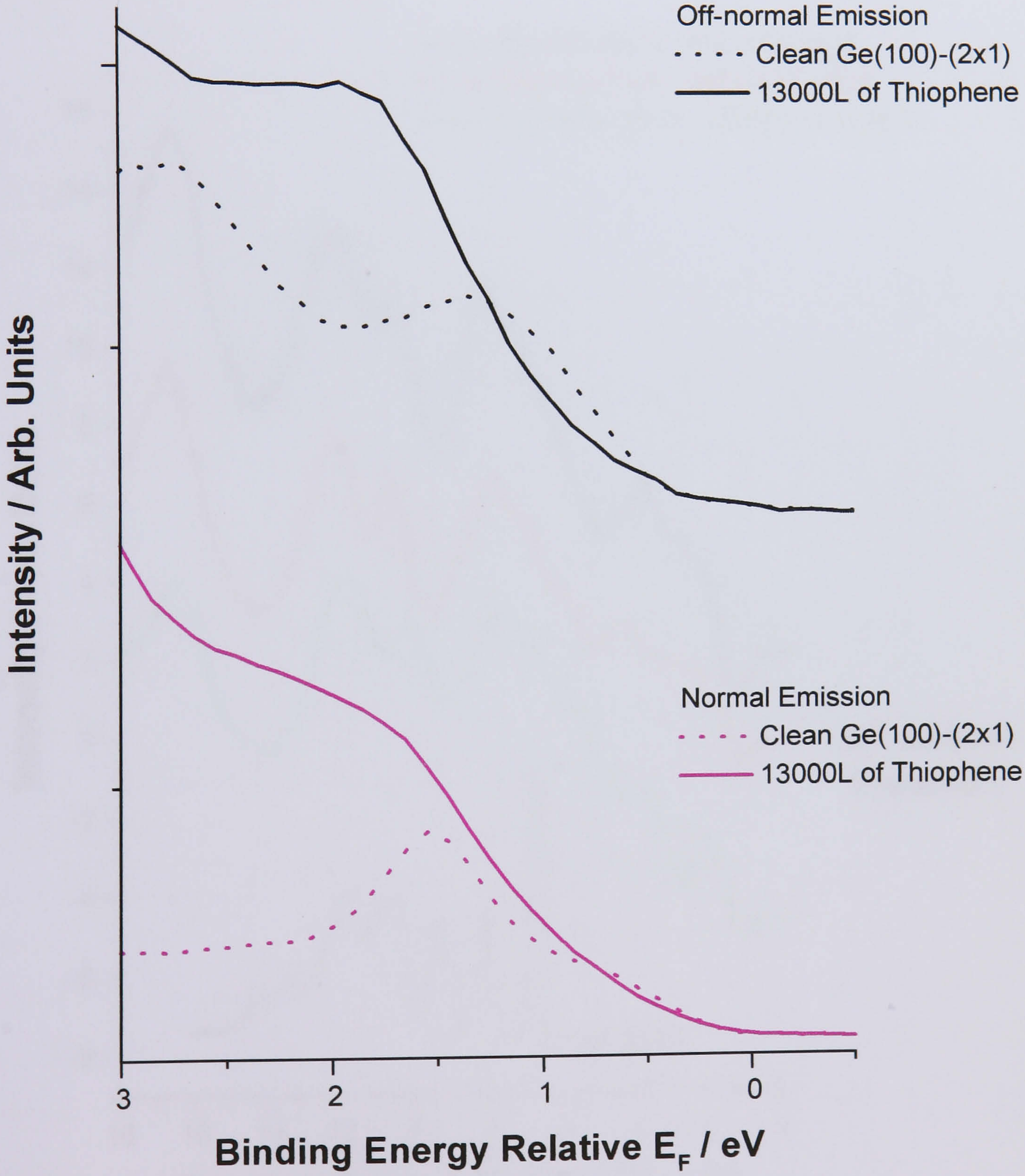

Fig.17. *Off-normal difference spectra (hν = 40 eV) collected from the Si(100)-(2×1), Si(111)-(7×7) and Ge(100)-(2×1)surfaces, which had been exposed to 60, 300 and 13 000 L of thiophene respectively, are compared with gas phase spectrum of 2,5-dihydrothiophene (2,5-DHT). The gas phase spectrum has been shifted by 2 eV to lower BE.*

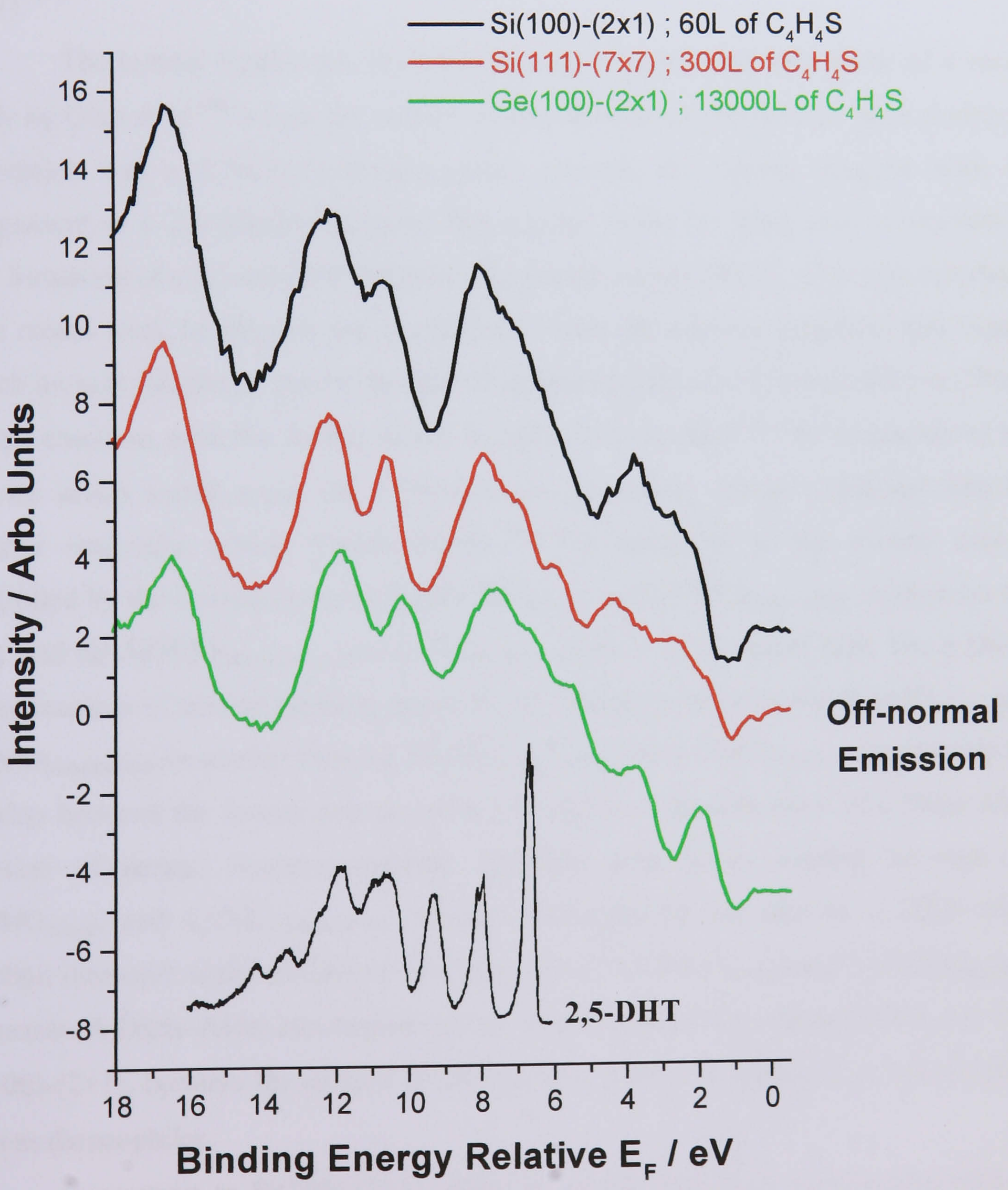

6.3 Discussion

What is unique about this current study is that we have investigated the adsorption of a single organic molecule on a series of substrates using a single technique under identical experimental conditions. This approach allows us to readily compare data from each system and hence facilitate the establishment of structure/reactivity relationships. The results of the current work can be directly compared with previous investigations of thiophene on Si(100)-(2×1)[13,14] and Si(111)-(7×7).[16]

The current results for Si(100)-(2×1) are in agreement with those of a recent study by Qiao *et al.*[14] where the surface moiety formed on this surface upon thiophene adsorption was a 2,5-dihydrothiophene-like species, but clearly disagree with the assignment of a 2,3-dihydrothiophene-like species made by Jeong and co-workers.[13] The formation of a 2,5-dihydrothiophene-like moiety on Si(100)-(2×1) is also consistent with recent work by Hamers and co-workers where the authors suggested that dienes, which include thiophene, can be thought of as undergoing a [4+2] cycloaddition (Diels–Alder) reactions with the dimers of the Si(100)-(2×1) surface.[9] The formation of this species which would occur *via* a Diels–Alder mechanism can be explained with the frontier molecular orbital (FMO) theory.[30] The reactivity in the present case is controlled by the overlap between the $HOMO_{(diene)}$ and $LUMO_{(dieneophile)}$ orbitals on one side, and the $HOMO_{(dieneophile)}$ and $LUMO_{(diene)}$ orbitals on the other side. For a Diels–Alder reaction of normal electron demand, the separation between the $HOMO_{(diene)}$ and $LUMO_{(dieneophile)}$ is smaller than the $HOMO_{(dieneophile)}$ and $LUMO_{(diene)}$, consequently the overlap between the former pair dominates reactivity. The efficiency of a Diels Alder reaction of normal electron demand increases with better overlap between the $HOMO_{(diene)}$ and $LUMO_{(dieneophile)}$ orbitals. Consequently the rate of a Diels–Alder reaction increases as the difference of energy between $HOMO_{(diene)}$ and $LUMO_{(dieneophile)}$ decreases. A Diels–Alder mechanism can be used to explain the reactions of dienes with Si(100)-(2×1), because the surface Si dimers have weak π character and hence can be seen as dieneophiles.

In contrast to Si(100)-(2×1), there is no previous study of the adsorption of thiophene on Ge(100)-(2×1) available in the literature. However our results for the Ge(100)-(2×1) surface are entirely consistent with the known behaviour of the

germanium substrate reported in the literature. Using similar arguments to those invoked to explain the reactivity of Si(100)-(2×1), it has been proposed that dienes, specifically butadiene[31] and 1,3-cyclohexadiene,[32] can undergo Diels–Alder reactions on the Ge(100)-(2×1) surface. A Diels–Alder mechanism can be used to explain the reaction of thiophene with Ge(100)-(2×1) with the formation of the 2,5-dihydrothiophene-like moiety, but it can also explain why the Ge(100)-(2×1) surface is less reactive than the Si(100)-(2×1) surface. As illustrated in Fig. 18, the $HOMO_{thiophene}$ ($1a_2$ orbital) lies at 8.9 eV below E_V,[33] while the $LUMO_{thiophene}$ ($3b_1$ orbital) is located at 1.15 eV above E_V,[14] and these two molecular orbitals are of π symmetry. For both the silicon and germanium dimers the $LUMO_{Si}$ and $LUMO_{Ge}$ are unoccupied dangling bond states with π* character, and the $HOMO_{Si}$ and $HOMO_{Ge}$ are occupied dangling bond states with π symmetry. The $LUMO_{Si}$ and $LUMO_{Ge}$ are located 0.35 eV[34] and 0.90 eV[35] above E_F, and the $HOMO_{Si}$ and $HOMO_{Ge}$ lie 0.80[34] eV and 1.00 eV[35] below E_F, respectively. Given that the work functions of Si(100) and Ge(100) are 4.91 and 5 eV,[36] the positions of $LUMO_{Si}$, $LUMO_{Ge}$, $HOMO_{Si}$ and $HOMO_{Ge}$ with respect to the vacuum level E_V for the two surfaces are 4.56, 4.10, 5.71 and 6.00 eV respectively. These values provides:

- $HOMO_{thiophene} - LUMO_{Si} = 8.90 - 4.56 = 4.34$ eV
- $HOMO_{Si} - LUMO_{thiophene} = 5.71 - (-1.15) = 6.86$ eV
- $HOMO_{thiophene} - LUMO_{Ge} = 8.90 - 4.10 = 4.80$ eV
- $HOMO_{Ge} - LUMO_{thiophene} = 6.00 - (-1.15) = 7.15$ eV

Because ($HOMO_{thiophene} - LUMO_{Si}$) is smaller than ($HOMO_{Si} - LUMO_{thiophene}$), and ($HOMO_{thiophene} - LUMO_{Ge}$) is also smaller than ($HOMO_{Ge} - LUMO_{thiophene}$), the thiophene adsorbed on Si(100)-(2×1) and Ge(100)-(2×1) undergoes a Diels–Alder reaction of normal electron demand. The energy differences calculated above indicate that the direction of the electron donation flows from the adsorbate into the empty silicon and germanium dimer π* orbital, and also show a poorer orbital overlap for Ge(100)-(2×1), as ($HOMO_{thiophene} - LUMO_{Si}$) < ($HOMO_{thiophene} - LUMO_{Ge}$), indicating that the Diels–Alder reaction is less favourable for the Ge(100) surface. This could explain the lower sticking probability observed experimentally for the Ge(100)-(2×1) surface. A further possible explanation for the difference in reactivity between Si(100) and Ge(100) could stem from the electronic properties of the surface dimers. A study by

Chadi[7] suggested that a charge transfer from the down atom to the up atom takes place within the non-planar Si and Ge dimers which adds some Zwitterionic character to the dimers (see Fig. 3 in Chapter 1). In two recent high resolution core-level spectroscopy studies of the Si(100)-(2×1) and Ge(100)-(2×1) surfaces by Pi *et al.*,[39,40] it was found that the energy separations between the down atoms and the up atoms were 0.778 eV for Si(100)[39] and 0.259 eV for Ge(100).[40] These two energy separations therefore indicate that there a greater degree of polarisation between the Si dimer than the Ge dimer. This may also explain the difference in reactivity between the two semiconductor surfaces, as the probability for interaction is higher on Si than Ge.

Fig.18. *Schematic orbital energy correlation diagram of frontier molecular orbitals of thiophene with Si(100)-(2×1) and Ge(100)-(2×1). The HOMO and LUMO energy levels of thiophene, Si(100)-(2×1) and Ge(100)-(2×1) have been labelled. The Fermi level of both surfaces ($E_{F,Si}$ and $E_{F,Ge}$) are also indicated. This schematic diagram has been drawn to scale.*

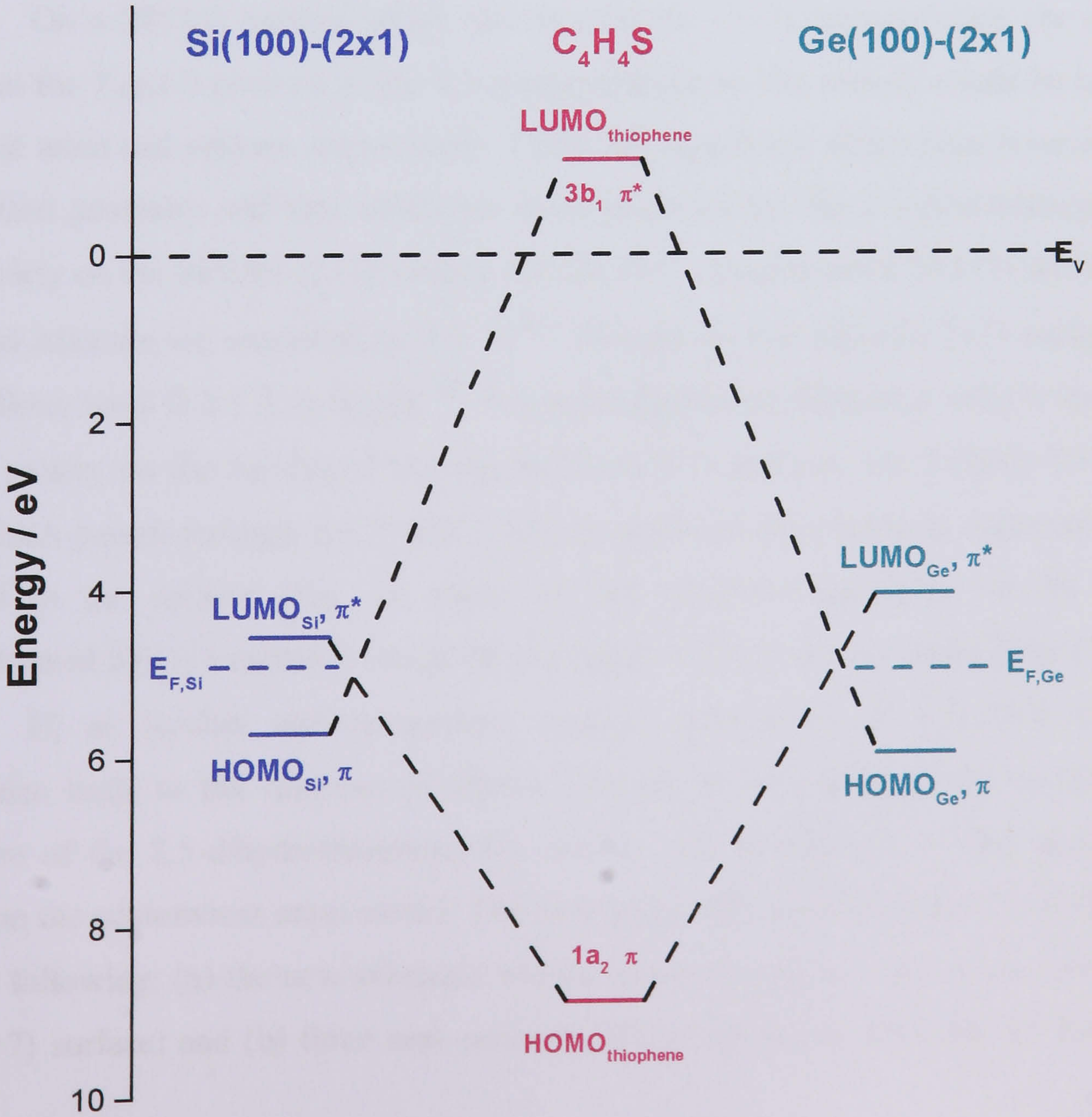

The assignment of the probable adsorption geometry of the 2,5-dihydrothiophene-like moiety on the Si(111)-(7×7) surface is more difficult than on Si(100)-(2×1) or Ge(100)-(2×1), because the latter surfaces are structurally simpler. This difficulty is reflected in the literature where there is some controversy as to the bonding geometry of organic adsorbates. For instance, for the adsorption studies of ethylene[25] and benzene[26] on Si(111)-(7×7), it was proposed that both C_2H_2 and C_6H_6 molecules are bonded to a pair of adjacent Si adatom – rest atom. However, in a photoemission study carried out by Rochet *et al.*, it has been suggested that the adsorption of organic molecules causes a re-arrangement of silicon atoms within the (7×7) reconstruction, which involves the removal of the adatom to an interstitial position under the plane containing the rest and pedestal atoms.[27] Work by MacPherson *et al.* where the adsorption of π bonded organic molecules led to an observed (7×1) LEED pattern provides further evidence for the re-arrangement of the (7×7) reconstruction.[28] Therefore the structure of the adsorbed 2,5-dihydrothiophene-like moiety will clearly be dependent on whether the (7×7) structure is retained upon thiophene adsorption.

On a Si(111) surface which has retained the (7×7) reconstruction the carbon atoms at the 2 and 5 position of the 2,5-dihydrothiophene-like moiety would be bonded to a rest atom and adatom respectively. There are significant differences between this adsorption geometry and that which has been proposed for the 2,5-dihydrothiophene-like moiety on the Si(100)-(2×1) surface. On the (7×7) reconstructed Si(111) surface the rest and adatoms are separated by 4.5 Å,[29] whereas for the Si(100)-(2×1) surface the Si–Si dimer bond is 2.3 Å in length.[27] A second significant difference is the orientation of the moiety on the Si(100)-(2×1) and Si(111)-(7×7) surfaces. On Si(100)-(2×1) the axis which passes through the 2 and 5 carbon atoms of the moiety is expected to be parallel to the surface (Fig. 3), while for the proposed geometry on the (7×7) reconstructed Si(111) surface it would be at a angle of 13° to the rest plane (Fig. 19).

If, as Rochet and co-workers suggest, adsorption of π-bonded organic molecules leads to the removal of silicon adatoms to interstitial positions, then the structure of the 2,5-dihydrothiophene-like moiety will be different to that postulated based on the adatom/rest atom model. The two major effects of the removal of adatoms are the following: (a) the new substrate will be less corrugated on an atomic level than the (7×7) surface; and (b) three new pedestal silicon atoms are available for bonding.

These two changes in the structure of the surface would influence the possible adsorption geometry and local registry of the 2,5-dihydrothiophene moiety because it could no longer bond in the AD/RA configuration. However, it could bond to the pedestal atoms exposed by the removal of the adatom. Bonding to the pedestal silicon atoms would have two effects on the geometry of the moiety. Firstly, assuming their positions remain the same as those adopted in the (7×7) structure, the separation between pedestal silicon atoms (3.7 Å) is shorter than the distance between adatoms and rest atoms (4.5 Å). Clearly, a shorter Si–Si separation will place different strains on the geometry of the 2,5-dihydrothiophene–surface complex, which would influence geometry. A second effect of the 2,5-dihydrothiophene moiety bonding to pedestal silicon atoms is that it could adopt a geometry where the axis passing through the 2 and 5 positions is parallel rather than inclined to the rest-atom plane, geometry which is similar to that adopted on Si(100)-(2×1). If the moiety bonded in a more tilted AD/RA configuration, one may have expected the Si(111)-(7×7) and Si(100)-(2×1) off-normal emission spectra to display greater differences, however the relative positions and relative intensities of peaks of these two spectra depicted in Fig. 11 are almost identical.

Although the current photoemission data does not provide any detailed quantitative information on the structure of the underlying Si(111) substrate, we believe from our valence band photoemission spectra that the Rochet model of a re-arranged (7×7) reconstruction (with the removal of the adatom) is the best description of the Si(111)-(7×7) surface after thiophene adsorption. It should be stressed that our suggestion of a re-arrangement of Si(111)-(7×7) is only tentative, to provide a more unambiguous answer, experiments which give quantitative structural information are required.

Fig.19. *Schematic diagrams of (a) the clean Si(111)-(7x7) surface where the rest atoms (RA), adatom (AD) and pedestal atom (PA) have been labelled, (b) the 2,5-dihydrothiophene-like moieties bonded to the RA and AD in a bridging geometry and (c) the 2,5-dihydrothiophene-like species bonded to the RA and PA.*

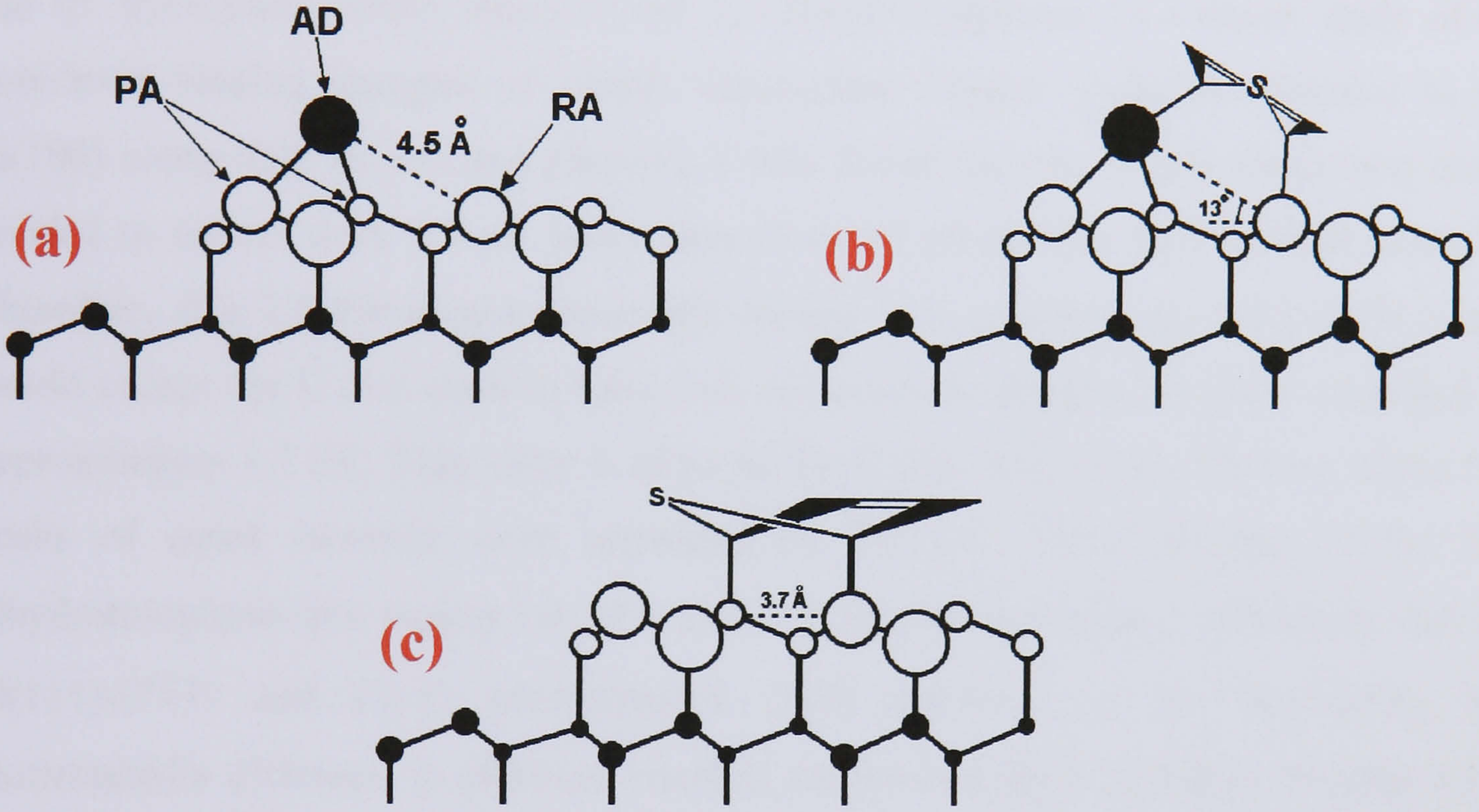

The formation of the 2,5-dihydrothiophene-like moiety on Si(111)-(7×7) is perhaps the most interesting aspect of the current study. From our results we have drawn significantly different conclusions to those reached by MacPherson and co-workers in the only other previous study of thiophene adsorbed on Si(111)-(7×7).[12] In this previous work MacPherson *et al.* suggested that C_4H_4S adsorption on Si(111)-(7×7) occurred in a similar manner to the one found when the molecule adsorbed on Cu(111).[11] On this surface, thiophene adsorbs in a roughly flat geometry at low coverage and then adopts a more upright geometry at high coverage. The driving force for such a compressional phase transition is the energy advantage of increasing the thiophene packing density. MacPherson and co-workers used the observation of two chemically shifted components in C (1s) photoemission spectra as the basis for the assignment of compressional phase transition observed. The two chemically shifted

components were assigned to two adsorbed thiophene species with different bonding geometries. We believe that the data presented by MacPherson and co-workers does not allow for an unambiguous assignment of a compressional phase transition for thiophene adsorption on Si(111)-(7×7). If we re-interpreted the experimental data obtained by MacPherson and co-workers, it can be shown these results are entirely consistent with the formation of a 2,5-dihydrothiophene-like moiety upon thiophene adsorption. We believe that the two components of the C (1s) peak can be assigned to emission from sp^3 and sp^2 hybridised carbon atoms of the 2,5-dihydrothiophene. In a recent study of the core-level binding energies of simple unsaturated organic molecules bonded to the Si(100) using XPS by Liu and Hamers, it was found that the 1s BE for carbon atoms bonded to silicon were 1.7 eV lower than those of alkene-like (sp^2) carbon atoms.[37] Therefore, if a 2,5-dihydrothiophene-like moiety was adsorbed on Si(111)-(7×7) one would except the C (1s) peak to have two components of equal intensity separated by approximately 1.7 eV. This value is close to the C (1s) data of MacPherson where two peaks of equal intensity were separated by 2.2 eV. The formation of the 2,5-dihydrothiophene-like moiety on Si(111)-(7×7) appear surprising, considering that the Si(111)-(7×7) and (2×1) reconstructed (100) surfaces are so structurally and electronically different. A different reaction mechanism must therefore be responsible for the formation the 2,5-dihydrothiophene-like moiety on Si(111)-(7×7) since the surface does not possess the π-bonded dimer required for a Diels–Alder reaction. Although initially surprising, the results of this current study are consistent with previous work on benzene adsorption on Si(100)-(2×1),[18] Si(111)-(7×7),[26] Ge(100)-(2×1).[38] These three previous studies showed that a 1,4-cyclohexadiene-like moiety was formed on these three surfaces upon benzene adsorption. Therefore from the current study and previous work it would appear that the product formed in a reaction between an aromatic molecule and silicon or germanium surface is not influenced by the electronic and physical structures of the surface, but the actual reaction mechanism is dependent upon the surface electronic and physical structure.

6.4 Summary

The most significant findings of the current study are outlined below:

- The same moiety is formed when thiophene is adsorbed on Si(100)-(2×1), Si(111)-(7×7) and Ge(100)-(2×1). From comparison with a gas phase photoemission spectrum we have assigned this moiety to a 2,5-dihydrothiophene-like species.

- The relative reactivity of Si(100)-(2×1) and Ge(100)-(2×1) is consistent with a Diels–Alder mechanism being responsible for the reaction on both surfaces.

- The formation of a 2,5-dihydrothiophene-like species on Si(111)-(7×7) would imply that although reaction mechanism is influenced by surface electronic/structural properties the actual product of the surface reaction is not.

6.5 References

1. D.J. Chadi, Phys. Rev. Lett., 43 (1979) 43
2. R.I.G. Uhrberg, G.V. Hannson, J.M. Nicholls, S.A. Flodstrom, Phys. Rev. B, 24 (1981) 4684
3. R.J. Hamers, R.M. Tromp, J.E. Demuth, Surf. Sci., 181 (1987) 346
4. R.I.G. Uhrberg, G.V. Hannson, J.M. Nicholls, S.A. Flodstrom, Phys. Rev. B, 24 (1981) 4684
5. J.E. Rowe, H. Ibach, Phys. Rev. Lett., 32 (1974) 421
6. R.I.G. Uhrberg, E. Landemark, Y.C. Chao, J. Electron. Spectrosc. Rel. Phenom., 75 (1995) 197
7. D.J. Chadi, Phys. Rev. Lett., 43 (1979) 43
8. E. Landemark, C.J. Karlsson, Y.C. Chao, R.I.G. Uhrberg, Phys. Rev. Lett., 69 (1992) 1588
9. R.J. Hamers, S.K. Coulter, M.D. Ellison, J.S. Hovis, D.F. Padowitz, M.P. Schwartz, C.M. Greenlief, J.N. Russell, Acc. Chem. Res., 33 (2000) 617
10. R.I.G. Uhrberg, G.V. Hannson, J.M. Nicholls, S.A. Flodstrom, Phys. Rev. B, 24 (1981) 4684
11. P.K. Milligan, B. Murphy, D. Lennon, B.C.C. Cowie, M. Kadodwala, J. Phys. Chem. B, 105 (2001) 140
12. C.D. MacPherson, K.T. Leung, Phys. Rev. B, 51 (1995) 17995
13. H.D. Jeong, Y.S. Lee, S. Kim, J. Phys. Chem., 105 (1996) 5200
14. M.H. Qiao, Y. Cao, F. Tao, Q. Liu, J.F. Deng, G.Q. Xu, J. Phys. Chem. B, 104 (2000) 11211
15. I. Novak, S.C. Ng, Y.T. Chua, C.Y. Mok, H.H. Huang, J. Electron. Spectrosc. Rel. Phenom., 63 (1993) 85
16. H.J. Kuhn, M. Klessinger, B. Ruscic, L. Klasinc, J. Electron. Spectrosc. Relat. Phenom., 43 (1987) 147
17. H. Schmidt, A. Schweig, Tetrahedron Lett., 16 (1973) 1437
18. S. Gokhale, P. Trischberger, D. Menzel, W. Widdra, H. Droge, H.P. Steinruck, U. Birkenheuer, U. Gutdeutsch, N. Rosch, J. Chem. Phys., 108 (1998) 5554
19. H.J. Kuhn, M. Klessinger, B. Ruscic, L. Klasinc, J. Electron. Spectrosc. Relat. Phenom., 43 (1987) 147

20. R.I.G. Uhrberg, G.V. Hannson, J.M. Nicholls, P.E.S. Persson, S.A. Flodstrom, Phys. Rev. B, 31 (1985) 3805
21. J. Hermanson, Solid State Commun., 22 (1977) 9
22. E. Landemark, C.J. Karlsson, L.S.O. Johannsson, R.I.G. Uhrberg, Phys. Rev. B, 49 (1994) 16523
23. J.G. Nelson, W.J. Gigac, R.S. Williams, S.W. Robey, J.G. Tobin, D.A. Shirley, Phys. Rev. B, 27 (1983) 3924
24. T.C. Hsieh, T. Miller, T.C. Chiang, Phys. Rev. B, 30 (1984) 7005
25. M.N. Piancastelli, N. Motta, A. Sgarlata, A. Balzarotti, M. De Crescenzi, Phys. Rev. B, 48 (1993) 17892
26. M. Carbone, M.N. Piancastelli, R. Zanoni, G. Comtet, G. Dujardin, L. Hellner, Surf. Sci., 407 (1998) 275
27. F. Rochet, F. Jolly, F. Bournel, G. Dufour, F. Sirotti and J.L. Cantin Phys. Rev. B, 58 (1998) 11029
28. C.D. MacPherson, D.Q. Hu, M. Doan, K.T. Leung, Surf. Sci., 310 (1994) 231
29. M. N. Piancastelli, N. Motta, A. Sgarlata, A. Balzarotti, M. De Crescenzi, Phys. Rev. B, 48 (1993) 17892
30. I. Fleming, *Frontier Orbitals and Organic Chemical Reactions*; Wiley: London; Chapter 4 (1976)
31. A.V. Teplyakov, P. Lal, Y.A. Noah, S.F. Bent, J. Am. Chem. Soc., 120 (1998) 7377
32. S.W. Lee, L.N. Nelen, H. Ihm, T. Scoggins, C.M. Greenlief, Surf. Sci., 410 (1998) L773
33. N.V. Richardson, J.C.Campuzano, Vacuum, 31 (1981) 449
34. R.J. Hamers, Ph Avouris, F. Bozso, J. Vac. Sci. Technol. A, 6 (1988) 508
35. L. Kipp, R. Manzke, M. Skibowski, Surf. Sci., 269/270 (1992) 854
36. The CRC Handbook of Chemistry and Physics, CRC Press, Boca Raton, FL, 1995
37. H. Liu, R.J. Hamers , Surf. Sci., 416 (1998) 354
38. A. Fink, D. Menzel, W. Widdra, J. Phys. Chem. B, 105 (2001) 3828
39. T.W. Pi, C.P. Cheng, I.H. Hong, Surf. Sci., 418 (1998) 113
40. T.W. Pi, J.F. Wen, C.P. Ouyang, R.T. Wu, Phys. Rev. B, 63 (2001) 153310

Chapter 7. Photoemission Studies of the Surface Reactivity of Benzene on Si(100)-(2×1), Si(111)-(7×7) and Ge(100)-(2×1)

7.1 Introduction

The electronic structure of benzene adsorbed on Si(100)-(2×1), Si(111)-(7×7) and Ge(100)-(2×1) at room temperature has been studied by valence band photoelectron spectroscopy using linearly polarised synchrotron radiation. Based on the direct comparison between the photoemission data collected in the current work and the ARUPS measurements and first-principles DFT calculations of the C_6H_6/Si(100)-(2×1) system by Gokhale *et al*,[(1)] we believe that the moiety formed on the three semiconductor surfaces corresponds to a 1,4-cyclohexadiene-like species. This previous investigation[(1)] is in good agreement with recent work in which it was proposed that the π-bonded dimers of the (2×1) reconstructed Si(100) and Ge(100) surfaces can undergo cycloaddition (Diels-Alder) reactions with dienes. In analogy to the previous TPD experiments of benzene adsorbed on the Ge(100)-(2×1) surfaces,[(2)] our photoemission data suggest that upon benzene coverage, the molecules initially react with the Ge dimers positioned next to the step edges, and upon high benzene exposure, adsorption on the terrace sites occurs. As for thiophene adsorbed on Si(111) described in the previous chapter,[(3)] firstly, due to the absence of the required $\pi-$bonded silicon dimers, the formation of a 1,4-cyclohexadiene-like species on the Si(111)-(7×7) surface implies that although the reaction mechanism is influenced by surface electronic and structural, properties the actual product of the surface reaction is not. Secondly we tentatively propose that the orientation of the moiety formed on Si(111)-(7×7) is not significantly different to that adopted on Si(100)-(2×1).

7.2 Results

7.2.1 Benzene/Si(100)-(2×1)

Fig. 1 depicts the normal and off-normal valence band spectra recorded at a photon energy of 40 eV for 9 L of benzene adsorbed on the Si(100)-(2×1) surface at room temperature. Bands centred at 1.0, 2.5, 4.0, 5.7, 6.6, 7.9, 8.4, 8.9, 10.3, 11.3, 12.9, 14.0, and 17.1 eV binding energy can be observed. The analysis of the photoemission spectra collected in the present work is based upon information provided in a recent study by Gokhale *et al.*[1] In this previous work, the C_6H_6/Si(100)-(2×1) system was characterised by performing a series of ARUPS measurements and first-principles density functional cluster calculations.[1] Their experimental data suggested a local C_{2v} symmetry for benzene chemisorbed on the silicon surface at 300 K. The comparison of their ARUPS data with their DFT calculations confirmed the formation of a 1,4-cyclohexadiene-like adsorption complex with the benzene molecule di-σ-bonded to a single Si surface dimer, as illustrated in Fig. 2. Their theoretical predictions indicated that the degeneracy of the benzene gas-phase e orbitals was lost with a decrease of symmetry, following the destruction of the delocalised aromatic π system of the benzene molecule upon the formation of the 1,4-cyclohexadiene-like moiety.[1] Their calculations also showed the emergence of a new set of molecular orbitals whose shapes are depicted in Fig. 3. As can be seen in Fig. 4 the energetic positions of the 1,4-cyclohexadiene molecular orbitals derived from the Gokhale work [1] and the eleven resolvable bands of the valence band difference UP spectra from the present study are in excellent agreement. This further reinforces the idea of the formation of a 1,4-cyclohexadiene-like species on Si(100)-(2×1) upon benzene exposure. We therefore believe that the features at 17.1 eV can be attributed to $3b_{3u}$ and $2b_{2u}$, 14.0 eV to $4a_g$, 12.9 eV to $2b_{1g}$, 11.3 eV to $5a_g$, 10.3 eV to $4b_{3u}$, 8.9 eV to $1b_{1u}$ and $3b_{2u}$, 8.4 eV to $1b_{2g}$ and $4b_{2u}$, 7.9 eV to $5b_{3u}$, 6.6 eV to $6a_g$, 5.7 eV to $3b_{1g}$, 4.0 eV to $1b_{3g}$, and 2.5 eV to $2b_{1u}$. As was previously mentioned, the degeneracy of the benzene gas-phase e orbitals is lifted upon adsorption and the former $2e_{2g}$ and $3e_{2g}$ molecular orbitals split into $4a_g$, $2b_{1g}$ and $6a_g$, $3b_{1g}$ orbitals, respectively.

Fig. 5 displays the same normal and off-normal emission benzene spectra (solid lines) in the 0 – 5 eV BE region, plotted along with the corresponding clean Si(100)-(2×1) surface spectra (dashed lines). As for thiophene adsorbed on Si(100),[3] the data from the current work clearly shows that the presence of adsorbed benzene changes the nature of the bonding within the silicon dimers. For instance, the overall intensities of the peaks associated with the density of states close to E_F are clearly affected by the presence of benzene. Furthermore we believe that the two bands located at 2.5 and 4.0 eV can be associated with the emission of photoelectrons from the remaining unreacted dangling bonds since only every second surface dimer is occupied,[2] and also from the two HOMOs denoted as $1b_{3g}$ and $2b_{1u}$ of the 1,4-cyclohexadiene-like moiety formed upon benzene adsorption.[1] In an early ARUPS study of the Si(100)-(2×1) surface, the electronic features observed in the BE range 2 – 4 eV were attributed by Uhrberg *et al.*[4] to photoemission from the σ bond of the silicon dimers. In a more recent investigation Hamers and co-workers[5] suggested that the Si–Si σ bond remained intact even after adsorption of organic molecules on the Si(100) surface. The $1b_{3g}$ and $2b_{1u}$ molecular orbitals of the 1,4-cyclohexadiene-like species are also depicted in Fig. 5, and the energetic positions deduced here (4.0 and 2.5 eV) are similar within the margin of error (estimated here at ± 0.2 eV) to those found by Gokhale and co-workers (4.0 and 2.3 eV).[1] These authors also pointed out that the two HOMOs consist of the symmetric and antisymmetric linear combinations of the remaining two π orbitals attributed to the C=C double bonds on the opposite sides of the carbon ring (Fig. 3).[1] The $1b_{3g}$ MO originates from the degenerate benzene gas-phase $1e_{1g}$ (π) orbital and the $2b_{1u}$ MO stems from the unoccupied $1e_{2u}$ (π*) orbital.[1]

In summary we believe that the adsorption of benzene on the Si(100)-(2×1) surface at room temperature leads to the formation of a 1,4-cyclohexadiene-like moiety. This assignment is based on the comparison between the valence band data collected in the current work and ARUPS measurements and first-principles DFT calculations of the C_6H_6/Si(100)-(2×1) system by Gokhale *et al.*[1] In the proposed adsorption geometry, this moiety would have a local C_{2v} symmetry, with two opposite carbons of the benzene ring di-σ-bonded to a single Si dimer and the two C=C double bonds on the opposite sides of the

carbon ring (Fig. 2). This conclusion is consistent with a [4+2] cycloaddition (Diels-Alder) reaction between benzene and the silicon dimers of the (2×1) reconstructed Si(100) surface.

Fig.1. *Normal and off-normal emission valence band photoemission spectra (hν = 40 eV) collected from a Si(100)-(2×1) surface that had been exposed to 9 L of benzene at room temperature.*

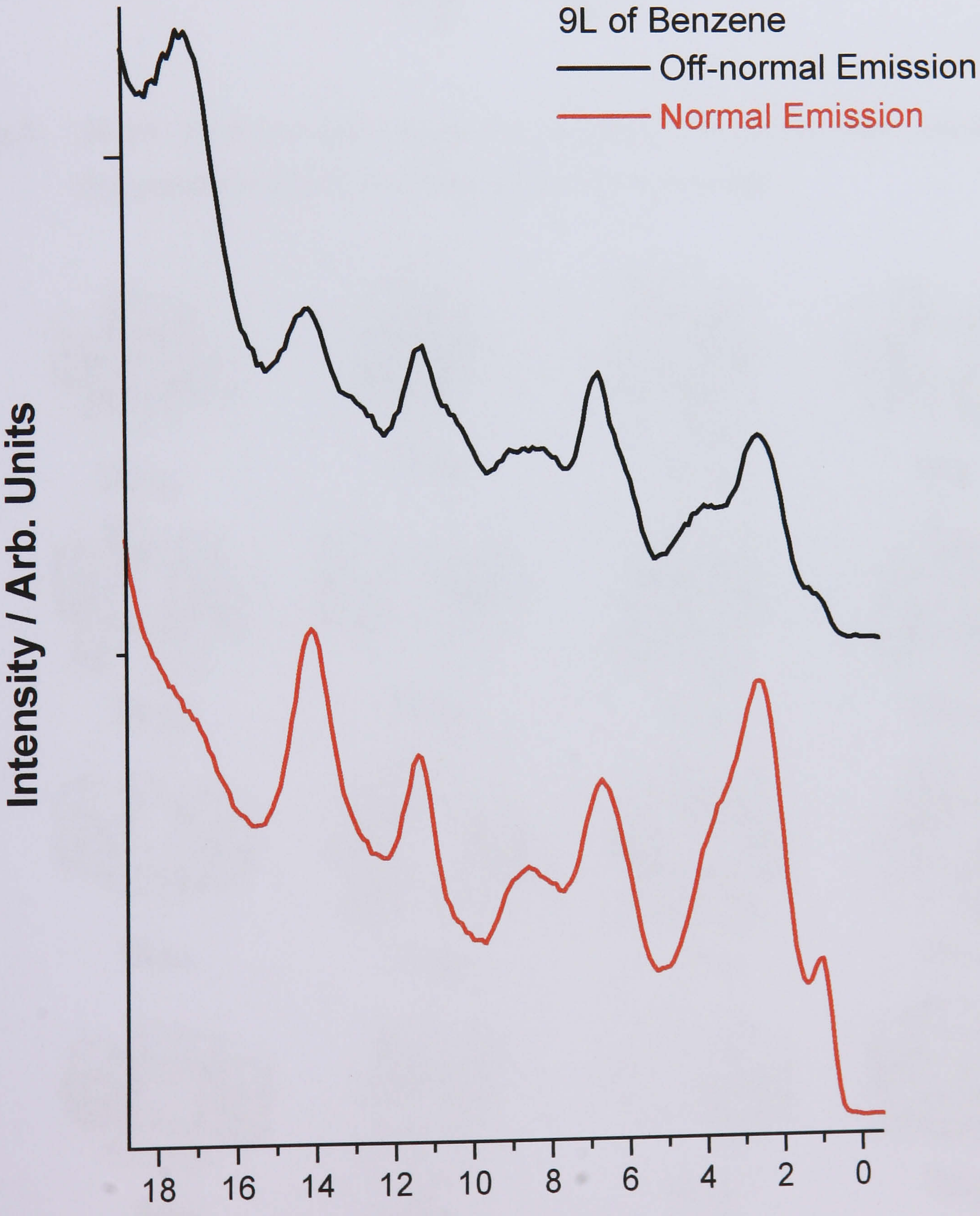

Fig.2. *Probable bonding geometry of the 1,4-cyclohexadiene-like moiety formed on Si(100)-(2×1) upon benzene adsorption at room temperature.*

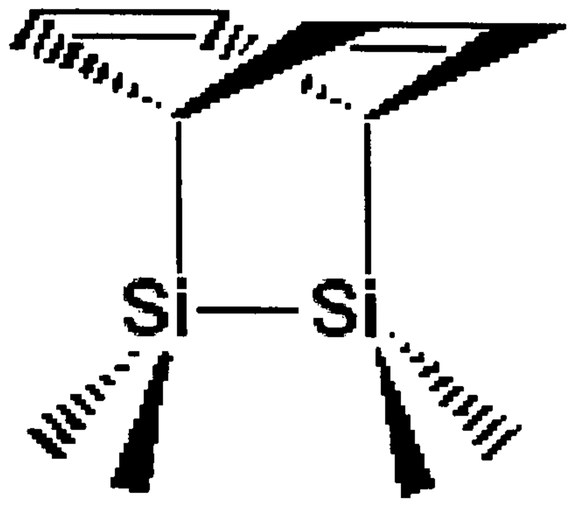

Fig.3. *Sketch of the molecular orbitals of gas-phase 1,4-cyclohexadiene calculated by first-principles density functional model cluster from Ref. 1.*

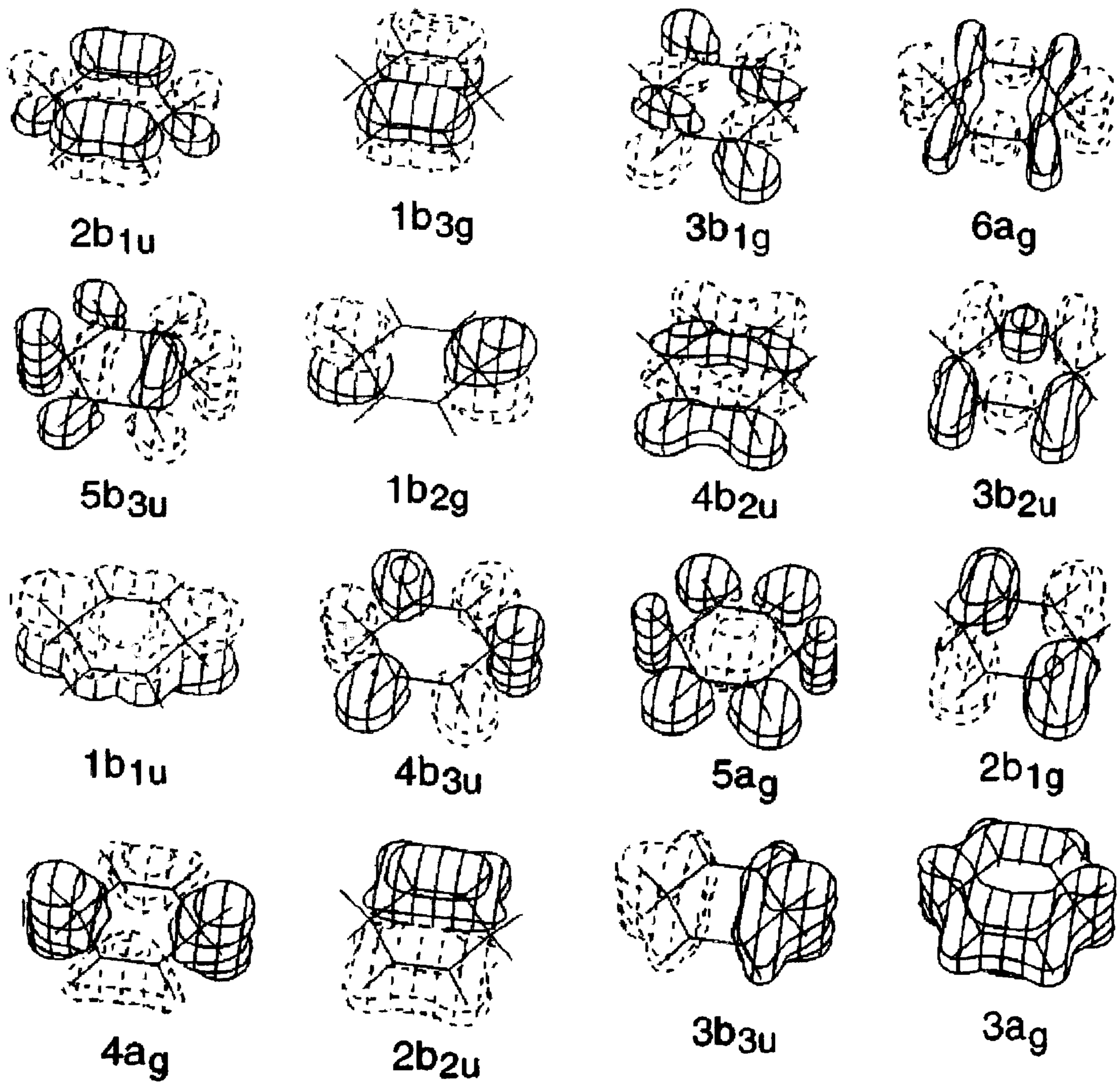

Fig.4. *Normal and off-normal difference spectra (hν = 40 eV) collected from Si(100)-(2×1) which had been exposed to 9 L of benzene at room temperature. The energetic positions of the molecular orbitals of 1,4-cyclohexadiene derived from the investigation of the same system by Gokhale et al.[1] are also displayed.*

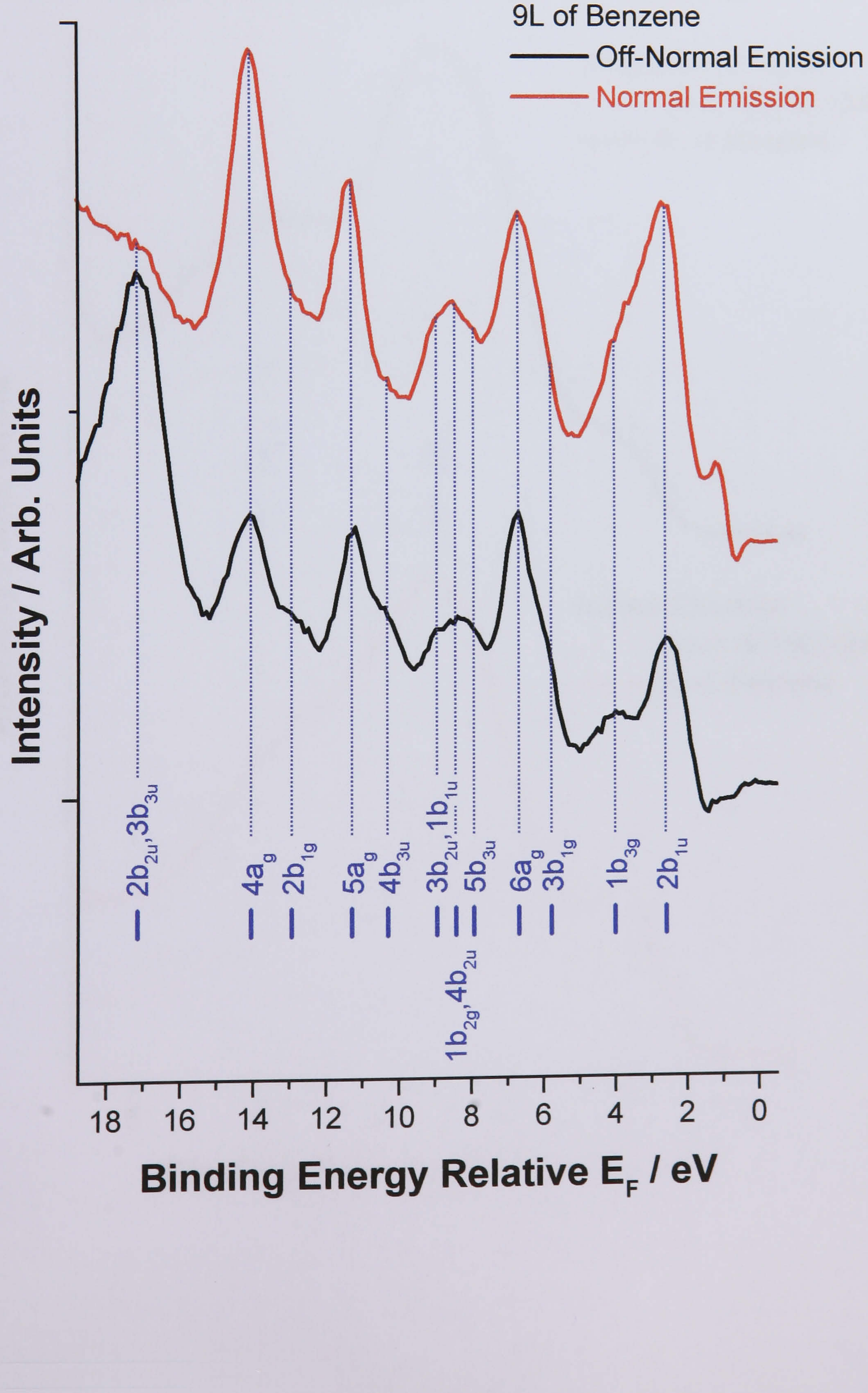

Fig.5. *Comparison between the off-normal and normal emission valence band photoemission spectra (hν = 40 eV) of the clean Si(100)-(2×1) surface and the same surface exposed to 9 L of benzene at room temperature. This plot shows the direct effects of adsorbed benzene on the density of states close to E_F and the increase in the bands at 2.5 and 4.0 eV BE. The energetic positions of the HOMOs of the 1,4-cyclohexadiene-like species from Ref. 1 are also displayed.*

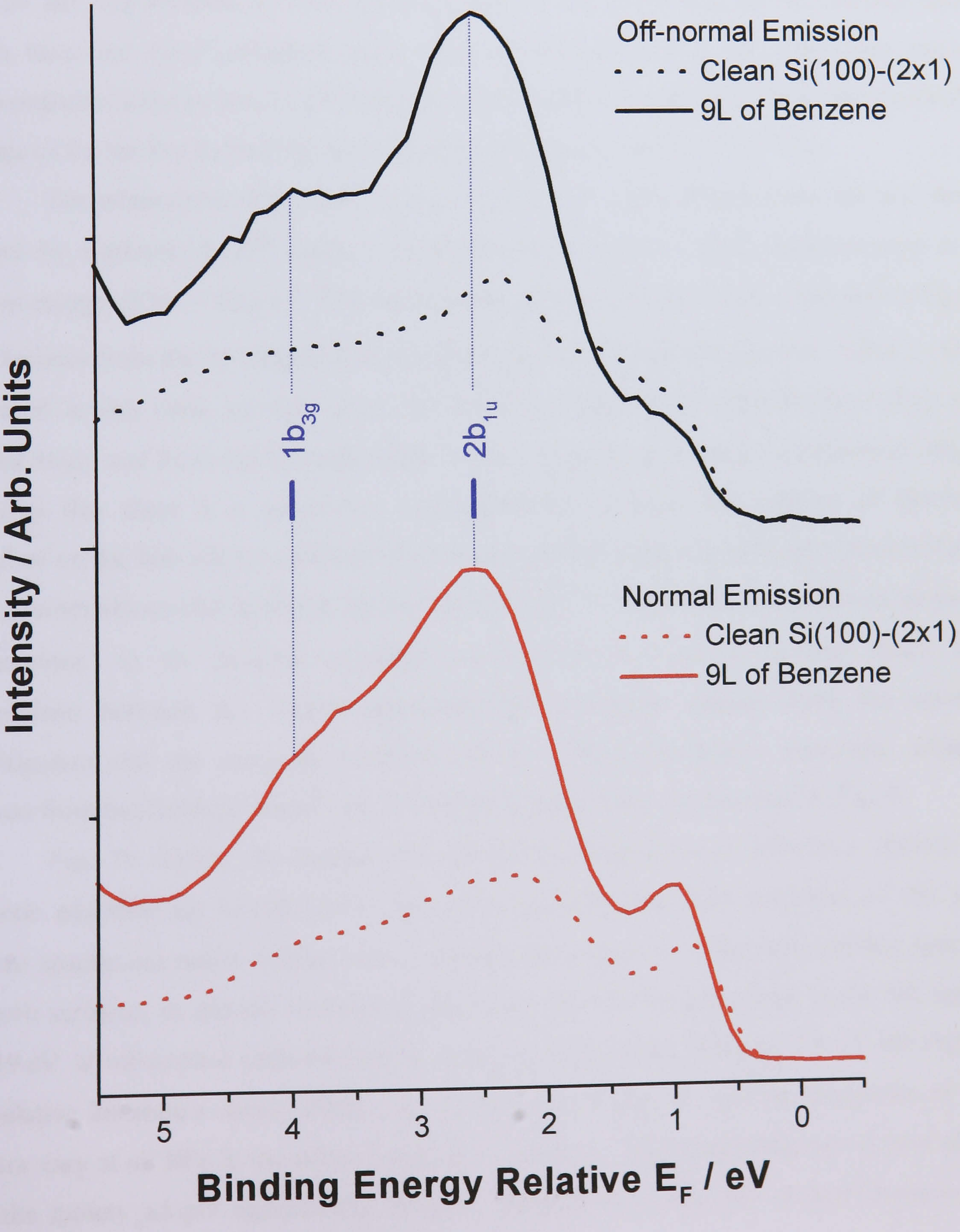

7.2.2 Benzene/Si(111)-(7×7)

The normal and off-normal valence band spectra collected from the Si(111)-(7×7) surface, which had been exposed to 300 L benzene dosed at room temperature, are shown in Fig. 7. The combination of both normal and off-normal emission spectra displays fourteen peaks centred at 0.5, 1.1, 2.6, 4.3, 5.9, 6.8, 7.9, 8.4, 8.9, 10.2, 11.0, 13.1, 14.1 and 17.3 eV BE. We attribute the features at 0.5 and 1.1 eV to the RA and AD surface states which have not been quenched upon benzene adsorption (Fig. 8). The other twelve photoemission features consist of individual bands which can be assigned to the molecular orbitals of the moiety formed by the adsorption of benzene on Si(111)-(7×7).

The adsorption of benzene on Si(111)-(7×7) at room temperature has also been studied by Carbone *et al.*[6] using synchrotron-based valence band photoemission at a photon energy of hν = 42.3 eV. The energy peak positions of the bands observed in Fig. 7 and the ones from the investigation by Carbone and co-workers are given in Table 1. Also indicated in this table are the values for benzene adsorbed on Si(100)-(2×1) from the current study and from the Gokhale work.[1] The comparison of these experimental values indicates that there is a one-to-one correspondence between the features of benzene adsorbed on the two silicon surfaces within experimental error, which further proves that a 1,4-cyclohexadiene-like moiety is formed on Si(111)-(7×7) upon benzene exposure at room temperature. As for benzene adsorbed on Si(100)-(2×1) in the present study, the comparison between the twelve resolvable UP difference spectra from the current investigation and the energetic positions of the 1,4-cyclohexadiene molecular orbitals derived from the Gokhale work[1] are in very good agreement, as presented in Fig. 9.

Fig. 10 depicts the normal and off-normal valence band difference spectra of benzene adsorbed on Si(100)-(2×1) and Si(111)-(7×7). The peak positions of the off-normal spectra are rather similar, which confirm the presence of the same surface species on both surfaces, as already mentioned. Although the relative intensities in the BE range 10-19 eV at off-normal emission appear rather similar, in the 10.0 and 1.5 eV BE region the relative intensities clearly differ. Fig. 10 also shows that the relative intensities of the spectra vary at all BEs in the normal emission geometry. This graph indicates at first sight that the moiety adopts significantly different geometries on the two surfaces because in

UPS the relative intensities of the molecular orbitals are correlated to the geometry of the surface moiety. This observation agrees with the conclusion drawn by Carbone and co-workers where it was suggested that adsorption of benzene on Si(111)-(7×7) involves the simultaneous interaction of one adatom (AD) and one rest atom (RA) of the reconstructed surface with two opposite carbon atoms of the benzene ring.[6] This produces a moiety tilted by an angle of 13° with respect to the rest plane (Fig. 6) and differs to the model depicted in Fig. 2. The AD/RA configuration, however, clearly contradicts the model proposed by Rochet *et al.*[7] where it was suggested that the adsorption of π bonded organic molecules caused the re-arrangement of silicon atoms within the (7×7) reconstruction of the Si(111) surface and involved the removal of the adatom to an interstitial position under the plane containing the rest and pedestal atoms. As already suggested in Chapter 6 for thiophene adsorbed on Si(111)-(7×7), the current photoemission data does not provide detailed quantitative information on the structure of the underlying Si(111) substrate after adsorption. The adsorption model proposed here is therefore only tentative and a more unambiguous answer from experiments which could provide quantitative structural information is therefore required. We defer further discussion of these possibilities to Section. 7.3.

To summarise, the similarity in peak positions between our photoemission spectra and the one collected by Carbone *et al.*[6] suggests the formation of a 1,4-cyclohexadiene-like species upon the adsorption of benzene on the Si(111)-(7×7) surface at room temperature.

Table 1 *Comparison of the binding energy (in eV) of the molecular orbitals of 1,4-cyclohexadiene-like species formed on Si(111)-(7×7) and Si(100)-(2×1) upon benzene exposure at room temperature. The error in determining the energy peak positions is estimated here at ± 0.2 eV.*

	Si(111)-(7×7)		Si(100)-(2×1)	
Molecular orbitals	Present work	Carbone *et al.*[6]	Present work	Gokhale *et al.*[1]
$2b_{1u}$	2.6	2.7	2.5	2.3
$1b_{3g}$	4.3	4.3	4.0	4.0
$3b_{1g}$	5.9	6.1	5.7	5.7
$6a_g$	6.8	6.8	6.6	6.5
$5b_{3u}$	7.9	8.2	7.9	7.9
$1b_{2g}$ and $4b_{2u}$	8.4	8.8	8.4	8.4
$1b_{1u}$ and $3b_{2u}$	8.9		8.9	8.9
$4b_{3u}$	10.2	10.0	10.3	10.2
5_{ag}	11.0	11.0	11.3	11.2
$2b_{1g}$	13.1	12.9	12.9	12.9
4_{ag}	14.1	13.9	14.0	14.1
$3b_{3u}$ and $2b_{2u}$	17.3	17.1	17.1	17.1

Fig.6. *Schematic diagrams of (a) the clean Si(111)-(7x7) surface where the rest atoms (RA), adatom (AD) and pedestal atom (PA) have been labelled, (b) the 1,4-cyclohexadiene-like moieties bonded to the RA and AD in a bridging geometry and (c) the 1,4-cyclohexadiene-like species bonded to the RA and PA.*

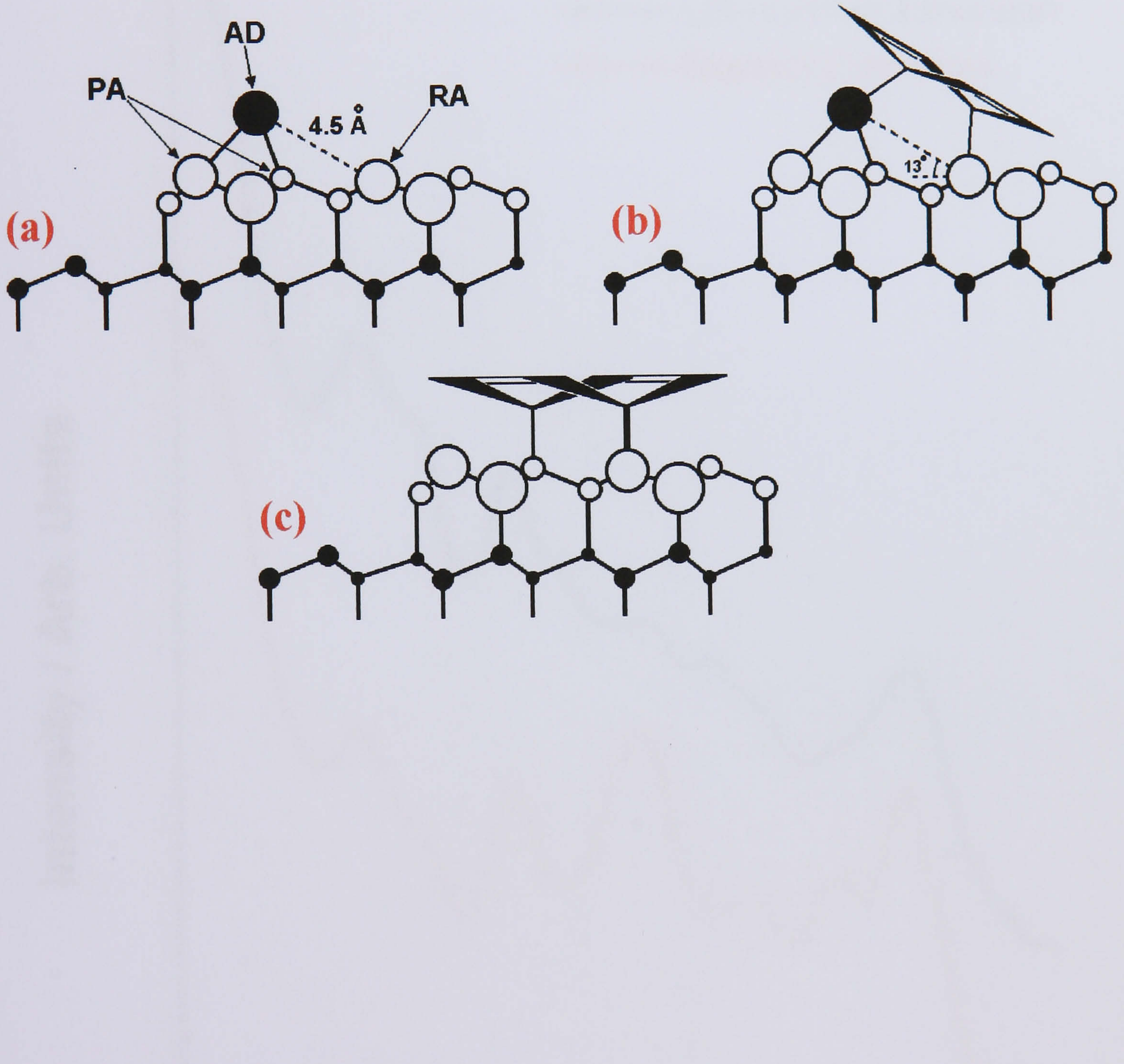

Fig.7. *Normal and off-normal emission valence band photoemission spectra ($h\nu = 40$ eV) collected from a Si(111)-(7×7) surface that had been exposed to 300 L of benzene at room temperature.*

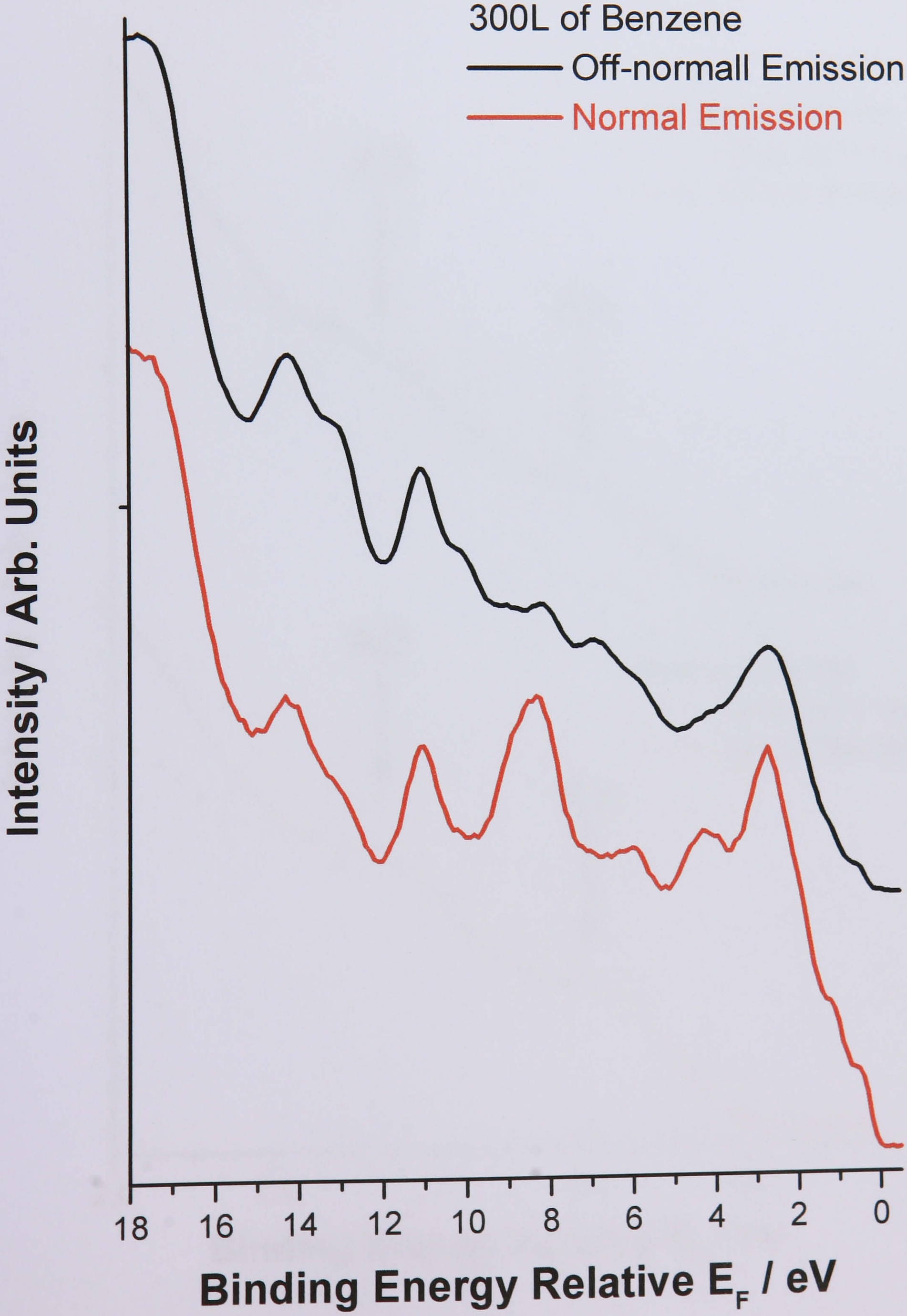

Fig.8. *Comparison between the off-normal and normal emission valence band photoemission spectra (hν = 40 eV) of the clean Si(111)-(7×7) surface and the same surface exposed to 300 L of benzene at room temperature. This plot shows the decrease in intensity of the RA and AD surface states upon benzene exposure.*

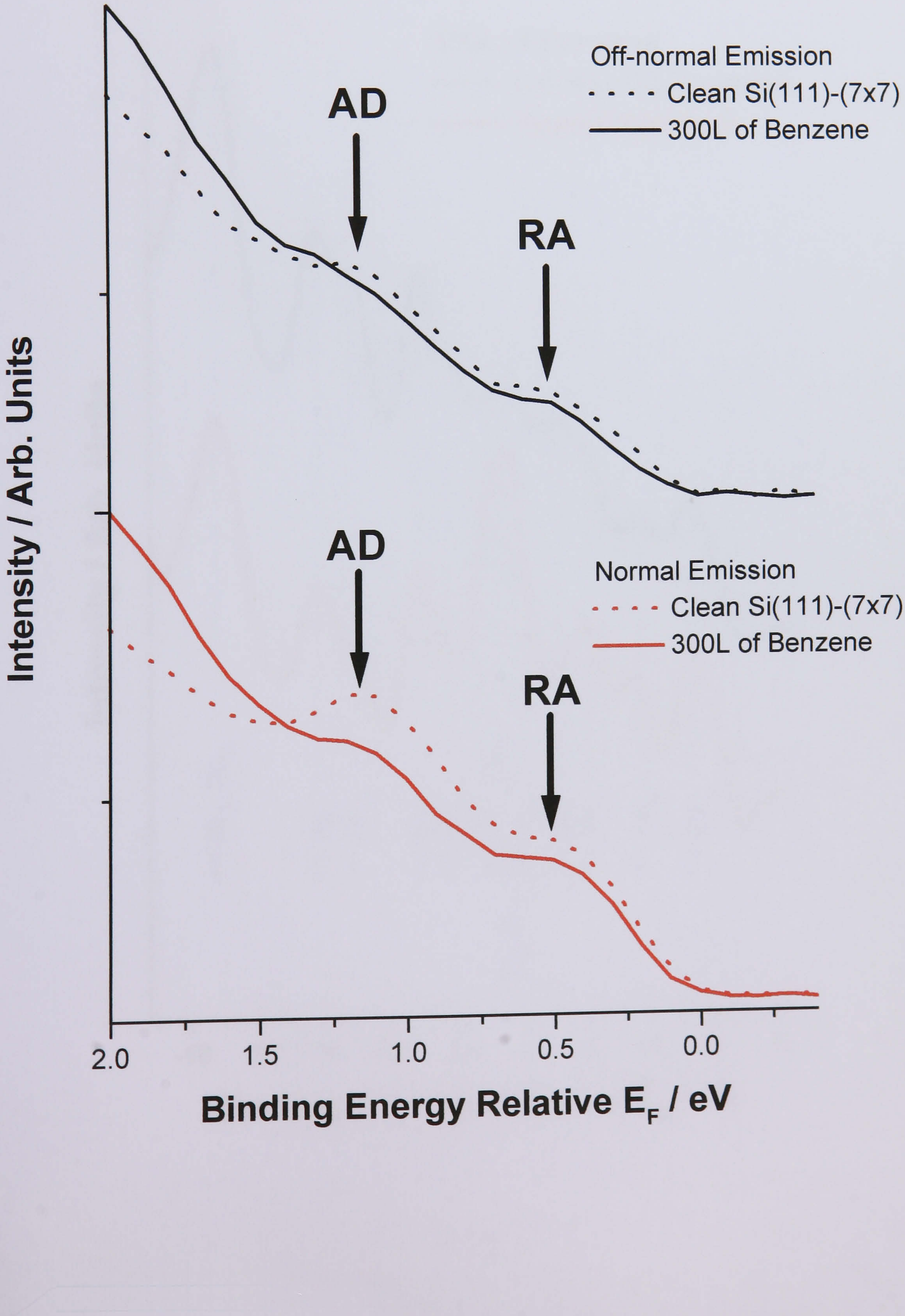

Fig.9. *Normal and off-normal difference spectra (hν = 40 eV) collected from Si(111)-(7×7) which had been exposed to 300 L of benzene at room temperature. The energetic positions of molecular orbitals of 1,4-cyclohexadiene derived from the investigation of the C_6H_6/Si(100)-(2×1) system by Gokhale et al.*[1] *are also displayed.*

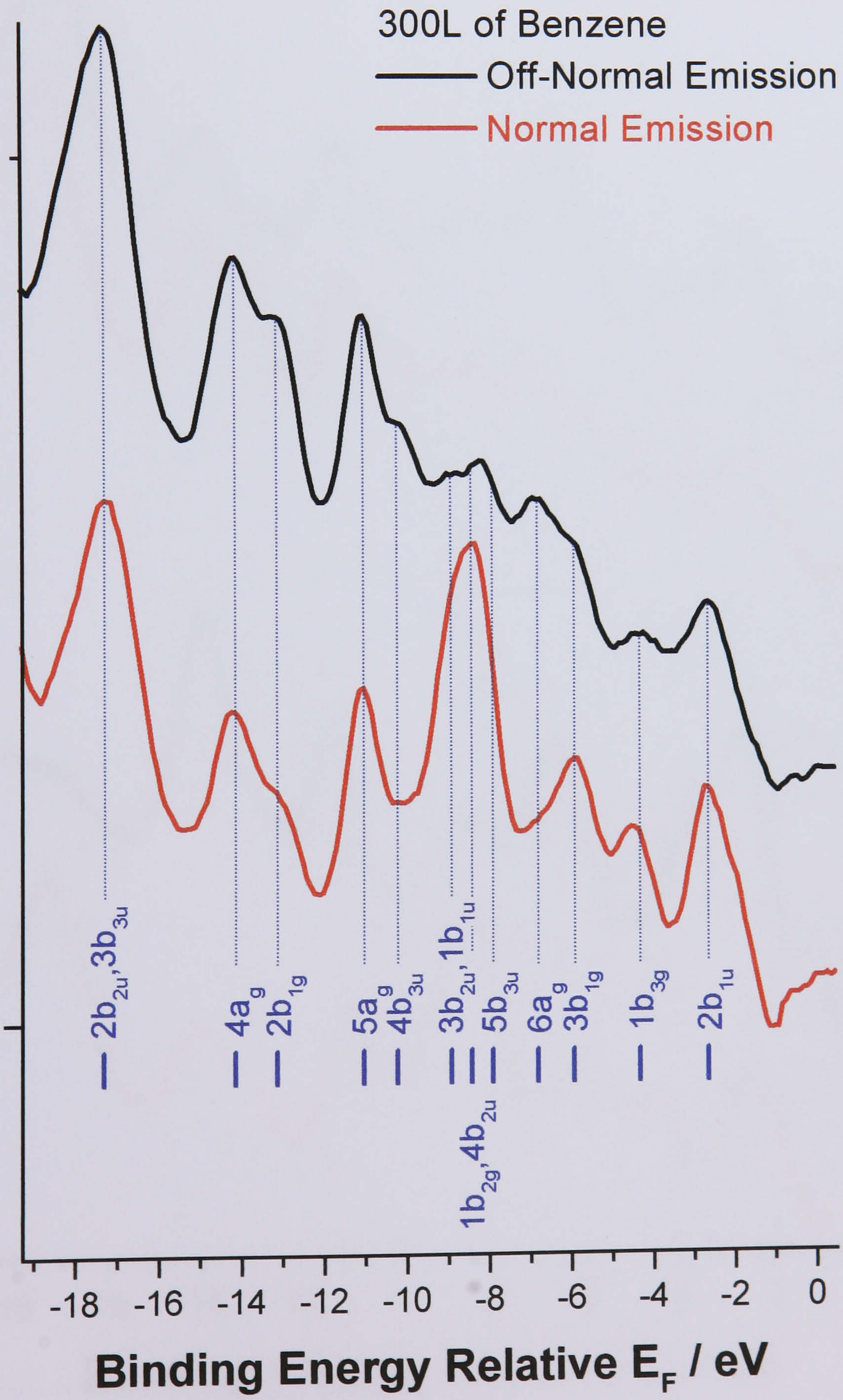

Fig.10. *Off-normal (a) and normal (b) difference spectra (hν = 40 eV) collected from the Si(100)-(2×1) and Si(111)-(7×7) surfaces which had been exposed to 9 and 300 L of benzene at room temperature respectively.*

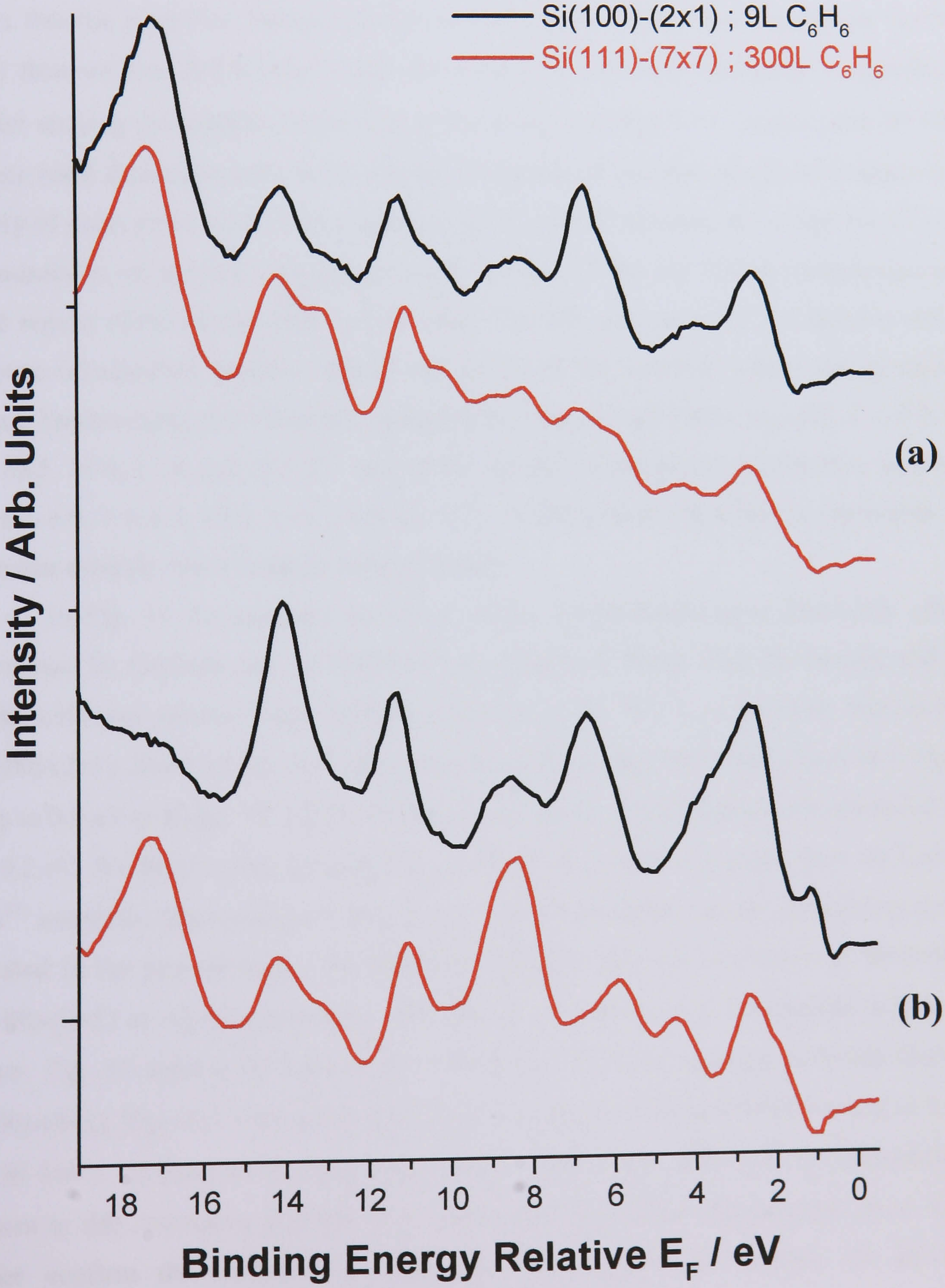

7.2.3 Benzene/Ge(100)-(2×1)

The normal and off-normal valence band and difference spectra collected from Ge(100)-(2×1) surfaces, which had been exposed to sequentially higher amounts of benzene, are displayed in Figs. 12 and 13 respectively. Comparison with Figs. 1 and 4 shows that the adsorbate induced photoemission bands develop less rapidly on Ge(100)-(2×1) than on the Si(100)-(2×1) and Si(111)-(7×7) surfaces, indicating a significantly smaller sticking probability. Inspection of the clean Ge(100)-(2×1) surface and 30 000 L valence band data collected reveals that the adsorption of benzene results in changes in the density of states close to E_F, with a decrease in the overall intensity at 0.6 and 1.4 eV (most pronounced in off-normal emission geometry in Figs. 12 and 13). These changes take place in the region where surface states of the clean Ge(100) surface occur and indicate that the presence of adsorbed benzene affects the nature of the bonding within the germanium dimers. Furthermore, the off-normal emission spectra present bands with BE 2.2, 6.0, 6.9, 9.1, 10.5, 11.6, 13.9 and 17.5 eV, and in the normal emission spectra features centred at 2.2, 4.4, 6.0, 7.7, 8.7, 10.5, 11.6, 13.9 and 17.5 eV BE appear which can be associated with molecular orbitals of the benzene derived moiety.

In Fig. 14 the energetic positions of the 1,4-cyclohexadiene molecular orbitals determined by Gokhale and co-workers[1] are displayed along with the normal and off-normal emission valence band difference spectra of 30 000 L of benzene deposited on Ge(100)-(2×1). Some of the energetic positions of the molecular orbitals have been shifted by up to 0.4 eV to higher BE (Table 2) but are still within experimental error estimated here at ± 0.2 eV. We believe that the energetic levels of the molecular orbitals from the Gokhale work[1] match the photoemission features of benzene adsorbed on the germanium surface collected in the present study, and therefore indicates that the adsorption of benzene on Ge(100)-(2×1) at room temperature leads to the formation of a 1,4-cyclohexadiene-like moiety. Fig. 15 depicts the normal and off-normal difference spectra collected from the Si(100)-(2×1), Si(111)-(7×7) and Ge(100)-(2×1) surfaces which had been exposed to 9, 300 and 30 000 L of benzene at room temperature respectively. Although the photoemission features in this respective plot are in the same position within experimental error, which further confirm the formation of the 1,4-cyclohexadiene-like species on all three

semiconductor surfaces upon benzene exposure, it is readily apparent that the relative intensities of the germanium spectra at both normal and off-normal emission geometries differ from the ones of the Si surfaces. This would suggest at first sight that the 1,4-cyclohexadiene-like moiety also adopts a different orientation on the Ge(100)-(2×1) surface.

The C_6H_6/Ge(100)-(2×1) complex has recently been studied by Fink *et al.* at cryogenic temperature using a combination of TPD and ARUPS techniques.[2] In this investigation, prior to collecting their photoemission data, the benzene molecules were dosed on the germanium surface at 90 K and the sample was then heated in order to desorb the benzene multilayers. Their ARUPS spectra, whose peak positions have been listed in Table 2 along with the results from the current study and from the Gokhale work of the C_6H_6/Si(100)-(2×1) system,[1] indicated that a 1,4-cyclohexadiene-like moiety was also formed upon the chemisorption of benzene on the Ge(100) surface.[2] Furthermore, their TPD spectra showed two desorption peaks at 234 and 252 K.[2] The former peak was attributed by the authors to desorption of chemisorbed benzene adsorbed on terraces, whilst the latter peak was assigned to desorption of chemisorbed benzene from the step edges. We therefore believe that the adsorption of benzene on Ge(100)-(2×1) in the present work, which was dosed at room temperature, would initially occur on the step edges. Interestingly, in their investigation of benzene adsorbed on the Si(100)-(2×1) surface, Gokhale and co-workers suggested from their ARUPS data that at low coverages the benzene molecules adsorbed on the step sites of the Si(100)-(2×1) surface were oriented in highly symmetric fashion.[1] The alignment of benzene molecules along the steps edges of the Ag(111) single crystal has also been observed by STM.[8]

In UPS, changes in the relative intensities of the peaks normally indicate a change in the adsorption geometry of the molecules. We do not believe, however, that the orientation of benzene adsorbed on the silicon and germanium surfaces differs. Based on the thermal desorption study of benzene on the Ge(100) surface previously reported,[2] we propose that a change in adsorption sites is responsible for the difference in the relative intensities of the photoemission peaks observed in the present study. As can be seen in Figs. 12 and 13, the relative intensities of the adsorbate bands at both emission geometries change with increasing amounts of benzene adsorbed on Ge(100)-(2×1). In the off-normal

emission spectra, close inspection of the peaks centred at 6.0 and 9.1 eV with respect to the other peaks shows an increase in height with increasing benzene coverage. Conversely, in the normal emission spectra the intensity of the photoemission features at 4.4 and 6.0 eV decreases and increases with increasing C_6H_6 coverage respectively. We hypothesise that at an exposure of ≤ 1110 L, benzene mainly reacts with the Ge dimers next to the step edges (Fig. 11), whilst at higher exposure the terrace sites become occupied as demonstrated by the change in the relative intensities. Finally, we believe that at an exposure of 30 000 L the Ge(100)-(2×1) surface is still unsaturated and further benzene adsorption on the remnant terrace sites is feasible.

Similar arguments employed in Chapter 6 to explain the difference in relative intensities observed for thiophene adsorbed on Si(100)-(2×1) and Si(111)-(7×7) at normal emission can also be applied here to justify the difference in relative intensities of the UP spectra observed at both normal and off-normal emission angles of the C_6H_6/Ge(100)-(2×1) system. The schematic diagram of benzene di-σ-bonded to a Ge dimer positioned next to the step edge depicted in Fig. 11 indicates the presence of two "non-equivalent" upper and lower levels. If we consider that benzene is mainly chemisorbed on the terraces of the Si(100) surfaces at room temperature,[1,10] and that benzene initially reacts with the Ge dimers positioned next to the step edges, we believe that the differing relative intensities of the normal and off-normal emission data between the germanium and silicon substrates reflects the difference of the overall symmetry of the C_6H_6/Si(100)-(2×1) and C_6H_6/Ge(100)-(2×1) complexes.

Three important conclusions can be drawn from our photoemission data. Firstly, as is the case for benzene adsorbed on Si(100)-(2×1) and Si(111)-(7×7), the adsorption of benzene on the Ge(100)-(2×1) surface at room temperature leads to the formation of a 1,4-cyclohexadiene-like moiety. Secondly, based on the TPD results of the C_6H_6/Ge(100)-(2×1) system performed by Fink *et al.*,[2] benzene can be considered to be adsorbed on the step edge sites of the Ge(100) surface followed by the terrace sites upon saturation of the step sites. We believe that the adsorption model depicted in Fig. 11 can explain the difference in relative intensities of the photoemission peaks observed in the present study. Finally,

applying similar arguments to those used for Si(100)-(2×1), the reactions of benzene with Ge(100)-(2×1) can be viewed as a [4+2] cycloaddition (Diels-Alder) reaction.

Table 2 *Comparison of the binding energy (in eV) of the molecular orbitals of 1,4-cyclohexadiene-like species formed on Ge(100)-(2×1) and Si(100)-(2×1), upon benzene exposure at room temperature. The error in determining the energetic positions of the photoemission peaks is estimated at ± 0.2 eV.*

Molecular orbitals	Ge(100)-(2×1)		Si(100)-(2×1)
	Present work	Fink *et al.*[2]	Gokhale *et al.*[1]
$2b_{1u}$	2.2	2.3	2.3
$1b_{3g}$	4.4	4.0	4.0
$3b_{1g}$	6.0	5.6	5.7
$6a_g$	6.9	6.4	6.5
$5b_{3u}$	7.7	7.8	7.9
$1b_{2g}$ and $4b_{2u}$	8.7	8.5	8.4
$1b_{1u}$ and $3b_{2u}$	9.1	8.9	8.9
$4b_{3u}$	10.5	10.0	10.2
5_{ag}	11.6	10.9	11.2
$2b_{1g}$	13.3	12.8	12.9
4_{ag}	14.3	13.7	14.1
$3b_{3u}$ and $2b_{2u}$	17.5	17.1	17.1

Fig.11. *Schematic diagram showing benzene adsorbed near the step edges of the Ge(100)-(2×1) surface.*

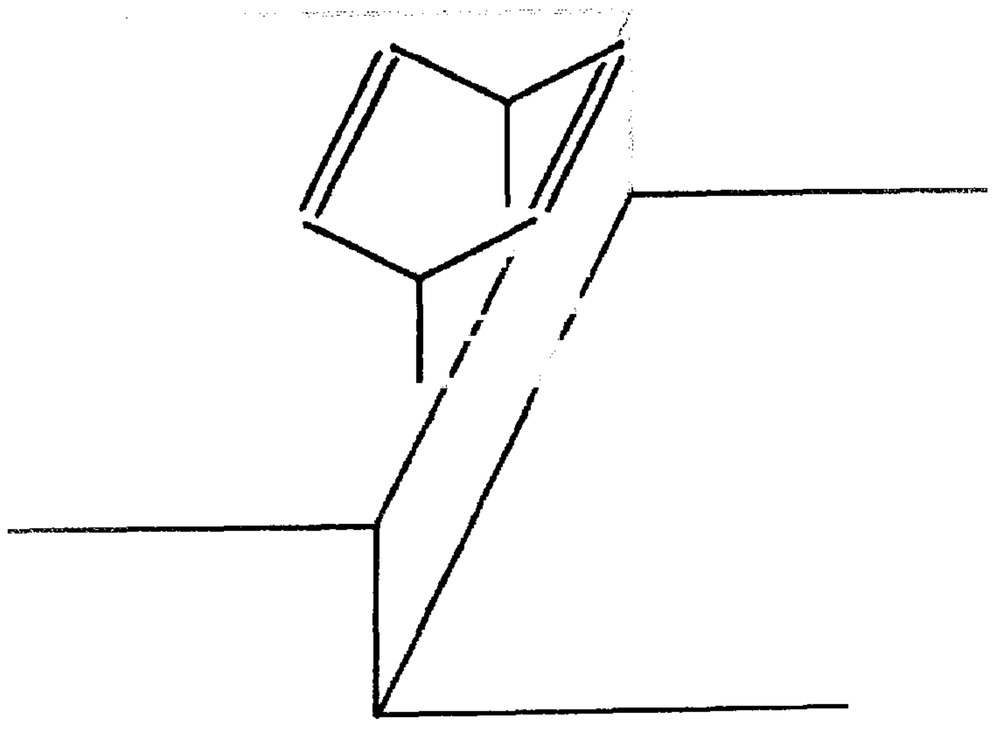

Fig.12. *Off-normal (a) and normal emission (b) valence band spectra ($h\nu$ = 40 eV) collected from clean Ge(100)-(2×1) and the same surface which had been exposed to 110, 1110, 11110, 20000 and 30000 L of benzene at room temperature.*

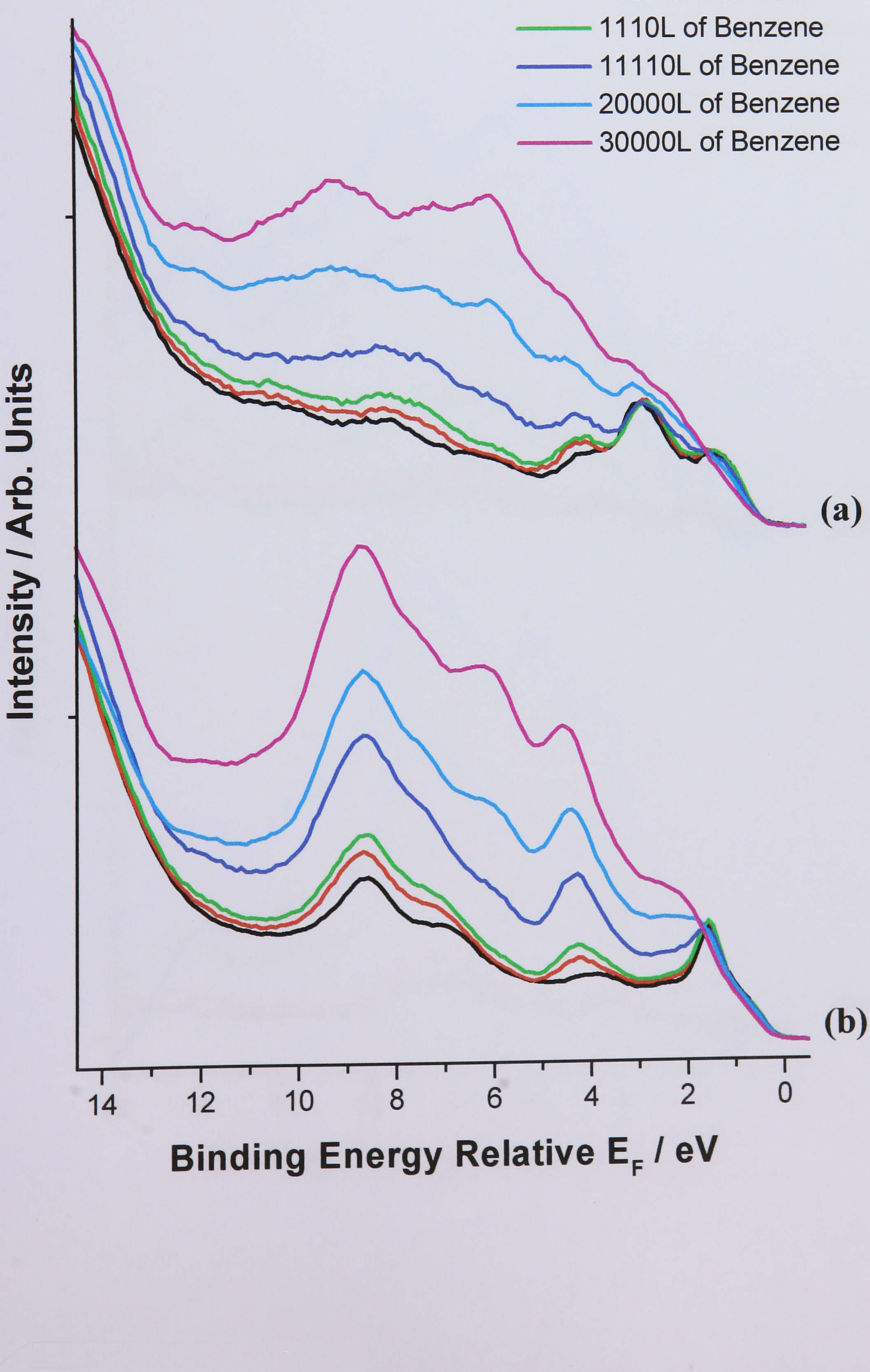

Fig.13. *Off-normal (a) and normal (b) emission difference spectra (hν = 40 eV) produced by subtracting clean surface spectrum from those taken after exposing the Ge(100)-(2×1) surface with 110, 1110, 11110, 20000 and 30000 L of benzene adsorbed at room temperature.*

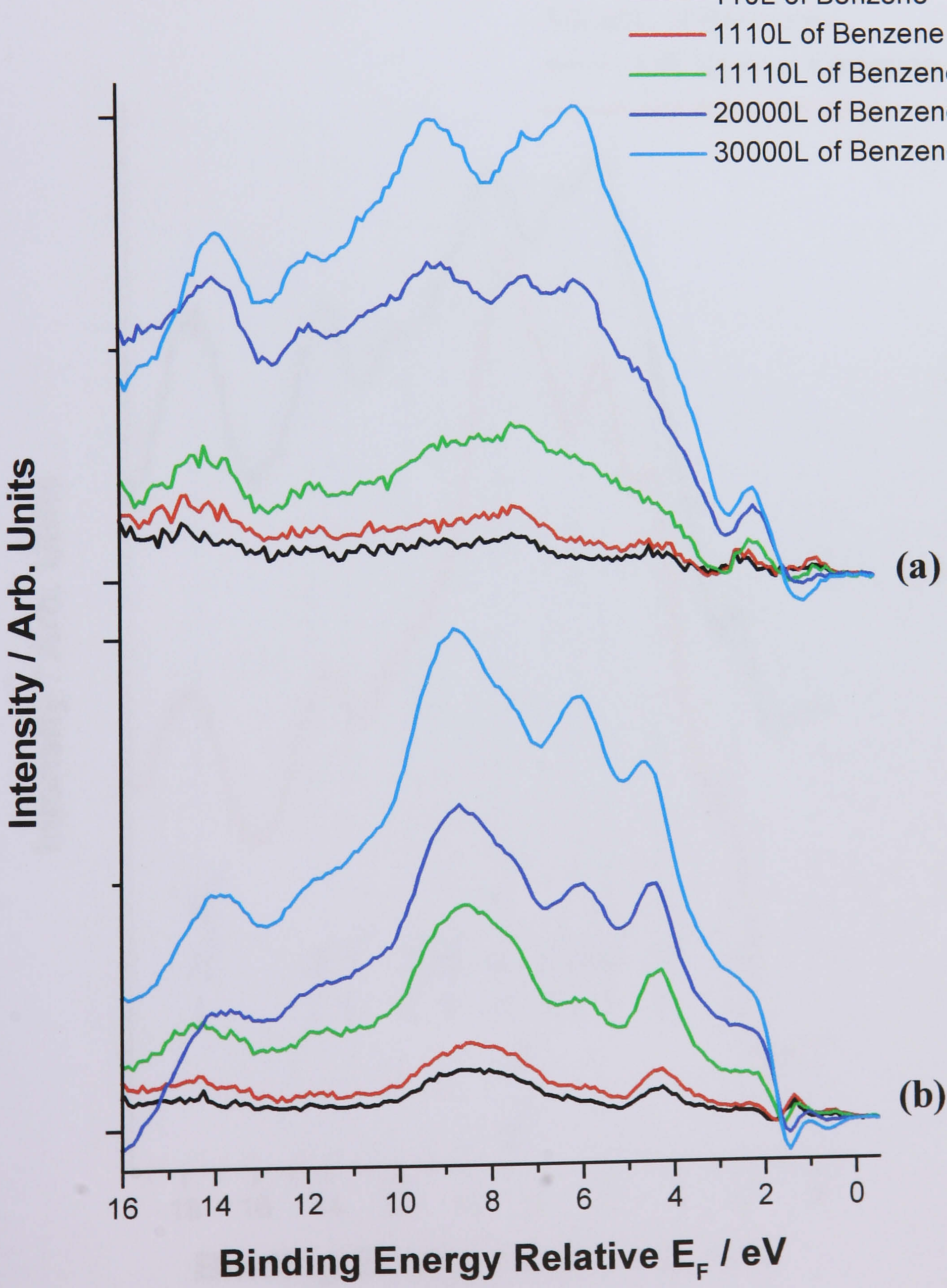

Fig.14. *Normal and off-normal difference spectra (hν = 40 eV) collected from Ge(100)-(2×1) which had been exposed to 30 000 L of benzene at room temperature. The energetic positions of molecular orbitals of 1,4-cyclohexadiene derived from the investigation of the C_6H_6/Si(100)-(2×1) system by Gokhale et al.*[1] *are also displayed.*

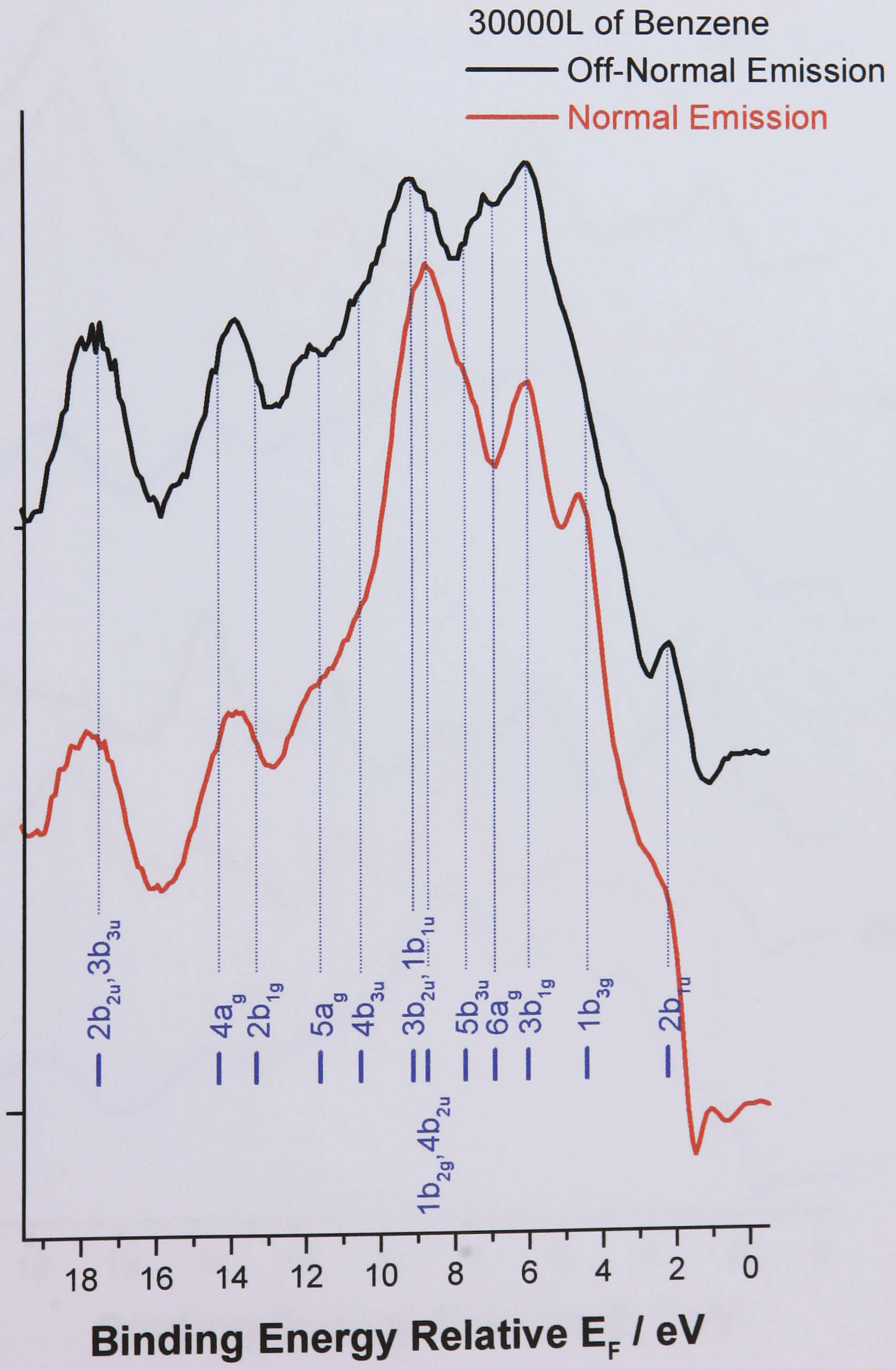

Fig.15. *Off-normal (a) and normal (b) difference spectra (hν = 40 eV) collected from the Si(100)-(2×1), Si(111)-(7×7) and Ge(100)-(2×1) surfaces, which had been exposed to 9, 300 and 30000 L of benzene at room temperature respectively.*

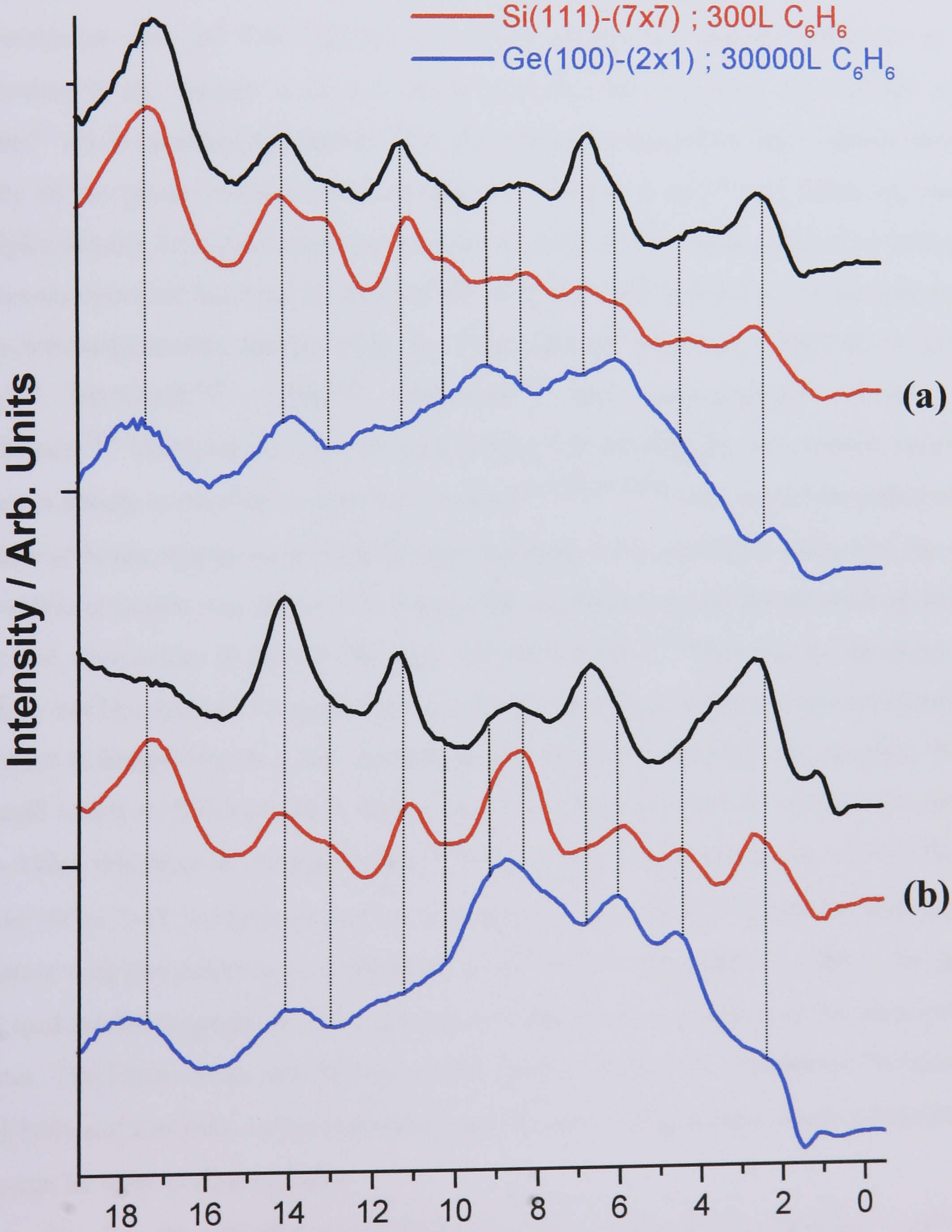

7.3 Discussion

Since the first investigation by Taguchi *et al.* in 1991,[10] the adsorption of benzene on Si(100)-(2×1) has been extensively studied and despite many experimental and theoretical investigations,[1,10-28] the exact adsorption model is still subject to controversy and therefore requires further investigation. Fig. 4 and Table 1 demonstrate that the photoemission data of the C_6H_6/Si(100)-(2×1) adsorption system collected at room temperature in the present work and in the previous ARUPS study by Gokhale and co-workers[1] are in excellent agreement. The similarities between both sets of data confirm the validity of the photoemission data collected by Gokhale *et al.*,[1] and following the first-principles density functional cluster calculations performed by these authors we believe that the chemisorption of benzene on the Si(100) surface at 300 K leads to the formation of the 1,4-cyclohexadiene-like species (Fig. 3). This structure has been supported by previous STM,[18] NEXAFS,[15] FTIR,[15] HREELS[23] and semiempirical cluster model calculations.[13] However the current work cannot rule out that the 1,4-cyclohexadiene-like species is ***slowly*** converted to a tetra-σ-bonded[16,17,20,22,24,28] or 1,3-cyclohexadiene-like[14] structure of lower energy as previously hypothesised, but it should be noted that the second more stable structure was detected in significant amounts only ***on a time scale of hours*** by Kong and co-workers in their FTIR and NEXAFS study.[15] This second structure would therefore not be expected to appear in our valence band photoemission spectra because our data were collected within a few minutes after exposure. Although the aromatic benzene molecule is not an efficient Diels-Alder reagent in organic chemistry and rarely undergoes Diels-Alder reactions in solution phase,[29] due to the unique properties of Si(100)-(2×1) and Ge(100)-(2×1), we believe that the formation of the 1,4-cyclohexadiene-like species is consistent with the recent work by Hamers *et al.*[5] which suggested that dienes can undergo [4+2] cycloaddition (Diels-Alder) reactions with the Si and Ge dimers of the semiconductor surfaces. The Diels–Alder mechanism can be used to explain the reactions of benzene with the Si(100) and Ge(100) surface because both Si and Ge dimers have weak π character and hence can be seen as dieneophiles.

As for the thiophene/Si(100)-(2×1) and thiophene/Ge(100)-(2×1) adsorption complexes,[3] FMO theory can be employed here to explain the reactivity between the

benzene molecules and the Si and Ge dimers and can also explain the lowest reactivity experimentally observed for Ge(100) when compared to the Si(100) surface. The two most important interactions which control the reactivity of the Diels-Alder reactions are the overlaps between the $HOMO_{benzene}$ and $LUMO_{Si\ or\ Ge}$ on one hand, and the $HOMO_{Si\ or\ Ge}$ and $LUMO_{benzene}$ orbitals on the other hand. For Diels-Alder reactions of normal electron demand, the separation between $HOMO_{benzene}$ and $LUMO_{Si\ or\ Ge}$ is smaller than the $HOMO_{Si\ or\ Ge}$ and $LUMO_{benzene}$, and the overlap between the former pair dominates the reactivity. The efficiency of a Diels-Alder reaction of normal electron demand increases with better overlap between the $HOMO_{benzene}$ and $LUMO_{Si\ or\ Ge}$ orbitals and consequently the rate of a Diels-Alder reaction increases as the ($HOMO_{benzene}$–$LUMO_{Si\ or\ Ge}$) energy separation decreases. The $HOMO_{benzene}$ is the well known $1e_{1g}$ orbital which has π character and lies at 9.2 eV below E_v.[30] For both Si(100) and Ge(100) the LUMOs are unoccupied dangling bond states with π* character and are located 0.35 eV[31] and 0.90 eV[32] above E_F, respectively. Given that the work functions of Si(100)-(2×1) and Ge(100) -(2×1) are 4.91 and 5 eV below E_v,[33] the positions of the π* state $LUMO_{Si}$ and $LUMO_{Ge}$ with respect to the vacuum level for the two surfaces are 4.56 and 4.10 eV below E_v, respectively. The energy separations from these values give:

- $HOMO_{benzene} - LUMO_{Si} = 9.20 - 4.56 = 4.64$ eV
- $HOMO_{benzene} - LUMO_{Ge} = 9.20 - 4.10 = 5.40$ eV

The above results show a poorer orbital overlap for Ge(100)-(2×1), as the ($HOMO_{benzene} - LUMO_{Ge}$) separation is bigger than the ($HOMO_{benzene} - LUMO_{Si}$) separation, which indicates that the Diels–Alder reaction is more favourable for the Si(100)-(2×1) surface and explains the lower sticking probability observed for the Ge(100)-(2×1) surface. As was previously mentioned in Chapter 6, the difference in sticking probability between Si(100) and Ge(100) could also stem from the difference in polarisation between the Si and Ge dimers. It was proposed that the degree of polarisation within the dimers is higher for Si than Ge, thereby making the probability for interaction of the adsorbates greater on Si than Ge. Furthermore our FMO calculations can be used to justify the lowest reactivity between benzene and the semiconductor surfaces when compared to thiophene,[3] because the ($HOMO_{thiophene} - LUMO_{Si\ or\ Ge}$) energy separations calculated for thiophene were smaller (4.34 and 4.80 eV for the Si(100) and Ge(100) separations respectively). Interestingly, it

was found by Qiao *et al.*[34] in their thermal evolution study of thiophene on the Si(100) surface using the XPS technique that, upon annealing, about 9% of the saturated thiophene monolayer desorbed molecularly while the remaining part underwent further reaction, and at 1000 K about 60% of the carbon from chemisorbed thiophene was left on the surface forming silicon carbide. On the other hand, the TPD experiments of benzene adsorbed on Si(100)-(2×1) performed in the temperature range 90–600 K showed no desorption of hydrogen or other hydrocarbon fragments, indicating a completely reversible molecular desorption.[1,10] These thermal desorption studies therefore indicate that thiophene is more strongly bonded to the Si(100) surface than benzene, and further confirm our theoretical predictions.

In contrast to the extensively studied C_6H_6/Si(100)-(2×1) system, the adsorption of benzene on the (2×1) reconstructed Ge(100) surface has only been the focus of one recent ARUPS and TPD investigation.[2] Although the experimental conditions employed by Fink *et al.* in this previous work differ from the present study, the detailed analysis of their ARUPS data also indicated that the chemisorption of benzene on Ge(100)-(2×1) led to the formation of a 1,4-cyclohexadiene-like species. One interesting aspect of the current study is that the differing relative intensities of the photoemission peaks observed in Figs. 12 and 13 illustrate the possible change of adsorption sites as a function of benzene exposure. Based on the conclusions drawn from the previous thermal desorption study of C_6H_6 adsorbed on the Ge(100)-(2×1) surface,[2] we believe that in the current study the C_6H_6 molecule initially reacts with the Ge dimers positioned next to the step edges at low benzene coverage. Interestingly, in the early investigation of benzene chemisorbed on Si(100)-(2×1), from their calculated heats of desorption Taguchi *et al.* estimated that the adsorption of benzene on the defect sites was thermodynamically more favourable than on the terrace sites.[10] Considering that the structure of the Ge(100)-(2×1) surface is very similar to that of Si(100)-(2×1),[5] we therefore believe that the step sites of the germanium surface are thermodynamically more favourable than the terrace sites for benzene adsorption. Again, the comparison between the valence band spectra of thiophene (Fig. 15 in Chapter 6) and benzene (Fig. 13 of present work) adsorbed on Ge(100)-(2×1) at room temperature illustrates the difference in reactivity between the two aromatic molecules and the germanium dimers. The benzene molecule is well known to be more stable than the

thiophene due to the complete delocalisation of its 6 π electrons around the ring.[39] In contrast, the presence of the electronegative sulfur heteroatom within the thiophene ring makes the carbon in position 2 electron-rich and likely subject to electrophilic attack.[39] Finally, close inspection of the relative intensities of the photoemission peaks in Figs. 12 and 13 possibly suggests that at high benzene exposure the terrace sites of the Ge(100)-(2×1) become occupied. In analogy to the previous TPD data of the C_6H_6/Si(100)-(2×1) adsorption complex collected by Gokhale *et al.*,[1] our valence band data indicate that adsorption on the Ge(100) terraces starts upon saturation of the step sites. We are however unable to detect the coexistence of benzene on the germanium terrace and step sites at low coverage as previously observed by Taguchi and co-workers for C_6H_6 on Si(100) at 300 K.[10]

The formation of the 1,4-cyclohexadiene-like moiety on the Si(111) surface is another interesting aspect of the current study since the Si(111)-(7×7) and the (2×1) reconstructed Si(100) and Ge(100) surfaces are structurally and electronically different. The 1,4-cyclohexadiene-like configuration in which the benzene molecule is di-σ-bonded to the Si(111) surface has been supported by previous UPS[6] and HREELS experiments,[40] and theoretical calculations.[41] As illustrated in Table 1 and Fig. 10, the small difference in orbital energies between the C_6H_6/Si(100) and C_6H_6/Si(111) systems confirm that adsorption of benzene on the silicon surfaces leads to the formation of the same species. This result is not entirely surprising in view of the recent thiophene[3,34] and ethylene[7,38] adsorption studies on the two surfaces. In contrast to the off-normal spectra of thiophene adsorbed on the Si(100) and Si(111) surfaces,[3] it is clearly evident that the relative intensities of the benzene photoemission peaks from Si(111)-(7×7) and Si(100)-(2×1) in the off-normal collection geometry differ (Fig. 10). This would suggest at first sight that the orientation of the 1,4-cyclohexadiene-like moiety on Si(111)-(7×7) could be different to the one adopted on the (2×1) reconstructed Si(100) surface. However, taking into consideration several recent investigations which suggested that the adsorption of π-bonded molecules leads to the re-arrangement of the silicon atoms within the (7×7) reconstruction,[3,7] we believe that benzene does not adopt a different orientation on Si(111). In a previous STM investigation of benzene adsorbed on Si(111) by Wolkow and Moffat[44] it was found that the activation barrier to diffusion was surprisingly low and also comparable to that for

desorption. More importantly the STM images indicated that the benzene molecules were mobile on the Si(111) at room temperature. In contrast, to the best of our knowledge, no benzene diffusion on Si(100) has ever been reported in the literature. Consequently, as previously suggested by Carbon *et al.*,[6] we believe that the surface mobility of benzene on Si(111)-(7×7) affects the intensity of the adsorption features and the difference in relative intensities displayed in Fig. 10 can be associated to the different level of mobility of the benzene molecule across the Si(111) and Si(100) surfaces.

Although it was initially proposed in the early investigations by Taguchi *et al.*[42] and MacPherson and co-workers'[43] that benzene was parallel to Si(111)-(7×7), in the more recent UPS,[6] HREELS[40] and STM[44] studies it was suggested that the C_6H_6 molecule was bonded to a pair of adjacent adatom/rest atom and tilted by 13° with respect to the surface. The proposed AD/RA model was based on the disappearance of bright spots associated to the AD in the STM images[44] and quenching of the surface states in the photoemission spectra.[6] The above experimental observations, however, could also indicate the re-arrangement of the silicon adatoms within the (7×7) reconstruction as described by Rochet and co-workers for the ethylene adsorbed on Si(111).[7] As a result the removal of the silicon adatoms to an interstitial position would have two major effects. The first effect would be to create a less corrugated substrate on an atomic level which could explain the unprecedented case of benzene on Si(111) where $E_{diff} \approx E_{desorb}$ as described by Wolkow and Moffat.[44] A large barrier to adsorbate diffusion would be normally expected for the highly corrugated Si(111)-(7×7) surface, but the decrease of the surface roughness associated with the removal of the AD would consequently decrease E_{diff} and increase the rate of spreading of the adsorbate across the surface. The second effect would be to produce three new pedestal silicon atoms available for bonding. By assuming that the positions of the pedestal atom remain the same as those adopted in the (7×7) structure, the separation between pedestal and rest atoms (3.7 Å) would be shorter than the distance between adatoms and rest atoms (4.5 Å). Because the distance between the two opposite carbon atoms of the benzene molecule is 2.78 Å,[6,45] a shorter Si – Si separation would clearly place different strains on the geometry of the 1,4-cyclohexadiene-like – surface complex. Another effect for the 1,4-cyclohexadiene-like moiety di-σ-bonded to neighbouring rest

and pedestal silicon atoms would be that the moiety could adopt a geometry where the axis passing through the 1 and 4 carbon positions would be parallel rather than inclined to the rest-atom plane (Fig. 6c). Since our photoemission data does not provide detailed quantitative information on the structure of the underlying Si(111) substrate, it should be stressed that the suggestions made here are only tentative and more unambiguous experiments which could give quantitative structural information are therefore required. Finally, as was the case for thiophene adsorbed on Si(100)-(2×1), Si(111)-(7×7) and Ge(100)-(2×1),[3] because the Si(111)-(7×7) surface does not possess the required π-bonded silicon dimers for the reaction to occur *via* a Diels–Alder mechanism, the formation of the 1,4-cyclohexadiene-like moiety on the three semiconductor surfaces shows that the product formed in a reaction between an aromatic molecule and silicon or germanium surface is not influenced by the electronic and physical structures of the surface, but the actual reaction mechanism is dependent upon the surface electronic and physical structure.

7.4 Summary

The most significant findings of the current study are outlined below:

- Comparisons between the photoemission data collected in the current work and the ARUPS measurements and first-principles DFT calculations of the C_6H_6/Si(100)-(2×1) system by Gokhale *et al.*[1] show that the adsorption of benzene on Si(100)-(2×1), Si(111)-(7×7) and Ge(100)-(2×1) at room temperature in the present work leads to the formation of a 1,4-cyclohexadiene-like moiety. This 1,4-cyclohexadiene-like species is the direct results of a [4+2] cycloaddition (Diels–Alder) reaction between π-bonded dimers of the (2×1) reconstructed Si(100) and Ge(100) and the benzene molecules.

- In analogy to the previous TPD experiments of benzene adsorbed on the Ge(100)-(2×1) surfaces,[2] our photoemission data suggest that benzene initially reacts with the Ge dimers positioned next to the step edges, and upon high benzene exposure, adsorption on the terrace sites occurs.

- We tentatively propose that the orientation of the moiety on Ge(100)-(2×1) and Si(111)-(7×7) is not significantly different to that adopted on Si(100)-(2×1). As for thiophene adsorbed on Si(111),[3] due to the absence of the π-bonded silicon dimers required for a Diels-Alder reaction, the formation of a 1,4-cyclohexadiene-like species on the Si(111)-(7×7) surface implies that although the reaction mechanism is influenced by surface electronic and structural properties the actual product of the surface reaction is not.

7.5 References

1. S. Gokhale, P. Trischberger, D. Menzel, W. Widdra, H. Droge, H.P. Steinruck, U. Birkenheuer, U. Gutdeutsch, N. Rosch, J. Chem. Phys., 108 (1998) 5554
2. A. Fink, D. Menzel, W. Widdra, J. Phys. Chem. B, 105 (2001) 3828
3. Chapter 6 of the present work
4. R.I.G. Uhrberg, G.V. Hannson, J.M. Nicholls, S.A. Flodstrom, Phys. Rev. B, 24 (1981) 4684
5. R.J. Hamers, S.K. Coulter, M.D. Ellison, J.S. Hovis, D.F. Padowitz, M.P. Schwartz, C.M. Greenlief, J.N. Russell, Acc. Chem. Res., 33 (2000) 617
6. M. Carbone, M.N. Piancastelli, R. Zanoni, G. Comtet, G. Dujardin, L. Hellner, Surf. Sci., 407 (1998) 275
7. F. Rochet, F. Jolly, F. Bournel, G. Dufour, F. Sirotti and J.L. Cantin Phys. Rev. B, 58 (1998) 11029
8. S.J. Stranick, M.M. Kamna, P.S. Weiss, Surf. Sci., 338 (1995) 41
9. P.K. Milligan, B. Murphy, D. Lennon, B.C.C. Cowie, M. Kadodwala, J. Phys. Chem. B, 105 (2001) 140
10. Y. Taguchi, M. Fujisawa, T. Takaoka, T. Okada, M. Nishijima, J. Chem. Phys., 95 (1991) 6870
11. B.I. Craig, Surf. Sci. Lett., 280 (1993) L279
12. H.D. Jeong, S. Ryu, Y.S. Lee, S. Kim, Surf. Sci., 344 (1995) L1226
13. U. Birkenheuer, U. Gutdeutsch, N. Rosch, Surf. Sci., 409 (1998) 213
14. B. Borovsky, M. Krueger, E. Ganz, Phys. Rev. B, 57 (1998) R4269
15. M.J. Kong, A.V. Teplyakov, J.G. Lyubovitsky, S.F. Bent, Surf. Sci., 411 (1998) 286
16. G.P. Lopinski, T.M. Fortier, D.J. Moffatt, R.A. Wolkow, J. Vac. Sci. Technol. A, 16 (1998) 1037
17. G.P. Lopinski, D.J. Moffatt, R.A. Wolkow, Chem. Phys. Lett., 282 (1998) 305
18. K.W. Self, R.I. Pelzel, J.H.G. Owen, C. Yan, W. Widdra, W.H. Weinberg, J. Vac. Sci. Technol. A, 16 (1998) 1031
19. Y. Taguchi, Y. Ohta, T. Katsumi, K. Ichikawa, O. Aita, J. Electron Spectrosc. Relat. Phenom., 88 (1998) 671

20. R.A. Wolkow, G.P. Lopinski, D.J. Moffatt, Surf. Sci., 416 (1998) L1107
21. S. Alavi, R. Rousseau, T. Seideman, J. Chem. Phys., 113 (2000) 4412
22. P.L. Silvestrelli, F. Ancilotto, F. Toigo, Phys. Rev. B, 62 (2000) 1596
23. M. Staufer, U. Birkenheuer, T. Belling, F. Nortemann, N. Rosch, W. Widdra, K.L. Kostov, T. Moritz, D. Menzel, J. Chem. Phys., 112 (2000) 2498
24. W.A. Hofer, A.J. Fisher, G.P. Lopinski, R.A. Wolkow, Phys. Rev. B, 63 (2001) 085314
25. Q. Li, K.T. Leung, Surf. Sci., 479 (2001) 69
26. M. Nagao,Y. Yamashita, S. Machida, K. Hamaguchi, F. Yasui, K. Mukai, J. Yoshinobu, Surf. Sci., 513 (2002) 413
27. A. Fink, W. Widdra, W. Wurth, C. Keller, M. Stichler, A. Achleitner, G. Comelli, S. Lizzit, A. Baraldi, D. Menzel, Phys. Rev. B, 64 (2001) 045308
28. P. Kruse, R.A. Wolkow, Appl. Phys. Lett., 81 (2002) 4422
29. S. F. Bent, J. Phys. Chem. B, 106 (2002) 2830
30. K. Kimura, S. Katsumata, Y. Achiba, T. Yamazaki, S. Iwata, *Handbook of HeI Photoelectron Spectra of Fundamental Organic Molecules*, Japan Scientific Societies Press, Tokyo, 1981
31. R.J. Hamers, Ph Avouris, F. Bozso, J. Vac. Sci. Technol. A, 6 (1988) 508
32. L. Kipp, R. Manzke, M. Skibowski, Surf. Sci., 269/270 (1992) 854
33. The CRC Handbook of Chemistry and Physics, CRC Press, Boca Raton, FL, 1995
34. M.H. Qiao, Y. Cao, F. Tao, Q. Liu, J.F. Deng, G.Q. Xu, J. Phys. Chem. B, 104 (2000) 11211
35. X. Torrelles, H.A. van der Vegt, V.H. Etgens, P. Fajardo, S. Alvarez, S. Ferrer, Surf. Sci., 364 (1996) 242
36. P. Kruger, J. Pollmann, Phys. ReV. Lett. 74 (1995) 1155
37. S.W. Lee, J.S. Hovis, S.K. Coulter, R.J. Hamers, C.M. Greenlief, Surf. Sci., 462 (2000) 6
38. A. Fink, R. Huber, W. Widdra, J. Chem Phys, 115 (2001) 2768
39. J. McMurry, *Organic chemistry*, Pacific Grove, California: Brooks-Cole, 3rd ed., Chapter 15 (1992)

40. Y. Cao, X.M. Wei, W.S. Chin, Y.H. Lai, J.F. Deng, S.L. Bernasek, G.Q. Xu, J. Phys. Chem. B, 103 (1999) 5698
41. Z.H. Wang, Y. Cao, G.Q. Xu, Chem. Phys. Lett, 338 (2001) 7
42. Y. Taguchi, M. Fujisawa, M. Nishijima, Chem. Phys. Lett., 178 (1991) 363
43. C.D. MacPherson, D.Q. Hu, K.T. Leung, Solid State Comm., 80 (1991) 217
44. R.A. Wolkow, D.J. Moffat, J. Chem. Phys., 103 (1995) 10696
45. The CRC Handbook of Chemistry and Physics, CRC Press, Boca Raton, FL, 1995

Chapter 8. Photoemission Studies of the Surface Reactivity of Benzonitrile on Si(100)-(2×1), Si(111)-(7×7) and Ge(100)-(2×1)

8.1 Introduction

The binding of the multifunctional benzonitrile molecule (C_6H_5-C≡N) on the Si(100)-(2×1), Si(111)-(7×7) and Ge(100)-(2×1) surfaces at room temperature has been studied by valence band spectroscopy using linearly polarised synchrotron-based radiation. The assignment of the bonding of benzonitrile on the three semiconductor surfaces has been made by comparing the valence band features obtained in the current work with the UP spectra of benzonitrile adsorbed on Si(100)-(2×1) and Si(111)-(7×7) by Tao *et al.*[(1)] and Wang and co-workers[(2)] respectively. Our experimental results are in excellent agreement with the photoemission data collected in the two previous investigations and indicate that a benzoimine-like species is formed upon adsorption of benzonitrile. In contrast to the silicon surfaces, to the best of our knowledge, the adsorption of benzonitrile on Ge(100)-(2×1) has not been previously studied and our valence band data suggest that the formation of the benzoimine-like moiety initially occurs on the Ge dimers positioned next to the step edges. We propose that the formation of the benzoimine-like species on Si(100)-(2×1) and Ge(100)-(2×1) is consistent with a 1,2-dipolar cycloaddition reaction between the unsaturated cyano group and the π-bonded dimers of the Si(100) and Ge(100) surfaces. The adsorption of benzonitrile on Si(111)-(7×7) also leads to the formation of a benzoimine-like species, and this result again implies that the actual product formed in the reaction between the aromatic molecule and the silicon or germanium surfaces is not dependent upon the electronic and structural properties of the three semiconductor surfaces. The results from the present study are in excellent agreement with Chapters 6 and 7 of the current project which suggest that the absorption of organic molecules on Si(100)-(2×1), Si(111)-(7×7) and Ge(100)-(2×1) lead to the formation of the same surface species.

8.2 Results

8.2.1 Benzonitrile/Si(100)-(2×1)

The normal and off-normal photoemission spectra, collected from a clean Si(100)-(2×1) surface which had been exposed to 45 L of benzonitrile at room temperature, are shown in Fig. 2. The difference UP spectra, which emphasise the states produced by the adsorbate, were obtained by subtracting the corresponding clean surface spectrum from the one obtained after benzonitrile adsorption and are also displayed in Fig. 2. The valence band spectra (Fig.2a) display bands centred at 1.0, 2.6, 4.0, 6.8, 9.5, 10.8, 12.2, 14.0 and 17.5. The peaks at 1.0 and 2.6 eV can be associated with the remnants of the silicon dangling bond (π) state and with photoemission from the σ bond between the two silicon atoms of the surface dimers, respectively. The feature at 4.0 eV also originates from the σ bond between the two Si surface dimers, but the height of this feature (most pronounced in off-normal emission) suggests that this band can also be attributed to one of the molecular orbitals of the moiety formed by the adsorption of benzonitrile on Si(100). Therefore the bands observed at BE $\geq$ 4.0 eV in Fig. 2 can be associated with the orbitals of the benzonitrile derived moiety.

Fig. 3 shows the comparison between the UP spectra of 0.4 L of benzonitrile adsorbed on Si(100)-(2×1) at 110 K collected by Tao *et al.*[1] using a He II source ($h\nu = 40.8\,eV$) and the normal and off normal valence band photoemission spectra obtained in the current work for 45 L of benzonitrile adsorbed on Si(100) at room temperature. Although some of the peaks are more pronounced in the present investigation, Fig. 3 displays a one-to-one correspondence between the peak positions of both sets of experimental data. By comparing the UP spectra of physisorbed (multilayer) and chemisorbed benzonitrile (both states were primarily identified by TPD), Tao and co-workers were able to detect a decrease in the intensity of the peak attributed to photoemission from the $\pi_{C\equiv N}$ molecular orbitals of chemisorbed benzonitrile, indicating that the cyano group of the molecule in this particular state directly interacted with Si(100) surface dangling bonds.[1] However, UPS was not the only technique used by the authors to characterise the moiety formed on Si(100)-(2×1) upon benzonitrile exposure.

By using a combination of HREELS, XPS and DFT calculations, the authors showed that the covalent attachment of chemisorbed benzonitrile on Si(100) occurred in a highly selective manner through the direct interaction of both C and N atoms of the cyano group with a Si dimer to form a four-member Si–C=N–Si ring at the interface, leaving a nearly unperturbed phenyl ring protruding into vacuum, as depicted in Fig. 1. These authors first identified both physisorbed and chemisorbed benzonitrile at an adsorption temperature of 110 K, with the desorption of condensed physisorbed benzonitrile layer taking place at 180 K, and chemisorbed benzonitrile desorbing at a temperature of 490 K. Their TPD results therefore suggest that in the present work, the adsorption of C_6H_5CN on Si(100) at room temperature leads to the formation of chemisorbed benzonitrile molecules. Furthermore, the vibrational features of chemisorbed benzonitrile obtained by HREELS showed the disappearance on the C≡N stretching mode coupled with the appearance of the C=N stretching mode and the retention of all vibrational signature of the phenyl ring, and their XPS data indicated that both the C 1s and N 1s of the cyano group displayed a large downshift to lower binding energy. Both techniques therefore indicated the direct interaction of the cyano group of the benzonitrile molecule with the Si dimers of the Si(100)-(2×1) surface, demonstrating the formation of a benzoimine-like moiety upon the adsorption of benzonitrile (Fig. 1). This assignment was also confirmed by performing DFT calculations where several possible binding modes were tested. It was found that the total energy of the model representing the 1,2-dipolar cycloaddition reaction occurring between the cyano group and the Si dimer was the lowest (because the N=C bond of the isothiocyanate group is polar, this cycloaddition reaction is labelled as a 1,2-dipolar rather than [2+2] cycloaddition). This theoretical prediction reinforces the idea of the formation of a benzoimine-like specie through the adsorption of benzonitrile on Si(100).

In summary, the valence band photoemission data collected in the present work are in excellent agreement with the UPS data of the same system collected by Tao *et al.*[1] Using a combination of TPD, HREELS, XPS, UPS and DFT calculations, the authors were able to demonstrate that the chemisorption of benzonitrile on Si(100)-(2×1) at 300 K leads to the formation of benzoimine-like species. This result is consistent with a 1,2-dipolar cycloaddition between benzonitrile and the silicon dimers of the Si(100)-(2×1) surface.

Fig.1. *The probable bonding geometry of the benzoimine-like moiety formed on Si(100)-(2×1) upon the adsorption of benzonitrile is shown schematically.*

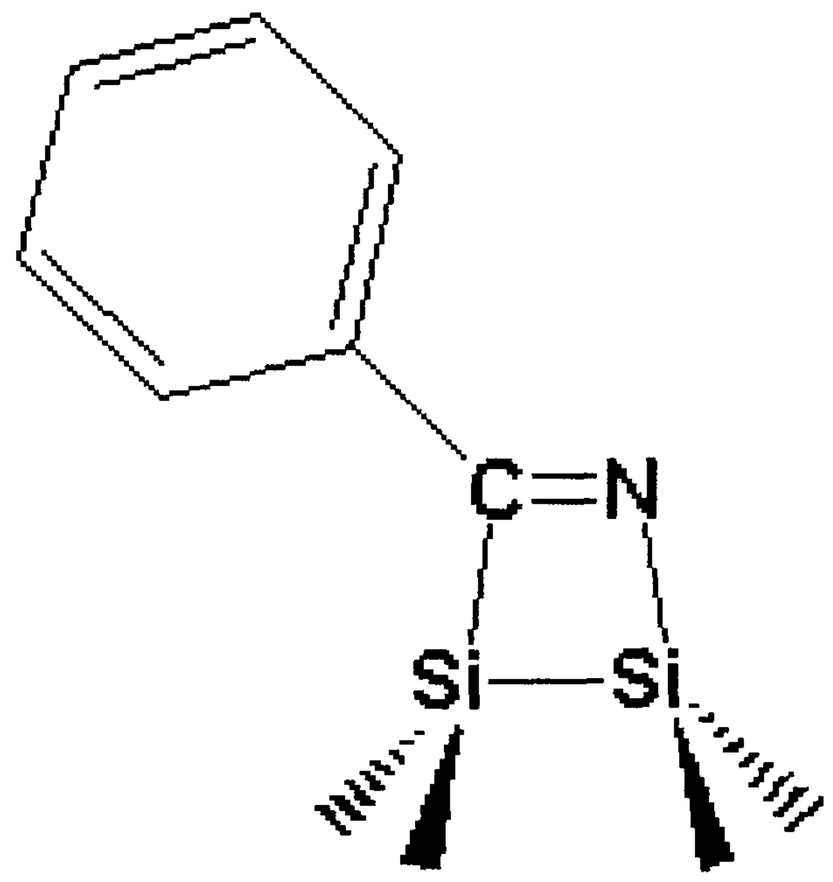

Fig.2. *Normal and off-normal emission valence band (a) and difference (b) UP spectra ($h\nu$ = 40 eV) collected from a Si(100)-(2×1) surface that had been exposed to 45 L of benzonitrile at room temperature.*

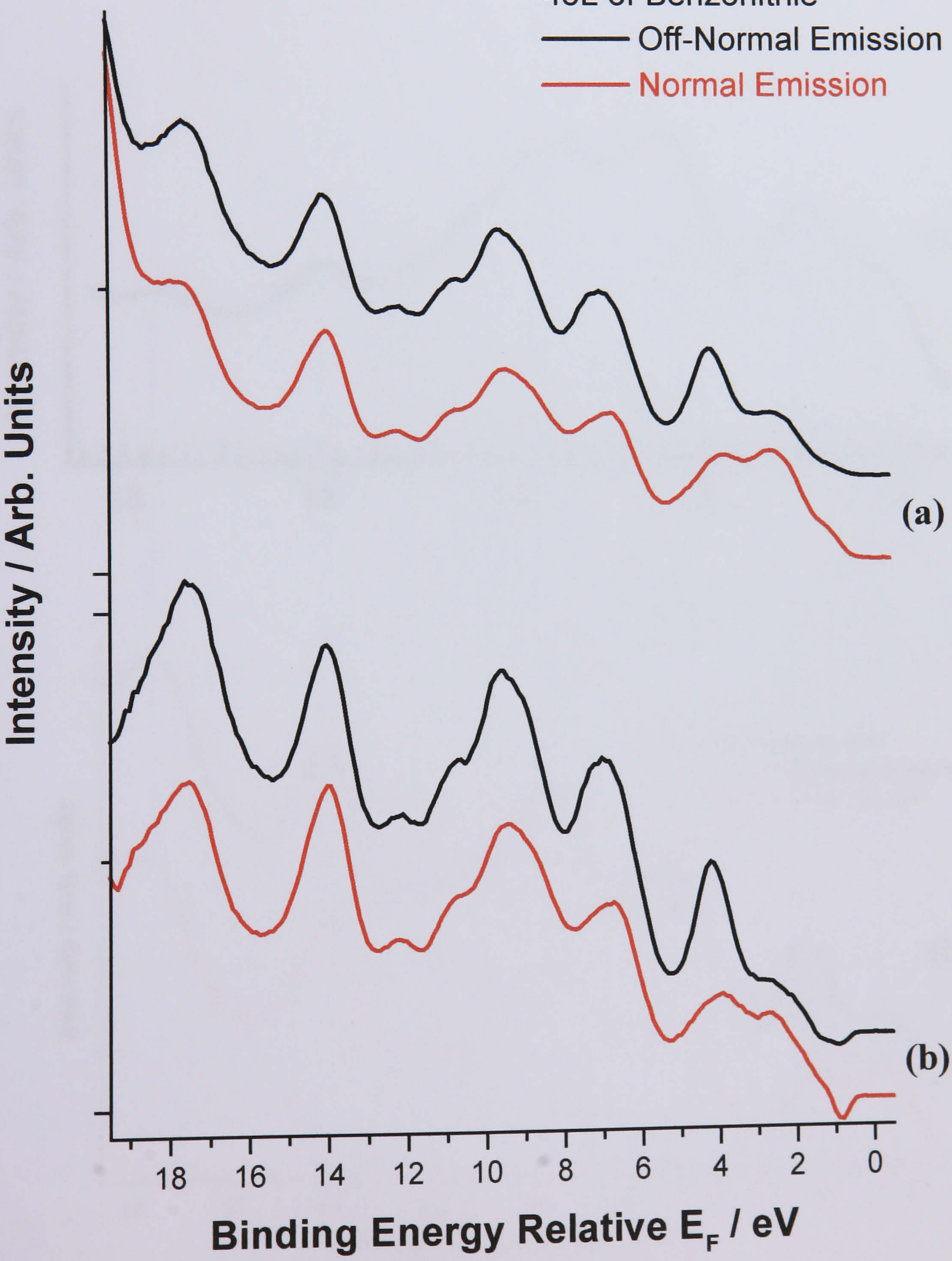

Fig.3. *Comparison between (a) the UPS data collected by Tao et al. of 0.4 L of benzonitrile adsorbed on Si(100)-(2×1) at 110 K using a He II source ($h\nu = 40.8\ eV$)* [1] *and (b) the normal and off normal valence band photoemission data of 45 L of benzonitrile adsorbed on Si(100)-(2×1) at room temperature obtained in the current study.*

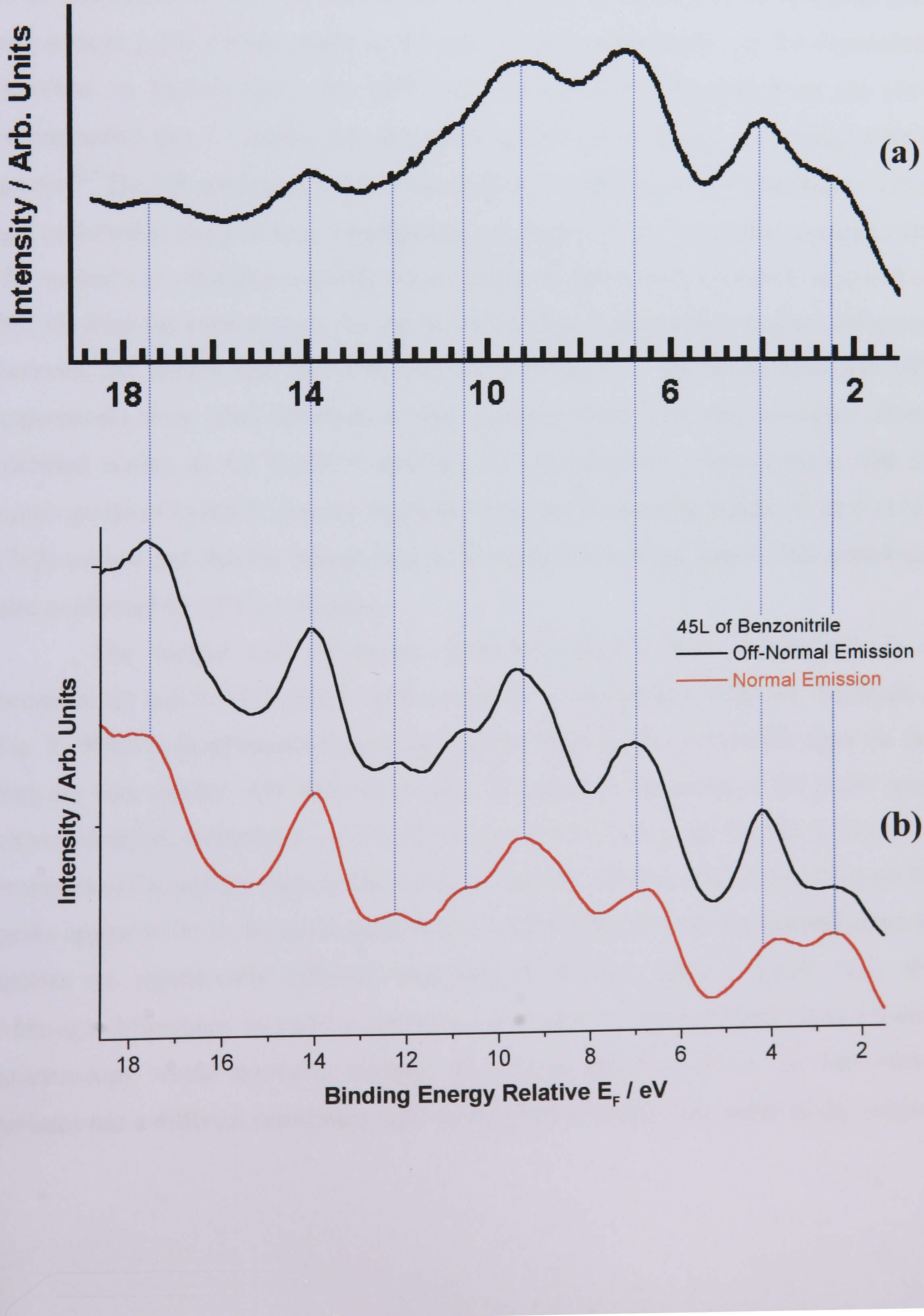

8.2.2 Benzonitrile/Si(111)-(7×7)

Fig. 5 depicts the spectra collected at normal and off-normal emission, along with the corresponding difference spectra, from a clean Si(111)-(7×7) surface which exposed to 300 L of benzonitrile at room temperature. Both spectra have six broad features in the regions which cover 0.0–3.0, 3.0–5.2, 5.2–8.0, 8.0–11.7, 11.7–15.3, and 15.3–18.6 eV BE. The bands observed at BE > 3.0 eV can be attributed to the molecular orbitals of the moiety derived from the adsorption of benzonitrile. As illustrated in Fig. 6, the adsorption of 300 L of benzonitrile leads to the attenuation of the rest atom (RA) and adatom (AD) surface states at 0.5 and 1.1 eV, respectively. As for benzonitrile adsorbed on Si(100)-(2×1), the UPS study of C_6H_5CN chemisorbed on the (7×7) reconstructed Si(111) surface has also been carried out by Wang *et al.* using a He II source.[2] The UP spectra of 3.0 L of benzonitrile on Si(111)-(7×7) adsorbed at 110 K and collected in this previous investigation are shown in Fig. 7 and are compared with the normal and off-normal valence band spectra of 300 L of benzonitrile adsorbed on Si(111) from the current work. As can be seen in Fig. 7, there is an excellent agreement between our results and the UPS data from the Ref. 2. HREELS, XPS and UPS experiments were also obtained in this previous work and they provided almost identical results as for C_6H_5CN adsorbed on Si(100)-(2×1), demonstrating that the cyano group of C_6H_5CN directly interacted with the Si dangling bonds of the Si(111)-(7×7) surface and that the phenyl ring of the molecule was left intact. This model was also confirmed by DFT calculations.

The normal and off-normal difference spectra from Si(100) (45 L of benzonitrile) and Si(111) (300 L of benzonitrile) of the current study are displayed in Fig. 8. When both ***off-normal*** spectra are compared (Fig. 8a), it is readily apparent that they are very similar, with both the position and relative intensities of the bands being almost identical. Differences exist in the region 0–5 eV in Fig. 8a, but this is due to the remnants of the surface states of both silicon surfaces. On the other hand, although the peaks appear to be in the same position, the relative intensities of the ***normal*** emission spectra are significantly different, especially in the BE range 5 - 12 eV (Fig. 8b). Although differences in relative intensities of peaks in valence band photoemission spectroscopy would normally indicate that the moiety formed on the two silicon surfaces has a different orientation with respect to the polarisation vector of the incident

radiation, the inconsistency between the normal and off-normal data sets can be resolved by considering the overall symmetry of the adsorbate–substrate complex. The same arguments were previously employed to explain the difference in relative intensities observed for thiophene adsorbed on Si(100)-(2×1) and Si(111)-(7×7) at normal emission [Chapter 6]. The symmetry of the benzoimine-like moiety is also strongly influenced by the symmetries of Si(100)-(2×1) and Si(111)-(7×7), and the differing relative intensities in the normal emission spectra reflect the difference in the overall symmetry of the benzoimine complex on the two silicon surfaces. We therefore believe that the same surface species is formed on the Si(100)-(2×1) and Si(111)-(7×7) surface upon the adsorption of benzonitrile at room temperature.

STM experiments were also performed at room temperature by Wang *et al.* in order to determine which surface atoms were involved in the adsorption process of benzonitrile on Si(111)-(7×7).[(2)] In their clean surface STM image, adatoms, corner holes and dimer boundaries could clearly be observed. However the bright spots attributed to the adatoms on the clean surface image disappeared upon benzonitrile exposure, and it was subsequently suggested that the darkness of the adatoms in the STM image could be attributed to the consumption of the adatom dangling bonds due to surface adsorbates bond formation. Consequently the authors proposed that the attachment of the benzonitrile molecules to the Si(111)-(7×7) surface involved the cyano group and the adjacent adatom/rest atom pair (Fig. 4b). In the photoemission study of thiophene adsorbed on Si(111)-(7×7), following the model proposed by Rochet *et al.*,[(3)] we tentatively suggested that the chemisorption of C_4H_4S caused a rearrangement of the silicon atoms within the (7×7) reconstruction, which involved the removal of the adatom to an interstitial position under the plane containing the rest atom and pedestal atoms. We believe that the same model could be applied here to explain the similarity of the off-normal data observed in Fig. 8a. On a re-arranged (7×7) surface where the benzonitrile molecule is bonded to a pedestal atom and a rest atom (PA/RA model), the geometry adopted by the surface moiety will be similar to that on Si(100)-(2×1), with the axis passing through the carbon and nitrogen atoms of the cyano group being roughly parallel to the surface (Fig. 4c). In this configuration, the strains placed on the C=N group will be less important than for the adatom/rest atom model. The removal of the adatoms to the interstitial sites could also explain the disappearance of the bright spots assigned to the adatom sites in the STM image obtained by Wang and

co-workers upon adsorption of benzonitrile.[2] It should also be noted that in the STM image the (7×7) reconstruction was preserved after adsorption, an experimental result which also agrees with our PA/RA model.

To summarise, the most important conclusions that can be drawn from our photoemission data are that a benzoimine-like moiety is formed by the adsorption of benzonitrile on the Si(111)-(7×7) surface through reaction between the cyano group and the dangling bonds of the adjacent pedestal atom – rest atom, and that the orientation of the moiety on the Si(111)-(7×7) surface is not significantly different to that adopted on Si(100)-(2×1).

Fig.4. *Schematic diagrams of (a) the clean Si(111)-(7x7) surface where the rest atoms (RA), adatom (AD) and pedestal atom (PA) have been labelled, (b) the benzoimine-like moieties bonded to the RA and AD in a bridging geometry and (c) the benzoimine-like species bonded to the RA and PA.*

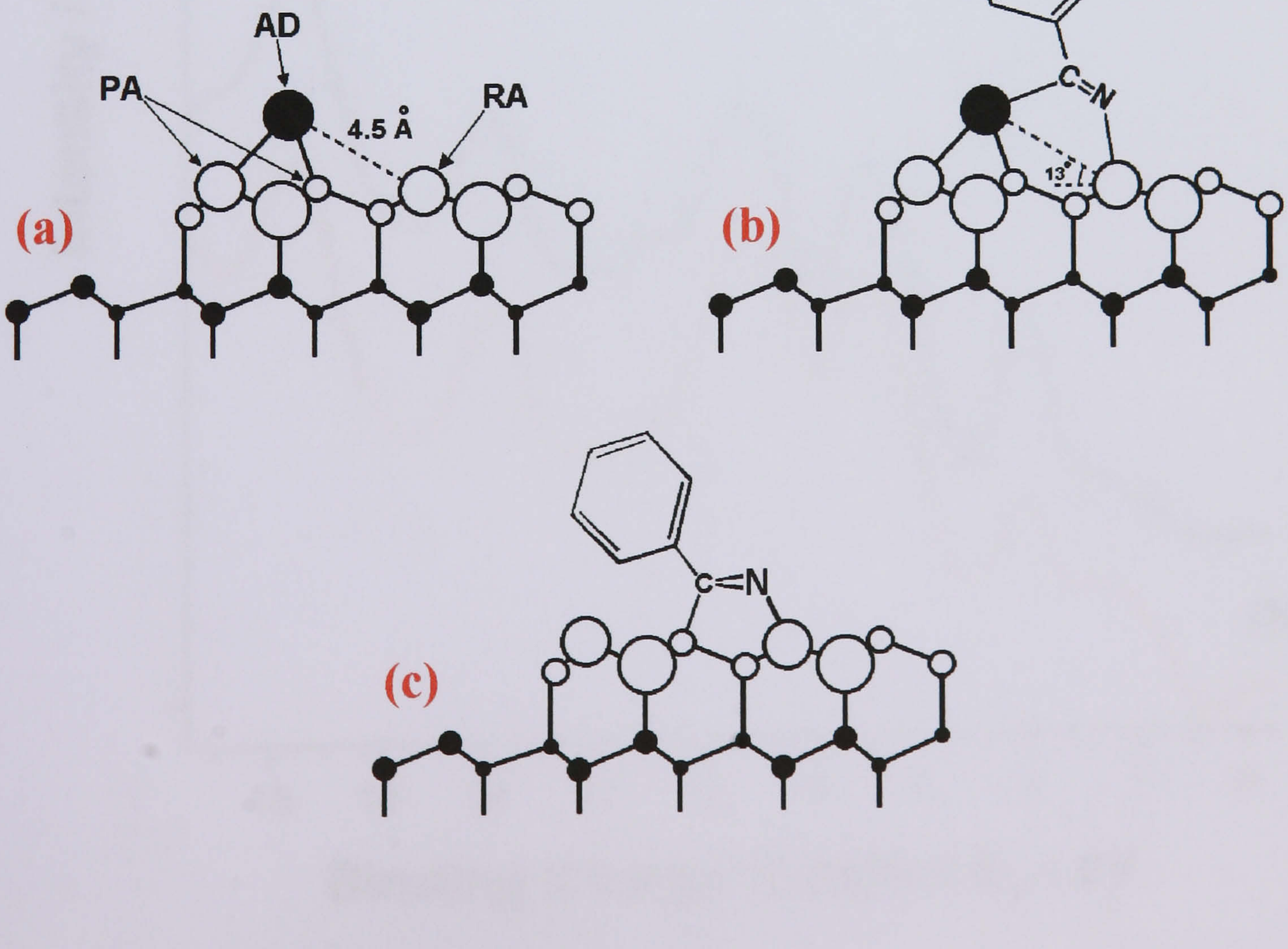

Fig.5. *Normal and off-normal emission valence band (a) and difference (b) UP spectra ($h\nu$ = 40 eV) collected from a Si(111)-(7×7) surface which had been exposed to 300 L of benzene at room temperature.*

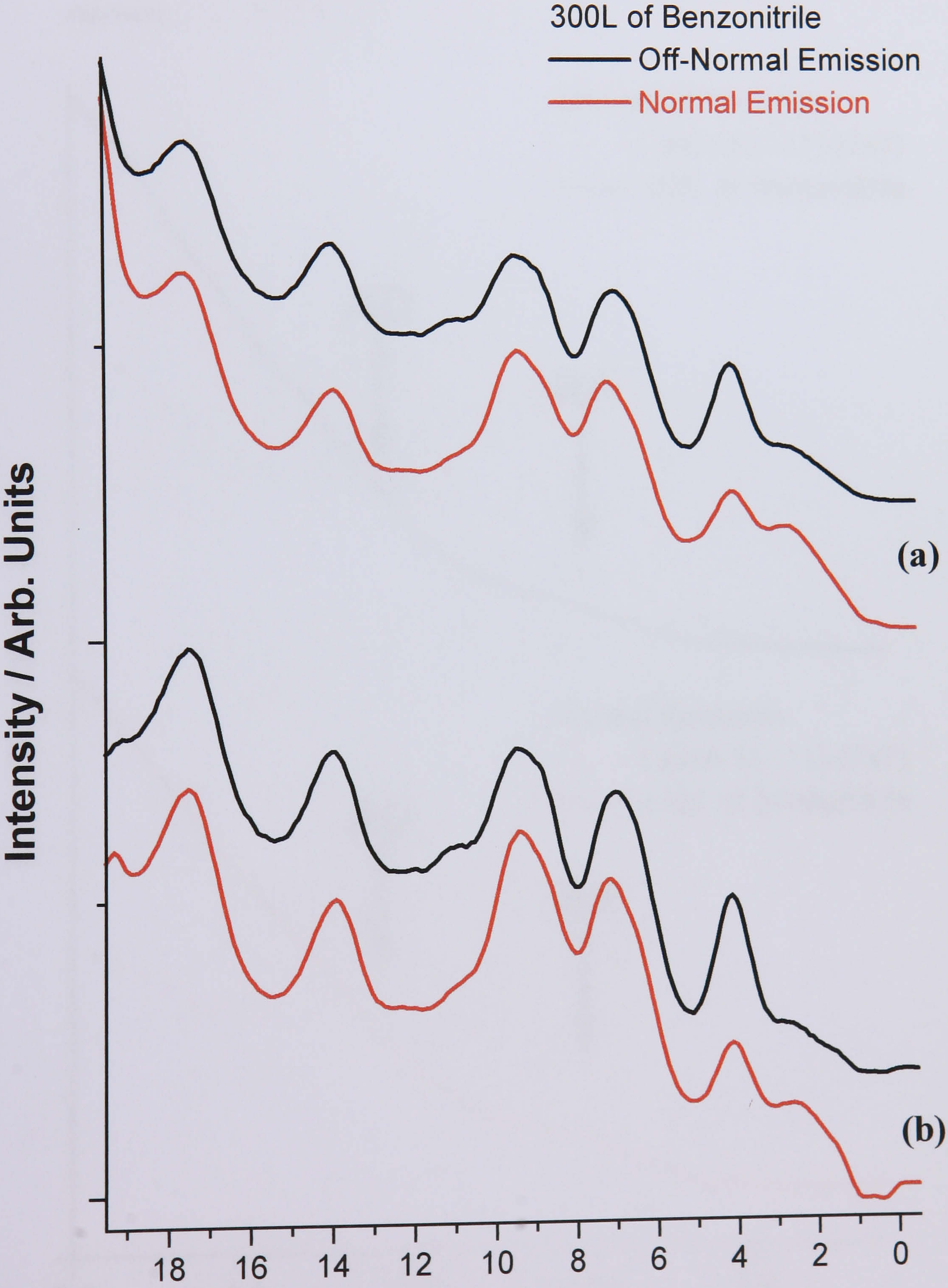

Fig.6. *Comparison between the off-normal and normal emission valence band photoemission spectra (hν = 40 eV) of the clean Si(111)-(7×7) surface and the same surface exposed to 300 L of benzene at room temperature. This plot shows the decrease in intensity of the RA and AD surface states upon benzene exposure.*

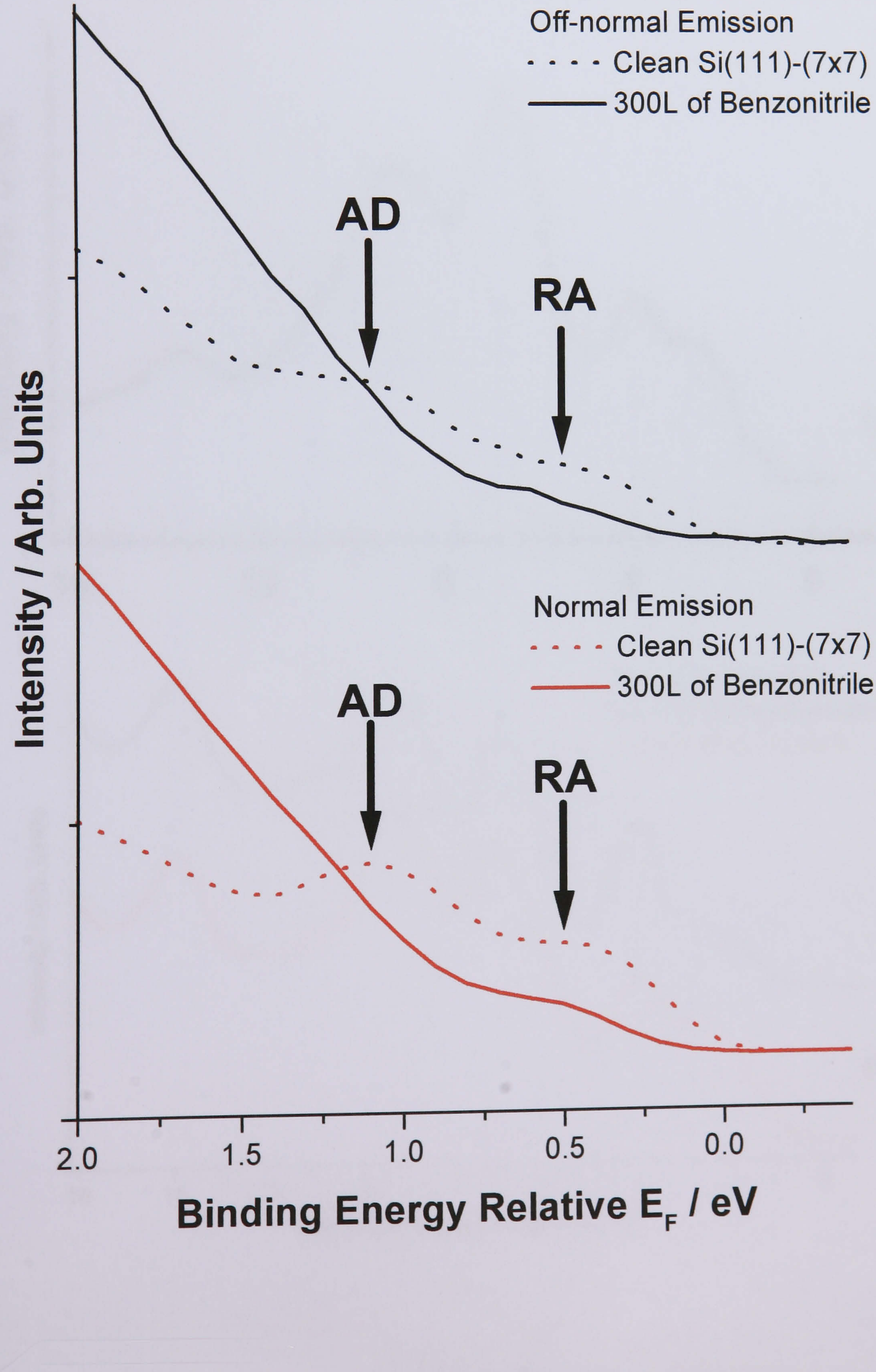

Fig.7. *Comparison between (a) the UPS data collected by Wang et al. of 3.0 L of benzonitrile adsorbed on Si(111)-(7×7) at 110 K using a He II source ($h\nu = 40.8\ eV$)* [2] *and (b) the normal and off normal valence band photoemission data of 300 L of benzonitrile adsorbed on Si(111)-(7×7) at room temperature obtained in the current study.*

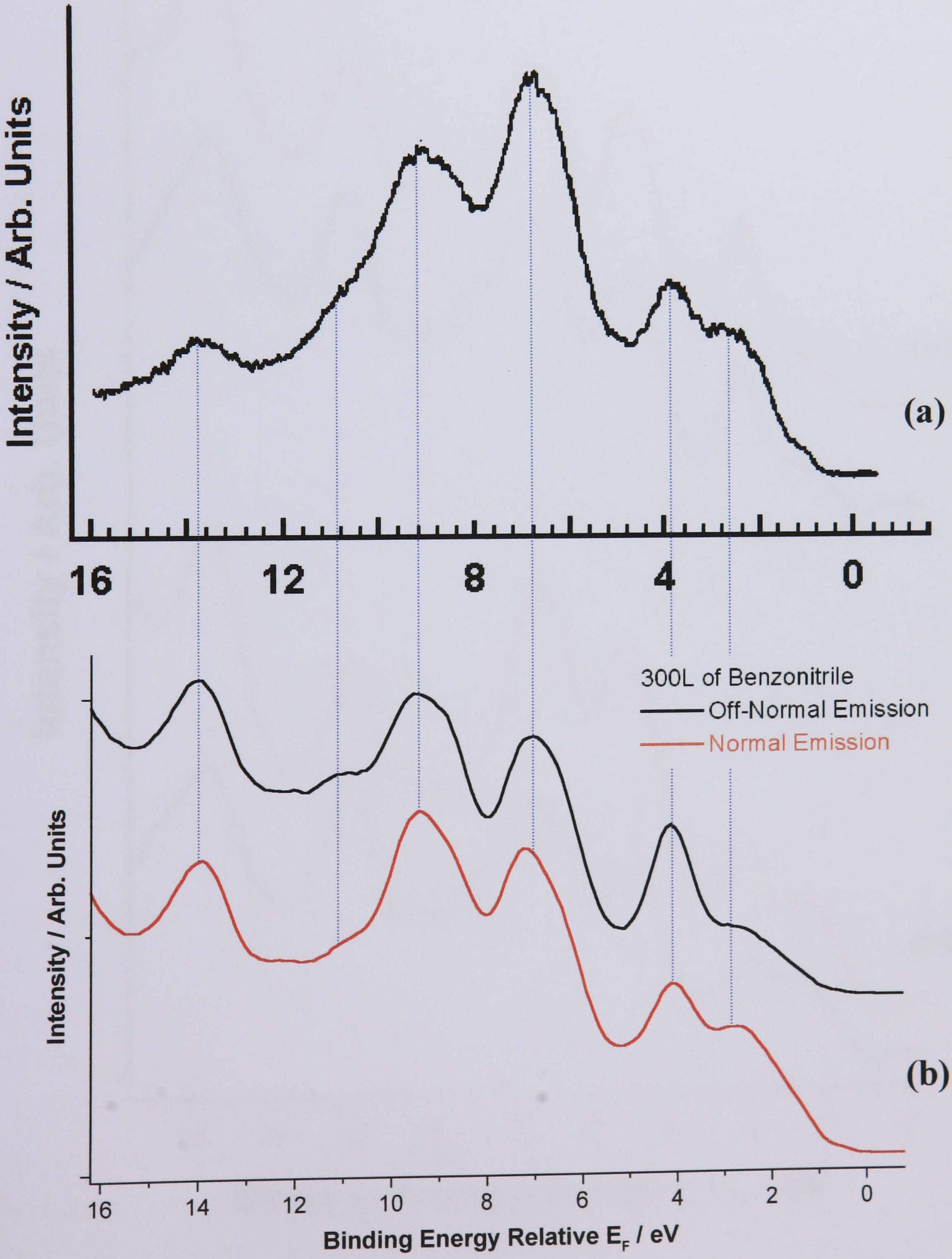

Fig.8. *Off-normal (a) and normal (b) difference spectra (hν = 40 eV) collected from the Si(100)-(2×1) and Si(111)-(7×7) surfaces which had been exposed to 45 and 300 L of benzonitrile at room temperature, respectively.*

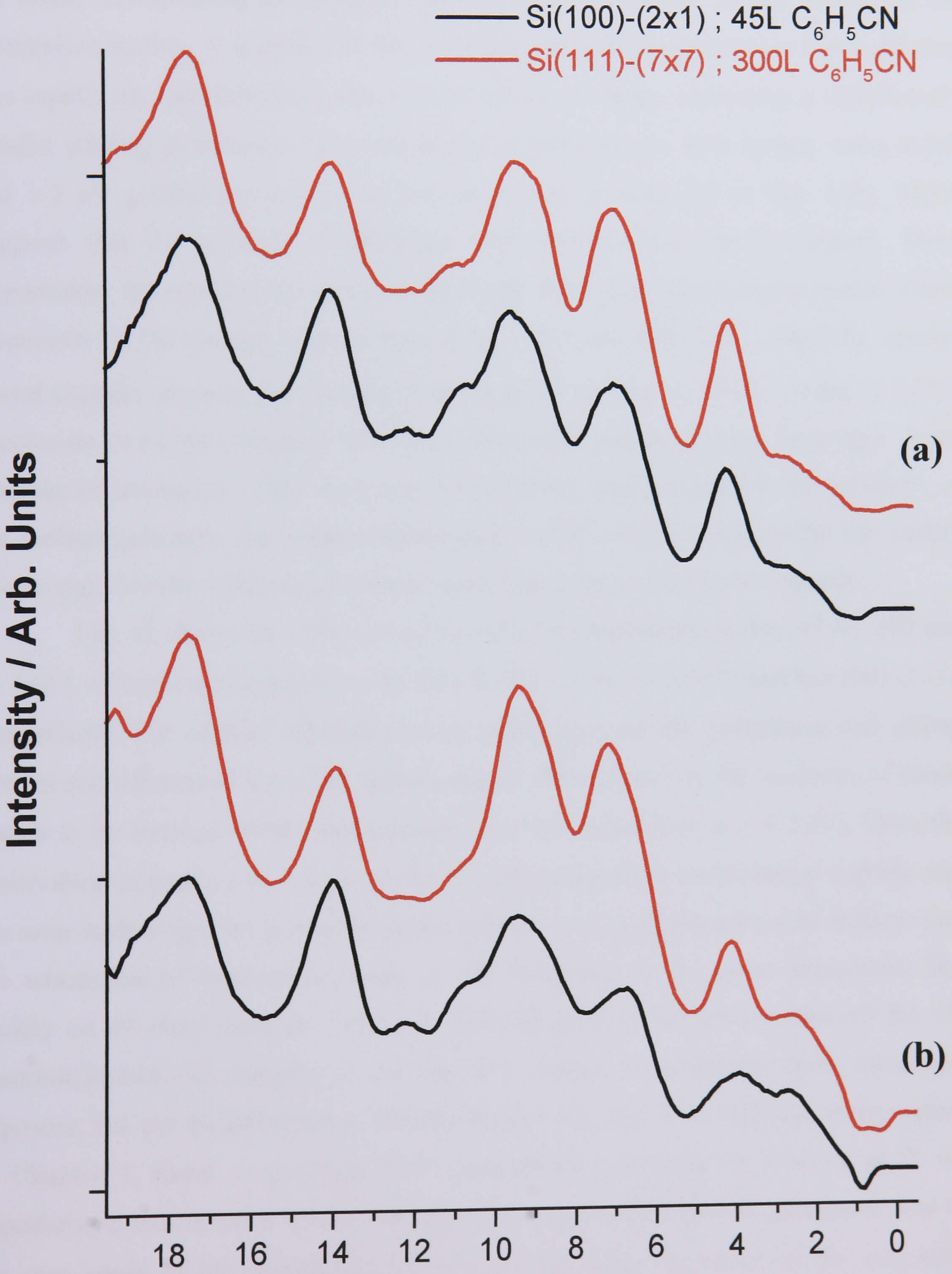

8.2.3 Benzonitrile/Ge(100)-(2×1)

Photoemission data taken of a Ge(100)-(2×1) surface, which was exposed to sequentially higher amounts of benzonitrile at room temperature, are displayed in Fig.10. Fig. 11 depicts the normal and off-normal difference spectra which emphasise the bands corresponding to the molecular orbitals of the surface moiety formed on the germanium surface. It is clear that the adsorbate induced photoemission bands develop less rapidly on Ge(100)-(2×1) than on the silicon surfaces, indicating a significantly smaller sticking probability. Upon adsorption of benzonitrile, both surface states at 0.6 and 1.3 eV gradually decrease in intensity (most pronounced in Fig. 11b), which suggests that the presence of adsorbed benzonitrile affect the Ge dimers. More importantly, the relative intensities of the bands differ with increasing exposure. Close inspection of the normal valence band (Fig. 10b) and difference (Fig.11b) spectra reveal changes, in particular the height of the peaks centred at 7.0 eV of the 11 110 L spectra are of higher intensities than the ones of benzonitrile at lower coverages. Since the relative intensities of the molecular orbital bands are correlated to the geometry of the surface geometry, our photoemission data would initially suggest that the moiety adopts significantly different geometries upon increasing benzonitrile exposure.

Fig. 12 shows the comparison between the photoemission data of 45, 300 and 11 110 L of benzonitrile dosed on the Si(100)-(2×1), Si(111)-(7×7) and Ge(100)-(2×1), respectively. The relative intensities of the peaks between the germanium and silicon normal and off-normal emission spectra clearly differ, however the positions of bands appear to be identical within experimental error (estimated here at ± 0.2 eV). Since the observation of bands with similar positions in photoemission spectroscopy indicate that the same surface species is present on the surfaces, our photoemission data indicate that the adsorption of benzonitrile leads to the formation of the same benzoimine-like moiety on all three surfaces. Thus the differing relative intensities observed for the benzonitrile/Ge(100) complex is not due to a change in orientation upon increasing exposure, but can be attributed to the adsorption of C_6H_5CN on different surface sites. In Chapter 7, based on previous TPD experiments performed by Fink *et al.*,[4] we hypothesised that benzene bonded initially to the germanium dimers positioned next to the step edges of the Ge(100)-(2×1) surface, and upon saturation of the step sites adsorption on the terraces started. Whilst to the best of our knowledge no thermal

desorption studies of benzonitrile on Ge(100) have been reported in the literature so far, we believe that the same model can be applied here to explain the difference in relative intensities observed in our photoemission data of the C_6H_5CN/Ge(100)-(2×1) complex. From the information provided in Figs. 10 and 11, for benzonitrile exposures of $\leq$1110 L we suspect that the adsorption involves the Ge dimers close to the step edges of the surface (Fig. 9). And at a higher exposure, the terraces sites become occupied as demonstrated by the change in the relative intensities observed for 11 110 L spectra. There is also some clear evidence that the Ge(100)-(2×1) surface remains unsaturated at this very high exposure. Finally it should be noted that the model presented here is only tentative and requires further investigation.

To summarise, from the similar peak positions our photoemission data clearly shows that the moiety formed by the adsorption of benzonitrile on Ge(100)-(2×1) at room temperature is the same as the one produced on both silicon surfaces. The differing relative intensities of the photoemission peaks suggest that the attachment of benzonitrile on Ge(100) occurs on the Ge dimers positioned next to the step edges and then terraces upon saturation of the step edge sites. As for C_6H_5CN adsorbed on the Si(100) surface, the formation of the benzoimine-like moiety on Ge(100)-(2×1) is the direct product of a 1,2-dipolar cycloaddition reaction between the cyano groups and the π-bonded Ge dimers.

Fig.9. *Schematic diagram showing benzonitrile adsorbed near the edges of the Ge(100)-(2×1) surface.*

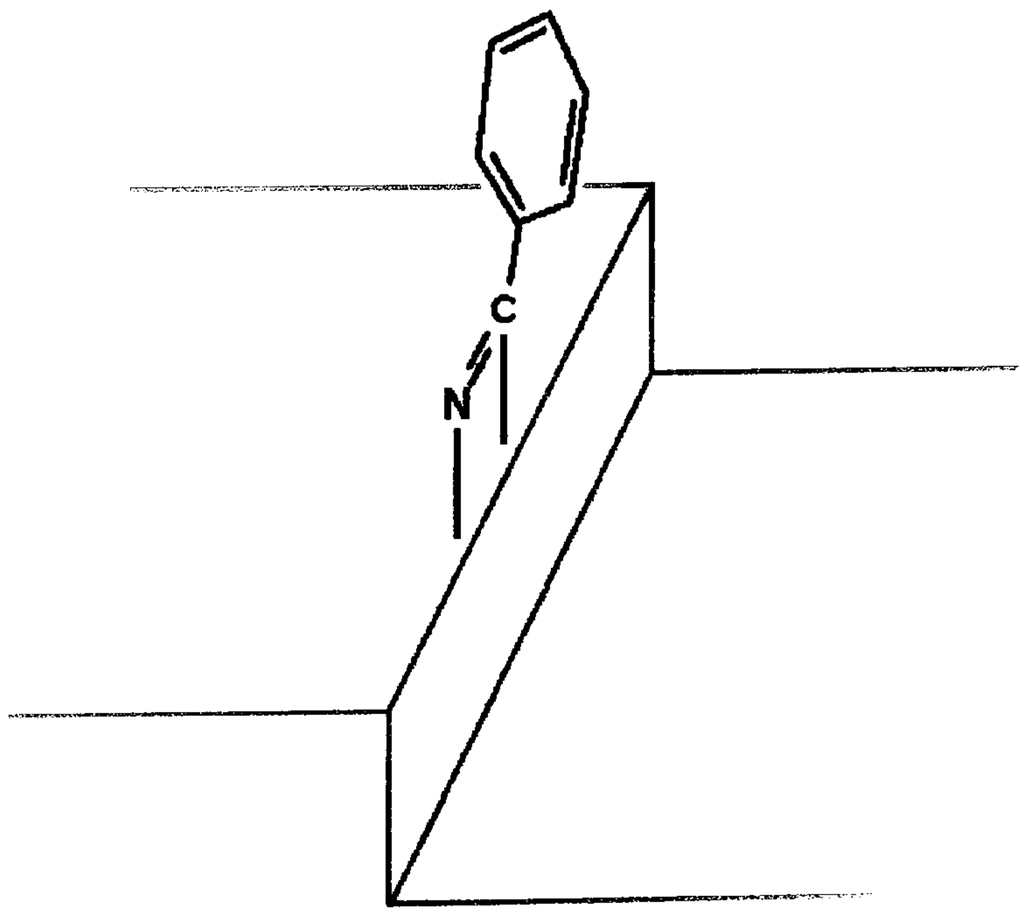

Fig.10. *Off-normal (a) and normal emission (b) valence band photoemission spectra ($h\nu$ = 40 eV) collected from clean Ge(100)-(2×1) and the same surface which had been exposed to 10, 20, 50, 110, 1110 and 11110 L of benzonitrile at room temperature.*

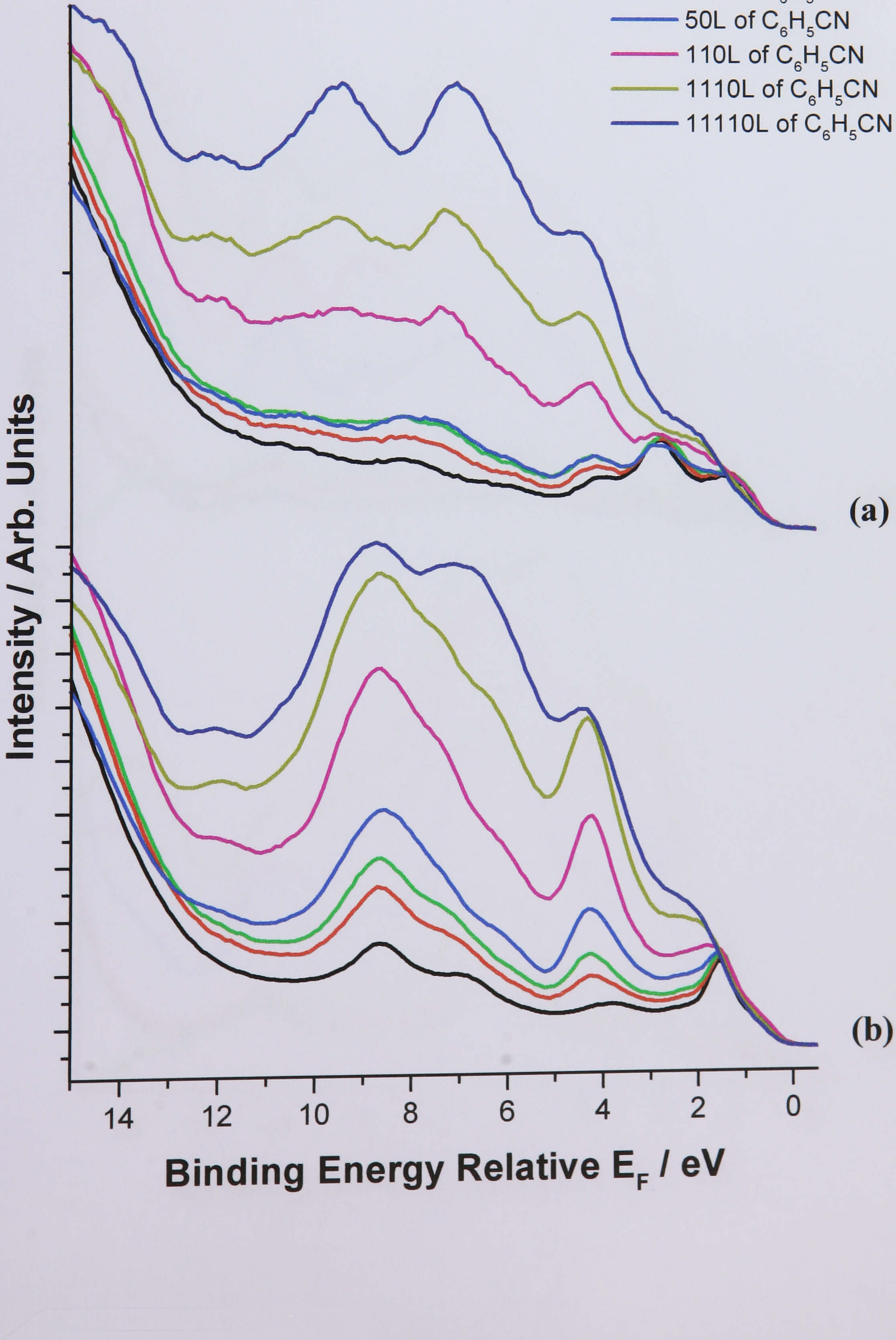

Fig.11. *Off-normal (a) and normal (b) emission difference UP spectra (hν = 40 eV) produced by subtracting clean surface spectrum from those taken after exposing the Ge(100)-(2×1) surface with 10, 20, 50, 110, 1110 and 11110 L of benzonitrile at room temperature.*

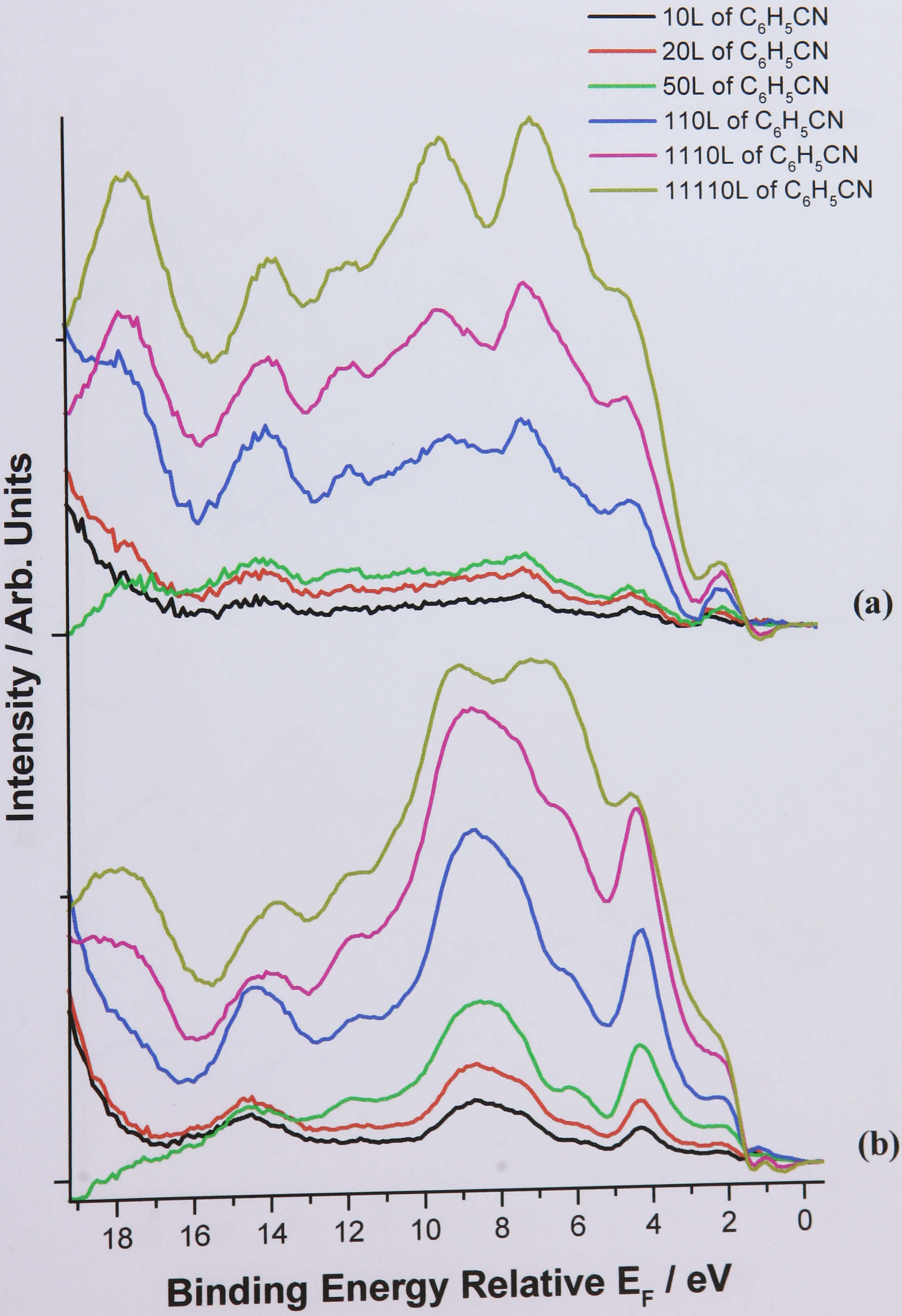

Fig.12. *Off-normal (a) and normal difference spectra (hν = 40 eV) collected from the Si(100)-(2×1), Si(111)-(7×7) and Ge(100)-(2×1) surfaces, which had been exposed to 45, 300 and 11110 L of benzonitrile at room temperature respectively.*

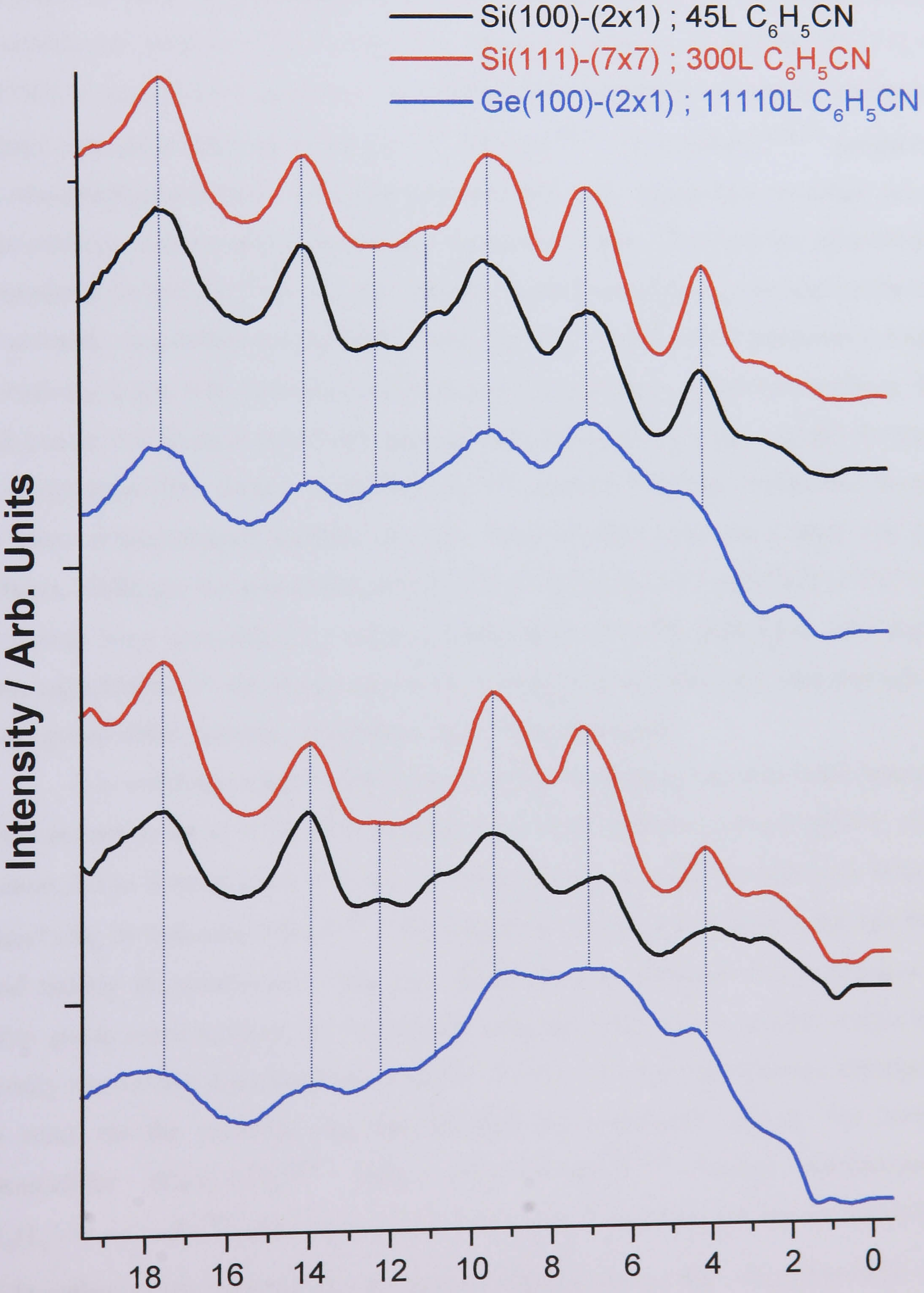

8.3 Discussion

The photoemission data depicted in Fig. 12 reveal that the same surface species is formed on Si(100)-(2×1), Si(111)-(7×7) and Ge(100)-(2×1) at room temperature upon benzonitrile exposure. Comparisons with work previously published by Tao *et al.*[1] and Wang and co-workers [2] confirm that a benzoimine-like moiety is produced on all three semiconductor surfaces. The formation of the same species on Si(100), Si(111) and Ge(100) is not entirely surprising, considering that adsorption of simple unsaturated organic molecules such as thiophene,[5,6] benzene[4,7-9] or ethylene[3,10-13] produces a 2,5-dihydrothiophene-like, 1,4-cyclohexadiene-like and ethane-like moieties on the three surfaces, respectively. Interestingly, it was previously found that the adsorption of benzonitrile on Ni(111)[14] occurs through the rehybridised nitrile group and not through the aromatic ring, whilst on Au(100)[15] and Cu(111)[16] benzonitrile produces a weakly π-bonded species, with both the C≡N axis and C_6-ring plane parallel to surfaces. It is well known that d-band metals are more reactive than noble metals, and the formation of a benzoimine-like moiety on Si(100), Si(111), and Ge(100) may be possible, because the three semiconductor surfaces are also more reactive than the copper and gold surfaces. Although the adsorption of C_6H_5CN on Si(100)-(2×1) and Si(111)-(7×7) has previously been determined by using a combination of UPS, HREELS, XPS and ab initio calculations,[1,2] the main reasons for benzonitrile to selectively bind through the cyano group rather than the phenyl have never been discussed.

It is well known that a substituent such as the nitrile group affects the reactivity of the aromatic ring to which it is attached. Due to the intrinsic electronegativity of the N atom and to bond polarity in C≡N, the cyano group can withdraw electrons from the phenyl ring by inductive effects.[17] This transfer of charge, which occurs through the σ bond linking the substituent to the ring, deactivates the aromatic ring and makes the cyano group more reactive. In conjunction with this observation, several studies have recently shown that functionalised aromatic systems, to which benzonitrile belongs, do not react *via* the aromatic ring but through the substituent instead. For instance benzenethiol (C_6H_5–SH),[18] aniline (C_6H_5–NH_2),[19-22] phenyl isothiocyanate (C_6H_5 - N = C = S)[23] and styrene (C_6H_5–CH=CH_2)[24] bond exclusively to the Si(100)-(2×1) surface *via* the external groups, and not through the C_6 ring. The benzenethiol and aniline molecules bind to Si(100) with Si-S(N) linkages through dissociation of the

S(N)-H bond,[18-22] whilst the C=N bond of phenyl isothiocyanate[23] and the external C=C bond of styrene[24] undergo a 1,2-dipolar and [2+2] cycloaddition reactions with the Si dimers, respectively. Interestingly, FTIR investigations have shown that toluene, para-xylene, meta-xylene and ortho-xylene [25] molecules possessing unreactive substituent groups, are chemisorbed onto Si(100) through their ring, in a similar manner as benzene.[7,8,25] However, the adsorption studies of phenyl isothiocyanate[23] and styrene[24] are relatively interesting in the present case, because they provide information which can be employed here to explain the high degree of selectivity in bonding of benzonitrile to the Si(100)-(2×1) and Ge(100)-(2×1) surfaces.

It is widely recognised that the difference in electronegativity between the C and N atoms of the cyano group makes the former atom positively charged (δ^+) and the latter one negatively charged (δ^-).[17] A study by Chadi also suggested that a transfer of charge occurs within the non-planar Si and Ge dimers.[26] This transfer of charge from the "down" atoms to the "up" atoms, which is associated with the tilting of the dimer units, adds some zwitterionic character to the surface dimers and makes the "down" atoms positively charged (δ^+) and the "up" atoms negatively charged (δ^-).[26] Consequently, the initial forces experienced by an impinging benzonitrile molecule on a Si(100) or Ge(100) surface will be controlled by the dipole-dipole interaction between the cyano group and the surface dimers (Fig. 13). Indeed, the ab initio calculations performed by Hamers and co-workers for the adsorption of styrene[24] and phenyl isothiocyanate[23] on Si(100)-(2×1) indicated that the long range interactions of the vinyl group and N=C bond of the isothiocyanate group with the ends of a Si dimer were attractive, while the interaction of the aromatic rings of both molecules were repulsive or essentially non-interacting. As a result, the initial dipole-dipole interaction, which is attractive at large separation and depicted in Fig. 13, "steers" the cyano group of the benzonitrile molecule towards the correct ends of the surface dimers. As was described in the two previous chapters, the degree of polarisation within the dimers is higher for Si than Ge, which may explain the different sticking probabilities between the Si(100) and Ge(100) observed in the current study.

We also believe that the reaction pathway involved in the present study is controlled by the unique geometry and electronic properties of the surface dimers. We believe that the 1,2-dipolar cycloaddition reaction between the C≡N group of the benzonitrile molecule and the π-bonded dimers of the Si(100)-(2×1) and Ge(100)-(2×1)

surfaces does not take place via a concerted manner but can be instead described as occurring through a low symmetry pathway. It is well known that the rate of this pericyclic reaction, controlled by the Woodward-Hoffmann rules in the present case, is normally low under normal (i.e. non-photochemical) condition.[24] However, the high sticking probability for benzonitrile on Si(100)-(2×1) observed and illustrated in Fig. 12 indicates that this 1,2-dipolar cycloaddition reaction is relatively facile phenomenon also experienced by other unsaturated molecules adsorbed on the same semiconductor surface.[27] To explain this, it was suggested by Hamers and co-workers that the charge transfer within the dimers produces a region of electron-deficiency located around the "down" atom and makes this end of the dimer an ideal site for nucleophilic attack.[23,24,27] Considering this argument, we believe that upon bonding the electron-rich cyano group reacts with the electron-deficient edge of the surface dimer, with initially N breaking its π bond to C and forming a new N–Si bond, then followed by creation of the C–Si σ bond further facilitated by the ability of the dimers to tilt back in the unbuckling process. Therefore the formation of benzoimine-like species on the Si(100)-(2×1) surface upon benzonitrile exposure occurs through a low-symmetry pathway to which the Woodward-Hoffmann rules do not apply. The unique properties of the Ge dimers can also explain the lower sticking coefficient observed for benzonitrile adsorbed on Ge(100)-(2×1).

To the best of our knowledge, the valence band data of benzonitrile adsorbed on Ge(100)-(2×1) at room temperature has not reported anywhere else, and Fig. 12 exhibits the difference in sticking probabilities between the Si(100) and Ge(100) surfaces. A possible explanation for this experimental observation may be due to the different structural properties of the two surfaces. In comparison to Si, the lattice constant of Ge is 4% enlarged[12] and makes the Ge dimer bond length 0.2 Å longer than the silicon-dimer bond length.[28] As for Si(100), the 1,2-dipolar cycloaddition reaction between C≡N and the Ge dimers is not a concerted reaction but rather proceeds through the formation of a three-membered intermediate, where the π bond of the cyano group first reacts with the "down" end of the germanium dimer before forming the four-membered ring in the final reaction product. The extra length of the Ge dimer may make it more difficult for the benzonitrile molecules, after forming the three-membered intermediate, to move over and create the benzoimine-like species on the surface, thereby lowering the sticking coefficient. This tentative description provides a possible

explanation of the data collected. As for the benzene/Ge(100)-(2×1) complex discussed in Chapter 7, the chemisorption of benzonitrile on the germanium surface appear to be more difficult than on the (2×1) reconstructed Si(100) surface. Our valence band spectra suggest that the adsorption of C_6H_5CN occurs initially on the Ge dimers positioned next to the step edges, followed by adsorption on the flat terraces upon saturation of the step edges.

The adsorption behaviour of benzonitrile on Ge(100)-(2×1) and Si(100)-(2×1) is clearly consistent with a 1,2-dipolar cycloaddition reaction between the C≡N group and the π-bonded Ge and Si dimers, however the formation of a benzoimine-like moiety on Si(111)-(7×7) is more surprising because the latter surface does not possess the π-bonded silicon dimers. A different reaction mechanism must therefore be responsible for the formation of this surface species. As already mentioned, the results of the current study are consistent with previous work on thiophene,[5,6] benzene[4,7-9] or ethylene[3,10-13] adsorbed on Si(100)-(2×1), Si(111)-(7×7) and Ge(100)-(2×1). The adsorption of these three molecules lead to the formation of a 2,5-dihydrothiophene-like,[5,6] 1,4-cyclohexadiene-like[4,7-9] and ethane-like moities[3,10–13] on all three semiconductor surfaces, respectively, which are the expected cycloadducts for pericyclic reactions. As for thiophene adsorbed on Si(111)-(7×7),[5] our photoemission data also suggest that the adsorption of benzonitrile on this surface causes the re-arrangement of the silicon atoms within the (7×7) reconstruction and involves the pedestal and rest atoms in the bonding process. So from the present investigation and previous work, because the Si(100), Si(111) and Ge(100) surfaces are structurally and electronically different, it again appears that the product formed on the silicon or germanium surfaces is not influenced by the electronic and physical structures of the surface, however the actual reaction mechanism is dependent upon the surface electronic and physical structure.

Fig.13. *Schematic illustration of dipole-dipole interaction and low-symmetry pathway for adsorption of benzonitrile on (a) Si(100)-(2×1) and (b) Ge(100)-(2×1). The arrows indicate the relative attractive polar interactions.*

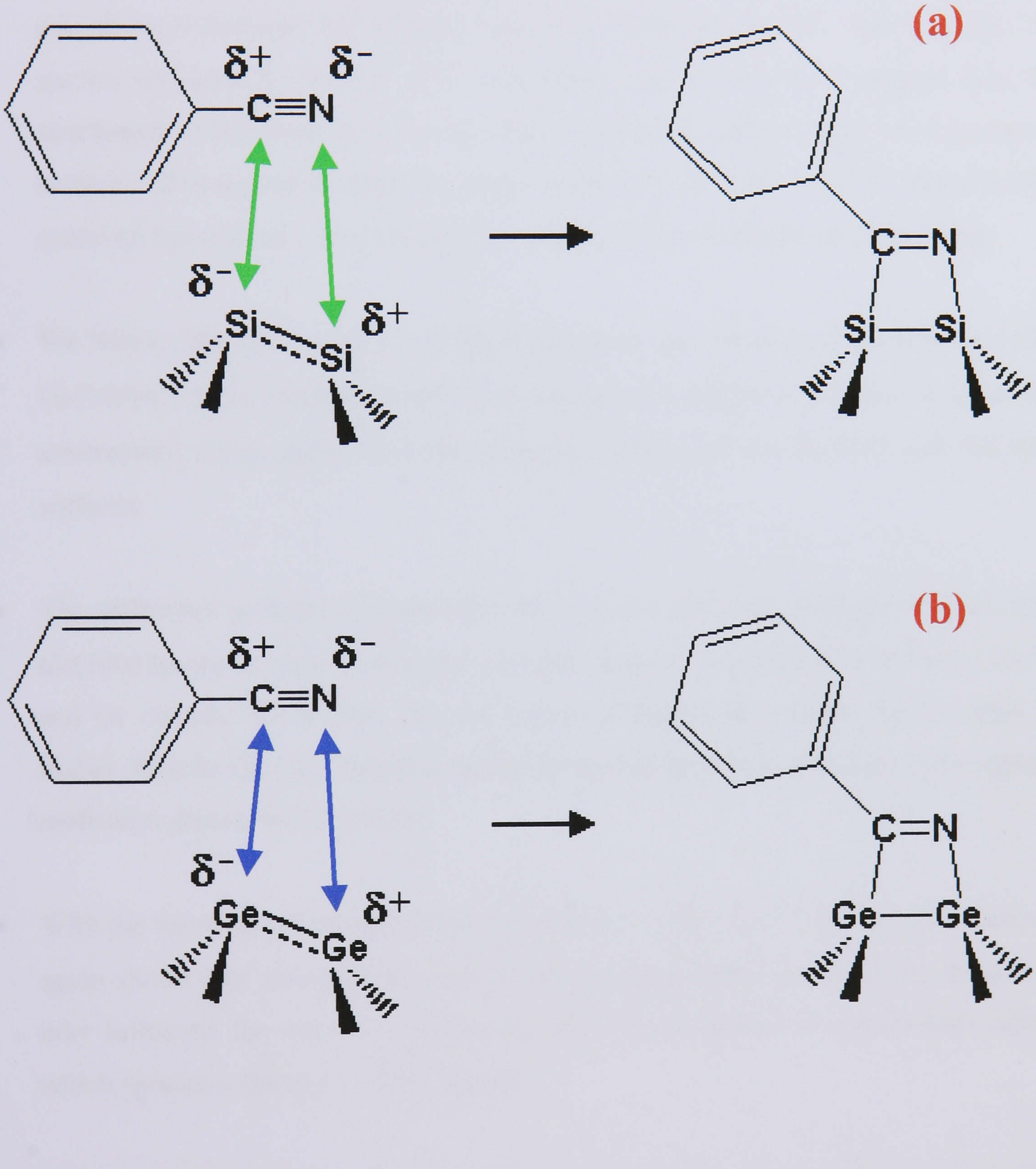

8.4 Summary

The most significant findings of the current study are outlined below:

- The adsorption of benzonitrile on Si(100)-(2×1), Si(111)-(7×7) and Ge(100)-(2×1) at room temperature lead to the formation of the same surface species. The direct comparisons between the valence band data from the current work and the UP spectra collected by Tao *et al.*[1] and Wang and co-workers[2] suggest that the attachment of benzonitrile occurs in a highly selective manner on the semiconductor surfaces. This occurs through the direct interaction of both C and N atoms of the cyano group to form a benzoimine-like species and not through the phenyl ring.

- We believe that the formation of the benzoimine-like species on Si(100)-(2×1) and Ge(100)-(2×1) is consistent with a1,2-dipolar cycloaddition reaction between the unsaturated cyano group and the π-bonded dimers of the Si(100) and Ge(100) surfaces.

- The difference in sticking probability between the (2×1) reconstructed Si(100) and Ge(100) has been associated to the different degrees of polarisation between the Si and Ge dimers. We believe that the degree of polarisation within the Si dimer is higher than the Ge one, thereby making the probability for interaction of the organic molecules greater on Si than Ge.

- With the formation of a benzonitrile-like species on Si(111)-(7×7), this investigation again shows that although the electronic/physical properties of the three substrates may influence the reaction mechanism, they do not appear to significantly affect which species is the most stable product.

- Finally, the three semiconductor studies performed in the current project show that the absorption of organic molecules on Si(100)-(2×1), Si(111)-(7×7) and Ge(100)-(2×1) lead to the formation of the same surface species.

8.5 References

1. F. Tao, Z.H. Wang, G.Q. Xu, J. Phys. Chem. B, 106 (2002) 3557
2. F. Tao, Z.H. Wang, X.F. Chen, G.Q. Xu, Phys. Rev. B, 65 (2002) 115311
3. F. Rochet, F. Jolly, F. Bournel, G. Dufour, F. Sirotti, J.-L. Cantin, Phys. Rev. B, 58 (1998) 11 029
4. A. Fink, D. Menzel, W. Widdra, J. Phys. Chem. B, 105 (2001) 3828-3837
5. Chapter 6 of the current work
6. M.H. Qiao, Y. Cao, F. Tao, Q. Liu, J.F. Deng, G.Q. Xu, J. Phys. Chem. B, 104 (2000) 11211
7. Chapter 7 of the current work
8. S. Gokhale, P. Trischberger, D. Menzel, W. Widdra, H. Droge, H.-P. Steinruck, U. Birkenheuer, U. Gutdeutsch, N. Rosch, J. Chem. Phys., 108 (1998) 5554
9. M. Carbone, M.N. Piancastelli, R. Zanoni, G. Comtet, G. Dujardin, L. Hellner, Surf. Sci., 407 (1998) 275
10. M. Carbone, R. Zanoni, M.N. Piancastelli, G. Comtet, G. Dujardin, L. Hellner, A. Mayne, J. Electron. Spectrosc. Relat. Phenom., 76 (1995) 271
11. M.N. Piancastelli, N. Motta, A. Sgarlata, A. Balzarotti, M. De Crescenzi, Phys. Rev. B, 48 (1993) 17892
12. A. Fink, R. Huber, W. Widdra, J. Chem. Phys., 115 (2001) 2768
13. P. Lal, A.V. Teplyakov, Y. Noah, M.J. Kong, T. Wang, S.F. Bent, J. Chem. Phys., 110 (1999) 10545
14. K. Kishi, Y. Okino, Y. Fujimoto, Surf. Sci., 176 (1986) 23
15. T. Solomun, K. Christmann, H. Baumgartel, J. Phys. Chem., 93 (1989) 7199
16. M.E. Kordesch, W. Feng, W. Stenzel, M. Weaver, H. Conrad, J. Electron. Spectrosc. Rel. Phenom., 44 (1987) 149
17. J. McMurry, *Organic chemistry*, Pacific Grove, California: Brooks-Cole, 3rd ed., Chapter 16 (1992)
18. S.K. Coulter, M.P. Schwartz, R.J. Hamers, J. Phys. Chem. B, 105 (2001) 3079
19. X. Cao, S.K. Coulter, M.D. Ellison, H. Liu, J. Liu, R.J. Hamers, J. Phys. Chem. B, 105 (2001) 3759
20. R.M. Rummel, C. Ziegler, Surf. Sci., 418 (1998) 303
21. T. Kugler, C. Ziegler, W. Gopel, Mater. Sci. Eng. B, 37 (1996) 112
22. T. Bitzer, T. Alkunshalie, N.V. Richardson, Surf. Sci., 368 (1996) 202

23. M.D. Ellison, R.J. Hamers, J. Phys. Chem. B, 103 (1999) 6243
24. M.P. Schwartz, M.D. Ellison, S.K. Coulter, J.S. Hovis, R.J. Hamers, J. Am. Chem. Soc., 122 (2000) 8529
25. S.K. Coulter, J.S. Hovis, M.D. Ellison, R. J. Hamers, J. Vac. Sci. Technol. A, 18 (2000) 1965
26. D.J. Chadi, Phys. Rev. Lett., 43 (1979) 43
27. R.J. Hamers, S.K. Coulter, M.D. Ellison, J.S. Hovis, D.F. Padowitz, M.P. Schwartz, C.M. Greenlief, J.N. Russell Jr., Acc. Chem. Res., 33 (2000) 617
28. S.W. Lee, J.S. Hovis, S.K. Coulter, R.J. Hamers, C.M. Greenlief, Surf. Sci., 462 (2000) 6

Summary 2. Semiconductor Studies

The results from these three semiconductor studies indicate that the absorption of organic molecules on Si(100)-(2×1), Si(111)-(7×7) and Ge(100)-(2×1) leads to the formation of the same surface species. From the analysis of the respective doses required for the photoemission peaks to be observed in our valence band spectra, the relative reaction rates give: Si(100) > Ge(100). We suggested that the Si(100) surface is more reactive than the Ge(100), because the degree of polarisation within the dimers is higher for Si than Ge, thereby making the probability for interaction of the organic molecules greater on Si than Ge.

The formation of 2,5-dihydrothiophene-, 1,4-cyclohexdiene- and benzoimine-like moieties on the Si(100) and Ge(100) surfaces, which possess π-bonded dimers, are consistent with cycloaddition mechanisms such as those proposed by two group led by Hamers and Bent. The relative reactivities the Si(100)-(2×1) and Ge(100)-(2×1) surfaces towards thiophene and benzene are consistent with a [4+2] cycloaddition (Diels-Alder) mechanism. On the other hand, a 1,2-dipolar cycloaddition reaction between the unsaturated reactive cyano group of the benzonitrile molecules and the surface dimers is responsible for the formation of the benzoimine-like surface species.

Finally we have seen that the same surface species are formed on Si(111)-(7×7). Because this surface does not possess the required "π-bonded" dimers, this result would imply that although the reaction mechanisms are influenced by the surface electronic and structural properties, the actual products of the surface reaction are not.